Historical and future trends in global snow conditions – observed by remote sensing and forecasted by spatio-temporal modelling.

Darri Eyþórsson

Faculty of Civil and Environmental Engineering
University of Iceland
2023

Historical and future trends in global snow conditions – observed by remote sensing and forecasted by spatio-temporal modelling.

Darri Eyþórsson

Dissertation submitted in partial fulfillment of a
Philosophiae Doctor degree in Environmental Engineering

Advisor
Dr. Sigurdur M. Gardarsson

PhD Committee
Dr. Sigurdur M. Gardarsson
Dr. Bart Nijssen
Dr. Birgir Hrafnkelsson
Dr. Óli Grétar Blöndal Sveinsson

Opponents
Dr. Halldór Björnsson
Dr. Kostas Andreadis

Faculty of Civil and Environmental Engineering
School of Engineering and Natural Sciences
University of Iceland
Reykjavik, 2023

Historical and future trends in global snow conditions – observed by remote sensing and forecasted by spatio-temporal modelling.
Dissertation submitted in partial fulfillment of a *Philosophiae Doctor* degree in Environmental Engineering

Faculty of Civil and Environmental Engineering
School of Engineering and Natural Sciences
University of Iceland
Hjardarhaga 2-6
107, Reykjavik
Iceland

Telephone: 525 4000

Bibliographic information:
Eythorsson, D. 2023, *Historical and future trends in global snow conditions – observed by remote sensing and forecasted by spatio-temporal modelling,* PhD dissertation, Faculty of Civil and Environmental Engineering, University of Iceland

Author ORCID: 0000-0003-3653-3936
ISBN: 978-9935-9742-2-8

Printing: Haskolaprent
Reykjavik, Iceland, 2023

Abstract

Snow resources worldwide are undergoing extensive changes in response to widespread and rapid changing of the global climate. These resources are vital in many areas and changes to them have and will continue to impact human societies and ecosystems in cold regions. The research presented in this dissertation entails the assessment and comparison of historical trends in the climate and snow regimes and the projection of these trends until the end of the 21st century, under different emission scenarios. The results show that extensive changes have occurred to the frequency of Northern Hemisphere (NH) snow cover since the beginning of the 21st century, as estimated based on remote sensing data from the MODIS satellite instrument. The future evolution of NH snow resources was modelled for the period 1950-2100 for each of the 21 downscaled and bias corrected CMIP5 climate models for two emission scenarios (RCP45 and RCP85) using the Snow17 model. The simulations show that the Snow Cover Frequency (SCF) is in general projected to diminish substantially across the NH. However, the NH 1st April Snow Water Equivalent (SWE) is projected to increase slightly at the beginning of the period, driven by increased snowfall at high latitudes in the Arctic and then decline back to 1950-1975 levels under RCP45 and 10% under those given RCP85. These trends were analyzed specifically for Icelandic circumstances revealing a trend of increasing SCF in many parts of the country over the period 1930-2021, whereas the simulated results project a decrease in SCF across Iceland between 1950 to 2100.

Útdráttur

Snjóauðlindir víðsvegar um heiminn eru nú breytingum undiropnar í kjölfar hnattrænna loftlagsbreytinga. Þessar auðlindir eru mikilvægar víðsvegar og breytingar á eðli þeirra hafa haft og munu halda áfram að hafa áhrif á mannleg samfélög og vistkerfi á kvöldum svæðum. Rannsókn sú er birt er í þessari ritgerð fjallar um greiningu og samanburð á sögulegri þróun loftlags og snjós og gerð forspár um það hvernig væntar loftlagsbreytingar munu hafa áhrif á snjóauðlindir út 21 öldina miðað við mismunandi sviðsmyndir í hlýnun. Niðurstöður rannsóknarinnar sýna fram á að víðtækar breytingar hafa þegar orðið á snjóþekju á Norður Hveli jarðar (NH) frá byrjun 21 aldarinnar útfrá fjarkönnunargögnum frá MODIS gervihnattamælinum. Spáð var fyrir um framtíðarþróun snjóauðlinda á NH fyrir tímabilið 1950-2100 með Snow17 snjólíkaninu útfrá 21 CMIP5 loflagslíkönum fyrir tvö hlýnunartilvik (RCP45 og RCP85). Niðurstöður líkansins gefa til kynna að tíðni snjóhulu (SCF) muni almennt minnka verulega um allt NH en að hinsvegar, muni meðal rúmál vatns sem geymt er í snjóalögum NH aukast lítillega í byrjun tímabilsins, aðallega vegna aukinnar snjókomu og norðlægum breiddargráðum innan norðurheimskautsbaugs, en minnka svo aftur að því sem var um 1950 fyrir RCP45 en 10% neðar en svo fyrir RCP85.. Þróun í loftlagi og snjóauðlindum var rannsökuð sérstaklega á Íslandi, sem leiddi í ljós tölfræðilega marktækta aukningu á SCF stórum svæðum frá aldamótum, spá um þróun snjóauðlinda út 21 öldina gerir hinsvegar ráð fyrir verulegri minnkun á SCF í öllum hæðarbilum á Íslandi.

This work is dedicated to my daughter, Eldey.

Table of Contents

List of Figures ..... **ix**

List of Tables ..... **xi**

List of Publications ..... **xiii**

Abbreviations ..... **xiv**

Acknowledgements ..... **xvii**

1. Introduction **1**
1.1 Statement of purpose 1
1.2 Research objectives 1
1.3 Dissertation organization 4

2. Background **5**
2.1 Historical and predicted changes in the climate and snow regimes 5
2.1.1 Global trends in climate and snow conditions 5
2.1.2 Changes in the Icelandic climate and snow 9
2.2 Snow Observations 12
2.2.1 In situ observations 12
2.2.2 Remote sensing of snow 13
2.3 Snow modelling 15
2.3.1 Physical representation of snow 15
2.3.2 Physical models 18
2.3.3 Empirical models 19
2.3.4 Conceptual models 20
2.3.5 Calibration and Validation 21
2.3.6 Spatial representation 22

3. Application and results **23**
3.1 Simulating seasonal glacier mass balance – Application to Brúarjökull glacier 23
3.1.1 Data 24
3.1.2 Variable selection 25
3.1.3 Multivariate model ensemble 26
3.1.4 Multi-model inference 26
3.1.5 Selecting an optimal subset of models for inference 27
3.1.6 Model Evaluation and results 27
3.2 Observing global snow cover changes 29
3.2.1 Estimating Snow Cover Frequency 29
3.3 Estimating and predicting changes to global climate classifications 32
3.3.1 Köppen-Geiger classification system 32
3.3.2 Projecting future Climate Classifications 33

3.4 Comparing trends in climate classifications and Snow Cover - an Arctic case study 38
3.5 Projecting changes to NH snow resources under different climate change scenarios 42
3.5.1 Methods 42
3.5.2 Results 47
3.6 Analyzing historical and predicted snow cover and climate trends – a case study for Iceland 56
3.6.1 Historical Snow Cover Trends 56
3.6.2 Estimating and Projecting Climate Classifications 61
3.6.3 Projecting Changes to Snow Resources in Iceland 63

4. Conclusion and future perspectives 67
4.1 Conclusion 67
4.2 Future Perspectives 70

References 73

Appendix A - Statistical Summer Mass-Balance Forecast Model with Application to Brúarjökull Glacier, South East Iceland 101

Appendix B - Arctic Climate and Snow Cover Trends – Comparing Global Circulation Models with Remote Sensing Observations 111

Appendix C - Observed and Predicted Trends in Icelandic Snow Conditions for the period 1930-2100 123

Appendix D - Projected Changes to Northern Hemisphere Snow Conditions over the period 1950-2100, given two emission scenarios 135

List of Figures

Figure 3-1 Location of mass-balance sites and Automatic Weather Stations (AWS) where the glaciological and meteorological data used in Eythorsson et al., (2018), were collected (from Eythorsson et al. 2018) 25

Figure 3-2 Model-average forecasts of Brúarjökull summer mass balance for all five folds used for cross validation (from Eythorsson et al., 2018) 28

Figure 3-3 Areas of increasing (blue) and decreasing (red) SCF, as estimated using Sen's slope estimation method at the $\alpha = 0.05$ confidence level. 31

Figure 3-4 Examples of annual Köppen-Geiger (KG) classification maps for year 1951 (upper) and 2099 given the RCP45 emission scenario (lower). 34

Figure 3-5 Snapshot of the KG classification app developed from the results of Eythorsson et al., (2019). 35

Figure 3-6 Proportional areal coverage of the most common groups of KG classes in the Arctic, below 500 m.a.s.l., for the period 1950-2100. A 15-year rolling mean is shown as a solid line (from Eythorsson et al., 2019) 36

Figure 3-7 The Arctic area (AMAP, 2015) and the 10 pollution prevention areas in the Arctic which were selected for comparing changes in the snow and climate domains (from Eythorsson et al., 2019) 38

Figure 3-8 Snow Cover Frequency (SCF) and proportional coverage of the two most common KG classes in each study area over the period 2001-2016 (from Eythorsson et al., 2019). 39

Figure 3-9 Snow Cover Frequency (SCF) for the 2004 water year, i) as simulated using the ensemble average of the NASA NEX-GDDP dataset ($GDDP_{sim}$), ii) as simulated using GLDAS-2 data ($GLDAS_{sim}$), iii) as observed in the GLDAS-2 data ($GLDAS_{hist}$) and iv) as observed by MODIS/TERRA (MOD_{obs}) (from Eythorsson et al. 2023b) 47

Figure 3-10 Mean annual SWE for the 2004 water year, i) as simulated using the ensemble average of the NASA NEX-GDDP dataset ($GDDP_{sim}$), ii) as simulated using the GLDAS-2 dataset ($GLDAS_{sim}$) and iii) as observed in the GLDAS-2 dataset ($GLDAS_{hist}$) (from Eythorsson et al., 2023b) 48

Figure 3-11 Pearson's Correlation, R, for daily SCA values over the 2004 water year as estimated between: i) $GDDP_{sim}$ and $GLDAS_{hist}$ ii) $GDDP_{sim}$ and MOD_{obs} iii) $GDDP_{sim}$ and $GLDAS_{sim}$ iv) $GLDAS_{sim}$ and MOD_{obs} SCA v) $GLDAS_{sim}$ and $GLDAS_{hist}$ and vi) $GLDAS_{hist}$ and MOD_{obs}. 48

Figure 3-12 Pearson's Correlation, R, for daily SWE values during the 2004 water year as estimated between i) $GDDP_{sim}$ and $GLDAS_{hist}$ ii) $GDDP_{sim}$ and $GLDAS_{sim}$ and iii) $GLDAS_{sim}$ and $GLDAS_{hist}$ 49

Figure 3-13 i) Mean number of Snow-Covered Days (SCD) for the period 1950-1975, ii) percentage change in SCD between 2075-2100 and 1950-1975 under RCP45 and iii) same as ii) but for RCP85 (from Eythorsson et al., 2023b). 50

Figure 3-14 1 Snow Water Equivalent (SWE) for the period 1950-1975, ii) percentage change in SWE between 2075-2100 and 1950-1975 under RCP45 and iii) same as ii) but for RCP85 (from Eythorsson et al., 2023b). 51

Figure 3-15 Annual Snow Cover Frequency (SCF) (right) and 1st of April Snow Water Equivalent (SWE) across the NH (left). The shaded areas represent the upper and lower quantiles of the ensemble simulations, and the solid line a 10-year moving average. (From Eythorsson et al., 2023b). 52

Figure 3-16 Changes to 1st April SWE in the study basins selected in Eythorsson et al., (2023b). Blue basins showed more than 10% increase in SWE, red basins showed more than 10% decrease in SWE while grey basins showed less than 10% change in SWE, under the RCP45 emission scenario (from Eythorsson et al., 2023b). 53

Figure 3-17 Topographical map of Iceland and the locations of the Icelandic Meteorological Office (IMO) observation stations where snow data recorded (from Eythorsson et al., 2023a) 57

Figure 3-18 Left panel: Average annual temperature and precipitation in Iceland over the period 1950-2021 as estimated by the ensemble average of the 21 GCM‘s in the NASA NEX-GDDP dataset and the IMO. Center panel: Annual average SCF for all IMO monitoring stations for the period 1930-2021, calculated for local (circles) and mountain (triangles) snow cover for observations of fully snow covered ground, SNC or SNCM = 4 (blue) and including patchy snow cover, SNC or SNCM ≥ 2 (red), the average annual SCF estimated from the MODIS TERRA/AQUA snow cover products (black markers) is shown for observations above (stars) and below (crosses) 500 m a.s.l. Right panel: average annual snow depth of all IMO monitoring stations. (from Eythorsson et al., 2023a) 58

Figure 3-19 Left panel: trend in annual SCF over Iceland as estimated from MODIS. Right panel: areas where the trendline is statistically significant ($\alpha = 0.05$) for both MODIS and in situ observations (SNC = 4). 2019 outlines of glaciers and the ice divides of their major outlet glaciers are shown with black lines (RGI Consortium, 2019). (from Eythorsson et al., 2023a) 59

Figure 3-20 Time series of annual SCF in locations where known land surface changes have taken place over the period of MODIS observations (2000-2016)..... 60

Figure 3-21 Examples of annual KG classification maps calculated for Iceland in the study for the years 1951 (upper) and 2099 (lower) 62

Figure 3-22 Time series of the annual proportional coverage of the three main KG Classes in each elevation zone in Iceland for the period 1951-2099 (from Eythorsson et al., 2023a). 63

Figure 3-23 Left panel: simulated average winter SWE across Iceland for both RCP45 (green) and RCP85 (red). Right panel: simulated average annual SCF across Iceland as projected by RCP45 (green) and RCP85 (red). Observations from monitoring stations of mountain (crosses) and local (stars) snow cover and MODIS observations (triangles) are shown in black. The shaded area represents the upper and lower quantiles of the ensemble simulations, and the solid line shows a 10-year moving average of the ensemble. (from Eythorsson et al., 2023a) 64

List of Tables

Table 3-1 Predictor variable selected for development of a multimodel forecast ensemble and their correlation to the observed summer mass balance of Brúarjökull, given as r^2 values (from Eythorsson et al., 2018). 26

Table 3-2 Evaluation metrics, NSE, RSR, PBIAS for forecasts made between the 15th of May and 1st of July (from Eythorsson et al., 2018) 27

Table 3-3 Criteria for Köppen-Geiger classifications and their symbols 33

Table 3-4 Proportional coverage of Polar and Cold climate classes within the Arctic AMAP boundary and the changes between the periods 1951-1960 and 2090-2099 (from Eythorsson et al., 2019). 36

Table 3-5 Changes in coverage of the two main KG classes in the period 2001-2016 and the percentage of study areas below 500 m.a.s.l. showing a significant SCF trend. Significant results at the $\alpha = 0.05$ confidence level are in bold. (From Eythorsson et al., 2019) 40

Table 3-6 Datasets used for snow modelling and parameter estimation and model evaluation (from Eythorsson et al. 2023b) 43

Table 3-7 Snow17 parameters, description, value ranges and estimation methodology (from Eythorsson et al. 2023b) 43

Table 3-11 Relative change in SWE and SCD (in %) between 1950-1975 and 2075-2100 in the study basins. Basins colored blue have more than 10% increase in mean winter SWE over the period, red colored basins showed more than 10% decrease in SWE and grey colored basins had less than 10% change in SWE, under the RCP45 emission scenario (from Eythorsson et al., 2023b). 53

Table 3-12 Statistical significance of the linear snow trends, estimated using the Mann-Kendall (MK) trend test, for both the period of historical records (1930-2021) and the MODIS period (2001-2021), of p values Statistically significant trendlines at the $\alpha = 0.05$ level shown in bold. 59

Table 3-13 Results of Mann-Whitney-Wilcoxon (MWW) on two sample means, before and after known land surface changes in three locations in Iceland 60

List of Publications

Journal Articles

Eythorsson D., Gardarsson S.M., Nijssen B., (2023), Projected Changes to Northern Hemisphere Snow Conditions over the period 1950-2100, given two emission scenarios, *Remote Sensing Applications: Society and Environment, 30,* 100954, https://doi.org/10.1016/j.rsase.2023.100954

Eythorsson, D., Gardarsson, S. M., Gunnarsson, A., and Sveinsson, O. G. B, (2023) Observed and predicted trends in Icelandic snow conditions for the period 1930–2100, *The Cryosphere*, 17, 51–62, https://doi.org/10.5194/tc-17-51-2023

Eythorsson D., Ahmad SK, Gardarsson S.M, Hossain F, Nijssen B, (2019), Arctic Climate and Snow Cover Trends – Comparison of Global Circulation Models with Remote Sensing observations, *International Journal of Applied Earth Observations and Geoinformation*, *80,* 71-81, https://doi.org/10.1016/j.jag.2019.04.003

Eythorsson D., Gardarsson S.M., Gunnarsson A., Hrafnkelsson B., (2018), Statistical summer mass-balance forecast model with application to Brúarjökull glacier, South East Iceland. *Journal of Glaciology*, *64*(244), 311-320. https://doi:10.1017/jog.2018.22

Conference presentations

Eythorsson D., Gardarsson SM., Nijssen B., (2020), "Projecting Changes to Northern Hemisphere Snow Resources Under Different Emission Scenarios, Using Google Earth Engine", Conference presentation – *AGU Fall Meeting 2020*, C063-0010

Eythorsson D., Ahmad SK, Gardarsson SM, Hossain F, Nijssen B, (2019), Arctic Climate and Snow Cover Trends – Comparing Global Circulation Models with Remote Sensing Observations, Conference presentation, *AGU Fall Meeting 2019*, C52A – 02

Abbreviations

Antarctic Ice Sheet (AIS)

Advanced Very High-Resolution Radiometer (AVHRR)

Active Microwave (AM)

Arctic Assessment and Monitoring Program (AMAP)

Atlantic Meridional Oscillation (AMO)

Advanced Microwave Scanning Radiometer-EOS (AMSR-E)

Advanced Spaceborne. Thermal Emission and Reflection Radiometer (ASTER)

Assessment Report (AR)

Automatic Weather Stations (AWS)

Coupled Model Intercomparison Project (CMIP)

Degree Day Factor (DDF)

Digital Elevation Model (DEM)

European Climate Assessment & Data Set (ECA&D)

Gauge Catch Factor (GCF)

Global Circulation Model (GCM)

Google Earth Engine (GEE)

Global Daily Downscaled Projections (GDDP)

Global Land Cover Facility (GLCF)

Global Land Data Assimilation System (GLDAS)

Global Surface Air Temperature (GSAT)

Greenland Ice Sheet (GIS)

Hydro Power Plant (HPP)

Icelandic Meteorological Office (IMO)

International Panel on Climate Change (IPCC)

Inferometric Synthetic Aperature Radar (InSAR)

InfraRed (IR)

Köppen-Geiger (KG)

Modern Eera Retrospective analysis for Research and Applications (MERRA)

MODerate Resolution Imaging Spectroradiometer (MODIS)

Nasa Earth Exchange (NEX)

Nash-Sutcliffe Efficiency (NSE)

North Atlantic Oscillation Index (NAOI)

National Oceanic and Atmospheric Administration (NOAA)

US National Oceanic Data Center (NODC)

Mann-Kendall (MK)

Maximum Melt Factor (MFMAX)

Minimum Melt Factor (MFMIN)

Mann-Whitney-Wilcoxon (MWW)

Northern Hemisphere (NH)

Numerical Weather Prediction Model (NWPM)

National Weather Service River Forecast System (NWSRFS)

Percent Bias (PBIAS)

Physical Liquid Water Holding Capacity (PLWHC)

Passive Microwave (PM)

Polarimetric Synthetic Aperature Radar (PolSAR)

Regional Arctic System Model (RASM)

Representative Concentration Pathway (RCP)

Root Square Ratio (RSR)

Snow Water Equivalent (SWE)

Snow Covered Area (SCA)

Snow Cover Extent (SCE)

Snow Covered Days (SCD)

Snow Cover Frequency (SCF)

Snow Depth (SD)

Surface Energy Balance (SEB)

Scanning Multichannel Microwave Radiometer (SMMR)

Solid Precipitation Measurement Intercomparison Project (SPMIP)

Special Sensor Microwave Image (SSM/I)

Visible spectrum (VIS)

World Climate Research Program (WCRP)

World Glacier Monitoring Service (WGCM)

World Meteorological Office (WMO)

Acknowledgements

Above all, I express my most sincere gratitude to my supervisor Dr. Sigurður Magnús Garðarsson for his consistent support throughout this project. For his guidance, encouragement and understanding, which helped me persevere to complete this dissertation. I am forever grateful for the trust to take on this project with me and the skillful and compassionate counsel which has helped me rise to the challenges faced along the way.

I extend my sincere gratitude to the members of my doctoral committee: Dr. Óli Grétar Blöndal Sveinsson for valued comments, Dr. Birgir Hrafnkelsson for his constructive feedback and finally, I extend my deepest gratitude to Dr. Bart Nijssen for graciously welcoming me to his team at the UW and his guidance throughout my stay in Seattle, as well as for his continuous support and invaluable influence and contribution to this work.

I would like to thank the Google Earth Engine team, especially Noel, Simon, Michael, and Sufi, for their time, patience, and dedication in helping me troubleshoot and find solutions to programming and modelling approaches.

I would like to thank the organizers at the facilitators at a workshop on scientific writing, arranged by Aalto University, Helsinki, Finland, and IWA/YWP Finland in August 2018, especially Dr. Gustaf Olsson who influenced the way I think about academic writing.

This work was made possible by the University of Iceland Research Fund through the doctoral grants of the University of Iceland, a doctoral grant from the Icelandic National Energy Company, Landsvirkjun, which supported this work through the Energy Research Fund grant no DOK-02-2017.

I would like to thank my fellow PhD students both at HÍ and UW. Orianna, Andrew, Liz, Yifan, Hörður, Yixin and Diana, thank you for welcoming me into the group in Wilson and for all your help, kindness, and friendship while I was in the US. Majid, Tarek, and Narges thank you for the support and comradery at HÍ. Andri, thank you kindly for the opportunity to work with you at LV and the insight and inspiration I have gained from researching this subject alongside you.

Finally, I want to thank my colleagues at the University of Iceland. Brynhildur, Hrund and Guðmundur Freyr, it’s been a pleasure and a privilege to learn from and then teach alongside you over these past years. I am ever grateful for the trust and faith you have placed in me over the past years and for your guidance and kind counsel.

1. Introduction

1.1 Statement of purpose

Snow and ice play a significant role in the surface hydrological cycle in large parts of the world, primarily in mountainous areas and above 40° latitude. (e.g. Adam et al., 2009). Snow accumulates on the ground when precipitation falls at temperatures below the freezing point of water, where it stays until it melts or sublimates. Snowmelt begins to occur when the temperature of the accumulated snow cover increases above the melting point. The thermal flux between the snow and its environment is mainly governed by local meteorological conditions, which in turn are determined by the regional and then global climate. As snow melts, the water finds its way into streams, lakes, and rivers where it may provide important ecosystem functions as well as water resources for human communities.

Water resources managers seek to utilize the snow resource as efficiently and responsibly as possible. In current practice, information about the state of snow is combined with meteorological data to model changes in the snow cover and derive important parameters relating to the state of the snow, e.g., the water stored in snow, the timing of snow melt and the volume of meltwater. In a changing climate these parameters can be expected to change, and the nature of these changes may vary by region. Understanding how snow and ice will change with changing climate is, therefore, important for water resources managers in cold regions across the globe to estimate future infrastructure requirements and resource availability.

1.2 Research objectives

The doctoral research of past and future changes to the snow conditions was structured according to the following main research objectives.

Research objective 1: *Identify the environmental drivers of snow and ice mass balance*

The first objective of the research was to investigate the relationships between the snow and climate regimes and to identify the dominant climatological and meteorological factors that govern snow and ice mass balance. To accomplish this objective the seasonal mass balance of the Brúarjökull glacier was used as a case study. The relative importance of different meteorological, climatological, and hydrological conditions in determining daily and seasonal mass balance of the glacier were assessed, using both statistical and physical modelling approaches. The findings of the analysis of key drivers of variability in snow and ice are discussed in Section 3.1.

The obtained results of the statistical modelling framework is published as an article with the title *Statistical summer-mass balance forecast model with application to Brúarjökull Glacier, South-East Iceland* in the Journal of Glaciology (Eythorsson et al., 2018), presented herein as Appendix A.

Research objective 2: *Assess and compare historical trends in the snow and climate regimes*

The results from research Objective 1 reveal a correlation between long term climate trends and glacier mass balance. These results are congruent with multiple studies on the climate impact on glacier changes (e.g. Christian et al., 2018; O'Neel et al., 2019; Putnam et al., 2012). Daily snow accumulation and melt behavior is largely dependent on short term local meteorological conditions, thus, short term (1-10 day) snow predictions may be achieved by using meteorological forecasts applied to a snow model. The reliability of short-term meteorological forecasts decreases as lead time increases, however, seasonal mass balance can to some extent be predicted based on climatological conditions. Thus, medium term (2-4 months) mass balance predictions can be accomplished using information on the state of the snow and its surrounding climatology applied to a snow model. To achieve long term (1-100 years) predictions of snow cover, climate forecasts must be used for modelling.

Therefore, analysis and comparison of historical changes in snow cover and climate is the main topic of research Objective 2. Changes in snow cover vary, and have varying significance for water resources management in, depending on the region. Thus, understanding the historical spatio-temporal relationship between the climate and snow conditions on a regional scale is important for successful adaptation of water resources management to climate change.

In this research, recent changes to climate and snow conditions in the Arctic were used as a case study. Changes to snow cover were estimated based on MODIS satellite data while changes to the arctic climate were estimated as changes to Köppen-Geiger (KG) climate classifications calculated from an ensemble of 21 downscaled Global Circulation Models (GCM's). The observed changes were compared in 10 regions of the Arctic over the period of MODIS observations (2001-2016) revealing varying responses of local snow conditions to climate changes in the region. The findings of are discussed in Section 3.2 and 3.4.

The results of the analysis and comparison of historical changes in the snow and climate regimes across the arctic are published as an article with the title *Arctic climate and snow cover trends – Comparing Global Circulations Models with remote sensing observations* in the International Journal of Applied Earth Observation and Geoinformation (Eythorsson et al., 2019) presented herein as Appendix B.

Research objective 3: *Estimate future changes in snow conditions based on predicted climate changes.*

The analysis of climate trends across the Arctic showed that in all but the 3 northernmost regions there had occurred a statistically significant change in one or both most common KG climate classes over the study period. In the 7 regions where, significant changes had occurred to the climate, the largest changes to the Snow Cover Frequency (SCF) had also occurred. The analysis of snow cover trends revealed that at lower latitudes SCF had decreased during the period, while further north by the shores of the Arctic Ocean, SCF had

increased. Averaged across the entire Arctic SCF had decreased by 0.91 days/decade, which is congruent with other recent findings (Hori et al., 2017; Liston & Hiemstra, 2011; Yunlong et al., 2018). The climate trends were forecast until the end of the present century and showed that warmer climate classes will continue to replace the dominant climate classes in the Arctic, tundra, and cold summer climates throughout the present century, even under a scenario where global radiative forcing by greenhouse gas emissions is stabilized by 2100 (RCP4.5). Hence, to understand whether the observed trends in snow cover in the Arctic will continue given the expected climate changes, the snow response to these climate forcing's needs to be modelled.

Thus, the main topic of research Objective 3 is to estimate and analyze future changes to snow conditions based on different climate scenarios. The main source of uncertainty in the future progression of climate change is future anthropogenic greenhouse gas emissions. Understanding how snow conditions respond to an emission reduction scenario as compared to "business-as-usual" emissions is fundamental to adaptation and mitigation policymaking on both a regional and global scale.

Predicted changes to KG climate classifications across the globe have been estimated and published as an article with the title *Arctic climate and snow cover trends – Comparing Global Circulations Models with remote sensing observations* in the International Journal of Applied Earth Observation and Geoinformation (Eythorsson et al., 2019) presented herein as Appendix B. The findings are discussed in Sections 3.3 and 3.4

In this research future snow conditions were modelled and analyzed across the Northern Hemisphere (NH). A snow model (Snow17) was run with climate projections from 21 downscaled GCSs for both an emission stabilization scenario (RCP4.5) and a "business-as-usual" emission scenario (RCP8.5). The findings are discussed in Section 3.5 The results from the simulation of snow resources across the NH have been submitted as an article with the title *Projected Changes to Northern Hemisphere Snow Conditions over the period 1950-2100, given two emission scenarios* to the journal; Remote Sensing Applications: Society and Environment, presented herein as Appendix D. (Eythorsson et al., 2023b).

Furthermore, these results combined with the historical trends in the climate/snow regimes were used to estimate future snow conditions in Iceland. The findings are discussed in Section 3.6 and published as an article with the title *Observed and Predicted Trends in Icelandic Snow Conditions for the period 1930-2100* to the journal; *The Cryosphere*., presented herein as Appendix C, (Eythorsson et al., 2023a).

1.3 Dissertation organization

This dissertation is composed two parts. Part I contains the following four chapters: Introduction, Background, Applications and Results, Conclusion, and future perspectives.

The *Introduction* chapter contains the statement of purpose and outlines the objectives of the doctoral research presented in this dissertation. It summarizes the motivation for the research described herein and describes how these results have been published and disseminated to the research community. The *Background* chapter describes the state of knowledge within the fields that concern this doctoral research. It contains an overview of the state of climate change, both globally and in Iceland, the state of knowledge about past, present and future changes to snow resources, the methods used to observe changes to snow resources and lastly the state of the art in snow modelling. The *Applications and results* chapter describes the results that have been achieved in of this doctoral research with appropriate references to the four academic papers that have been prepared or published because of it. The *Conclusion and future perspectives* chapter summarizes the findings of this doctoral research, how they relate to the present state of knowledge within its field and which future questions they pose.

Part II is presented as an Appendix with the scientific papers which are based on this work. Two ISI papers have been published based on the research presented in the current dissertation. The manuscripts of the third and fourth papers have been submitted and are in the peer review process. The papers are presented in full as appendices. Following is a summary of the outline presented in of each of the papers:

Paper 1: The main goal in this paper is to develop a comprehensive framework for developing a site specific and optimized set of melt models, given a wide range of environmental data, to forecast the seasonal glacial mass balance in a catchment in Eastern Iceland.

Paper 2: The main goal in this paper is to estimate the historical spatio-temporal trends of changes in the climate and snow regimes based on extensive distributed environmental datasets. The observed trends are analyzed and compared across the Arctic.

Paper 3: The main goal in this paper is to simulate future snow conditions under different climate scenarios using spatially distributed environmental data and a conceptual snow model. The simulated spatio-temporal snow characteristics are then analyzed across the Northern Hemisphere and throughout the 21st century.

Paper 4: In this paper the historical trends the climate and snow regimes which were estimated in Paper 2 are compared to the in-situ observed trends in both regimes in Iceland. These are combined with the snow simulations from Paper 3 to derive a plausible forecast for the evolution of the Icelandic climate and snow resources under different global emission scenarios.

2. Background

2.1 Historical and predicted changes in the climate and snow regimes

2.1.1 Global trends in climate and snow conditions

Climate Change

The just published 6th Assessment Report (AR6) by the Intergovernmental Panel on Climate Change (IPCC) states that the scientific evidence for the anthropogenic warming of the atmosphere, ocean and land is unequivocal, that the scale of this change to the climate system is unprecedented and these changes are already affecting every inhabited region across the world. The changes observed to global surface temperatures to date will continue until at least the mid-21st century under all emission scenarios causing many changes in the climate system, including further intensifying the water cycle and its variability. Many of these changes are irreversible on the scale of centuries to millennia (IPCC, 2021).

To derive such predictions the research community employs a range of climate models, which simulate the global climate system based on fundamental physical laws and knowledge of the initial state of the system to explain and predict the movement of air, water, particles, and energy. Due to computational limits the spatio-temporal resolution of these models is restricted, although the model resolution continues to increase with further advances in computational sciences. Climate models which model the circulation of mass and energy over the entire globe are referred to as General Circulation Models (GCM) and are used as basis for predicting future changes to the global climate. The Coupled Model Intercomparison Project (CMIP) is tasked by the World Climate Research Program (WCRP) to assess the performance of competing state of the art GCM and to summarize and disseminate their findings to policy makers, research communities and the general public. The 6th phase of the CMIP project has recently been concluded with 23 CMIP6-endorsed models which were used to lay the scientific basis for the policy recommendations published by IPCC in AR6 (Eyring et al., 2021)

As stated in AR6 the results of CMIP6 show that global climate system has been changing rapidly since the start of the industrial evolution and that these changes will continue at least until the middle of the present century (Lee et al., 2021). The results of CMIP6 have been applied at global and regional scale to investigate different climate change impacts. Among the projected impacts are increased drought risk and severity (Cook et al., 2020; Ukkola et al., 2020; Zhai et al., 2020), increased flood risk (Hirabayashi et al., 2021; Sante et al., 2021), increased monsoon precipitation (Chen et al., 2020; Wang et al., 2020) changes to the intensity, frequency and distribution of tropical cyclones (Emanuel, 2021; Roberts et al., 2020), rising sea levels (Hofer et al., 2020; Jevrejeva et al., 2020; Lyu et al., 2020), decreasing snow cover, especially in the Northern Hemisphere (NH) (Mudryk et al., 2020;

Paik & Min, 2020; Zhu et al., 2021), decreasing concentrations of sea ice in both the Arctic and Antarctic seas (Notz et al., 2020; Notz et al., 2016; Roach et al., 2020; Shu et al., 2020) and increased melt rates of the ice sheets in Greenland and Antarctica (Bracegirdle et al., 2020; Hofer et al., 2020; Nowicki et al., 2016; Payne et al., 2021).

One way to visualize and parameterize climate change is to classify different climate regions based on some abstract categorization of what constitutes a distinctive climate, in terms of climatological parameters such as air temperature and precipitation. Thus, climate regions that are similar in some physical or biological sense can be identified and classified. One of the most common climate classification systems is the Köppen-Geiger system (Köppen, 1884; Köppen & Geiger, 1968), which has been used in a range of studies in various disciplines (e.g. Beck et al., 2018; Kottek et al., 2006; Peel et al., 2007). Using spatio-temporal estimates of climate classifications to visualize and quantify climate variation and change is a valuable method for researching the impacts of climate change (e.g. Chen & Chen, 2013) and to disseminate the work of the scientific community to the general public in way that resounds with their experiential reality (e.g. Jylhä et al., 2010).

Changes to the Earth's energy budget are expected with high confidence to lead to an increase in the global mean precipitation and evaporation, although the predicted rate varies between climate models (Douville et al., 2021). A warmer climate is expected with high confidence to increase moisture transport intensifying heavy precipitation events and season. Warming over land is expected with high confidence to increase potential evaporation and intensify the severity of droughts. There is high confidence that mountain glaciers will diminish globally, and that seasonal snow duration will generally decrease. Furthermore, the variability of the water cycle and its extremes are expected with high confidence to increase faster than the average under all emission scenarios in most regions of the world (Douville et al., 2021).

In the research presented in this dissertation CMIP5 models were used as a representation of future climate conditions as the work was performed prior to the release of the CMIP6 model ensemble.

Changing Seasonal Snow Dynamics

Snow cover represents a major geophysical feature on earth and impacts hydrology, ecology, and geology to a varying extent in many regions of the planet. Fluctuations in the characteristics of snow cover in an area (i.e., depth, extent, timing, duration) represent changes to the local climatology. On a global scale, fluctuations in snow cover impact the planetary energy balance of earth. Snow cover reflects more of the inbound solar radiation than bare ground, leading to further heat adsorption which may in turn reduce snow cover even further in a process named the "ice-albedo-feedback" (e.g. Callaghan et al., 2011). Changes to seasonal snow cover associated with global climate change have and are expected to continue to impact human societies and ecosystems in cold regions.

Connolly et al., (2019), compared observed changes to the snow cover in the Northern Hemisphere (NH) to that predicted by all available CMIP5 models over the period 1967-2018. The results showed a trend of decreasing snow cover across all estimates; however the magnitude of the observed trend was greater than what most of the models had predicted. Mudryk et al., (2020), analyzed historical snow cover trends, as estimated from an ensemble of 6 observation-based products, and projected changes in the CMIP6 multi-model ensemble

over the NH until the end of the 21st century. Their results showed a mass loss trend of approximately -5 Gt/yr for all months from December to May for the period 1981-2018 and that the NH spring snow extent will decrease by approximately 8% per degree of Global Surface Air Temperature (GSAT) increase relative to the 1995-2014 average.

Yunlong et al. (2018) analyzed variations in NH snow cover using snow cover data from MODIS, AMSR-e and the IMS snow cover extent product for the period 2000-2015. Their results showed that the SCD over the NH had decreased by an average of 5.3 days/decade and the seasonal variation in SCA showed a decreasing trend for all seasons but winter. Hori et al. (2017), analyzed snow cover trends in the NH based on a daily SCE product calculated from a combination of MODIS and AVHRR data for the period 1979-2009. Their results showed a that the SCE had decreased by approximately 10 days per decade during the study period and that the SCD in western Eurasia has decreased by up to two months in the past 30 years. Liston & Hiemstra (2011), analyzed pan-Arctic snow trends for the period 1979-2009 for the period by creating a distributed snow dataset based on MERRA reanalysis data. Their results showed a decrease in SCD by 2.5 days per decade averaged across the Arctic. Choi et al. (2010), studied changes to NH snow seasons over the period 1967 to 2008 using weekly snow cover extent data generated mainly from visible satellite imagery by NOAA and National Ice Center meteorologists (Robinson, 1993). Their results showed that NH Full Snow Seasons (FSS) have decreased on average by 5.3 days/decade, these changes were primarily attributed to progressively earlier spring melt.

Malmros et al. (2018), estimated snow cover changes in the Andes based on MODIS observations over the period 2000-2016 and found that the Snow Cover Extent (SCE) and number of Snow-Covered Days (SCD) decreased on average by 13 ± 2% and 43 ± 20 days, respectively. Saavedra et al. (2018), estimated snow cover changes in the Andes based on MODIS observations over the period 2000-2016. Their results showed that large areas showed statistically significant decreasing trends in snow cover, especially on the eastern side of the Andes.

Zhang & Ma (2018), analyzed the variability in the continental Eurasian SCE using the NH EASE-Grid data for the period 1972-2006. Their results showed a significant decrease in the spring and summer SCE and an earlier loss of snow in the spring whereas the onset of snow cover in autumn was not found to have changed significantly during the period. Zhong et al. (2021), studied the spatiotemporal variability of snow cover duration in Eurasia over the period 1966-2012 based on in-situ data from 1103 station with ground-based snow measurements. Their results showed that on average the first day of snow and the last day of snow delayed and advanced by approximately 1 day/decade, respectively and that the ratio of SCD to snow season length increased by about 0.01 per decade. Bach et al. (2018) analyzed in situ observational records of mean and extreme snow depths over Europe based on the European Climate Assessment & Data Set (ECA&D; Klein Tank et al., 2003). Their results showed an average decrease of -12.2% and -11.4%/decade for mean and maximum snow depths, respectively, for the period since 1951.

The published literature, summarized in this section, agrees that on average and across estimates, the extent and duration of global snow cover has been decreasing in recent decades and that this decrease is projected to continue under all emission scenarios. The magnitude of this change, however, varies significantly in space and time as well as across estimates, both for the historical period and future predictions. The 6th AR by the IPCC states that there is very high confidence that the NH spring snow cover has been decreasing since 1978 and

that further decrease of the NH seasonal snow extent is virtually certain under all plausible emission scenarios (Fox-Kemper et al., 2021).

Glaciological trends

Glaciers and ice caps represent most of the freshwater storage on earth. Fluctuations in the extent of a single glacier, (measured i.e., in length, mass, area, or volume) represent changes in the energy balance of that glacier, due to some external changes that affect the transfer of energy to and from the glacier. On a global scale such glacier fluctuations are recognized as high confidence indicators of climate change (Bojinski et al., 2014). Glacier fluctuations associated with climate change have and are expected to continue to impact geophysical features and processes that are of key importance to both human societies and ecosystems in cold regions.

Zemp et al. (2015), used observational datasets from the World Glacier Monitoring Service (WGMS) to estimate glacier fluctuations over the last century. Their results showed that the rates of glacier mass loss in the 21st century are without precedent on a global scale for the period observed and that this loss is likely to continue, even if the present climate remains stable at present day levels. Marzeion et al. (2014), showed that the anthropogenic signal in glacier mass balance observations during the period 1991-2010 is detectable with high confidence, being responsible for 69 ± 24 % of the global glacier mass loss, whereas over the period 1851 – 2100 the anthropogenic signal is weaker, constituting only 25 ± 35 % of the global glacier mass loss Sommer et al. (2020), computed changes in glacier fluctuations in the European Alps between 2000-2014 using optical and radar remote sensing imagery. Their results revealed a rapid glacier retreat across the Alps amounting to an annual loss of 39 km^2 in areal coverage and an average annual mass loss of -1.03 m of water equivalent. Kulkarni & Karyakarte (2014), analyzed observed changes in glacial extent and mass balance in Himalayan Glaciers. Their results showed a decrease in both extent and volume across the Himalaya, with the rate of decrease more than doubling between the time periods 1975-85 and 2000-2100.

Glacier mass loss has and will contribute to sea level rise globally. Marzeion et al. (2012) estimated sea-level changes due to global glacier mass of all individual glaciers of the world (excluding the Greenland Ice Sheet (GIS) and Antarctic Ice Sheet (AIS) and found their mass loss to have contributed 114 ± 5 mm of sea level rise between 1902 and 2009. Gardner et al. (2013), estimated from satellite gravimetry and altimetry and local glaciological records that glaciers were losing mass in all regions of the world, with the largest changes occurring around the Arctic, in the Andes and high-mountain Asia and that over the period 2003-2009 the global glacier mass loss amounted to 259 ± 28 gigatons per year. (Marzeion et al., 2014) projected the expected future mass loss of the earths glaciers under different emission scenarios based on 15 coupled General Circulation Models (GCM) from the CMIP5 ensemble, which suggest a future glacier derived sea level rise ranging from 148 ± 35 mm (RCP26) to 424 ± 46 mm (RCP85). Radić et al. (2013), modelled that volume changes of all glaciers in the world based on 14 GCMs from the CMIP5 project for two emission scenarios (RCP45 and RCP85) and estimated a future glacier derived sea level rise of 155 ± 41 mm (RCP45) and 216 ± 44 mm (RCP85) over the period 2006-2100). Zemp et al. (2019), used an extrapolation of glaciological and geodetic observations to estimate a glacier derived sea level rise of 27 ± 22 mm over the period 1961-2016 which equals the contribution of the GIS and exceeds the loss from the AIS, amounting to a total 25-30% of the observed sea-level rise.

Glacier fluctuations have been shown to impact the regional water cycle in a number of ways. Huss & Hock (2018), estimated global glacier runoff changes for 56 large scale glacierized basins over the 21st century. Their results showed a significant interbasin variability, however, a general pattern of increasing annual glacier runoff until a maximum is reached, after which runoff will be in steady decline. Bliss et al. (2014), projected monthly runoff for all glaciers and icecaps outside Antarctica based on 14 global climate models for the period 2006-2100. Their results showed continuous glacier mass loss in all regions, however, the hydrological response varied significantly between region which depends on the balance between higher melt rates and decreased storage as glaciers retreat. Kaser et al. (2010), estimated the contribution of changes to water availability in large rivers systems due to a projected delay in seasonal glacier melt. Their results showed that the seasonal delay contribution was greatest in seasonally arid basins and negligible in monsoon regions. Huss (2011) estimated the glacial runoff contribution to large scale drainage basins in Europe based on monthly mass balance data for the period 1908-2008. The results showed that glacial meltwaters are relevant to the hydrology of macroscale watersheds and water shortages will intensify as summer glacial runoff contribution decreases water shortages. Cauvy-Fraunié & Dangles (2019), conducted a global meta-analysis of published bio-diversity studies and found that biodiversity in general increases as glaciers recede, however, the species that are removed are generally highly specialized.

Glacier fluctuations are expected to impact local hazard situations as the dynamics glacierized areas changes. Bajracharya & Mool, (2009), analyzed changes to glaciers, glacial lakes, and glacial outburst floods in Nepal over the period 1976-2000. Their results showed a total decrease in glacial lakes in the region, however they also recorded an increase in the moraine-dammed lakes which is associated with an increased risk of glacial outburst flooding. Kääb et al. (2003), used satellite imagery from the ASTER instrument on the NASA TERRA satellite to assess the conditions of a rock/ice avalanche in Russia and a glacial lake in the Alps in 2002. The results showed that the ASTER imagery is a valuable source of estimating and quantifying glacier fluctuations and for the timely identification of glacier hazards.

2.1.2 Changes in the Icelandic climate and snow

Climate

The Icelandic climate is characterized by its maritime nature causing mild winters and cold summers, with frequent precipitation and heavy winds. The location and mountainous topology of Iceland creates large spatio-temporal variations in both weather and climate (e.g. Bjornsson et al., 2007; Ólafsson et al., 2007). Studies show that since the last glacial maximum the temperature fluctuations in Iceland have been about 4°C, which is significantly higher than the global average (Geirsdóttir et al., 2013; Knudsen et al., 2008; Langdon et al., 2011; Larsen et al., 2011; Sicre et al., 2011). This large variability in temperature is caused by spatio-temporal changes in the location of warm and cold ocean currents around the island (Cabedo-Sanz et al., 2016).

Continuous meteorological records exist in Iceland since the middle of the 19th century. Since records began the average temperature in Iceland has risen by about 0.8°C per century, like the global average warming over the same period. Over the period 1980-2015 the average annual precipitation has increased by 7-13 % while the average temperature has increased by 0.5 °C per decade (Björnsson et al., 2018).

The average temperature in Iceland is expected to increase by 1.3-2.3°C by the middle of the 21st century compared to the average of the period 1986-2005 and if global emissions are not significantly reduced, the warming could exceed 4 °C by the end of the 21st century. The uncertainty in projected changes in precipitation are greater than for temperature changes but estimates predict a 1.5 – 4.5% increase in average precipitation volume per degree of warming (Dee et al., 2011; Nawri et al., 2017; Poli et al., 2016).

The projected climate changes in Iceland are expected to impact the local hydrological cycle, as winters become milder and less water is stored as snow, causing streamflow to increase in winter and decreasing peak flow during spring melt. Runoff from glaciers is expected to increase, especially in summer, until at least the middle of the 21st century (Blöschl et al., 2017; Jónsdóttir et al., 2008; Ministerrådet, 2012)

Snow

Snow is a key feature of the hydro-climatological cycle in Iceland, storing precipitation in winter and releasing melt runoff in spring. Icelandic snow cover has been categorized as a mixture of tundra, taiga and maritime snow types with shallow snow depth on average, high density, frequent melt cycles and high wind stress (Sigurðsson & Jóhannesson, 2014). Understanding changes to key snow parameters such as the amount, spatio-temporal distribution and physical characteristics are important for managing the water resources in Iceland. Analysis of trends in discharge, precipitation and temperature time series has revealed that spring snowmelt occurs earlier in the year and that spring peak flows have decreased between the periods 1996-2007 and 1963-1995 (Jónsdóttir et al., 2008).

Long term trends in snow cover have been studied by Jónsson (2001), which analyzed manual snow cover observations around the country over the duration of continuous measurements (~1930 – 2000). The results showed no clear trends over the entire study period, although the average snow cover had decreased towards the end of the period. An analysis of the relationship between snow cover and ambient air temperatures revealed an estimated 10% loss of snow cover in each winter month, per 1°C of warming.

Gunnarsson et al., (2019) analyzed Icelandic snow cover characteristics based on a gap-filled MODIS snow cover product for the period 2000-2018. They compared MODIS snow cover data to in situ data from the Icelandic Meteorological Office (IMO) and remotely sensed data from Landsat and Sentinel with good agreement. Their results showed a trend of increasing snow cover duration for all months except October and November. The trendline for June was significant at a the $\alpha = 0.05$ level and the trendlines in May and June were significant at the $\alpha = 0.1$ level. The results of Gunnarsson et al., (2019) shows a significant decreasing trend of average snow cover in spring/summer. These results are of particular importance as they illustrate a significant decrease in snow cover during the season of minimum snow cover.

The snow cover trends studied by Jónsson (2001), were based on manual observations from manned observation stations, mostly located in lowland areas close to urban areas. Sigurðsson & Jóhannsson, (2014), analyzed snow depth records from 4 observation sites in the central highlands over the period 1975-2014 which revealed a slightly decreasing, albeit not statistically significant, trend in snow depth over the period although the measurement locations are too few to draw any conclusions for the extensive highland region. The trend of increasing snow cover duration observed in Gunnarsson et al. (2019) over the period

2000-2017 is in the opposite direction to long term projections which predict snow cover to decrease across the country over the 21st century (Johannesson et al., 2007).

Glaciers

Changes to Icelandic glaciers have been studied based on a range of sources including in situ mass balance measurements, reconstructed surface maps, published maps, aerial photographs, satellite stereo imagery and airborne lidar (e.g. Belart et al., 2020). The results show that Icelandic glaciers reached their maximum extent since the settlement of Iceland at the end of the 19th century. Over the period 1890-2019 the mass loss of Icelandic glaciers has been estimated as 16 ± 4%, which corresponds to 1.50 ± 0.36 mm of sea level equivalent. This glacier recession was mostly confined to two periods 1920-1940 and the period since 1995 whereas during the three decades between 1960-1990 most Icelandic glaciers remained stable or even advanced (Aðalgeirsdóttir et al., 2020). While the surface mass balance is the main source of mass flux in Icelandic glaciers, internal and basal melt contribute a non-negligible portion of the overall mass balance, especially in geothermal and volcanic zones (Jóhannesson et al., 2020).

The retreat of the large and outlet glaciers in Iceland is well documented both through remote sensing and in situ observations. (Brynjólfsson et al., 2014; Hannesdóttir et al., 2015; Hannesdóttir et al., 2016; Pálsson et al., 2012). The mass loss of the three largest ice caps in Iceland (Vatnajökull, Hofsjökull and Langjökull) since 1890 has been well documented (e.g. Bjornsson et al., 2013). The surface of the Icelandic glaciers was lidar mapped in high resolution during the period 2007-2013 increasing the accuracy of ice volume estimates (Jóhannesson et al., 2013). The observed recession and increased volume of melt water from the Icelandic glaciers has resulted in changes to river channels to glacial rivers (Magnússon et al., 2009) and to the extent and placement of subglacial and moraine lakes (Björnsson et al., 2001; Jóhannesson et al., 2013). A key factor in the mass balance of Icelandic glaciers is the ice surface albedo, which is influenced by a number of environmental variables, such as snow metamorphism, dust loading and tephra depositions from nearby volcanoes, there is a large spatio-temporal variability in the albedo of Icelandic glaciers and the country's largest glacier, Vatnajökull has experienced a positive albedo trend over the period 2000-2019 (Gunnarsson et al., 2021).

Modelling of the future evolution of the Icelandic glaciers has shown that they will almost disappear completely over the next two centuries given projected changes to the global climate (Adalgeirsdottir et al., 2011; Guðmundsson et al., 2009; Hannesdóttir et al., 2015). This projected retreat will significantly impact runoff from glaciated areas, with significant challenges and opportunities to water resource managers and renewable energy producers in the country (Johannesson et al., 2007; Thorsteinsson & Björnsson, 2013). The increased rate of melt water is projected to continue to affect river channels in glacial rivers (Pálsson et al., 2016) as well as the extent and character of ice-marginal lakes (Magnússon et al., 2013; Schomacker, 2010) .

2.2 Snow Observations

Monitoring of snow resources, both on a local and global scale, is important for water resources management, hazard assessments and improved geophysical understanding of the earth's hydro-climatological system. Many snow datasets have been recorded and presented in the literature, based on a range of measurement technologies and covering many snow parameters (e.g. Dong, 2018). Snow observations of all kinds can be assimilated in land surface models to derive best estimates of spatio-temporally distributed snow parameters (e.g. Clark et al., 2006; Slater & Clark, 2006).

2.2.1 In situ observations

The traditional method of measuring snow is the observation of snow properties on the ground, most often concomitantly with observations of other meteorological parameters. Measurements of snow depth (SD) and new snowfall amounts have been recorded in Europe and North America for centuries. However, the methods and means of snow monitoring varied significantly between locations, limiting the utility of such observations for global snow research. The Solid Precipitation Measurement Intercomparison Project (SPMIP) showed up to 700% variability in the proportional amount of solid precipitation recorded at in national precipitation gauges (with wind shields) at 6 m/s wind speed (Goodison et al., 1998).

Several international projects have been undertaken to improve the comparability of snow measurements across the globe, with observation stations located world-wide. These projects include the Global Cryosphere Watch – CryoNet (WMO, 2014), The Global Historical Climatology Network (Menne et al., 2012), The WCRP – Climate and Cryosphere (CliC) Project (Barry, 2003), The CMC – Daily Snow Depth Analysis Data (Brown & Brasnett, 2010), The Historical Soviet Daily Snow Depth (HSDSD) (Armstrong, 2001), The Historical Climatology Network (HCN) (Easterling, 2002), The European Climate Assessment & Dataset (Tank et al., 2002) and the Solid Precipitation Measurement Intercomparison Project (SPMIP) (Goodison et al., 1998).

At manned meteorological stations manual snow observations of a range of snow parameters are made at the frequency requested by the procurer of the data. Snow Depth (SD) is one of the most frequently collected snow parameters due to the relative ease of measurement. In recent decades the use of automated sensors for recording snow parameters such as SD and Snow Water Equivalent (SWE). SWE can be measured using weighing systems often referred to as snow pillows (Engeset et al., 2017) and snow height above ground can be monitored using e.g. ultrasonic sensors (Ryan et al., 2008) and time lapse photography of snow stakes (Parajka et al., 2012). The use of automatic snow monitoring has improved both the spatial and temporal resolution of snow measurements, as the limits to measurement frequency and data storage are continually being pushed and the operational cost of automatic stations is a fraction of that of manned stations.

Where the density of in situ snow observations is sufficient the spatial distribution of snow parameters can be estimated using different statistical interpolation methods (e.g. Carrera-Hernández & Gaskin, 2007; Foppa et al., 2007; Jarvis & Stuart, 2001; Molotch et al., 2005). Achieving the required density of point observations for adequate estimation of the spatial distribution of snow parameters is especially challenging in regions with complex

topography as it affects both the distribution of snow and the logistics of snow monitoring. Studies have shown that there are significant discrepancies between point-measurements and regional estimates of snow parameters, even in relatively well documented regions (López-Moreno & Nogués-Bravo, 2006; Meromy et al., 2013). As a result of the sparse distribution of point-based snow monitoring stations globally global scale monitoring of changes to snow resources are not feasible based only on in-situ observations (Dong, 2018).

2.2.2 Remote sensing of snow

Snow resources are inherently most abundant in cold regions with high precipitation. Incidentally these are also the regions least favored by humans for habitation and leisure. As a result, in situ observations of snow are logistically challenging, and therefore sparse, in many areas where significant quantities of the resource are located. Monitoring the snow resources by means of remote sensing, either by airborne vehicles or satellites has therefore been an important research topic since the dawn of the satellite era in the 1960's when the TIROS-1 satellite became the first satellite to allow monitoring of snow cover from space (Lucas & Harrison, 1990). Since the start of satellite monitoring, snow covered areas have been observed to decrease on average across the globe (R. D. Brown, 2000; Lemke et al., 2007). Although increases in snow cover have been observed in some regions such a China (e.g. Che et al., 2008; Xuejin et al., 2019)

Snow can be detected from remotely sensed data by observations of its physical and spectral properties, these however can vary based on many different factors, such as Snow Depth (SD), liquid water content, impurities, snow temperature, ice content, grain size and shape etc. (J. Foster et al., 1996; Kelly, 2009; Painter et al., 2009; Sturm, Holmgren, & Liston, 1995; Tait, 1998). The influence of these factors on the estimation of snow conditions varies depending on sensor technology and resolution. Many different sensor technologies have been developed and are in use for measuring land surface properties like snow. However they can be broadly divided in two categories, optical sensors that record reflective data in the visible and infrared wavelengths and microwave sensor that record either microwave radiation emitted from the land surface that can be measured with passive microwave sensors or radiation backscattered by active microwave sensors (Dietz et al., 2012).

In the visible (VIS) wavelengths snow reflects up to 80-90% of the solar radiation depending on grain size, age and purity (König et al., 2001; Winther et al., 1999) whereas at longer wavelengths, in the infrared (IR) spectrum the reflectivity of snow drops to near zero (Pepe et al., 2005; Wang et al., 2005). A key issue in snow monitoring is discerning between clouds and snow, which have similar reflective properties in the VIS and IR spectra (Hall et al., 2010; Hyvärinen et al., 2009; Miller et al., 2005) rendering satellite scenes exceeding a threshold cloud cover useless for snow monitoring (Rodell & Houser, 2004)

The land surface emits microwave radiation which can be observed by Passive Microwave (PM) sensors (König et al., 2001). PM data which has been applied to snow mapping has been collected by the Advanced Microwave Scanning Radiometer-EOS (AMSR-E), the Scanning Multichannel Microwave Radiometer (SMMR), the Special Sensor Microwave Imager (SSM/I) Microwave emissions from the underlying ground are weakened under snow cover at wavelengths similar in size to the snow grains and thus, the weaker the microwave signal recorded by the sensor, the more snow covers the ground (Chang et al., 1987). The microwave signal recorded by the sensor is determined by several factors including liquid

water content, grain size, grain shape and the dielectric discontinuities of snow and air (Amlien, 2008; Clifford, 2010; Foster et al., 1999). Several factors influence the accuracy of PM derived snow parameters. Vegetation absorbs microwaves in similar wavelengths as snow (Derksen, 2008) and thus snow cover is hard to detect in forested areas (Foster et al., 1999; Hall et al., 1982). Liquid water magnifies the microwave absorption of the snow causing underestimates of snow depth (Amlien, 2008). The crystal properties of the snow, especially the crystal size can have impact the estimation of SWE (Foster et al., 1999)

Snow cover characteristics can also be estimated based on Active Microwave (AM) data, where the microwave sensor measures the backscatter of a signal emitted by the instrument. However, because the penetration depth of microwaves into the snow depends heavily on its liquid water content only wet snow can be detected reliably using active microwave data (Wang et al., 2008), since the underlying ground is the main source of the back scattering signal under dry snow (König et al., 2001). The research interest remains high as AM sensors can provide higher spatial resolution monitoring than PM sensors (Foster et al., 2011) and AM data from the Sentinel-1 mission has shown promising results in mapping snow depth (e.g. Lievens et al., 2019).

Many algorithms have been developed to identify snow parameters based either on spectral data from optical sensors such as the Advanced Very High-Resolution Radiometer (AVHRR), the Moderate Resolution Imaging Spectrometer (MODIS), Landsat and Sentinel which collect the appropriate spectral data to both detect snow and discern between snow and clouds or from Microwave sensors. These snow mapping algorithms can be broadly categorized into algorithms that estimate: binary snow cover classifications from optical sensors (Fernandes & Zhao, 2008; Hall et al., 1995; Rosenthal & Dozier, 1996), fractional snow cover algorithms (Metsämäki et al., 2005; Painter et al., 2009; Salomonson & Appel, 2006; Solberg et al., 2010), algorithms that estimate snow cover beneath clouds from reflective data (Gafurov & Bárdossy, 2009; Parajka et al., 2010; Wang & Xie, 2009), algorithms that detect both snow cover and SWE with data from PM sensors (Chang & Rango, 2000; Derksen et al., 2003; Kelly, 2009; Pulliainen & Hallikainen, 2001; Pulliainen et al., 1999) and methods that utilize both PM and reflective data to estimate snow parameters (Foster et al., 2011; Gao et al., 2010; Liang et al., 2008; Romanov et al., 2000).

A promising remote sensing technology for high resolution snow monitoring is the use of airborne laser altimetry (lidar) which can detect vertical elevation with decimeter scale precision and meter scale horizontal resolution also complex terrain such as forests (Kraus & Pfeifer, 1998; Reutebuch et al., 2003). Snow depth can be estimated based on the difference between two lidar derived Digital Elevation Models (DEMs), one with snow free conditions and the other with snow covered ground (Deems et al., 2006; Hopkinson & Demuth, 2006; Miller et al., 2003). The technology of lidar offers a method for high resolution and accuracy mapping of snow depth (Deems et al., 2013). However, a key limitation is that remotely sensed lidar data is only acquirable from airborne vehicles and not from satellites in orbit. This causes logistical constraints for lidar monitoring at spatial scales larger than individual watersheds. Thus, lidar monitoring is currently restricted to high value snow resources in areas that are important for local water resources management.

Other promising methods for monitoring snow resources remotely include the use of Interferometric Synthetic Aperture Radar (InSAR) and Polarimetric Synthetic Aperature Radar (PolSAR) (e.g. Tsai et al., 2019) and snow depth mapping based on satellite stereo imagery (e.g. Deschamps-Berger et al., 2020; Marti et al., 2016).

2.3 Snow modelling

To understand and predict future behavior of the snow models are used to represent the physical processes that occur within the snow cover (state variables) as well as the interactions between the snow and its surroundings (energy and mass fluxes). Over the past several decades a wide range of snow models have been developed, see e.g. Magnusson et al., 2015 and Krinner et al., 2018 for a detailed description and comparison of some of the more common snow models. Snow models are generally grouped two categories: physical models that attempt to simulate all the physical processes occurring in the snow and empirical models, that rely on statistical relationships between the snow and its surroundings (e.g. Debele et al., 2010). In between these approaches are attempts to combine the advantages of each class of models, by using empirical relationships to derive a full physical representation of the snow (e.g. Schaefli et al., 2010). Many different models have been developed within each model class. Each of which are associated with their own advantages and disadvantages, that must be understood when selecting a model for a specific purpose.

2.3.1 Physical representation of snow

When temperatures are below the freezing point of water, precipitation falls as snow. If temperatures remain below freezing the snow will accumulate on the ground between precipitation events forming snowpack. In perpetually cold environments snow continuously accumulates, turning to ice under the pressure from its own weight and forms glaciers and ice sheets that can store frozen water for centuries to millennia. In warmer regions, where temperatures rise above freezing for some part of the year, the accumulated winter snowpack melts in spring to early summer. As temperatures rise ice crystals that absorb enough energy melt and percolate down the snowpack where it refreezes until the entire snowpack is isothermal at the melting point. When the whole snowpack has reached the melting point melt water begins to form runoff which then takes part in the surface hydrological cycle.

A snowpack is in constant thermodynamic flux with its environment. The energy budget of a snowpack can be described as the sum of all heat transfer components that transport heat between the snowpack and its surroundings, as shown in Equation 2.1 (e.g. U.S. Army Corps of Engineers, 1998),

$$Q_m = Q_{sn} + Q_{ln} + Q_h + Q_e + Q_g + Q_p - \Delta Q_i, \qquad (2.1)$$

where Q_{sn} symbolises net short-wave radiation flux from solar radiation, Q_{ln} represents the long-wave radiation flux from the environment, Q_h and Q_e represent the turbulent fluxes of thermal convection from the atmosphere (sensible energy) and latent energy due to phase changes, respectively. Q_g represents heat conducted from the underlying ground and Q_p represents the energy advected with precipitation. ΔQ_i represents the internal energy that is stored within the snowpack. The total energy available for snowmelt then becomes the sum of the individual energy fluxes or Q_m.

In winter, or in periods of freezing temperatures, precipitation will accumulate in the snowpack forming layers of snow with varying physical characteristics, e.g. density, crystal structure, hardness etc. (e.g. Fierz et al., 2009). In the spring, or when the energy flux into the snowpack increases, Q_m in Equation 2.1 becomes positive, and some ice crystals will begin to melt. The melt water percolates into the porous matrix of the snowpack where it

either refreezes or is stored as liquid water between the snow grains, increasing the density and water content of the snowpack. In this initial stage of snowmelt thermal energy is transferred from the surface boundary into the body of the snowpack, until it has reached an isothermal state where the temperature of the entire snowpack is at the melting point. When the snowpack that has reached the isotherm and when the interstices between snow grains are fully saturated with liquid water it is referred to as "ripe", as any additional energy it absorbs will result in surface runoff.

When the snowpack has become isothermal and is fully saturated with water, melt water begins to form and flow from the snowpack. The amount of melt water, M, produced is governed by the amount of thermal energy, Q_m, absorbed by the snowpack and can be described by Equation 2.2. (e.g. U.S. Army Corps of Engineers, 1998),

$$M = \frac{Q_m}{L_f \rho_w B}\,, \tag{2.2}$$

Where L_f represents the latent heat of fusion of the ice-crystals, ρ_w represents the density of liquid water and B represents the thermal quality of the snowpack, defined as the ratio of its water content that is in the solid phase. The accuracy with which the snow melt rate can be calculated based on Equation 2.2. depends on the accuracy that the individual heat transfer components in Equation 2.1. can be measured or estimated.

Short wave radiation, Q_s

The main source of thermal energy across the surface of the Earth comes from solar radiation. The amount of solar energy absorbed by a snowpack varies significantly depending on latitude, time of day, time of year, aspect, slope, cloud cover and the reflectivity of the snow surface. Cloud cover is the greatest source of uncertainty regarding the amount of solar radiation that reaches the surface of the snowpack, whereas the reflectivity of the snowpack surface determines the amount of inbound solar radiation that is absorbed by the snow. The albedo of the snowpack surface, α, is defined as the defined as the ratio of reflected solar radiation. The amount of solar radiation absorbed by the snowpack, Q_{sn}, can be described by Equation 2.3,

$$Q_{sn} = (1 - \alpha) I_i\,, \tag{2.3}$$

Where, I_i is the incident solar radiation.

Solar short wave radiation can be measured using different instruments and techniques (e.g. Paulescu et al., 2013) or modelled, using a range of models (e.g. Zhang et al., 2017). The snow and Ice albedo can be estimated using remote sensing imagery at different wavelengths (Corripio, 2004), numerical parameterization methods (Gardner & Sharp, 2010) or by assimilation of numerical modelling and observation (Kumar et al., 2020)

Long wave radiation, Q_{ln}

A snowpack also exchanges radiative energy with its surroundings at longer wavelengths than radiation from the sun (6.8-100 µm). A portion of the energy contained in the snowpack is lost to the surrounding atmosphere as blackbody radiation and in turn the snowpack absorbs from back reflection of the atmosphere and the surrounding terrain.

The long wave radiation emitted by the snowpack can be approximated by the Stefan-Boltzmann law, presented in Equation 2.4.

$$Q_{lnup} = \varepsilon * \sigma * T_s^4, \quad (2.4)$$

Where Q_{lnup} is the radiation of a blackbody, ε = 0.99 for clean snow, σ is the Stefan-Boltzmann constant and T_s is the temperature of the blackbody, in this case the surface temperature of the snow. Contrary to solar radiation in the visible spectrum, long-wave radiation is almost completely absorbed by snow, which can thus be modelled as a near perfect black body (Warren, 2019).

The long wave radiation absorbed by a snowpack Q_{lndown} can be estimated using a range of parameterization techniques based on temperature, vapor pressure and cloud factor for different regions (Formetta et al., 2016; Juszak & Pellicciotti, 2013; Kok et al., 2020; Marthews et al., 2012) it can be measured in situ or by remote sensing (e.g. Ellingson, 1995) and several distributed large scale observational datasets of surface long wave radiation have been developed for the research community, including FLUXNET (Baldocchi et al., 2001) and SURFRAD (Augustine et al., 2000). An analysis of the key global long wave radiation datasets has shown an increasing trend (1.8 Wm^{-2} per decade) over the period 2003-2018 (Feng et al., 2021).

The net long wave radiation budget of the snowpack Q_{ln} equals the radiation absorbed subtracted Q_{lndown} by the energy emitted by the snowpack Q_{lnup}, as presented in Equation 2.5.

$$Q_{ln} = Q_{lndown} - Q_{lnup} \quad (2.5)$$

Turbulent heat fluxes, Q_h and Q_e

The turbulent motion of the air at the snow-atmosphere boundary is responsible for heat transfer between the snowpack and the atmosphere, both due to thermal convection (sensible heat transfer) and phase changes of the snow (latent heat transfer). The vertical eddy fluxes of heat and water vapor transfer energy to and from the snowpack surface. The turbulent heat transfer components Q_h and Q_e that occur due to these vertical eddy fluxes can be estimated based on measurements of the factors that govern the intensity of these fluxes, including temperature and vapor gradients between the snow surface and the open atmosphere, surface roughness, atmospheric stratification, horizontal wind movement, air density and atmospheric pressure.

There have been developed several ways to parameterize the turbulent heat fluxes Q_h and Q_e including Obukhov length parameterization (Zeng et al., 1998), Richardsson number parameterization (Louis, 1979) and constant exchange coefficient parameterization (Martin & Lejeune, 1998).

Heat Conduction at the soil/snow boundary, Q_g

Thermal energy is not only transferred at the snow surface boundary, but also through thermal conduction at the snow bottom boundary if there is a temperature gradient between the bottom of the snow and the underlying ground. The energy flux at the snow-ground boundary can be described by Equation 2.6,

$$Q_g = k * \frac{\Delta T_s}{\Delta z}, \quad (2.6)$$

where, k is the thermal conductivity of the soil and $\Delta T_s/\Delta z$ is the temperature gradient between the ice and soil.

Heat convection by precipitation, Q_p

In events when liquid precipitation falls on a snowpack the thermal energy contained in the precipitation is absorbed by the snow. The heat transfer from such rain-on-snow events can be described by Equation 2.7. (e.g. U.S. Army Corps of Engineers, 1998),

$$Q_p = C_p \rho_w P_r (T_r - T_s)/1000, \quad (2.7)$$

where, C_p is the specific heat of rainwater, ρ_w is the density of rainwater, P_r is the volume of rainwater, T_r is the temperature of the rain and T_s is the snow temperature. If liquid precipitation freezes it will release the latent heat of fusion of water in the snowpack.

Internal energy of the snowpack, ΔQ_i

As the snowpack exchanges energy with its environment the internal energy of the snowpack is in constant flux. During cold periods the snowpack loses thermal energy to its surroundings and its internal heat deficit (defined as the amount of heat required to reach an isothermal state at the melting point temperature) increases. As a melt event approaches, the snowpack absorbs energy from its surroundings, decreasing the internal heat deficit until the pack reaches the isothermal state and surface runoff begins. The internal energy of the snowpack can be described by Equation 2.8. (e.g., Gray and Prowse, 1992),

$$\Delta Q_i = d_s(\rho_i C_{pi} + \rho_l C_{pl}) T_m, \quad (2.8)$$

where, d_s, is the depth of the snowpack, ρ_i is the snow density and ρ_l is the density of liquid water, C_{pi} is the specific heat of ice, C_{pl} is the specific heat of liquid water and T_m is the mean snow temperature. If the temperature of the snowpack is below the freezing point of water the internal energy of the pack, then, by definition, ΔQ_i, is positive.

2.3.2 Physical models

Physical snow models attempt to estimate the complete mass and energy balance between the snow and its surroundings to simulate the internal conditions of the snow at specified time intervals. Snow accumulation is calculated by addition of the precipitation that falls while temperature are below freezing while the rate of snow melt is estimated based on the energy that is available to heat and melt the snow (e.g. Hock, 2005). The net energy exchange between the snow cover and its surroundings can be quantified as the product to the net short wave (solar) radiation, net long wave (thermal) radiation, sensible and latent convection heat fluxes, heat advection from rain and conduction from the underlying soil (e.g. Anderson, 2006), as described in section 2.3.1. The advantages of energy balance models lie in their ability to represent the actual physical processes occurring in the snow. This ability allows for a detailed analysis of the snowpack and how it is affected by each component of the energy balance and therefore, how it is likely to respond to different meteorological forcing's (e.g. Marks et al., 1998).

Over the course of the last century many physical snow models have been developed, with varying degrees of complexity and for different applications. Selecting any "best" model or a set of optimal models is highly application and location dependent. At least five large model intercomparison projects have been undertaken to compare the performance of different snow models: PILPS2d (A. G. Slater et al., 2002), PILPS2e (Nijssen et al., 2003), Rhone-AGG (Boone et al., 2004), SnowMIP (Etchevers et al., 2004) and SnowMIP2 (Essery et al., 2009). None of these projects resulted in the identification of an overall "best" snow model. Most of the snow models surveyed in these projects use similar parameterizations for the key processes that occur in a snowpack. A study by Essery et al., 2013 used all possible combinations of the parameterizations commonly used in physically based snow models to develop an ensemble of 1701 snow models which were compared to observations from an alpine site. The results showed that there did exist a group of models that consistently provided good results, however, the optimal models are still likely to be location dependent.

The disadvantages of energy balance models are associated with their high data requirements, their complexity, and the uncertainty of the data. For an accurate representation of the energy balance, accurate data on solar radiation, thermal radiation, temperature, wind speed, humidity, precipitation and soil conditions are required, preferably in a dense grid across the entire catchment that is being modelled (Gabbi et al., 2014). Acquiring these data in enough quality to simulate snow melt accurately is a challenging and costly effort in real time and to forecast these parameters is associated with a high degree of uncertainty. As many catchments in the world are relatively poorly documented, energy balance models may be unsuitable for hydrological modelling of them (Sivapalan, 2003).

2.3.3 Empirical models

Empirical snow models rely on the statistical relationship between snowmelt and any of the variables affecting the surface energy balance. Most empirical models use air temperature as a predictor variable and are thus often referred to as temperature index models. These were the first melt models to be developed and the first application of temperature index snow model was in 1887 on an Alpine glacier, Der Suldenferner, (Finsterwalder & Schunk, 1887). Temperature index models have been widely applied and have shown good performance despite their computational simplicity (Hock, 2003). The simplest case of the temperature index models is the degree day model is presented in Equation 2.9:

$$M = DDF \sum_{i=1}^{n} T^{+} \Delta t, \tag{2.9}$$

Where T+ is the sum of positive air temperature over a time interval Δt, M is snowmelt and DDF is the degree day factor which must be calibrated for each area. Many extensions to this simple degree day model have been developed, e.g. by adding other components of the energy balance, each with their own calibration factor (e.g. Kustas et al., 1994; Zuzel & Cox, 1975)

The main advantage of empirical snow models is their low data requirements. Temperature is among the simplest meteorological parameters to measure, and temperature data is widely available in many areas. Net radiation is on average the main source of energy flux between a snowpack and its surroundings, as discussed in section 2.1.1. However, air temperature usually has a high correlation to snowmelt, since many of the components affecting the energy balance, such as the net solar radiation, are also highly correlated to air temperature

(e.g. Lang & Braun, 1990; Ohmura, 2002). Temperature index models provide good estimates of snowmelt and have been shown to outperform energy balance models in certain catchments (Gabbi et al., 2014).

In recent years efforts have been made to use machine learning and artificial intelligence methods for many hydrological modelling applications (e.g. Mosavi et al., 2018). These models are based on empirical relationships between snowmelt and the selected input data but limit the requirements for human data analytics to determine that relationship. These models are attractive due to their performance and operation simplicity and have shown good performance in stream flow predictions in snow impacted catchments (Kalra et al., 2013; Molotch et al., 2005)

The disadvantage of the empirical modelling approach is mainly the lack of analytical capacity of the models. An empirical model may provide good or even better results than a physically based model but may not provide the necessary information required to develop further scientific insight into the physical processes occurring in the snowpack. The empirical calibration factors that need to be determined from historical data are also subject to significant uncertainty, they have been shown to range significantly depending on catchments (Hock, 2003; Singh et al., 2000), location within catchments (Braithwaite, Konzelmann, Marty, & Ulesen, 1998), time of day (Sing & Kumar, 1996) and time of year (Kuusisto, 1980). All empirical models require some amount of calibration of model parameters. If these parameters are contingent upon prevailing climate conditions the use of the models for long term climate change scenarios may be problematic, as the underlying climate is changing while the model predicts future snow conditions. Studies on temperature index models have for example shown that models calibrated with historic data will overestimate snow melt rates when applied in a warmer climate (Raleigh & Clark, 2014).

2.3.4 Conceptual models

Conceptual models attempt to take advantage of the key benefits of both the empirical and physical models by retaining the low data requirements of the former while gaining the analytical capabilities of the latter. Conceptual models try to explicitly include most of the important physical processes that occur within the snow cover but do so only in a simplified way (e.g. Anderson, 2006). Thus, many of the energy balance components of the snow surface are indexed to simpler parameters like temperature allowing for the analysis of the sensitivity of a snowpack to individual heat flux components.

Among the disadvantages of conceptual models is that while they retain the low data requirements of empirical models, they can be relatively computationally complex. The internal relations and indexing between parameters may not be straightforward or universally applicable and these models are as reliant upon calibration as their empirical counterparts (Kavetski et al., 2006). Thus, while conceptual models may provide improved analytical capabilities their accuracy is contingent on accurate calibration and the more calibration parameters, they contain the more susceptible they are to the problem of equifinality, that is they provide good simulations but for the wrong reasons. This may lead to models that perform well on calibration data, but provide poor results when applied to data outside of the calibration set (Beven & Freer, 2001).

2.3.5 Calibration and Validation

Snow models use environmental information to simulate the physical state of a snowpack. Most snow models need to be calibrated to each specific application by inferring their parameters from observed data (Beven & Binley, 1992). For a model to be considered reliable, the calibrated model must be validated by comparison with independent data that was not used in calibration. Many methods have been developed for both calibration and validation although none has yet been widely recognized as superior (Beven et al., 2003).

Several variables can be used for calibration and validation of a snow model, they can broadly be broken into two categories: data on the state of the snowpack (e.g., depth, extent, Snow Water Equivalent (SWE), temperature, density) and data that describes the progression of snow melt (e.g., river discharge, reservoir inflow, mass balance) over some spatio-temporal scale. These data may be obtained from in situ measurements or through remote sensing (Corbari et al., 2009). Calibration and validation can be performed using any single type of observation or a combination of observations (Seibert, 2010).

Snow models can be applied either at a single point or in a distributed grid across a larger area. Point models are often used to simulate a snowpack at a measurement site and are then generally calibrated and validated based on the snowpack observations from that station, such models are most often calibrated and validated using snow depth or SWE (e.g., Franz et al., 2008). Snow models can be calibrated and validated based on different types of observations and at varying scales, e.g., a model can be calibrated based on meteorological point observations from single measurement station and then applied at basin scale and validated by discharge or mass balance data (e.g., Engelhardt et al., 2014).

Distributed snow models are applied using distributed meteorological forcing data but can be calibrated and validated by using data at varying scales. Either by using point observations that are representative of the area being modelled (e.g., discharge data) or by distributed observations (e.g., satellite measurements of Snow-Covered Area (SCA)). Studies have shown that calibrations using both satellite derived Snow-Covered Area (SCA) and discharge measurements provide quality simulations (Franz & Karsten, 2013). While discharge and snow depth data have historically been favored metrics for calibration, the inclusion of satellite derived SCA data in recent years has generally been shown to improve the validation and calibration of hydrological models (e.g., Konz et al., 2010; Parajka & Blöschl, 2008).

The purpose of calibrating and validating snow melt models is to reconcile environmental theory with observed data (Gupta et al., 2008). The quality or skill of a model is measured by the capability of the model to replicate observed data and can quantified by a range of different efficiency criteria. A number of these efficiency criteria exist, each with its own set of advantages and disadvantages (Krause et al., 2005). Whether the model output is considered satisfactory is determined by the values of the efficiency criteria. The selection of any value of these efficiency criteria for a model to be considered satisfactory is often arbitrary and application dependent studies have been conducted to provide some general guidelines for threshold values (e.g., Moriasi et al., 2007).

2.3.6 Spatial representation

Snow models can be applied at a point, in a lumped formulation or distributed. Point models simulate snow conditions at individual ablation sites whereas lumped and distributed models consider a basin scale. The lumped model, where variables are averaged or estimated over the watershed has historically been the favored formulation for many snow modelling applications due to computational constraints and data availability. With improved computation technology and data acquisition, applications of distributed temperature-index models have increased (e.g., Daly et al., 2000).

Simulating snow conditions in a distributed grid over a basin should improve the representation of local topographic. By incorporating topographical information into the model, a better representation of local snow conditions patterns can be achieved. Such modelling efforts generally try to include information on slope, aspect, elevation, local shading, and weather patterns. One approach has been to relate melt to the radiation index computed from digital elevation models at each grid point (Dunn and Colohan, 1999).

Distributed models have been shown to outperform simple lumped approaches, especially in representing diurnal melt cycles (Hock, 1998). Performance improvements of distributed temperature index models have been shown to marginally improve with a more complete representation of the energy balance (Hock, 1999). These results indicate that a large improvement in model performance can be achieved without a need for increased data acquisition of other energy balance variables. Nonetheless, recent studies in well documented catchments show that distributed energy balance models outperform distributed temperature index models where data is sufficient (Kumar et al., 2013 and Jost et al., 2012).

3. Application and results

The main discussion in this chapter revolves around the methods, applications and results developed in this dissertation and is in accordance with the objectives outlined in Chapter 1, with reference to the four papers prepared in this PhD project.

3.1 Simulating seasonal glacier mass balance – Application to Brúarjökull glacier

Understanding the spatio-temporal impact of climate change on snow resources requires a means of simulating the cryosphere portion of the water cycle, either as part of the larger terrestrial water cycle or as an individual portion of it. Many models have been developed to this end and a review of the major classes of snow models that have been described in the hydrological literature as is discussed in Section 2.3 of this dissertation. All these snow models are associated with their own advantages and weaknesses and no consensus has been reached within the snow hydrological community on the optimal snow model configuration (Essery et al., 2013; Etchevers et al., 2004; Krinner et al., 2018). Thus, to achieve Objective 1 of this dissertation, to identify the meteorological and climatological drivers of changes in snow and ice mass balance, the snow melt behavior of the well-documented Brúarjökull glacial catchment in South-Eastern Iceland was simulated using a novel data-driven modelling framework. The results of which are presented in this subsection and published in Eythorsson et al. (2018).

Previously published studies on melt modelling of Icelandic glaciers in general have focused on simulating the behavior of these resources in a daily or finer time resolution (Carenzo et al., 2009; de Wildt et al., 2003; de Wildt et al., 2003; Marshall et al., 2005). These studies have considered both physical energy balance models and empirical degree day models, which have both shown good performance in simulating diurnal melt rates. These models all rely on data on some or all the factors that govern snow accumulation and snow melt. Given meteorological forecasts snow models can be used to forecast snow conditions with lead times roughly equal to those of the meteorological data used to force the model. Current meteorological models can forecast weather conditions with reasonable accuracy several days in advance. However, the uncertainty in the forecast increases rapidly with longer lead times. Although the skill of Numerical Weather Prediction Models (NWPM) has been continuously increasing in the past years (e.g. Hoffman et al., 2018), snow forecasting based on the output of these NWPM's is limited to lead times of several days to a few weeks.

The ability to predict snow melt behavior with longer lead times than those currently achieved by modern day NWPM's would be valuable for the water resource management in catchments heavily impacted by snow, either due to glaciation or large amounts of seasonal snow. The Brúarjökull catchment represents an ideal study area for seasonal snow modelling as it is extensively glacierized and the amount of summer melt water that can be stored each year is one of the key parameters in operating the Kárahnjúkar HPP. Making the ability to

forecast the summer mass balance of the Brúarjökull glacier an important goal to optimize power plant operations.

3.1.1 Data

The Brúarjökull glacier is the largest outlet glacier of the Vatnajökull ice cap in South-Eastern Iceland. The glacial meltwater from the Brúarjökull glacier in South-Eastern Iceland has been mostly utilized in the Kárahnjúkar Hydro Power Plant (HPP) and represents most of the inflow into the plant's major reservoir, Hálslón. As a result of the powerplant development, the environmental conditions in Brúarjökull catchment are extensively monitored and time series of hydro-meteorological and glaciological data have been collected for decades. The inflow into Hálslón, the main reservoir of the Kárahnjúkar HPP, is measured by Landsvirkjun, the operator of the power plant. A time series of inflow extending from the commissioning of the plant in 2007 with hourly temporal resolution was made available for the purposes of this research.

Mass balance data is collected in several measurement points across the Vatnajökull glaciers, biannually. In spring, the winter snow accumulation is measured by ice core measurements while in the fall, summer ablation is measured from ablation wires or rods that are placed on the glacier during the spring survey (e.g. Thorsteinsson et al., 2004). The net annual mass balance of the glacier in each measurement point can then be estimated as the winter accumulation subtracted by the summer ablation. Figure 3-1 shows the location of the mass balance sites on the Brúarjökull glacier.

Palsson et al., 2014 used these mass balance measurements to estimate the annual bass balance in each of the glacial catchments on the Vatnajökull glacier. As a result, there is available a time series of the annual glacial mass balance in the Brúarjökull catchment extending back to the year 1992. It should be noted that this time series of glacial mass balance only represents the change in snow mass between the spring and fall measurement surveys and does not consider any liquid precipitation that may fall on the glacier during the summer nor snow that melts outside of the survey period (after the fall survey or before the spring survey). It does however provide a reasonable proxy estimate of reservoir inflow, which has only been measured since the commissioning of the power plant in 2007.

Several Automatic Weather Stations (AWS) are located on the Vatnajökull glacier, three of whom are situated on the Brúarjökull outlet. These AWS are designed to measure all the components of the Surface Energy Balance (SEB). Additionally, several AWS are operated on land in or in the vicinity of the Brúarjökull catchment. While these land-based AWS do not measure the radiative components of the SEB they do collect data on other parameters important for estimating the SEB, such as air temperature, humidity, wind speed and precipitation. Figure 3-1 shows the location of the AWS site locations on and around the Brúarjökull glacier.

The Icelandic climate, and consequently mass balance of the Icelandic glaciers, is significantly influenced by conditions in the surrounding ocean (e.g. Hanna et al., 2001, 2004). Large scale circulation patterns in the North Atlantic Ocean can be estimated by several indices and variables. Atmospheric circulation patterns over the North Atlantic have been shown to correlate with seasonal temperature and precipitation patterns in Iceland (Hanna et al., 2004). In Eythorsson et al., (2018) the North Atlantic Multidecadal Oscillation Index (NAOI) (Barnston & Livezey, 1987), as estimated by the National Oceanic and

Atmospheric Administration (NOAA), the Atlantic Meridional Oscillation (AMO) (Kerr, 2000), the US National Oceanic Data Center (NODC) estimated quarterly heat content of the northern Atlantic (60-0° W, 30-65° N) (Levitus et al., 2012) and measurements of sea surface temperatures, from three locations around Iceland, observed by the Icelandic Marine Research Institute, were evaluated as predictor variables for seasonal melt forecasting. The North Atlantic Ocean indices have been shown to correlate with seasonal climate patterns in northern Europe (e.g Palter, 2015; Zampieri et al., 2017).

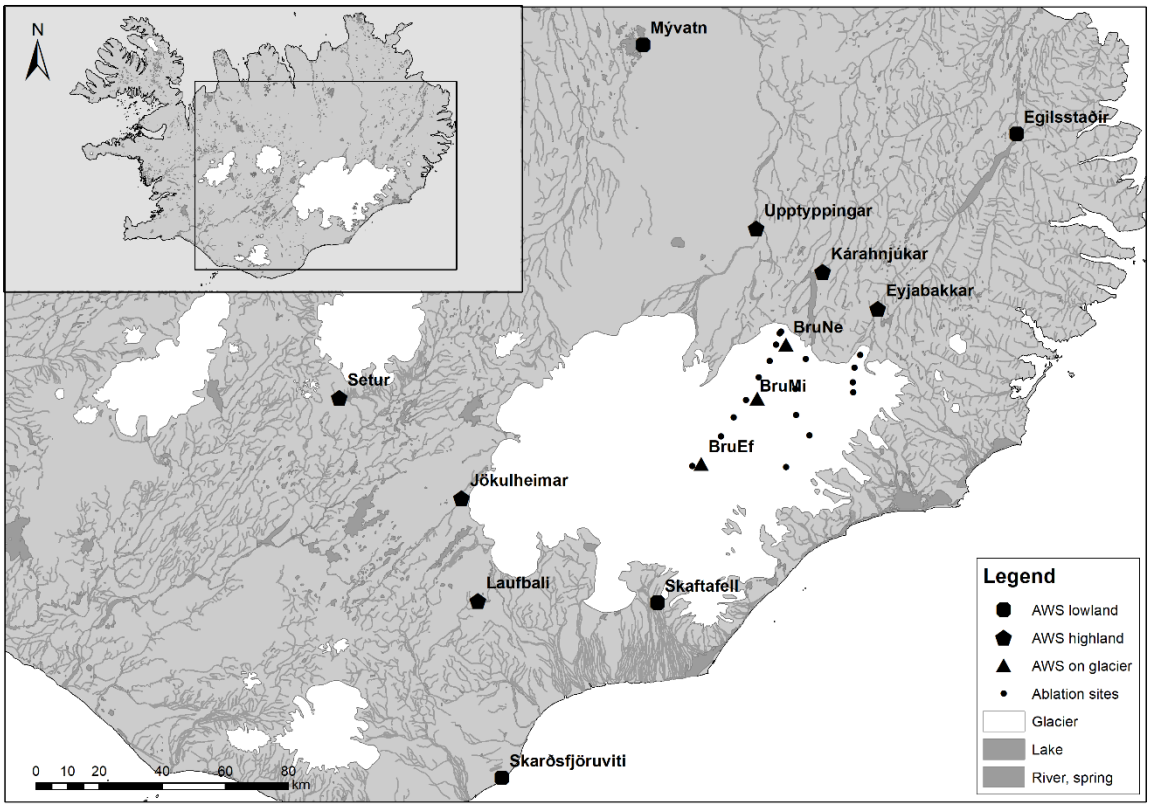

Figure 3-1 Location of mass-balance sites and Automatic Weather Stations (AWS) where the glaciological and meteorological data used in Eythorsson et al., (2018), were collected (from Eythorsson et al. 2018)

3.1.2 Variable selection

The response variable in in Eythorsson et al., (2018), was the annual summer mass balance of the Brúarjökull glacier, as estimated using the methods of Pálsson et al., (2014). All the available environmental data described in section 3.1.1 was assessed in terms of their predictive potential by estimating their correlation to the response variable, estimated as the square of the Pearson's correlation coefficient, *r*. Variables were ranked according to their r^2 value, and variables with an r^2 value above a certain threshold value, r_t, were selected to develop an ensemble of forecast models. The value of r_t, was optimized by performing a sensitivity analysis of the model results for model forecasts made on the 1st of July, as described in Eythorsson et al., 2018. The variables which were ultimately selected to create the final model ensemble are summarized in Table 3-1 with their correlation to the observed summer mass balance of Brúarjökull.

Table 3-1 Predictor variable selected for development of a multimodel forecast ensemble and their correlation to the observed summer mass balance of Brúarjökull, given as r^2 values (from Eythorsson et al., 2018).

Variable	Location	r^2
Net radiation	BruNe (850 m a.s.l)	0.65
AMO index	Atlantic Ocean	0.48
Albedo	BruNe (850 m a.s.l)	0.47
Albedo	BruMi (1,200 m a.s.l)	0.36
Atmospheric Pressure	Karahnjukar	0.35
Precipitation	Egilsstadir	0.33
Ocean Heat Content	North Atlantic	0.32

3.1.3 Multivariate model ensemble

The variables that showed the best predictive performance and are summarized in Table 4-1 were used to create an ensemble of all possible multivariate linear regression models with five or fewer input variables. The number of input variables were restricted to five or fewer due to the risk of potential overfitting of the models. The number of models to include in the ensemble was optimized by performing a sensitivity analysis of the model results, as described in Eythorsson et al., 2018.

3.1.4 Multi-model inference

Many multivariate regression models can be created by combining five or fewer of the input variables which showed predictive potential and are presented in Table 4-1. To select any single one of these models to infer information about the response variable would recognize the existence of several other competing models and reject their predictive potential. Thus, the selection of any one of the possible models is a source of uncertainty in the estimation of the response variable. Unless this uncertainty due to model selection is accounted for, overconfident predictions may be made (Wang et al, 2009).

To eliminate model selection as a source of forecast uncertainty the average of the response variable can be calculated over a range of plausible models, a method commonly referred to as model averaging (Hjort & Claeskens, 2003) and is commonly used in many earth science disciplines in cases where many competing models are possible (Dormann et al., 2018; Fragoso et al., 2018; Höge et al., 2019). Eythorsson et al., (2018)., used the frequentist model averaging technique and estimated the response variable, the summer mass balance of the Brúarjökull glacier, *M*, as the arithmetic mean of all the plausible models according to Equation 3.1.1.

$$M = \frac{1}{K}\sum_{k=1}^{K} M_k, \qquad (3.1.1)$$

where the index k denotes the k^{th} model considered, K is the total number of models, M_k is the estimated ablation based on the k^{th} model. The uncertainty in the estimate is taken as the spread in predicted values of the ensemble of plausible models.

3.1.5 Selecting an optimal subset of models for inference

The predictive quality of each of the models in the multimodel ensemble was assessed by three evaluation metrics: The Nash-Sutcliffe efficiency (NSE), the ratio of the root mean square error to the standard deviation of the measured data (RSR) and the percent bias. These three metrics were recommended by Moriasi et al., (2007), for watershed simulations, their mathematical formulae are described in Equations 3.1.2 - 3.1.4

$$NSE = 1 - \frac{\sum_{i=1}^{n}\left(Y_i^{obs} - Y_i^{sim}\right)^2}{\sum_{i=1}^{n}\left(Y_i^{obs} - Y^{mean}\right)^2}, \quad (3.1.2)$$

$$RSR = \frac{RMSE}{STDEV_{obs}} = \frac{\sqrt{\sum_{i=1}^{n}\left(Y_i^{obs} - Y_i^{sim}\right)^2}}{\sqrt{\sum_{i=1}^{n}\left(Y_i^{obs} - Y^{mean}\right)^2}}, \quad (3.1.3)$$

$$PBIAS = \frac{\sum_{i=1}^{n}\left(Y_i^{obs} - Y_i^{sim}\right)*(100)}{\sum_{i=1}^{n}\left(Y_i^{obs}\right)}, \quad (3.1.4)$$

where n is the number of data points in the dataset, Y_{obs} is the observed mass balance of Brúarjökull in the i^{th} year, Y_{sim} is the simulated mass balance in the i^{th} year and Y_{mean} is the mean observed mass balance. Moriasi and others (2007) suggested that a model simulation could be judged as satisfactory if NSE > 0.5, RSR < 0.7 and PBIAS < ±25%. In Eythorsson et al., (2018) an ensemble of optimal models was created by only selecting those models from the multimodel ensemble which met these three criteria.

3.1.6 Model Evaluation and results

The skill of the multi-model forecast ensemble created in Eythorsson et al., (2018) was evaluated in its ability to forecast the summer mass balance of the Brúarjökull glacier, in terms of the evaluation metrics NSE, RSR and PBIAS described in Equations 3.1.2 - 3.1.4. The model forecasts were evaluated using five-fold cross-validation, meaning that the data were split five ways where $4/5^{ths}$ of the observations were used for calibration and $1/5^{th}$ was used for evaluation of the results. Table 3-2 shows the evaluation metrics NSE, RSR and PBIAS for forecasts made between the 15^{th} of May and the 1^{st} of July.

Table 3-2 Evaluation metrics, NSE, RSR, PBIAS for forecasts made between the 15^{th} of May and 1^{st} of July (from Eythorsson et al., 2018)

Forecast Date	NSE	RSR	PBIAS (%)
15^{th} May	-0.95	1.39	9.2
1^{st} June	0.13	0.93	3.2
15^{th} June	0.45	0.75	2.7
1^{st} July	**0.71**	**0.54**	**0.27**

Figure 3-2 shows the model averaged forecasts of the Brúarjökull summer mass balance for all the five folds used for cross validation for forecasts made on the 1^{st} of July, the 1^{st} and 15^{th} of June and the 15^{th} of May.

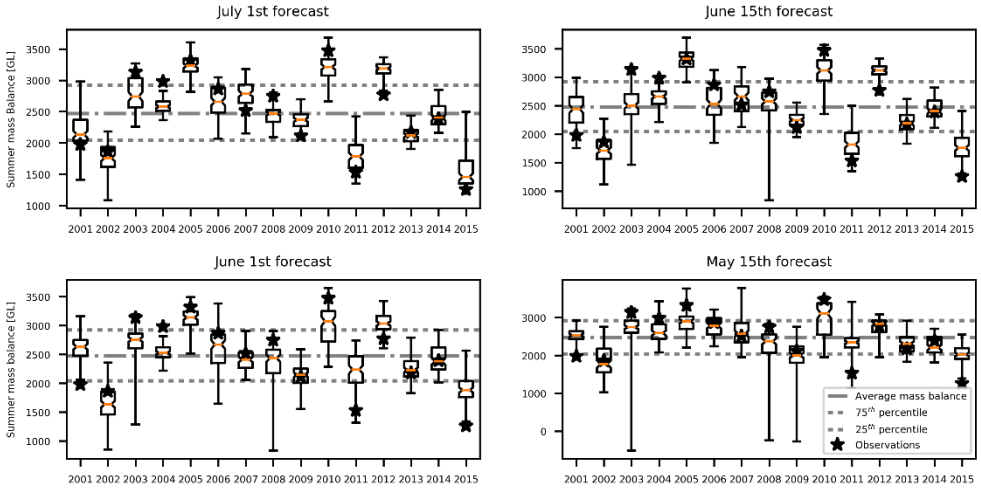

Figure 3-2 Model-average forecasts of Brúarjökull summer mass balance for all five folds used for cross validation (from Eythorsson et al., 2018)

The results in Figure 3-2 and Table 3-2 illustrate that satisfactory predictions of the summer mass balance of the Brúarjökull glacier were achieved when the models were run with data that are available at the 1st of July, at which time the glacial summer melt season is starting.

3.2 Observing global snow cover changes

Climate change can be expected to impact the extent, duration and volume of snow in areas with both seasonal and perpetual snow cover (e.g. Adam et al., 2009; Kapnick & Delworth, 2013). Understanding how these changes are distributed spatially and temporally requires reliable measurements of the parameters that are important for understanding and simulating snow dynamics. Many snow datasets have been described in the literature and made available to the research community, collected in various spatio-temporal resolution and extent, using different measurement technologies, and containing a wide range of snow parameters. These data sets range from individual snow pit measurements to time series of point based in situ measurements, to distributed datasets of remotely sensed snow cover extent (e.g. Dong, 2018). Thus, to achieve part of Objective 2 of this dissertation (assessing the historical changes to snow conditions), the spatio-temporal changes in snow cover were estimated using satellite derived snow cover data from the MODIS instrument on NASA's Terra and Aqua satellites, as it provides with a widest spatial coverage and finest temporal resolution of any of the observational snow cover datasets available in the literature. These results are presented in this subsection and published in Eythorsson et al., (2019)

3.2.1 Estimating Snow Cover Frequency

Snow cover, which persist on the ground for extended periods and occurs regularly, is one of the key elements governing the hydrology and ecology of an area (Vavrus, 2007). The duration of snow cover over the year determines which species of flora and fauna can inhibit a place (e.g. Billings & Mooney, 1968). Snow Cover Frequency (SCF) is an estimate of how impacted by snow an area is and can be calculated as the number of snow-covered days divided by the number of days in the year. The SCF is an important geophysical feature, as it is a key determinant of the local surface albedo, regulating solar absorption (e.g. Cohen, 1994) and has also be used to estimate species habitat suitability (Barichivich et al., 2013). With the advent and availability of large scale open source satellite data observations and sophisticated computational platforms the estimation and mapping of SCF data has been made possible for the research community, in a way hitherto impossible, to analyze and investigate snow dynamics (e.g. Basang et al., 2017; Choudhury et al., 2021).

Many methods have been applied to remotely estimate key parameters in the terrestrial snow cover, from both airborne vehicles and satellites using a range of sensor technologies (Dietz et al., 2012). Data from these sensors are commonly used in hydrological modelling (e.g Dong, 2018; Helmert et al., 2018). With improved sensing technologies and a maturing satellite industry, global datasets with high temporal resolution observations or estimates of snow cover have been made readily available and routinely used in snow research. One of the key snow cover datasets for the present-day snow research community is the Moderate Resolution Imaging Spectroradiometer (MODIS) snow cover product, which has been available since 2000 and provides global daily snow cover extent in 500 m spatial resolution. The MODIS snow dataset has been evaluated based on many other observational snow datasets (e.g. Arsenault et al., 2014; Hall et al., 2019) and is frequently used to study the observed snow dynamics over the period which has passed since the year 2000 (e.g. Dariane et al., 2017; Li et al., 2018). In Eythorsson et al., (2019), the MODIS MOD10A1 snow cover product was used to calculate the annual SCF globally for the period 2000-2016, and to identify the areas where there had occurred a statistically significant change in the SCF over that period.

The annual SCF was calculated in 500 m spatial resolution across the globe, based on the MODIS10A1.005 snow cover product. The MOD10A1 snow cover product was re-mapped to classify each pixel as snow/ice (1) or no snow/ice (0) for each valid observation in the dataset. To reduce the panoramic distortion caused by the curvature of the earth, which causes overlapping satellite scan lines, observations with zenith angles greater than 25° were removed excluded from the analysis. As this panoramic distortion has been shown to be a cause of systematic error in snow mapping with MODIS data (Ackerman et al., 2008; Frey et al., 2008; H Souri & Azizi, 2013). Metadata on sensor nadir angle was extracted from the MOD09GA dataset and merged with the MOD10A1 data. The MOD10A1 data was not subjected to any additional cloud masking as the improvements made to the fifth collection of MODIS imagery has resulted in significant improvements of its inherent cloud masking algorithm (Frey et al., 2008) and has been shown to be in good agreement with other cloud detection datasets (Ackerman et al., 2008; Ault et al., 2006; Wang et al., 2016). Missing observations (due to e.g., cloud cover, sensor malfunction or polar night) were indiscriminately excluded from the analysis.

The annual SCF was subsequently estimated for each 500x500m pixel globally as the number of days which each pixel was covered with snow, divided by the total number of valid observations in that pixel, for each year in the period 2000-2016. The trend in annual SCF in each pixel over the study period was estimated using two statistical slope estimation methods: linear regression and Sen's estimator of slope method (Sen, 1968). The statistical significance of the estimated trend lines was then estimated using two non-parametric hypothesis tests: the Mann-Kendall trend test (Maurice & Kendall, 1975) and Sen's slope test (Sen, 1968). In general, comparable results were achieved using both statistical slope estimation methods. However, the Mann-Kendall method was more sensitive to misclassified pixels, especially over permanent snow cover. Sen's slope estimation method showed more resilience to outliers due to misclassified pixels and was thus used in all subsequent analysis. Statistically significant changes to snow cover in each pixel was reported at two confidence levels ($\alpha = 0.01$ and $\alpha = 0.05$).

Figure 3-3 shows a map of the areas which were shown to have experienced a statistically significant increase in SCF (blue) and a statistically significant decrease in SCF (red) over the period 2000-2016, as estimated using the Sen's slope estimation method for the $\alpha = 0.05$ confidence level. The results presented in Figure 3-3 show that over the period that the MODIS data has been collected (2000-2016) there has been a statistically significant decrease in the SCF in large areas of the continental subarctic. At higher latitudes, especially near the Arctic coastline extended areas where the SCF had increased during this period were observed. This pattern of increasing SCF is observed in the north-western Canadian and Alaskan arctic coastline, the eastern Siberian coastline and to a slightly lesser extent in northern Fenno-Scandia and Iceland. However, on the western coast of Greenland and the southern part of Novaya Zemlya the opposite trend, of increasing SCF was observed. This incongruity of SCF patterns on the coastline surrounding the Arctic seas is interesting. It is most likely explained by that in Western Greenland and Novaya Zemlya the decreasing SCF is observed due to deglaciation and the loss of permanent snow cover (Carr et al., 2014; Melkonian et al., 2016; Straneo & Heimbach, 2013), whereas in the North American, Eurasian Arctic the patterns of increasing SCF may be due to an increasing volume of winter precipitation which causes a deeper winter snowpack and may extend the duration of the annual snow cover (Kopec et al., 2016; Singarayer et al., 2006).

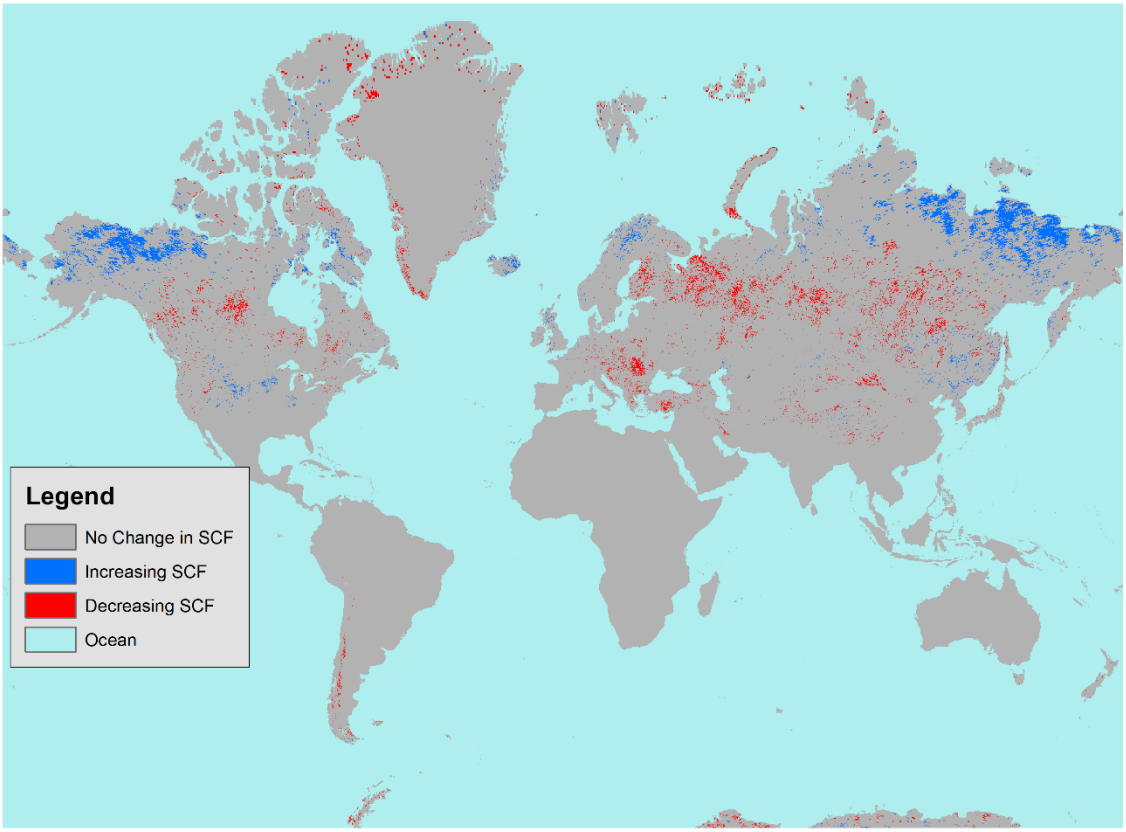

Figure 3-3 Areas of increasing (blue) and decreasing (red) SCF, as estimated using Sen's slope estimation method at the α = 0.05 confidence level.

Eythorsson et al. (2019) estimated that 8.3% of the Arctic land surface has experienced a statistically significant (α = 0.05) change in the local SCF over the MODIS period (2001-2016). Over the same period the average Arctic SCF, below 500 m.a.s.l., was found to have decreased by 0.25% per year, or by 9.1 days per decade. These results are in line with the findings of prior research which have estimated changes to the snow regime in this area. The number of snow covered days (SCD) in the Northern Hemisphere (NH) was estimated to have decreased by 5.3 days/decade over the MODIS period by Yunlong et al., (2018) using remotely sensed MODIS, IMS and AMSR-e data. Hori et al., (2017) showed that over the period 1979-2009 the frequency of snow cover over the NH had decreased by 10 days / decade, estimated using remote sensing data from MODIS and AVHRR. This trend of decreasing NH SCF has also been simulated based on hydro-climatological datasets. Liston & Hiemstra, (2011), used the MERRA reanalysis product to model NH snow cover over the period 1979-2009 and observed an average decrease in NH SCD by 2.5 days/decade.

3.3 Estimating and predicting changes to global climate classifications

Climate projections, like those produced by GCM's, estimate future conditions in climate state variables based on predicted changes to forcing variables that determine spatio-temporal changes in the state of the climate. The output of such models are thus the values of the state variables at each time increment that the model is run in, distributed across the spatial extent over which the model is run. Although such information about parameters such as temperature and precipitation in a distributed grid across the globe is valuable for many applications, further abstractification of the climate model output can provide insight into important aspects of climate change and the impacts it will have on many processes on the earth's surface. One way to abstractify this data is to use it to categorize areas of climate regions that are meaningful in some physical or biological sense. One of the most commonly used climate classifications systems is the Köppen-Geiger system, which has been applied to a range of studies in many scientific disciplines (Beck et al., 2018; Kottek et al., 2006; Peel et al., 2007). Thus, in order to achieve the second part of Objective 2 of this dissertation (assess the historical changes in the climate regime), the spatio-temporal changes in Köppen-Geiger climate classifications were estimated using the ensemble of Global Circulation Models (GCM's) from the fifth project phase of the Coupled Model Intercomparison Project (CMIP5) (Taylor et al., 2012), as these models make up the key scientific background for the International Panel on Climate Change (IPCC) policy recommendation for global policymakers, and thus represent the one of the most relevant estimates of future climate conditions for humanity. These results are presented in this subsection and published in Eythorsson et al., (2019).

3.3.1 Köppen-Geiger classification system

The local climate of an area is a key characteristic of that region in the minds of most of its human inhabitants. It determines which species of animals and plants can reside there and it impacts our level of comfort, our lifestyles and can even impact our mental health. It is one of the most distinctive feature changes that we notice while travelling from place to place. Using spatio-temporal estimates of climate classifications to visualize and quantify climate variation and change is a valuable method for researching the impacts of climate change (e.g. Chen & Chen, 2013) and to disseminate the work of the scientific community to the general public in way that resounds with their experiential reality (e.g. Jylhä et al., 2010).

The Köppen-Geiger (KG) climate classification system has been widely used in a range of disciplines to classify local climates. The system classifies the climate of an area based on monthly average measurements of air temperature and precipitation and can be applied to point measurements from individual weather stations or in a distributed grid, using a distributed meteorological dataset. The classification criteria of the Köppen-Geiger classification system are presented in Table 3-3. The system assigns climates into five main groups, *A* (tropical), *B* (Arid), *C* (temperate), *D* (continental) and *E* (polar). All groups except the polar climates (group *E*) are further divided into seasonal precipitation subgroups, marked by the second letter in the climate class, and finally all groups except the tropical climates (group *A*) are assigned a temperature subgroup, indicated by the third letter in the climate class. Thus, for example, climate class *Csa* represents temperate climate with dry and hot summers.

Table 3-3 Criteria for Köppen-Geiger classifications and their symbols

1st	2nd	3rd	Description	Criteria*
A			Tropical	$T_{cold} \geq 18$
	f		-Rain forest	$P_{dry} \geq 60$
	m		-Monsoon	Not Af and $P_{dry} \geq 100\text{-}MAP/25$
	w		-Savannah	Not Af and $P_{dry} < 100\text{-}MAP/25$
B			Arid	$MAP < 10*P_{threshold}$
	w		-Desert	$MAP < 5*P_{threshold}$
	s		-Steppe	$MAP \geq 5*P_{threshold}$
		h	-Hot	$MAT \geq 18$
		k	-Cold	$MAT < 18$
C			Temperate	$T_{hot} > 10$ & $0 < T_{cold} < 18$
	s		-Dry Summer	$P_{sdry} < 40$ & $P_{sdry} < P_{wwet}/3$
	w		-Dry Winter	$P_{wdry} < P_{swet}/10$
	f		-Without dry season	Not Cs or Cw
		a	-Hot Summer	$T_{hot} \geq 22$
		b	-Warm Summer	Not a & $T_{mon}10 \geq 4$
		c	-Cold Summer	Not a or b & $1 \leq T_{mon}10 \leq 4$
D			Cold	$T_{hot} > 10$ and $T_{cold} \leq 0$
	s		-Dry Summer	$P_{sdry} < 40$ & $P_{sdry} < P_{wwet}/3$
	w		-Dry Winter	$P_{wdry} < P_{swet}/10$
	f		-Without dry season	Not Ds and Not Dw
		a	-Hot Summer	$T_{hot} \geq 22$
		b	-Warm Summer	Not a & $T_{mon}10 \geq 4$
		c	-Cold Summer	Not a, b or d
		d	-Very Cold Winter	Not a or b & $T_{cold} < -38$
E			Polar	$T_{hot} < 10$
	T		-Tundra	$T_{hot} > 0$
	F		-Frost	$T_{hot} \leq 0$

* MAP = Mean annual precipitation, MAT = mean annual temperature, T_{hot} = temperature of the hottest month, T_{cold} = temperature of the coldest month, T_{mon10} = number of months with mean temperatures above 10, P_{dry} = precipitation in the driest month, P_{sdry} = precipitation in the driest month in summer, P_{wdry} = precipitation in the driest month in winter, P_{swet} = precipitation in the wettest month in summer, P_{wwet} = precipitation in the wettest month in winter, $P_{threshold}$ = varies according to: (if 70% of MAP occurs in winter then $P_{threshold} = 2*MAT$, if 70% of MAP occurs in summer then $P_{threshold} = 2*MAT+28$, otherwise $P_{threshold} = 2*MAT + 14$). Summer (winter) is defined as the warmer (cooler) six-month period of ONDJFM and AMJJAS.

From Peel et al., 2007

3.3.2 Projecting future Climate Classifications

In Eythorsson et al., (2019) a code was developed in Google Earth Engine (GEE) (Gorelick et al., 2016) to classify local climates according to the KG classification criteria presented in Table 3-3. The code was applied to classify the climate of each pixel (0.2-degree horizontal resolution) globally for each year in the time period 1950-2100, using temperature and precipitation data calculated from the ensemble average of the downscaled and bias corrected CMIP5 GCM results as published in the NASA-NEX GDDP dataset (Thrasher et

al., 2006), for both the Representative Concentration Pathway (RCP) RCP4.5 and RCP8.5 scenarios (van Vuuren et al., 2011).

Figure 3-4 shows an example of the global annual KG classifications for the years 1951 and 2099 produced in Eythorsson et al. (2019). The results show a general trend across the globe where warmer climate classes migrate to higher latitudes, replacing the colder climate classes. Nowhere is this warming trend as apparent as in the Arctic and continental sub-Arctic where climate classes associated with warm and hot summers are expected to replace cold summer and polar climates over large areas. This migration of warmer climate classes into high latitude areas was found to be more rapid and widespread under RCP85 as compared to RCP45. However, under RCP45 the coverage of the currently most common climate class in the Arctic (Cold climate with cold summers and no dry season, *Dfc*) is expected to decrease by about 40% by the year 2100.

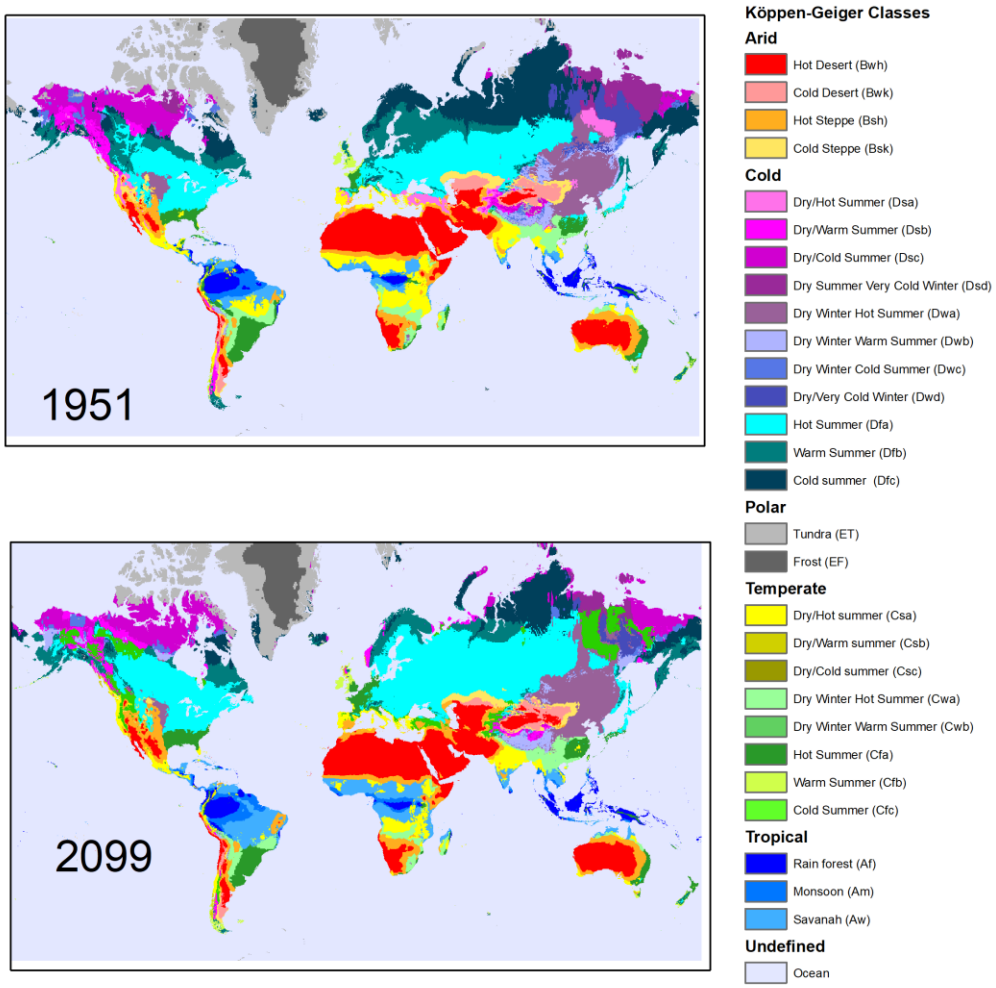

Figure 3-4 Examples of annual Köppen-Geiger (KG) classification maps for year 1951 (upper) and 2099 given the RCP45 emission scenario (lower).

The Köppen-Geiger classifications projected in Eythorsson et al. (2019), can be explored in more detail in an online app developed by the first author. The app, available through the following url: https://dareyt.users.earthengine.app/view/koppengeiger2 presents an

interactive map of the global KG classifications for the periods 1950-1960 and 2090-2100 under both the RCP4.5 and the RCP8.5 emission scenarios based on the ensemble average of the 21 CMIP5 GCMs in the NASA NEX GDDP database. The application allows the user to compare side by side how local climates are expected to change over the period 1950-2100 depending on future emission scenarios.

Figure 3-5 shows a screenshot of the KG classification app developed by the author. The KG classification for the period 1950-1960 are shown on the leftmost pane, the middle pane shows the KG classifications for the period 2090-2100 under the RCP45 emission scenario and the rightmost pane shows the classifications for the period 2090-2100 under the RCP85 emission scenario.

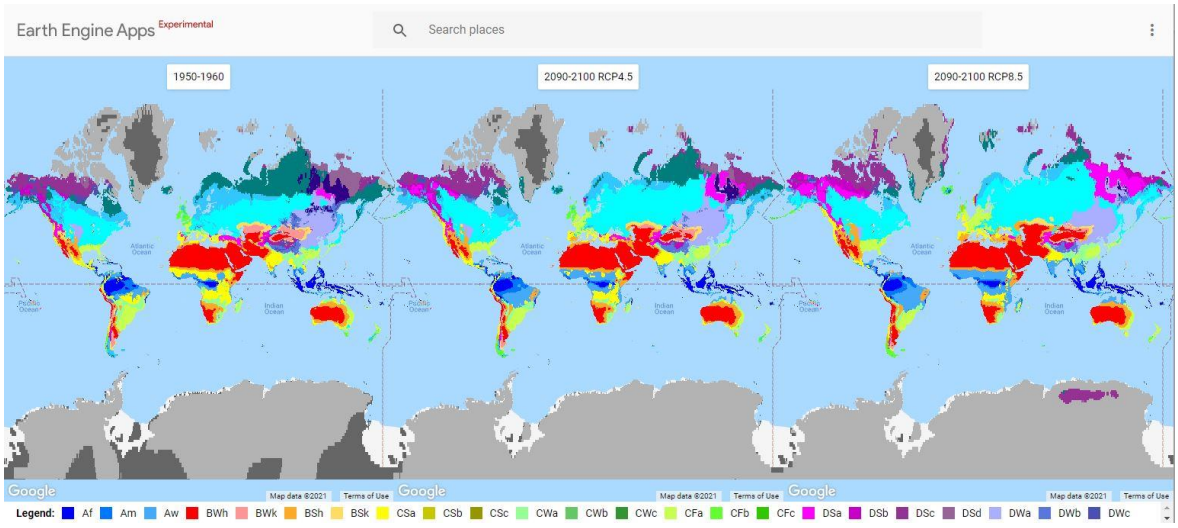

Figure 3-5 Snapshot of the KG classification app developed from the results of Eythorsson et al., (2019).

In Eythorsson et al., (2019) climate change over an area was estimated as a change in KG classification over that area due to a change in local temperature and precipitation patterns over time, given the RCP45 emission scenario. Figure 3-6 shows the proportional coverage of the Polar climate classes (ET and EF) and the four tertiary subgroups of the Cold climate classes, Warm summer (Dsb, Dwb, Dfb), Hot summer (Dsa, Dwa, Dfa), Cold summer (Dsc, Dwc, Dfc) and Very cold winter (Dsd, Dwd, Dfd), across the Arctic for each year in the period 1950-2100 with a 15 year rolling average. The most common climate classes in the Arctic, covering about 50% of its area at present, are the cold climate classes with cold summers (Dfc, Dsc and Dwc). Climate classes associated with very cold winters (Dwd and Dsd) and polar climates (ET and EF) are expected to decrease in coverage steadily throughout the study period. Climate classes associated with warm (Dfb, Dsb and Dwb) and hot summers (Dfa, Dsa and Dwa) were shown to increase in their coverage throughout the period, with a notable acceleration in the rate of increase after the turn of the 21st century. The results of Eythorsson et al., (2019), showed that during the period 1950-2020 cold summer classes are rapidly replacing polar (ET and EF) and very cold winter (Dwd and Dsd) climate classes, with cold summer classes reaching a peak coverage around year 2020, whereas in the latter part of the study period (2020-2100) classes with warm (Dfb, Dwb and Dsb) and hot summers (Dfa, Dwa and Dsa) were projected to advance further north into the Arctic, resulting in net decline in the coverage of the cold summer climate classes.

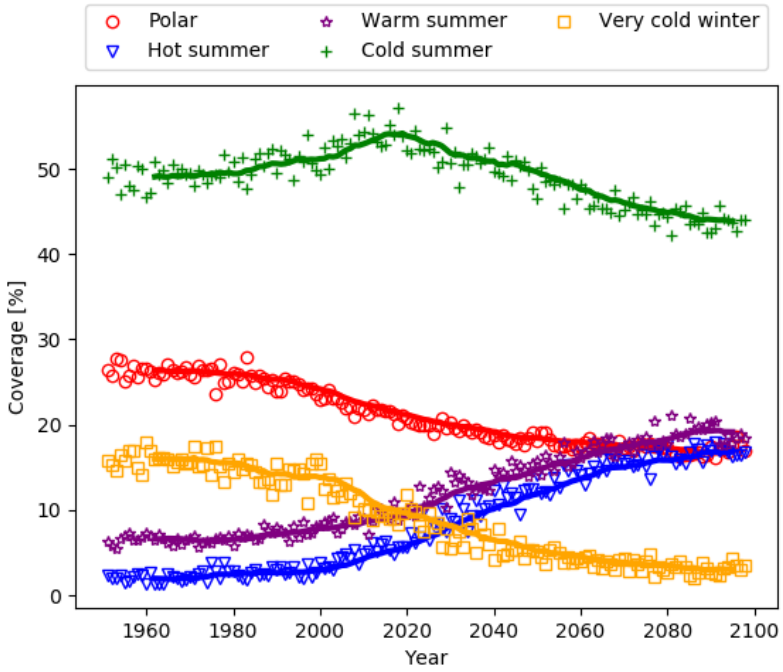

Figure 3-6 Proportional areal coverage of the most common groups of KG classes in the Arctic, below 500 m.a.s.l., for the period 1950-2100. A 15-year rolling mean is shown as a solid line (from Eythorsson et al., 2019)

Table 3-4 shows the proportional areal coverage of the Polar and Cold Climate classes within the Arctic and the changes in that proportional coverage between the periods 1951-1960 and 2090-2099. The results show that over the study period the coverage of the most common Arctic climate class in the beginning of the period, cold climate with cold summers and no dry season (Dfc) is expected to decrease by 41% while the second most common class, Polar tundra (ET) is expected to decrease by 34%. The results showed that as these colder climate classes recede further north, climate classes associated with warm and hot summers are expected to expand in coverage by 185% and 733% respectively, under the RCP45 scenario.

Table 3-4 Proportional coverage of Polar and Cold climate classes within the Arctic AMAP boundary and the changes between the periods 1951-1960 and 2090-2099 (from Eythorsson et al., 2019).

		1951-1960	2090-2099	Net Change
	Polar	**26.4%**	**17.3%**	**-35%**
	Polar Frost (EF)	0.4%	0.1%	-86%
	Polar Tundra (*ET*)	26.0%	17.2%	-34%
Cold Climate	**Very Cold Winters**	**15.9%**	**3.1%**	**-80%**
	Dry Winters (*Dwd*)	4.3%	0.1%	-97%
	Dry Summers (*Dsd*)	11.5%	3.0%	-74%
	Cold Summers	**49.1%**	**43.8%**	**-11%**
	No Dry Season (*Dfc*)	30.4%	18.0%	-41%
	Dry Winters (*Dwc*)	2.9%	1.8%	-36%
	Dry Summers (*Dsc*)	15.8%	23.9%	51%
	Warm Summers	**6.6%**	**18.7%**	**185%**
	No Dry Season (*Dfb*)	4.3%	12.9%	197%
	Dry Winters (*Dwb*)	0.2%	1.2%	518%

Dry Summers (*Dsb*)	2.1%	4.6%	126%
Hot Summers	**2.0%**	**16.9%**	**733%**
No Dry Season (*Dfa*)	0.9%	7.6%	770%
Dry Winters (*Dwa*)	0.5%	1.1%	125%
Dry Summers (*Dsa*)	0.7%	8.3%	1099%

3.4 Comparing trends in climate classifications and Snow Cover - an Arctic case study

Eythorsson et al., (2019), compared the changes in KG climate classifications with changes in the local Snow Cover Frequency (SCF), as estimated from the MOD10A1.005 dataset, described in Section 4.2, within 10 selected study areas in the Arctic. Figure 3-7 shows the location of the study areas which were selected as they have been defined by the Arctic Monitoring and Assessment Program (AMAP) as specific pollution prevention areas, because they are considered to be especially vulnerable to human development and climate change (AMAP, 2015). The study areas were restricted to the Arctic lowlands, under 500 m.a.s.l., as these are the areas which are most important for human development in the region. Figure 3-7 also shows the Arctic area, as delineated by AMAP, with a red dotted line.

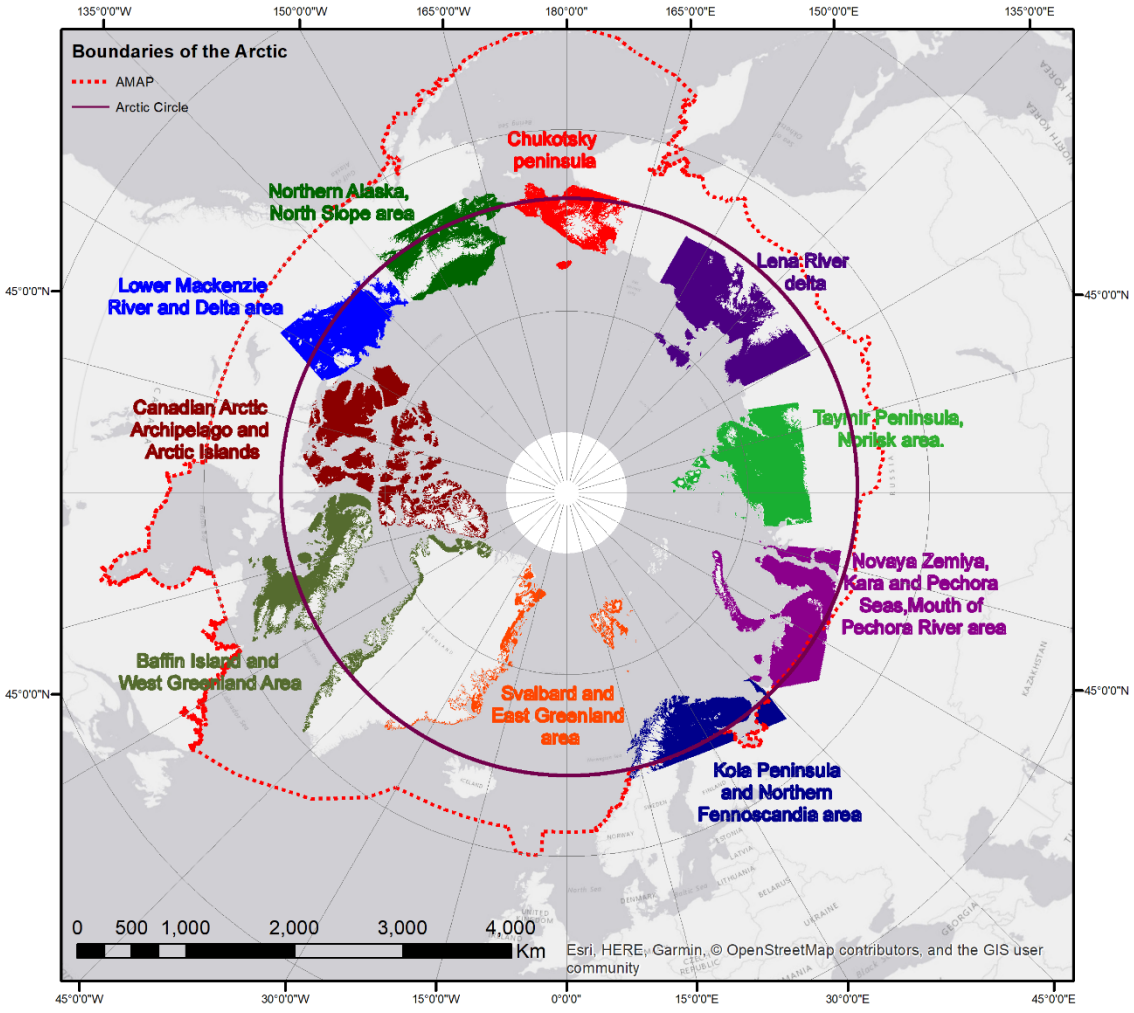

Figure 3-7 The Arctic area (AMAP, 2015) and the 10 pollution prevention areas in the Arctic which were selected for comparing changes in the snow and climate domains (from Eythorsson et al., 2019)

Figure 3-8 shows the annual SCF and the proportional coverage of the two most common KG classes in each of the study areas shown in Figure 3-7, for the period 2001-2016. The trends were estimated using least square linear regression and the significance of the slope of the proportional coverage of the KG classes was estimated using the non-parametric Sen's estimator of slope and Mann-Kendall methods.

The results showed evidence for statistically significant changes ($\alpha = 0.05$) to one or both main KG climate classes in seven of the ten study areas over the period 2001-2016. In all these cases there had occurred a warming trend, which was observed as either a statistically significant decrease in a colder climate class or an increase in a warmer climate class, or both. When compared to the changes in SCF in these same areas three distinct patterns were revealed: (i) in the northernmost areas of the Arctic (Canadian Arctic Archipelago, Svalbard & East Greenland, Taymir Peninsula & Norilsk Area) no significant trends were observed in the KG climate classifications as well as the smallest changes to the SCF, (ii) in the study areas closer to the Atlantic Ocean (Baffin Iceland & West Greenland, Kola Peninsula & Northern Fennoscandia, Novay Zemlya & Kara and Pechora Areas) significant warming trends were observed over the same period that the SCF had decreased significantly in many areas, and (iii) in the study areas closer to the Pacific Ocean (Lower Mackenzie river and delta area, Northern Alaska, Chuckotsky peninsula, Lena river delta) significant warming trends were observed over the same period that the SCF had increased.

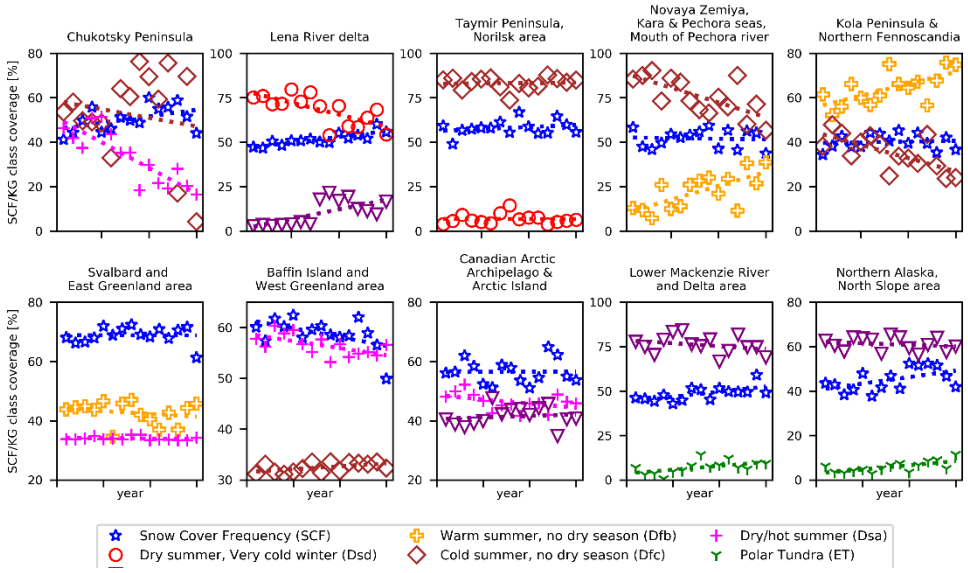

Figure 3-8 Snow Cover Frequency (SCF) and proportional coverage of the two most common KG classes in each study area over the period 2001-2016 (from Eythorsson et al., 2019).

Table 3-5 shows the estimated changes in the coverage of the two main KG classifications in each of the 10 areas studied in Eythorsson et al. (2019), over the period 2001-2016 and the percentage of the study areas which are below 500 m a.s.l. where a statistically significant SCF trend was observed. The results presented in Table 3-5 show a statistically significant trend in one or both most common climate classes in seven of the ten study areas considered. These same areas had proportionally the largest areas where the SCF had experienced a statistically significant change in the local SCF (4.8 – 13.6% at $\alpha = 0.05$).

Table 3-5 Changes in coverage of the two main KG classes in the period 2001-2016 and the percentage of study areas below 500 m.a.s.l. showing a significant SCF trend. Significant results at the α = 0.05 confidence level are in bold. (From Eythorsson et al., 2019)

	1st KG Class				2nd KG class				SCF significant area [%] (%pos. / %neg.)	
Area	**Name**	**Change 2001-2016 [%]**	**MK p-value**	**Sen's slope**	**Name**	**Change 2001-2016 [%]**	**MK p-value**	**Sen's slope**	**α = 0.05**	**α = 0.01**
Arctic AMAP area	Cold summer no dry season (Dfc)	-7.7%	0.255	inSign	**Tundra (ET)**	**-5.99%**	**0.025**	**Sign**	3.6 (+0.8/-2.8)	0.9 (+0.2/-0.7)
Chukotsky Peninsula	Cold summer no dry season (Dfc)	-21.60%	0.72	inSign	**Tundra (ET)**	**-77.00%**	**0.0006**	**Sign**	11.5 (+11.4/-0.07)	3.7 (+3.7/-0.0)
Lena River Delta	**Cold summer very cold winter (Dfd)**	**-25.30%**	**0.006**	**Sign**	**Cold/dry summers (Dsc)**	**490.50%**	**0.005**	**Sign**	13.6 (+12.9/-0.7)	6.4 (+6.2/-0.2)
Taymir Peninsula, Norilsk Area	Cold summer no dry season (Dfc)	0.70%	0.881	inSign	Dry summer very cold Winter (Dsd)	13.30%	0.805	inSign	1.8 (+1.4/-0.4)	0.4 (+0.3/-0.1)
Novaya Zemiya, Kara & Pechora Seas, Mouth of Pechora River	**Cold summer no dry season (Dfc)**	**-30.20%**	**0.009**	**Sign**	**Warm summer no dry season (Dfb)**	**198.60%**	**0.006**	**Sign**	4.8 (+0.5/-4.3)	1.6 (+0.1/-1.5)
Kola Peninsula & Northern Fennoscandia	**Warm summer no dry season (Dfb)**	**29.60%**	**0.009**	**Sign**	**Cold summer no dry season (Dfc)**	**-62.20%**	**0.003**	**Sign**	9.1 (+2.3/-6.8)	3.6 (+0.7/-0.29)
Svalbard and Eastern Greenland	Warm summer no dry season (Dfb)	-3.40%	0.52	inSign	Tundra (ET)	-1.30%	0.21	inSign	1.2 (+0.6/-1.6)	0.9 (+0.2/-0.7)
Baffin Island and West Greenland Area	**Tundra (ET)**	**-7.00%**	**0.025**	**Sign**	**Cold summer no dry season (Dfc)**	**5.00%**	**0.042**	**Sign**	7.8 (+3.1/-4.7)	3.0 (+1.1/-1.9)
Canadian Arctic Archipelago & Arctic Islands	Tundra (ET)	-8.10%	0.255	inSign	Cold/dry summers (Dsc)	6.50%	0.22	inSign	1.3 (+0.08/-1.2)	0.5 (+0.2/-0.3)
Lower Mackenzie River and Delta area	Cold/dry summers (Dsc)	-11.29%	0.21	inSign	**Dry/hot summers (Dsa)**	**32.78%**	**0.02**	**Sign**	11.3 (+10.7/-0.6)	4.5 (+4.3/-0.2)
Northern Alaska and North slope area	Cold/dry summers (Dsc)	4.03%	0.45	inSign	**Dry/hot summers (Dsa)**	**84%**	**0.006**	**Sign**	11.1 (+11.05/-0.05)	4.3 (+4.3/-0.0)

The warming trend observed across the Arctic in Eythorsson et al., (2019), is unsurprising as there is a consensus that the Arctic is warming at an amplified rate as compared to the global average. A phenomenon known as polar amplification which has been documented in present and historical periods of rapid climate change (J. Cohen et al., 2014; Serreze & Barry, 2011; Serreze & Francis, 2006). However, the observed regional differences in how snow resources respond to this warming are notable, and important for local hydrological and ecological adaptation strategies in these areas. In the northernmost areas (i) the local temperature has indeed risen; however, this rise has not resulted in a change in climate classification. Since there has not been any notable change in the general climatology of these regions, they are not expected to have undergone major snow hydrological changes. In the regions closer to the Atlantic Ocean (ii) cold climates are replacing polar climate and warm and hot summer climates are replacing cold summer climates within the Cold climate group, in line with this shift toward warmer climates the local SCF has decreased in large areas. In the study areas closer to the Pacific Ocean (iii) the same climate warming trends are observed as in ii), however, this rise in temperature has been accompanied with a larger increase in precipitation, as sea ice concentrations in these areas has decreased significantly in recent years, increasing local evaporation- and, subsequently, precipitation rates (Maslanik et al., 2011; Serreze & Stroeve, 2015), which is likely to increase both the frequency and volume of snowfall.

3.5 Projecting changes to NH snow resources under different climate change scenarios

The conclusions of Eythorsson et al., (2019) showed that significant changes were estimated to have occurred in the climate and snow regimes in the Arctic over the last decades. To understand how snow resources will continue to be impacted by a changing climate, future snow conditions must be simulated based on current best estimates of future climate conditions. As demonstrated by Eythorsson et al., (2018) seasonal ablation behavior in areas with abundant snow and ice resources can be predicted reasonably well a few months in advanced based on the initial conditions of the surrounding hydro-climatological system and as discussed in Section 2.3 of this dissertation, reliable shorter term forecasts can be produced based on initial state variables and meteorological forecasts. However, to simulate large scale snow response to climate change over a longer time frame, snow conditions should be simulated based on the results of scientifically accepted climate model results. Thus, in order to achieve Objective 3 of this dissertation, snow conditions were simulated based on the CMIP5 GCM ensemble for the time period 1950-2100 in a 0.2-degree horizontal resolution, using the Snow17 conceptual snow model which has been used by the National Weather Service River Forecast System (NWSRFS) since the 1970's (E. Anderson, 2006). The results of which are presented in this subsection and Eythorsson et al., (2023b).

3.5.1 Methods

As discussed in Section 2.3 of this dissertation there exists a wide selection of snow models which have been developed for a range of applications. In Eythorsson et al. (2023b) the Snow17 model (Anderson, 2006) was selected since: it has low input data requirements (temperature and precipitation); it has an extensive record of operational use with the National Weather Service River Forecast System (NWSRS); it provides estimates of many key snow variables which are empirically approximated; and it has been applied to several regional studies on climate change impacts to snow resources (e.g. Miller et al., 2011; Notaro et al., 2014).

The Snow17 model is a conceptual snow accumulation and snow melt model simulates the most relevant processes that occur within a snowpack, including heat storage, water retention, transmission of liquid water and snow melt. The model simulates these key processes based on a temperature index approach and the only data inputs required are temperature and precipitation. The Snow17 model simulates the snowpack as a single layer and can be applied to point measurements or in a distributed grid. The outputs of the Snow17 model are the Snow Water Equivalent (SWE) of stored snow and the outflow (precipitation runoff and snowmelt) in each grid point for each time step with which the model is run.

Tools and datasets

In Eythorsson et al. (2023b), Google Earth Engine (GEE) (Gorelick et al., 2016) was used to access the data used in the study, to perform the model simulations as well as to perform all spatio-temporal and statistical analysis of the results. ArcMap 10.7.1 was used to produce the illustrations of the results presented in the Article and this section. Table 3-6 summarizes the datasets used in Eythorsson et al. (2023b).

Table 3-6 Datasets used for snow modelling and parameter estimation and model evaluation (from Eythorsson et al. 2023b)

Dataset	*Description*	*Purpose*	*Reference*
MOD10A1 v006	MODIS/Terra snow cover product.	Model evaluation	(D. K. Hall, Salomonson, & Riggs, 2016)
GLDAS-2	Global daily hydro- meteorological data	- Model evaluation - Model forcing - Parameter estimation	(Rodell et al., 2004)
NASA NEX-GDDP	Ensemble of 21 daily downscaled and bias corrected GCMs from the CMIP5 project.	Model forcing	(Thrasher et al., 2006)
GTOPO30	Global Digital Elevation Map (DEM)	Parameter estimation	(LP-DAAC, 2004)
GLCF	Global Land Cover Data	Parameter estimation	(Sexton et al., 2013)
WGS43261	Arctic permafrost map	Parameter estimation	(Brown et al., 2002)

Parameter estimation

The Snow17 model requires eleven model parameters to operate. These model parameters must be specified by the user of the model and if the model is run in a distributed fashion, the model parameters must be evaluated in each grid cell to which the model is applied. In Eythorsson et al., (2023b), model parameters were determined based on previously published guidelines for the Snow17 model depending on local conditions, as estimated from global hydro-climatological datasets. The following are descriptions of the Snow17 model parameters along with the methodology applied to parameter estimation for each. The parameter values and source methodology used for the parameter estimation in Eythorsson et al. (2023b) are summarized in Table 3-7.

Table 3-7 Snow17 parameters, description, value ranges and estimation methodology (from Eythorsson et al. 2023b)

Parameter	Description	Range	Units	Methodology
GCF	Gauge under-catch factor	1.0	-	Andersson, (2006)
MFMAX	Maximum Melt Factor	0.7 – 2.4	mm/°C*6h	Mizukami & Koren, (2008)
MFMIN	Minimum Melt Factor	0.001 – 1.5	mm/°C*6h	Mizukami & Koren, (2008)
UADJ	Average wind during rain on snow	0.02 – 0.4	mm/mb	Andersson, (2006)
PXTEMP	Temperature determining rain/snow	-1 – 3	°C	Andersson, (2006)
MBASE	Base temp. where melt occurs	0	°C	Andersson, (2006)
NMF	Maximum negative melt factor	0.05 – 0.3	mm/°C*6h	Andersson, (2002)
TIPM	Antecedent temperature index	0.05 – 0.2	-	Andersson, (2002)
PLWHC	Liquid water holding capacity	0.02 – 0.3	%	Andersson, (2002)
DAYGM	Constant basal melt rate	0 – 0.3	mm/day	Andersson, (2006)

Gauge Catch Factor (GCF)

The GCF corrects the amount of new snow recorded for each time step to account for gage catch deficiency, blowing snow across areal divides and sublimation. The forcing datasets that were used in this project do not suffer from gage catch deficiencies since the GLDAS precipitation is estimated from satellite observations (Matthew Rodell et al., 2004) and the NASA-NEX GDDP dataset is downscaled and bias corrected using the GMFD dataset which has been corrected for gauge undercatch errors (Sheffield et al., 2006). Also, when simulation across long time periods with multiple snow fall events, gage catch efficiencies can be assumed to cancel out (E. Anderson, 2006). When simulation snow cover across large areas, the amount of snow transferred across areal divides can be assumed to be negligible (Anderson, 2002). The GCF was therefore set to be 1 globally in Eythorsson et al., (2023b).

Maximum Melt Factor (MFMAX)

The Snow17 model uses a melt factor to estimate the amount of surface snowmelt that occurs based on air temperature, precipitation volume and precipitation temperature (Anderson, 2006). The melt factor oscillates sinusoidally between a maximum value, MFMAX, which occurs at the summer solstice (21st of June) and a minimum value, MFMIN, which occurs at the winter solstice (21st of December). MFMAX was estimated for each model grid cell based on the average surface energy balance in that grid cell, as proposed by Mizukami & Koren, (2008), as described by Equation 3.5.1 :

$$MFMAX = \frac{1.03 * (1 - g) * R_{DB} + 2.04 + 0.42 * u}{2(R + 1)} \quad (3.5.1)$$

Where g is the percent forest cover in each grid cell, R_{DB} is the ratio between solar insolation at ground level with topography and without topography, R is the ratio between solar insolation in the winter and in the summer and u is the wind speed at 10m above the surface. The percent forest cover in each grid cell, g, was estimated based on the tree canopy cover dataset from the Global Land Cover Facility (GLCF) (Sexton et al., 2013). In Eythorsson et al., (2023b), R_{DB} was estimated in a distributed grid using the methods of McCune & Keon, (2002) and elevation data from the Global Digital Elevation Map (GTOPO30) dataset (LP-DAAC, 2004). To estimate R, the average winter and summer solar insolation were estimated in a distributed grid as the net average incident shortwave radiation in winter (December-February) and summer (June-August) from the GLDAS dataset (Matthew Rodell et al., 2004) for the period 1950-1999. The average wind speed, u, was estimated in a distributed grid as the mean wind speed in June from the GLDAS dataset for the period 1950-1999.

Minimum Melt Factor (MFMIN)

MFMIN occurs on the winter solstice and represents the smallest value of the melt factor in each grid cell over the year as it occurs at a time with the lowest amount of surface radiation. In Eythorsson et al., (2023b), MFMIN was estimated in a distributed grid based on the local Surface Energy Balance (SEB) according to the methods proposed by Mizukami & Koren, (2008), as described by Equation 3.5.2:

$$MFMIN = R * MFMAX \quad (3.5.2)$$

Where R is the ratio between solar insolation in the winter and in the summer, which estimated as the ratio between the net average incident shortwave radiation in winter (December-Feb) and summer (June-August) from the GLDAS dataset for the period 1950-1999.

Snow cover Index (SI)

SI is a model parameter which describes the mean areal Snow Water Equivalent (SWE) above which there is always 100% areal snow cover. In Eythorsson et al., (2023b), the SI parameter was set at 999 mm globally based on the guidelines presented in Anderson, (2002). As the model resolution is course enough that a range of topography can reasonably be expected in each grid cell the SI parameter was not distributed spatially.

Areal Depletion Curve (ADC)

The ADC is a curve that defines the areal extent of snow cover as a function of how much of the original snow remains after significant bare ground has opened after a melt event and thus implicitly accounts for the reduction in areal melt rates as less area is covered by snow. In Eythorsson et al., (2023b) the ADC was varied linearly between 0-1 based on the ratio of the SWE state variable at each model timestep in each grid cell and SI according to the guidelines in Andersson., (2006) as described by Equation 3.5.3:

$$ADC = MAX\left(1, \frac{SWE}{SI}\right) \quad (3.5.3)$$

Adjusted wind speed (UADJ)

UADJ describes the average wind function during rain on snow events and is used in the model to estimate the sensible and latent heat transfer components of the snowpack SEB. In Eythorsson et al., (2023b) UADJ was estimated in a distributed grid based on the guidelines presented in Andersson., 2002, as described by Equation 3.5.4:

$$UADJ = 0.002 * u_1 \quad (3.5.4)$$

Where u_1 is the six-hour wind travel in km, one meter above the snow surface. In Eythorsson et al., (2023b), UADJ was estimated as the average wind speed from the GLDAS wind field for the period 1950-1999.

Precipitation Partition (PXTEMP)

The portion of precipitation that falls as snow vs. rain is described by the model parameter PXTEMP. The form of precipitation varies based on air temperature and below a set value, PXTEMP1, all precipitation falls as snow and above a set value, PXTEMP2, all precipitation falls as rain. In Eythorsson et al., (2023b) PXTEMP1 was set to -1°C and PXTEMP2 was set to 3°C globally and between these values the PXTEMP parameter was varied linearly, based on the guidelines presented in Anderson, (2006).

Melting Point Temperature (*MBASE*)

MBASE is to determine the temperature gradient for non-rain melt computations and represents the temperature at which snow begins to melt. In Eythorsson et al., (2023b) the MBASE parameter was set to 0°C globally, based on the guidelines presented in Anderson, (2006)

Negative Melt Factor (*NMF*)

The negative melt factor is used in the Snow17 model to determine the energy exchange at the snow-air boundary when melt is not occurring, and it has the same seasonal variation as the non-rain melt factor. Andersson, 2002, recommends a maximum NMF range of 0.05 to 0.30, where lower NMF values are associated with areas where the average snow density is less than 0.3 g/ml and higher values associated with areas where snow density is generally higher than 0.5 g/ml. In Eythorsson et al., (2023b), snow density was estimated in a distributed grid from the snow depth and snow water equivalent from GLDAS-2 for the period 1950-1999. For areas with low snow densities (<0.3 g/ml) NMF was set to 0.05, where snow density was high (>0.5 g/ml) NMF was set to 0.3, and linearly interpolated between these values elsewhere.

Antecedent Temperature Index (*TIPM*)

TIPM is an antecedent index of snow pack temperatures near the surface. Anderson, (2002) recommends TIPM values of 0.05 for areas with generally deep snowpack (greater than 3 feet maximum depth) and values of 0.2 for areas with shallow snowpack (less than 1 foot). In Eythorsson et al., (2023b) the mean annual maximum snow depth was calculated in a distributed grid from the GLDAS-2 dataset for the period 1950-1999. For areas with deep snowpack (> 3 ft) TIPM was set to 0.05, for areas with shallow snowpack (< 1 ft) TIPM was set to 0.2 and for areas with medium snowpack (1ft < & < 3ft) TIPM was interpolated linearly.

Physical Liquid Water Holding Capacity (*PLWHC*)

PLWHC is given as the decimal fraction of ice in the snow. Anderson, (2002) recommends *PLWHC* values between 0.02 and 0.05 with the lower values associated with areas with deep snow cover. In Eythorsson et al., (2023b) the mean annual maximum snow depth was estimated in a distributed grid from GLDAS for the period 1950-1999. For areas with deep snowpack (> 3 ft) PLWHC was set to 0.02, for areas with shallow snowpack (< 1 ft) PLWHC was set to 0.05 and for medium snowpack (1ft < & < 3ft) PLWHC was interpolated linearly between these values.

Basal Melt Rate (*DAYGM*)

DAYGM describes the constant daily amount of melt at the ground snow interface (mm/day). Anderson, (2002) recommends DAYGM values between 0 for generally frozen soils to 0.3 in areas with intermittent snow cover or temperate climates. In Eythorsson et al., (2023b) frozen soils were identified using the NH permafrost map from the National Snow and Ice Data Center (Brown et al., 2002). In areas with continuous permafrost DAYGM was set to 0.0, in areas with discontinuous permafrost DAYGM was set to 0.1, in isolated patches of permafrost DAYGM was set to 0.2 and in other areas DAYGM was set to 0.3.

Model Evaluation

In Eythorsson et al., (2023b) the Snow17 model results were evaluated based on distributed historical data on the Northern Hemisphere (NH) Snow Water Equivalent (SWE) and Snow-Covered Area (SCA). The model was run with two different forcing datasets for evaluation purposes: i) NASA NEX-GDDP and ii) GLDAS-2. The simulated snow conditions were compared to a) SCA from the MODIS/TERRA snow cover dataset (MOD10A1.v006). b) SCA calculated from the GLDAS-2 dataset and c) SWE from the GLDAS-2 dataset. The model was evaluated for the period of the 2004 water year. This year was selected as it is in the overlap between the data availability of MODIS/TERRA (2001- 2020), GLDAS-2 (1948-2010) and historic GDDP data (1950-2006) and it had an average SWE across the NH within that period of overlap.

The model was forced with both the NASA NEX-GDDP dataset and the GLDAS-2 dataset for the historical period to i) compare the accuracy of snow conditions simulated using bias corrected GCM results and simulations based on an assimilated data product that incorporates satellite- and ground based observational data with land surface modelling and data assimilation techniques and ii) to assess the NASA-NEX GDDP results in light of the model's capability to replicate the GLDAS-2 SWE field, using forcing data from that same dataset.

The correlation between the simulated and observed daily SWE and SCA was estimated by calculating the Pearson's Correlation coefficient, R, for all combinations of

simulations and observations. The ratio between the root mean square error and the standard deviation (RSR) was also calculated for all combinations of simulations and observations for both SWE and SCA. Simulations were considered satisfactory if $RSR < 0.7$ as suggested by Moriasi et al., (2007).

Snow Projections

In Eythorsson et al., (2023b) the Snow17 model was run in GEE to simulate daily snow conditions across the Northern Hemisphere (NH) over the period 1950-2100 in a 0.2° horizontal resolution. The model was forced with daily temperature and precipitation data from the ensemble of the 21 downscale and bias corrected GCM results from the CMIP5 study, as contained in the NASA-NEX GDDP dataset. The model was initialized at the beginning of each water year during the study period so that it would not store water between years.

3.5.2 Results

Model Evaluation

The model was evaluated based on both Snow Cover Frequency (SCF) and Snow Water Equivalent (SWE) for the 2004 water year. The model was run with input data from both the NASA NEX-GDDP and the GLDAS-2 datasets, the runs are referred to as ($GDDP_{sim}$) and ($GLDAS_{sim}$), respectively. Simulated SWE values were compared to GLDAS-2 SWE data ($GLDAS_{hist}$) and simulated SCA was compared to SCA estimated from both MODIS/TERRA data (MOD_{obs}) and GLDAS-2 ($GLDAS_{hist}$).

Figure 3-9 shows the Snow Cover Frequency (SCF) for the 2004 water year as estimated by: i) $GDDP_{sim}$ ii) $GLDAS_{sim}$ iii) $GLDAS_{hist}$ and iv) MOD_{obs}

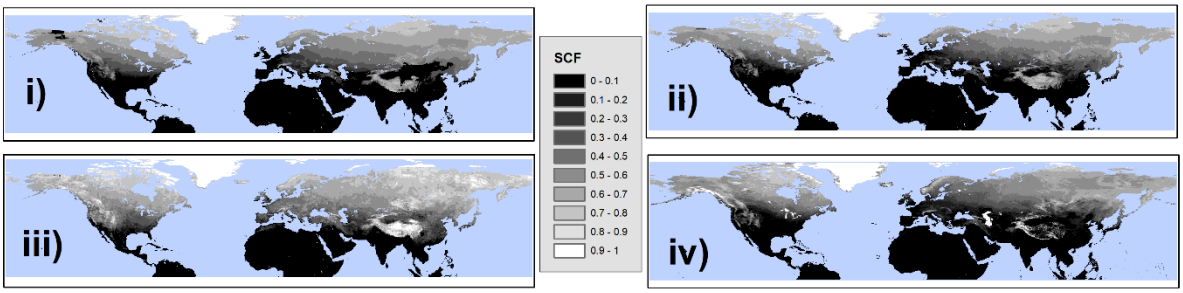

Figure 3-9 Snow Cover Frequency (SCF) for the 2004 water year, i) as simulated using the ensemble average of the NASA NEX-GDDP dataset ($GDDP_{sim}$), ii) as simulated using GLDAS-2 data ($GLDAS_{sim}$), iii) as observed in the GLDAS-2 data ($GLDAS_{hist}$) and iv) as observed by MODIS/TERRA (MOD_{obs}) (from Eythorsson et al. 2023b)

Figure 3-9 shows similar snow cover patterns across the four SCF estimates. However, there are a few minor discrepancies: In $GDDP_{sim}$ (i) there is a lack of snow cover in north-eastern Alaska due to minimal precipitation in this area, this is also visible in $GLDAS_{sim}$ (ii), though less pronounced. The largest SCF values were observed in $GLDAS_{hist}$ (iii), which especially showed a higher SCF on the Tibetan plateau. In general, MOD_{obs} (iv) was more consistent with the simulated SCF than $GLDAS_{hist}$.

Figure 3-10 shows the mean annual SWE for the 2004 water year as estimated by: i) $GDDP_{sim}$: ii) $GLDAS_{sim}$ iii) $GLDAS_{hist}$. Note that the $GLDAS_{hist}$ shows the full depth of the

Greenland glacier and thus the SWE data are not comparable there. As depicted in Figure 3-10 there were similar SWE patterns between the three SWE estimates. The highest values were consistently observed in Southern Greenland as well as in coastal regions around the Northern Atlantic Ocean and the pacific northwest in Northern America. The results show that $GLDAS_{hist}$ has generally lower SWE values as compared to both $GLDAS_{sim}$ and $GDDP_{sim}$. This may not be surprising as studies have shown that the GLDAS-2 snow field has a negative bias as compared to most other global SWE products (Mudryk et al., 2015).

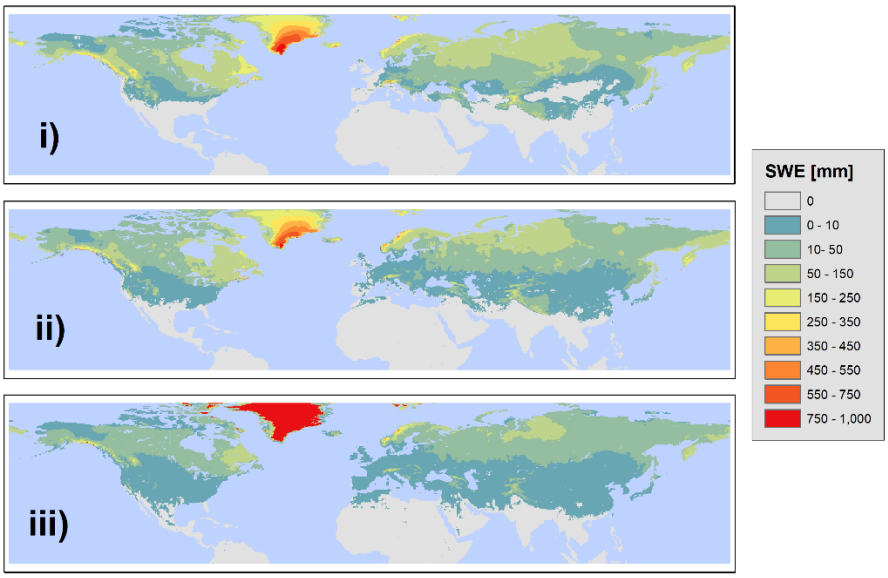

Figure 3-10 Mean annual SWE for the 2004 water year, i) as simulated using the ensemble average of the NASA NEX-GDDP dataset ($GDDP_{sim}$), ii) as simulated using the GLDAS-2 dataset ($GLDAS_{sim}$) and iii) as observed in the GLDAS-2 dataset ($GLDAS_{hist}$) (from Eythorsson et al., 2023b).

Figure 3-11 shows the correlation between simulated and observed daily SCA for the 2004 water year, as estimated by Pearson's Correlation coefficient, R, for the correlations between i) $GDDP_{sim}$ and $GLDAS_{hist}$ ii) $GDDP_{sim}$ and MOD_{obs} iii) $GDDP_{sim}$ and $GLDAS_{sim}$ iv) $GLDAS_{sim}$ and MOD_{obs} v) $GLDAS_{sim}$ and $GLDAS_{hist}$ and vi) $GLDAS_{hist}$ and MOD_{obs}.

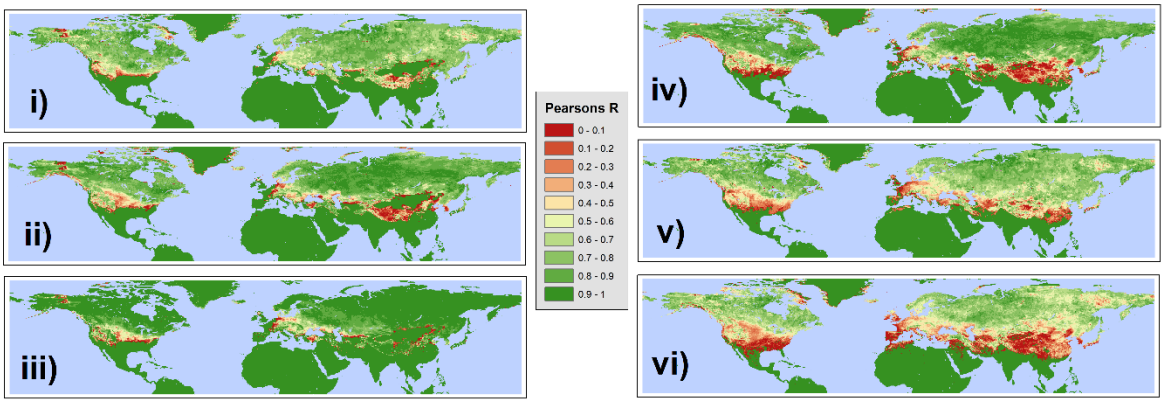

Figure 3-11 Pearson's Correlation, R, for daily SCA values over the 2004 water year as estimated between: i) $GDDP_{sim}$ and $GLDAS_{hist}$ ii) $GDDP_{sim}$ and MOD_{obs} iii) $GDDP_{sim}$ and $GLDAS_{sim}$ iv) $GLDAS_{sim}$ and MOD_{obs} SCA v) $GLDAS_{sim}$ and $GLDAS_{hist}$ and vi) $GLDAS_{hist}$ and MOD_{obs}.

The results in Figure 3-11 indicate that the lowest correlations were observed between the two observed data products, MOD_{obs} and $GLDAS_{hist}$ (vi). Generally, lower correlations were observed for the comparison between $GLDAS_{sim}$ and observations (v and iv) than for the comparison between $GDDP_{sim}$ and observed values (i and ii). The highest correlations were observed between the two simulated products (iii)). Consistently in all estimations, the lowest correlations are observed in areas close to the southern edge of the snow boundary, where freeze and thaw cycles are frequent. This is unsurprising as these areas have the most complex snow cover dynamics.

Figure 3-12 shows the correlation between simulated and observed daily SWE for the 2004 water year, as estimated by Pearson's Correlation coefficient, R, for the correlations between i) $GDDP_{sim}$ and $GLDAS_{hist}$ ii) $GDDP_{sim}$ and $GLDAS_{sim}$ and iii) $GLDAS_{sim}$ and $GLDAS_{hist}$.

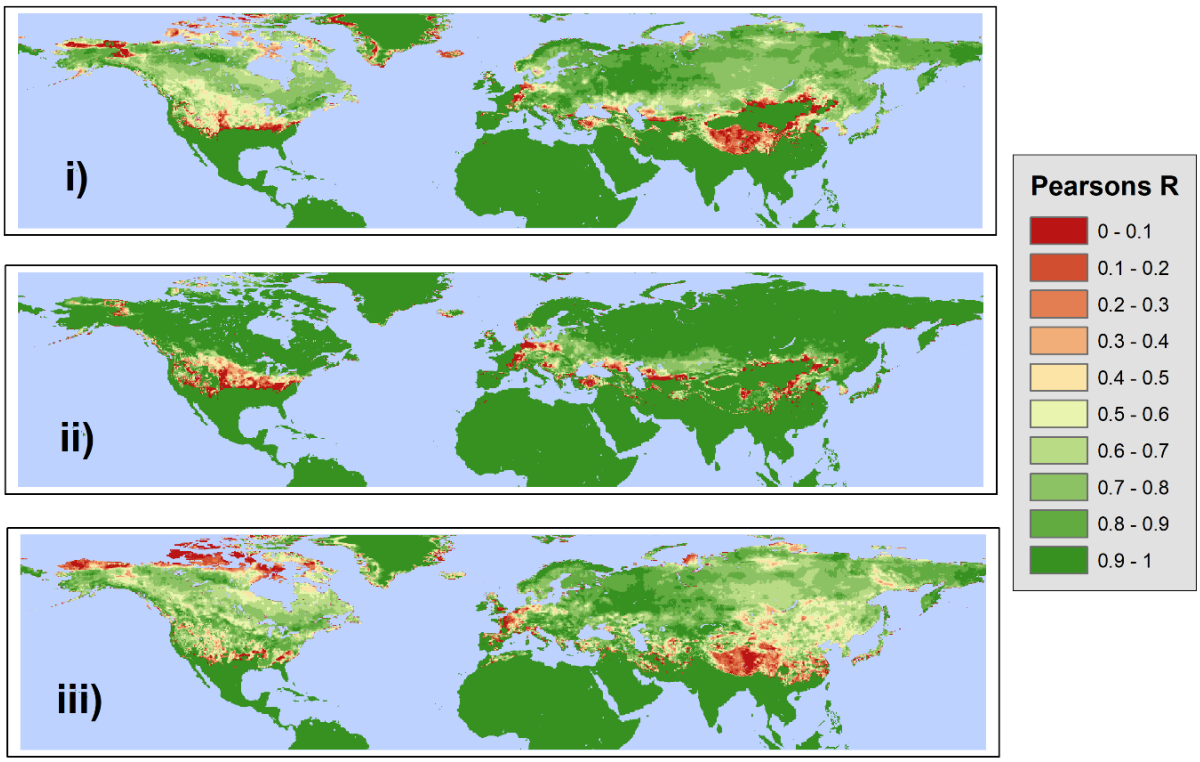

Figure 3-12 Pearson's Correlation, R, for daily SWE values during the 2004 water year as estimated between i) $GDDP_{sim}$ and $GLDAS_{hist}$ ii) $GDDP_{sim}$ and $GLDAS_{sim}$ and iii) $GLDAS_{sim}$ and $GLDAS_{hist}$

Figure 3-12 shows that the highest correlations were observed between the two simulated products (Fig 5-i)). The results showed that the highest inconsistencies between simulated and observed SWE are: on the Tibetan Plateau, the north Shore of Alaska and the Canadian Arctic Archipelago as well as in areas close to the southern edge of the snow boundary, where freeze and thaw cycles are frequent. These areas have in common that the average annual SWE is low and as is the absolute volume of precipitation that falls as snow.

The correlation between $GLDAS_{sim}$ and $GLDAS_{hist}$ was notably lower than the correlation between the $GDDP_{sim}$ and $GLDAS_{hist}$ as Figure 3-12 shows.

The model evaluation showed that the model produced similar SCA and SWE patterns as those observed by MODIS/Terra and GLDAS-2 snow cover data, as illustrated in Figure 3-9 and Figure 3-10. The correlations between simulated and observed daily SWE and SCA

values are high in most regions of the NH as depicted in Figure 3-11 and Figure 3-12. This suggests that the model provides as good an estimate of NH SCA and SWE as do either of the observed products. In terms of the evaluation metric RSR, the model provided satisfactory results when compared to SWE and SCA observations. Thus, the model is expected to provide a reasonable estimate of future snow conditions when forced with climate projections.

Projecting future snow conditions

The average annual number of Snow-Covered Days (SCD) was calculated for the first and last quarter centuries of the dataset, the 3rd quarter of the 20th century 1950-1975 and the 4th quarter of the 21st century 2075-2100, respectively.

Figure 3-13 shows i) the mean SCD for 1950-1975 ii) the percentage change in SCD between 2075-2100 and 1950-1975 under RCP45 and iii) same as ii) but for RCP85.

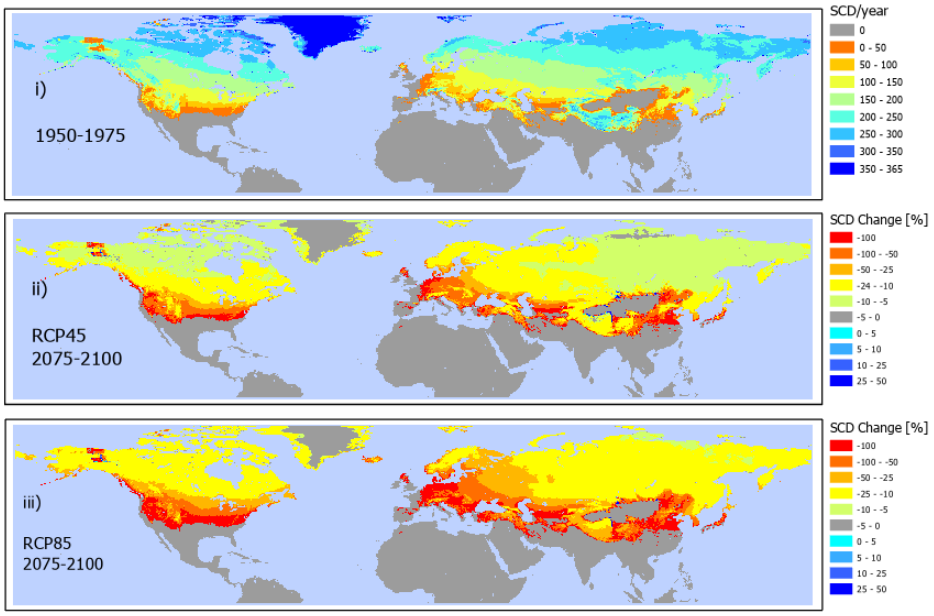

Figure 3-13 i) Mean number of Snow-Covered Days (SCD) for the period 1950-1975, ii) percentage change in SCD between 2075-2100 and 1950-1975 under RCP45 and iii) same as ii) but for RCP85 (from Eythorsson et al., 2023b).

The results shown in Figure 3-13 indicate that the frequency of snow cover is expected to decrease during the present century, across the NH. The only areas that show an increasing SCD are on the border of the Tibetan Plateau and the Gobi Desert. Snow cover is expected to disappear almost completely in many mid-latitude areas at the periphery of the current seasonal snow extent. Large regions in Central Europe, Northern Middle East, Northern China as well as in the Northern part of the conterminous USA are expected to be mostly snow free throughout the year by the end of the present century. Even in the northern Arctic SCD is expected to decrease by up to 25% given a “business-as-usual” emission scenario (RCP85).

The average annual Snow Water Equivalent (SWE) was calculated for the first and last quarter centuries of the dataset, respectively. Figure 3-14 shows i) the mean winter (SWE)

for 1950-1975, ii) the percentage change in SWE between 2075-2100 and 1950-1975 under RCP45 and iii) same as ii) but for RCP85.

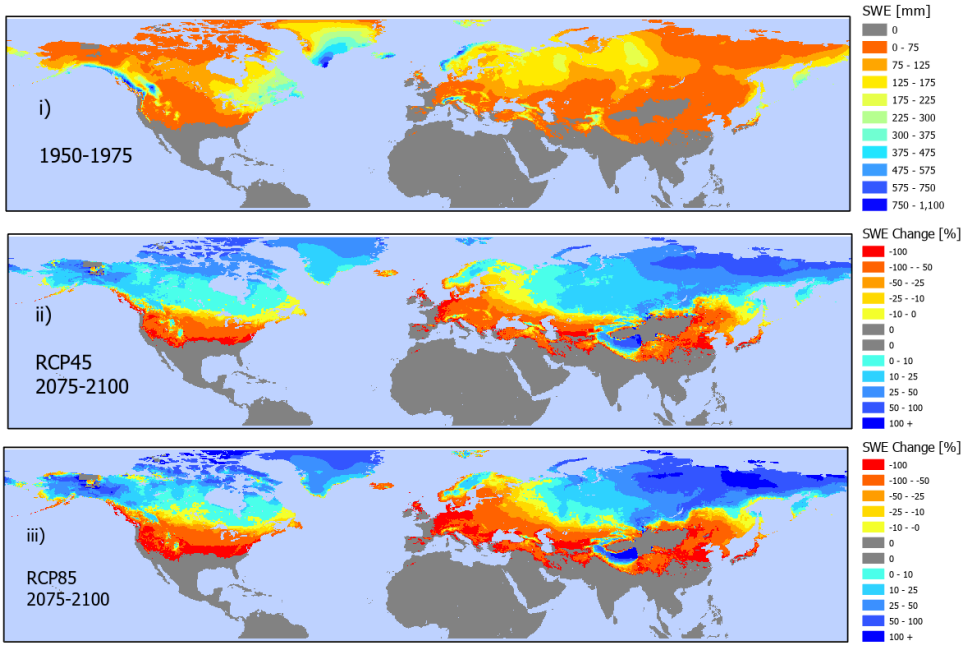

Figure 3-14 1 Snow Water Equivalent (SWE) for the period 1950-1975, ii) percentage change in SWE between 2075-2100 and 1950-1975 under RCP45 and iii) same as ii) but for RCP85 (from Eythorsson et al., 2023b).

Figure 3-14 shows that the mean winter SWE is expected to decrease in mid latitude areas of the NH during the present century. At higher latitudes however SWE is expected to increase, in some cases by more than 100%. The biggest relative increase in SWE is expected to occur in the high Arctic areas around the Bering strait, eastern Siberia and the north-western coast of North America as well as in the western Tibetan Plateau. These increases are more pronounced under a "business-as-usual" emission scenario (RCP85) than under a scenario where global radiative forcing due to anthropogenic GHG emissions is expected to stabilize around mid-century (RCP45). The decreasing SWE at lower latitudes is likewise expected to be more pronounced given RCP85 compared to RCP45.

Figure 3-15 shows the simulated NH average 1st April SWE over the period 1950-2100 (left panel) and the NH average annual SCF over the same period (right panel). The results show that under the RCP85 scenario SCF is expected to decrease nearly linearly throughout the present century, whereas given RCP45 the SCF is expected to stabilize at about 85% of 1950-1975 levels by the end of the 21st century. 1st April SWE is expected to increase slightly in the beginning of the period and then start to decline by about 2020, back to 1950-1975 levels under RCP45 and to 10% under those levels under RCP85.

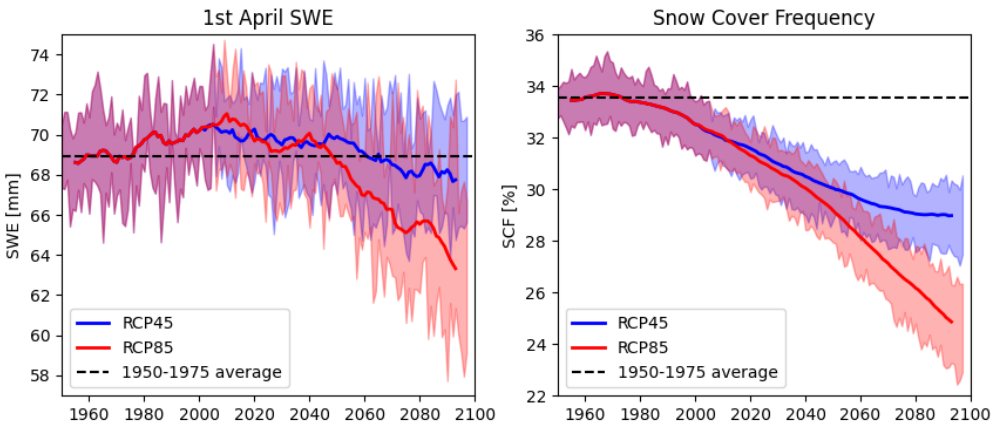

Figure 3-15 Annual Snow Cover Frequency (SCF) (right) and 1st of April Snow Water Equivalent (SWE) across the NH (left). The shaded areas represent the upper and lower quantiles of the ensemble simulations, and the solid line a 10-year moving average. (From Eythorsson et al., 2023b).

Figure 3-15 also shows that the frequency of snow cover is expected to decrease significantly throughout the 21st century given both emission scenarios. Figure 3-14 shows that most of this decrease will occur at lower latitudes where seasonal snow cover become less frequent. Figure 3-15 shows that this decrease in SCD is already underway, which is in an agreement with several earlier studies which have found decreasing snow cover in the NH in recent decades (Darri Eythorsson et al., 2019; Hori et al., 2017; Yunlong et al., 2018). Figure 3-15 also shows that despite decreasing SCF the NH 1st April SWE is expected to increase over the 21st century. Figure 3-14 shows that this increase is driven by increasing SWE in the Arctic, whereas at lower latitudes, SWE is decreasing.

This increase in snow in the high arctic is attributed to increasing precipitation, which in turn stems from decreasing sea-ice concentrations in the Arctic Ocean, which brings more atmospheric moisture to these areas. The increasing SWE at high latitudes is consistent with prior findings (e.g. Kopec et al., 2016; Singarayer et al., 2006). The results of this study show that under RCP45, increased precipitation in high latitude areas will result in an increasing 1st April SWE throughout the 21st century, whereas under RCP85 the NH 1st April SWE will peak in second half of the century as the declining snowpack at lower latitudes overtakes the increasing arctic SWE. This pattern of decreasing SWE at lower latitudes and increasing SWE in the Arctic has been observed in previous studies (e.g. Wang et al., 2018).

Eythorsson et al. (2023b) calculated the relative change in both SWE and SCD (in %) between 1950-1975 and 2075-2100 in some of the largest snow-impacted watersheds of the NH. Figure 3-16 shows the study basins, color coded by the change on 1st April SWE. Blue colored basins showed more than 10% increase in SWE, red colored basins showed more than 10% decrease in SWE while grey basins showed less than 10% change in SWE, under the RCP45 emission scenario.

Figure 3-16 Changes to 1st April SWE in the study basins selected in Eythorsson et al., (2023b). Blue basins showed more than 10% increase in SWE, red basins showed more than 10% decrease in SWE while grey basins showed less than 10% change in SWE, under the RCP45 emission scenario (from Eythorsson et al., 2023b).

Table 3-8 shows the relative average change in SWE and SCD between 1950-1975 and 2075-2100 in the river basins selected in Eythorsson et al. (2023b). The basins where mean winter SWE is expected to increase by more than 10% under RCP45 are colored blue, likewise the basins where SWE is expected to decrease by more than 10% are colored red, basins where SWE is expected to change by less than 10% are colored grey.

Table 3-8 Relative change in SWE and SCD (in %) between 1950-1975 and 2075-2100 in the study basins. Basins colored blue have more than 10% increase in mean winter SWE over the period, red colored basins showed more than 10% decrease in SWE and grey colored basins had less than 10% change in SWE, under the RCP45 emission scenario (from Eythorsson et al., 2023b).

Basin	*RCP45*		*RCP85*	
	Δ SWE [%]	*Δ SCD [%]*	*Δ SWE [%]*	*Δ SCD [%]*
Indigirka	56.7	-6.4	97.3	-10.9
Kolyma	46.5	-6.5	74.1	-11.4
Lena	31.8	-7.2	52.5	-12.5
Yukon	33.4	-14.0	48.4	-20.9
Ob	28.4	-9.2	18.7	-19.2
Yenisey	26.4	-7.8	42.0	-14.7
Mackenzie	12.3	-9.0	14.3	-16.2
Volga	2.5	-15.9	-9.8	-30.2
Dalälven	-3.9	-15.6	-22.6	-33.4
Fraser	-4.9	-20.2	-29.1	-36.6
Saskatchewan-Nelson	0.5	-12.9	-12.6	-23.6
Indus	-4.0	-14.6	-7.1	-23.1
Mekong	-8.0	-5.0	-11.8	-9.5
Ganges-Brahmaputra	-15.7	-12.9	-20.8	-18.7

St. Lawrence	-19.8	-20.9	-44.0	-43.7
Amur	-25.8	-20.0	-42.9	-26.4
Don	-24.1	-21.7	-61.6	-48.1
Dnieper	-34.7	-25.9	-84.0	-68.5
Yangtze	-27.0	-21.3	-31.4	-26.3
Seine	-46.8	-45.8	-46.9	-45.9
Colorado	-43.0	-40.7	-53.2	-51.3
Columbia	-55.9	-53.5	-73.2	-72.4
Mississippi	-58.4	-48.7	-73.4	-66.4
Rhone	-76.8	-70.6	-81.4	-76.9
Danube	-78.8	-67.5	-92.8	-89.0
Rhine	-94.3	-91.2	-97.5	-97.0
Vistula	-81.3	-58.7	-99.0	-96.2
Oder	-95.9	-90.9	-99.5	-99.0
Elbe	-92.0	-81.6	-99.8	-99.0

Figure 3-16 shows that all study basins flowing to the Arctic Ocean are expected to experience a more than 10% increase in mean winter SWE whereas in lower latitude basins SWE are mostly expected to decrease. This decrease is most pronounced in mid-latitude rivers of central Europe (Elbe, Oder, Rhone, Vistula, Danube and Dneiper) and North America (Mississippi, Columbia, and Colorado). Basins of the Himalaya region are expected to experience both decreasing SCD and SWE, however, not as pronounced as in the central European and North American basins.

Table 3-8 shows that in all basins the SCD is expected to decrease during the study period, under both emission scenarios. The decrease is greater under the RCP85 scenario than under RCP45, with some basins expected to experience an almost complete loss of snow cover given the business-as-usual (RCP85) scenario. Table 3-8 shows that despite decreasing SCD the 1st of April SWE is expected to increase in all the northernmost basins. This is attributed to increasing precipitation, as these historically arid areas receive more atmospheric moisture as sea ice cover decreases and more open water is exposed (eg. Kopec et al., 2016; Singarayer et al., 2006).

The declining snow pack in the basins in the subarctic North America has been well documented (e.g. Kang et al., 2016; Mote et al., 2005). A recent study showed that across the conterminous United States both SWE and SCD decreased significantly over the period 1982-2016 (Zeng et al., 2018) which is consistent with the results of this study. Previous studies on snow resources in the Himalaya region have shown decreasing frequency of snow cover as well as decreasing snow storage and snow melt runoff (Maurer et al., 2019; Stigter et al., 2017), which are consistent with the findings of the present study. A recent study of in-situ snow depth measurements found that the mean snow depth had decreased by 12% per decade over the period 1951-2017 (Fontrodona Bach et al., 2018). The increasing snowfall in Northern Eurasia has also been studied, and has been shown to have decreased the length of the growing season (Vaganov et al., 1999). In the Arctic region, the results of this study are consistent with prior studies which have found increasing snow cover (e.g. Cohen et al., 2012; Eythorsson et al., 2019) and snow storage (Callaghan et al., 2011) in recent decades. The findings presented in Eythorsson et al. (2023b) show that these observed

trends, decreasing snow resources at lower latitudes while increasing in the Arctic, will continue at a steady or increasing pace, at least for the next few decades.

3.6 Analyzing historical and predicted snow cover and climate trends – a case study for Iceland

Snow and ice are key components of the Icelandic ecology and hydro-climatology. Understanding how these resources are likely to respond to local climate changes is among the most important questions facing water resources managers and other natural resources planners in Iceland. Icelandic snow resources are highly sensitive to changes in the local climate as has been demonstrated (e.g. Bjornsson & Palsson, 2008; Eythorsson et al., 2018). In many of the cold regions of the Northern Hemisphere (NH) snow resources have undergone significant changes in recent decades, due to climate trends which are expected to continue throughout the 21st century at least, e.g., as shown in Eythorsson et al., (2019). Furthermore, Eythorsson et al., (2023b), showed that NH snow resources are generally expected to undergo significant further changes under all plausible emissions scenarios. Although these trends do have grave global implications in a myriad of ways, the practical adaptation to them must occur on a local scale. Thus, considering the aim of this dissertation, the trends in the climate and snow regimes were analyzed in terms of a local context with a case study for Iceland. The results of which are presented in this subsection and published in Eythorsson et al., (2023a).

3.6.1 Historical Snow Cover Trends

In situ observations

The Icelandic Meteorological Office (IMO) collects most in-situ meteorological observations in Iceland. Part of IMO routine measurements are daily manual observations of snow cover at 9am. The locations of these observation sites are shown in Figure 3-17. The figure notably shows how sparse these observational sites are, especially in the central highlands where most of the countries snow resources are located. Data were acquired from the IMO from a total of 266 manned sites over the period 1930-2021. Data includes observations of local snow depth (*SND),* Snow Cover (*SNC*), precipitation (*R*), precipitation class (*RTEG*), and a visual estimate of surrounding mountain snow cover (*SNCM*) (Icelandic Meterologocial Office, 2021). Snow depth, in cm, is measured for all days with snow covered ground at the monitoring site. SNC and SNCM are visually classified as: 0 = no snow, 2 = patchy snow cover, 4 = fully covered ground. (Icelandic Meterologocial Office, 2008). Gunnarsson et al. (2019), compared the IMO snow cover data to the MODIS snow cover products and observed a good agreement between the two datasets.

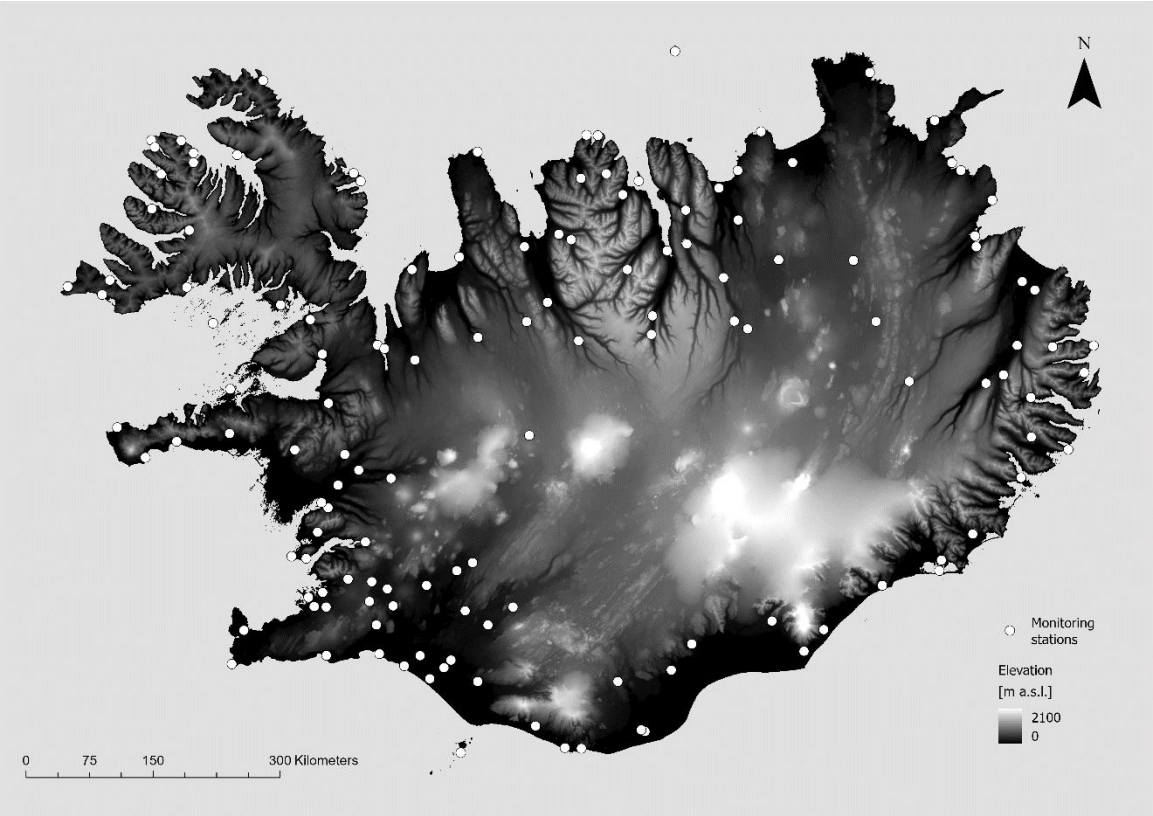

Figure 3-17 Topographical map of Iceland and the locations of the Icelandic Meteorological Office (IMO) observation stations where snow data recorded (from Eythorsson et al., 2023a)

The annual SCF was calculated for all stations by summing the number of snow-covered days and dividing by the number of observations for each year. The significance of the trendline in SCF over time was assessed for all stations which had more than 10 years of observations within the data period (2000-2016) using the non-parametric Mann-Kendall hypothesis test. The null hypothesis H_0 was that there is no trend in the data and the alternative hypotheses are that there is a statistically significant increase (H_1) or decrease (H_2) in the SCF.

Figure 3-18 (left panel) shows the average temperature and precipitation in Iceland over the period 1950-2021 as estimated from the ensemble average of the GDDP dataset and the average of an ensemble of long-term IMO station observations (Icelandic Meterological Office, 2023). The figure shows similar trends and averages in temperature and precipitation from both data sources. Figure 3-18 (center panel) shows the annual average SCF for all IMO monitoring stations for the period 1930-2021, calculated for local (circles) and mountain (triangles) snow cover based both on just observations of fully snow-covered ground (SNC or SNCM = 4) and including patchy snow cover (SNC or SNCM ≥ 2), the in-situ data is shown with a 10-year rolling average and a linear trendline. The figure shows the average annual SCF estimated from the MODIS TERRA/AQUA snow cover products (black markers) for observations above (stars) and below (crosses) 500 m a.s.l. Figure 3-18 (right panel) shows the average annual snow depth (SND) of all IMO monitoring stations for the period 1930-2021 along with a linear trendline. Note that most IMO stations are in the lowlands, which on average see less snow cover than the interior highlands, where the most snow is.

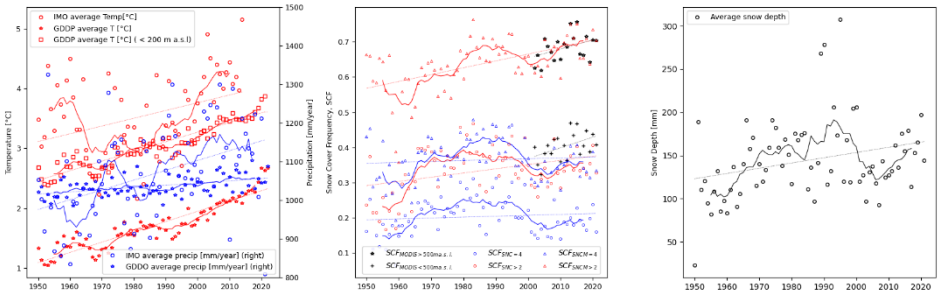

Figure 3-18 Left panel: Average annual temperature and precipitation in Iceland over the period 1950-2021 as estimated by the ensemble average of the 21 GCM's in the NASA NEX-GDDP dataset and the IMO. Center panel: Annual average SCF for all IMO monitoring stations for the period 1930-2021, calculated for local (circles) and mountain (triangles) snow cover for observations of fully snow covered ground, SNC or SNCM = 4 (blue) and including patchy snow cover, SNC or SNCM ≥ 2 (red), the average annual SCF estimated from the MODIS TERRA/AQUA snow cover products (black markers) is shown for observations above (stars) and below (crosses) 500 m a.s.l. Right panel: average annual snow depth of all IMO monitoring stations. (from Eythorsson et al., 2023a)

MODIS snow cover

Annual Snow Cover Frequency (SCF) was calculated with 500 m x 500 m resolution for Iceland based on the MOD10A1.005 MODIS/TERRA snow cover daily product (Dorothy K Hall, Riggs, & Salomonson, 2006) using the methods described in Eythorsson et al., (2019). The MOD10A1.005 dataset was remapped to provide a binary classification for valid observations. Observations with zenith angles > 25° were excluded to decrease the *panoramic bow tie effect* which is a panoramic distortion known to cause systematic errors in snow mapping (Souri & Azizi, 2013). Invalid observations due to cloud cover or polar night, for example, were masked by giving them a null value. The number of days a pixel is covered with snow was counted and divided by the number of valid observations of that pixel, per year. On average 60 valid observations/year per pixel were observed. The annual SCF was calculated for the period where MODIS observations are available (water years 2001-2016). The trend of annual SCF values in each pixel over the period was estimated by linear regression and Sen's estimator of slope methods. The statistical significance of the observed trend was assessed using both the non-parametric Sen's estimator of slope methods.

Figure 3-19 shows the trend in annual SCF over Iceland as estimated from MODIS observations (left) and areas where the trendline is statistically significant ($\alpha = 0.05$) for both MODIS and in situ observations (SNC = 4) (right). Blue regions and markers show areas where the SCF had increased significantly, and the red areas with decreasing SCF.

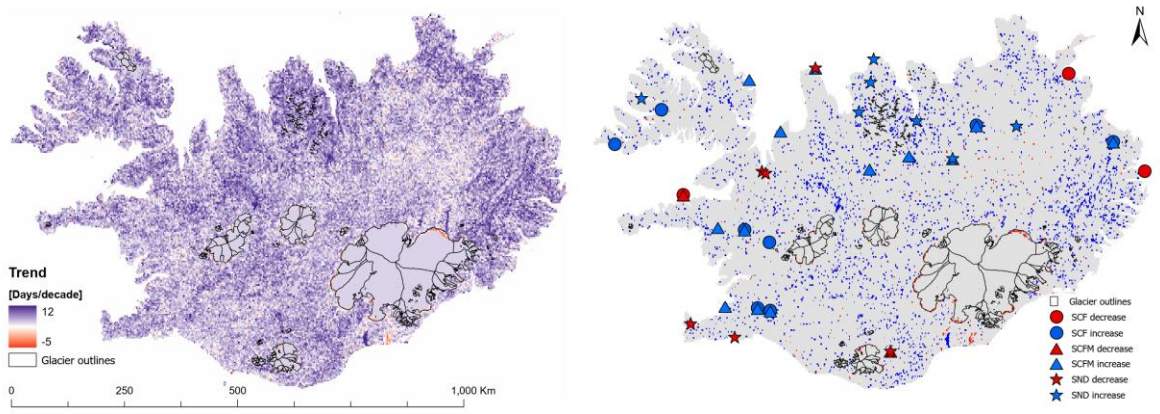

Figure 3-19 Left panel: trend in annual SCF over Iceland as estimated from MODIS. Right panel: areas where the trendline is statistically significant (α = 0.05) for both MODIS and in situ observations (SNC = 4). 2019 outlines of glaciers and the ice divides of their major outlet glaciers are shown with black lines (RGI Consortium, 2019). (from Eythorsson et al., 2023a)

Figure 3-19 show that many areas in Iceland have experienced a significant change in the local SCF, both as estimated from MODIS data and from manned snow cover observations over the period 2001-2021. Most of these areas have experienced an increase in SCF, especially the eastern highlands and the mountainous regions of Northern and Northwestern Iceland. A few small areas showed a statistically significant decrease in the local SCF over the period, these areas are located either in lowland areas or at the termini of the major outlet glaciers in Iceland, whose recession in recent years has been well documented (Aðalgeirsdóttir et al., 2020; Hauser & Schmitt, 2021).

Table 3-9 shows the statistical significance of the linear snow trends, estimated using the Mann-Kendall trend test, for both the period of historical records (1930-2021) and the MODIS period (2001-2021), of p values. Statistically significant trendlines at the α = 0.05 level are shown in bold

Table 3-9 Statistical significance of the linear snow trends, estimated using the Mann-Kendall (MK) trend test, for both the period of historical records (1930-2021) and the MODIS period (2001-2021), of p values Statistically significant trendlines at the α = 0.05 level shown in bold.

	Trend [% per year]		p-value	
	1930-2021	2001-2021	1930-2021	2001-2021
SCFM (SNCM > 2)	**0.15**	**0.43**	**$1.2 * 10^{-6}$**	**0.02**
SCFM (SNCM = 4)	0.038	0.21	0.2	0.07
SCF (SNC > 2)	**0.15**	**0.37**	**$1.8 * 10^{-6}$**	**0.01**
SCF (SNC = 4)	**0.076**	0.19	**$0.7 * 10^{-3}$**	0.06
SND	**0.081**	**0.30**	**$1.54 * 10^{-5}$**	**0.002**
MODIS below 500 m a.s.l.	**-**	**0.29**	-	**0.04**
MODIS above 500 m a.s.l.	-	0.24	-	0.11
MODIS all elevations	**-**	**0.26**	-	**0.04**

The results in Table 3-9 shows that the increasing SCF and SND trend shown in Figure 3-18 is statistically significant over the period 1930-2021 for all SCF estimates except for observations of SNCM = 4, fully snow-covered mountains. Over the MODIS period 2001-

2021 the trend is significant for all metrics except for observations of fully snow-covered mountains and for MODIS observations above 500 m a.s.l.

SCF in areas of recent land surface changes.

The annual SCF values were extracted for three locations in Iceland where land surface changes had physically impacted the local SCF during the MODIS period. The locations selected were: (a) Holuhraun volcano, which erupted in the winter of 2014; (b) the Hálslón area, where a major storage reservoir was commissioned in 2007 and an ice-covered lake replaced a deep canyon; and (c) Eystri Hagafellsjökull, where the glacier terminus has receded in recent years. The locations of these areas are shown in Figure 3-20.

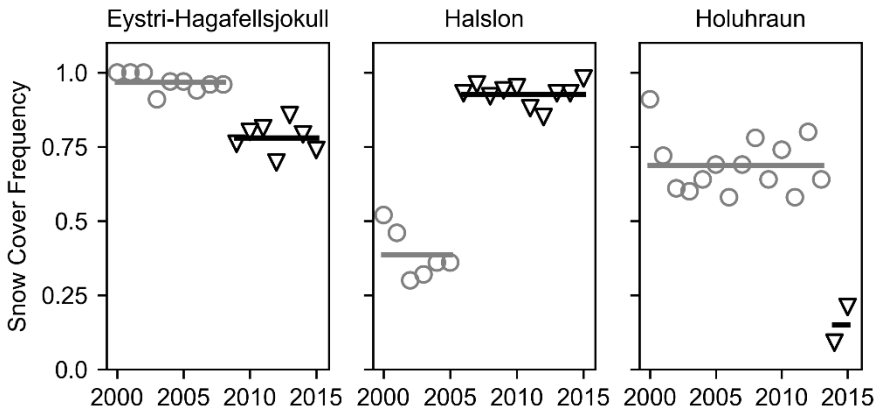

Figure 3-20 Time series of annual SCF in locations where known land surface changes have taken place over the period of MODIS observations (2000-2016)

The results shown in Figure 3-20 show a clear change in the time series of SCF around the time where the land surface changes describe above took place. To test whether the change observed in the SCF times series was statistically significant a Mann-Whitney-Wilcoxon (MWW) hypothesis test on two sample means, before and after the land surface changes. The null hypothesis was that the means of the two series are the same: H_0: $\mu_1 = \mu_2$ and the alternative hypothesis was that the means are not the same: H_1: $\mu 1 \neq \mu 2$.

Table 3-10 shows the results of the hypothesis tests. The results show that for all three locations the null hypothesis was rejected. Hence, the SCF record captures physical land surface changes that occurred during the period and the timing of these changes can be identified by the MWW test. We also note that, like the Hálslón reservoir, all other hydropower reservoirs constructed during the MODIS era, Sporðöldulón, Ufsarlón and Kelduárlón, could be clearly identified from the SCF maps.

Table 3-10 Results of Mann-Whitney-Wilcoxon (MWW) on two sample means, before and after known land surface changes in three locations in Iceland

Location:	Time of change	MWW p-value	SCF trend
Holuhraun	2014	0.017	Significant decrease
Hálslón	2007	0.00025	Significant increase
Eystri Hagafellsjokull	2008	0.00031	Significant decrease

3.6.2 Estimating and Projecting Climate Classifications

Köppen-Geiger climate classifications were calculated for Iceland in a 0.2-degree horizontal resolution using the methods described in Section 3.3 and published in Eythorsson et al., 2019. Climate classifications were assigned to each pixel based on the classification criteria outlined by Kottek et al. (2006) and Peel et al. (2007), as summarized in Table 3-3. The classification scheme contains five main classes, each with two levels of subclasses, in total 30 climate classes. As example, an area that has the main class *D – Cold*, second subclass *w – dry winter* and the third subclass a – *hot summer* would have the code *Dwa*.

The Icelandic climate was classified for each year in the period 1950-2100. We used the ensemble average of the NASA NEX dataset for both historical and predicted future climate conditions. The dataset contains an ensemble of 21 Global Circulation Models (GCM's) used in the CMIP5 model intercomparison project of the International Panel on Climate Change (IPCC) (Taylor et al., 2012). The climate classifications were calculated for the Representative Concentration Pathway (RCP) - RCP 4.5 as a more conservative prediction of future climate change. RCP 4.5 is a stabilization scenario where total radiative forcing is stabilized before 2100 by employment of a range of technologies and strategies for reducing greenhouse gas emissions, whereas RCP 8.5 is characterized by increasing greenhouse gas emissions over time and is representative for scenarios in the literature leading to high greenhouse gas concentration levels (van Vuuren et al., 2011). The proportion of each climate class was calculated for each year in four elevation bands *Coastline* (0-100 m a.s.l.), *Lowland* (100-500 m a.s.l.), *Highland* (500-1000 m. a.s.l.) *and Glaciers/Mountains* (1000 + m a.s.l.). A high resolution (20x20m) digital elevation model (DEM) from the National Land Survey of Iceland was used to calculate the elevation bands.

Figure 3-21 shows examples of the KG classification maps projected for Iceland in 0.2-degree horizontal resolution for the years 1951 and 2099. The four most common KG classes in Iceland in both periods were: *ET* – Polar Tundra, *Dfc* – Cold climate with cold summers and no dry season, *Dfb* – Cold climate with warm summer and no dry season, and *Dsc* – Cold climate with cold summers and dry summers.

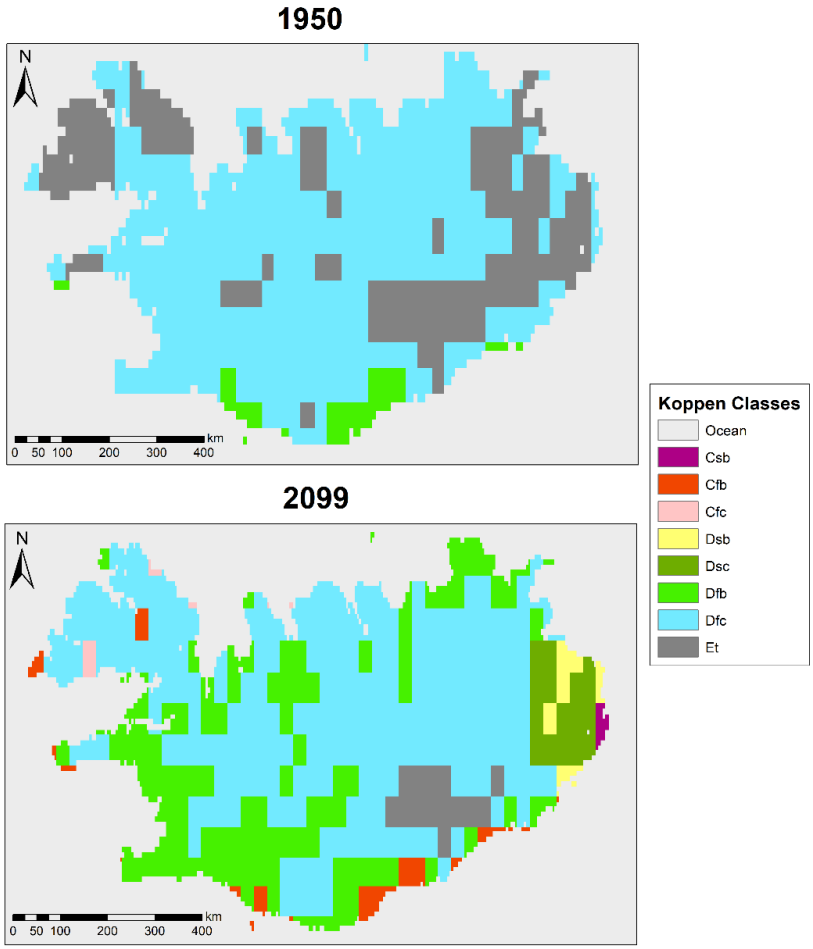

Figure 3-21 Examples of annual KG classification maps calculated for Iceland in the study for the years 1951 (upper) and 2099 (lower)

The results show that between 1950 and 2099 the polar tundra climate (ET) that initially covered a significant portion of the highlands will mostly disappear, except at the Vatnajökull Glacier. The *ET* is replaced by a cold climate with the cold summer classes *Dfc* and *Dsc*. A warm summer climate (*Dfb*), that in the first period was mostly limited to small areas in the southern lowlands on each side of the Myrdalsjökull Glacier, will by the end of the period have spread almost around the entire country and stretched far into the highlands. At the middle of the current century temperate climate classes (*Cfb, Cfc* and *Csb*) will start appearing consistently in coastal areas. This would be the first time that such climate classifications would be experienced in Iceland since records began.

Figure 3-22 shows the proportional coverage of the top climate classes for the period 1951-2099. The uppermost graph shows the results for the whole of Iceland and the lower graphs show the main climate classes within each elevation zone. The results in Figure 3-22 show that by the end of the current century the polar tundra climate (Class *ET*) in Iceland will decrease from about 20% coverage in 1950 to about 5%, by the middle of the current century and the ET class will disappear altogether in the coastal and lowland regions. Over the same period, warm summers (class *Dfb*) will increase by about the same amount. The net coverage of the most common climate class, *Dfc*, will not change much over the period. However, as

seen in Figure 3-21 and Figure 3-22, class *Dfc* is replaced by class *Dfb* in coastal areas while it replaces class *ET* in the highlands; thus we expect the spatial distribution of class *Dfc* to change significantly during the period.

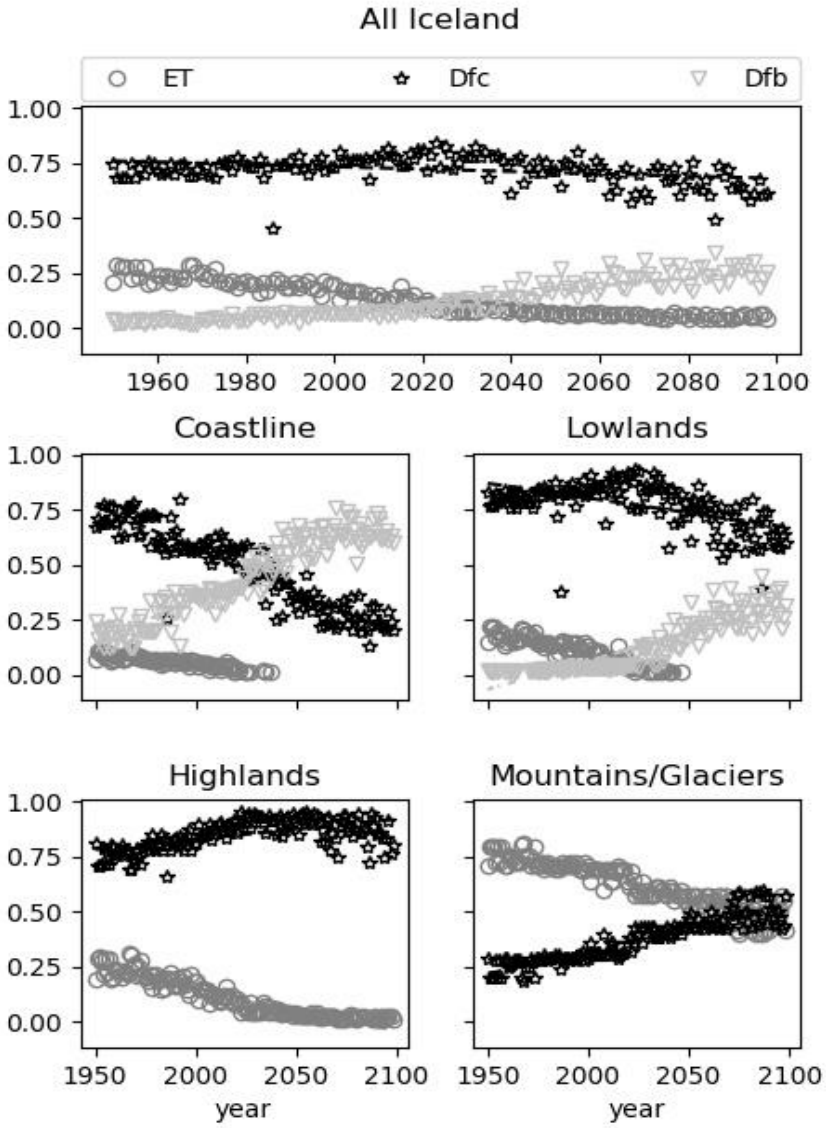

Figure 3-22 Time series of the annual proportional coverage of the three main KG Classes in each elevation zone in Iceland for the period 1951-2099 (from Eythorsson et al., 2023a).

3.6.3 Projecting Changes to Snow Resources in Iceland

Daily snow conditions in Iceland were simulated in 0.2-degree horizontal resolution for the period 1950-2100 for each of the 21 downscaled and bias corrected Global Circulation Models GCM's in the NASA NEX-GDDP dataset (Thrasher et al., 2006) using the Snow17 model for both the RCP45 and RCP85 emission scenarios. The methods used for the snow modelling are described in detail in section 3.5.1 and published in Eythorsson et al., (2023a).

Figure 3-23 shows on the left the simulated average winter SWE across Iceland for both RCP45 (green) and RCP85 (red). **Error! Reference source not found.** shows on the right the simulated average annual SCF across for RCP45 (green) and RCP85 (red). Observations from monitoring stations of mountain (crosses) and local (stars) snow cover and MODIS observations (triangles) are shown in black. The shaded area represents the upper and lower quantiles of the ensemble simulations, and the solid line represents a 10-year moving average of the ensemble.

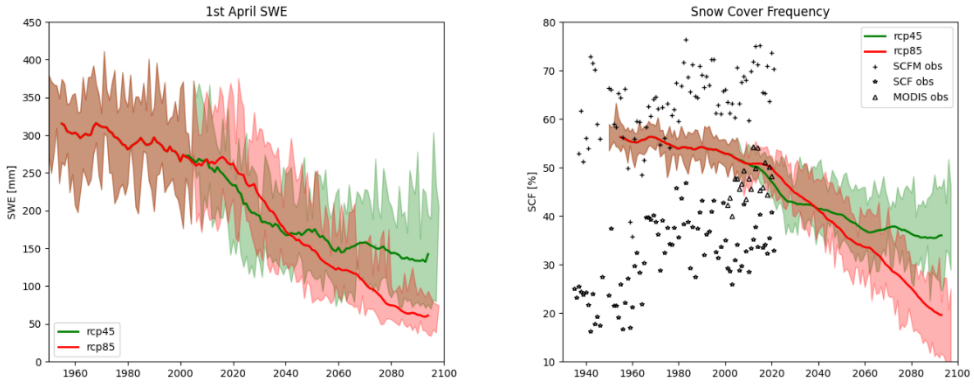

Figure 3-23 Left panel: simulated average winter SWE across Iceland for both RCP45 (green) and RCP85 (red). Right panel: simulated average annual SCF across Iceland as projected by RCP45 (green) and RCP85 (red). Observations from monitoring stations of mountain (crosses) and local (stars) snow cover and MODIS observations (triangles) are shown in black. The shaded area represents the upper and lower quantiles of the ensemble simulations, and the solid line shows a 10-year moving average of the ensemble. (from Eythorsson et al., 2023a)

The results in Figure 3-23 shows that both SWE and SCF are expected to decrease in Iceland over the course of the 21st century. The decrease is more severe given the RCP85 emission scenario as compared to RCP45. The simulated estimates of average annual SCF (right) are in line with MODIS observations over the period 2001-2021. In situ observations of local and mountain snow cover (SNC or SNCM > 2) fall below and above the simulated averages, respectively, as expected. The simulated SWE estimates show a decrease in SWE over the period 1950-2100 a trend which grows faster after the 2020s, whereas the observed snow depth measurements (shown in Figure 3-18) show a significant increase ($p = 1.54 * 10^{-5}$) over the period 1930-2021. The results presented in Figures 3-18 and 3-23 reveal an increasing trend in SCF and SND over a period where both metrics are projected to trend downward. The results also illustrate the substantial natural climate variability in Icelandic snow conditions.

The results in Figure 3-18 show a positive trend for temperature and precipitation in Iceland over the period 1950-2021. Increasing temperatures result in enhanced snow melt, which is apparent in a flat or decreasing SCF in coastal regions (as shown in Figure 3-19**Error! Reference source not found.**), whereas at higher elevation the increased precipitation enhances winter snow accumulation leading to higher SCF despite the enhanced melt rates during summer. With further climate change less, precipitation will fall as snow at higher elevations and both SND and SCF are expected to have decrease across the country by the end of the 21st century, as illustrated in Figure 3-23.

The results in Figure 3-23 show that there is a large variability in the average SCF from the observational IMO stations, shown as blue dots on the figure. The observational data shows that the SCF increases with elevation, however there is a large variability between stations especially at the lowlands. The figure also shows how few of the observational sites are located at high elevation, where most of Iceland's snow resources are located.

The results shown in Figure 3-23 show that snow resources are projected to diminish in Iceland at all elevation zones. These projected changes to Icelandic snow resources are in line with previous projections of the future evolution of Icelandic snow cover over the 21st century (Johannesson et al., 2007). The observed increase in snow cover, both by remote sensing and in situ measurements, over the period 2000-2021 also agree with the results of Gunnarsson et al. (2019) which also used satellite remote sensing data to show that there had been an increase in snow cover in Iceland for all months except October and November over the same period. The results of Eythorsson et al., (2023a) study suggest that the increase in snow cover in Iceland, observed both from remotely sensed and in situ data, is associated with increased precipitation causing a more frequent and thicker snowpack which persist longer, despite enhanced melt rates.

These results deserve further investigation. It should be noted that the MODIS period, 2000-2021, used to estimate the historical SCF changes in this study is short and trends observed during this period could be induced by low frequency cyclical climate patterns, or by a small amount of extreme weather events. However, the causes and the impacts of these changes to Icelandic snow resources needs to be better understood. Differences in future snowpack changes by elevation should be studied to understand the impact on the Icelandic hydrological cycle, which will further affect the local ecology, hazard assessments, water resources management, and hydropower production in the country.

4. Conclusion and future perspectives

The objective of this dissertation was to investigate from observations the impact of climate change on snow conditions that has already occurred and based on the best available assumptions on future climate change, to estimate by modelling how snow conditions are likely to continue to respond to changing climate forcings in different regions. In this dissertation and the scientifical journal articles that have been produced because of this work, this objective has been achieved in the following steps:

Firstly, a novel approach for predicting seasonal snow mass balance in glaciated catchments was published in (Eythorsson et al., 2018) and is discussed in detail in section 3.1of this dissertation. Secondly, the spatio-temporal changes in the climate and snow regimes were estimated globally and compared and analyzed within the context of the Arctic region, the results of which have been published in Eythorsson et al., (2019) and are discussed in detail in sections 3.2 - 3.4 of this dissertation. Future snow conditions were modelled across the Northern Hemisphere (NH) based on the expected changes to the climate regime, given different plausible emission scenarios, the results of which are presented in Eythorsson et al., (2023b) and are discussed in detail in section 3.5 of this dissertation. Lastly, the observed past and projected future changes in the climate and snow regimes are analyzed in a regional context for Iceland, the results of which are presented in Eythorsson et al., (2023a) and are discussed in detail in section 3.6 of this dissertation.

4.1 Conclusion

The main results of this dissertation are the large changes to snow resources, both observed and projected, in the NH. These results show that in general snow cover has been decreasing significantly, especially at lower latitudes, while some high latitude areas have experienced an increase in the frequency of snow cover. These trends were in general projected to continue throughout the 21st century with severe implications to societies and ecosystems in cold regions. These ongoing changes will affect the habitability of flora and fauna in cold regions, straining local ecosystems and inducing species migrations and extinctions. The projected changes to snow resources will impact the lifestyles and culture of societies and indigenous peoples across the NH providing complex problems and opportunities for water resources management and potential energy production in these regions as the local hydrological cycle is impacted by changing climate forcings.

Reliable forecasting of snow resources behavior is a key aspect of water resource management in cold regions. The Kárahnjúkar HPP in South-Eastern Iceland (by far the largest powerplant in Iceland) receives most of its inflow from the glacial meltwater of the Brúarjökull glacier. Several studies have considered the simulation of snow melt behavior on Brúarjökull using both empirical and physical approaches. These modelling efforts have all focused on the diurnal modelling of snow melt based on environmental input parameters that can only be forecast reliably a few days in advance. Eythorsson et al., (2018) showed

that the summer mass balance behavior of the Brúarjökull glacier can be predicted satisfactorily in the beginning of the melt season, using only the data on initial conditions of the hydro-climatological system that are available at that time, using a novel data driven modelling approach. These results are important for the water resource managers in glacially dominated catchments, like those managing the Kárahnjúkar HPP, as they demonstrate that the key source of runoff, glacial summer melt, in these areas can be satisfactorily predicted at the beginning of the melt season, 2-3 months in advance.

While glacial mass balance is a key hydrological parameter in few cold watersheds, water resources management in cold areas also require an understanding of seasonal snow cover dynamics, and especially at the present time how these dynamics can be expected to respond to a changing climate. Eythorsson et al., (2019) used MODIS snow cover data to estimate the changes that have occurred to the Snow Cover Frequency (SCF) in 500m horizontal resolution globally, during the period 2000-2016 and to identify those areas where the changes in SCF over that period have been statistically significant. The study revealed that large areas around the southern fringe of the Northern Hemisphere (NH) seasonal snow coverage have seen a significant decrease in SCF since the turn of the century. An opposite pattern was observed at the northern fringe of the NH seasonal snow coverage, where the SCF has increased in many coastal regions around the Arctic Ocean.

These historical SCF trends in the Arctic were compared to the regional climate change, which was estimated as changes to the proportional coverage of Köppen-Geiger (KG) Climate classes. The results showed a trend of climate classes associated with warmer weather migrating northward, which has persisted to date and was projected to continue at least until the end of the present century. This warming was observed in 7 of the 10 Arctic study areas considered in Eythorsson et al., (2019) and in Iceland as presented in Eythorsson et al., (2023a). The warming trend observed in these regions coincides with changing snow dynamics as the largest change to the local SCF in the arctic was seen in these same regions. It was only in the northernmost regions of the Arctic were little to no changes to either the SCF or the climate classifications was observed. Averaged across the Arctic the SCF was observed to have decreased by 9.1 days per decade over the study period, which corresponds to previous studies on snow cover in the general area (Hori et al., 2017; Liston & Hiemstra, 2011; Yunlong et al., 2018).

As warmer climate classes are expected to migrate ever northward until the end of the present century at least, as shown e.g. in Eythorsson et al., (2019) and (Beck et al., 2018), snow conditions can be expect to change drastically in regions where winter snow cover has historically been an important factor in the local hydro-climatology and ecology. Eythorsson et al. (2023b) modelled the evolution of NH snow resources over the period 1950-2100 using the Snow17 model forced with the ensemble of the downscaled and bias corrected CMIP5 projections as contained in the NASA-NEX GDDP dataset, for both the RCP45 and RCP85 emission scenarios. The simulated snow conditions for the historical period showed a high correlation to remotely sensed Snow-Covered Area (SCA) from the MODIS/Terra snow cover dataset and to the Snow Water Equivalent (SWE) field from the GLDAS-2 dataset. The results from Eythorsson et al., (2023b) showed that NH snow resources are expected to undergo considerable changes until the end of the present century. The average SCF in the NH was projected to decrease by 12.5% and 23.1% between the periods 1950-1975 and 2075-2100, under the RCP45 and RCP85 scenarios, respectively. While the frequency of snow cover is expected to decrease significantly, the average winter SWE was projected to

increase by 3.9% and 2.2% between the same periods under the RCP45 and RCP85 emission scenarios, respectively.

The decrease in NH SCF shown in the results of Eythorsson et al., (2023b) is primarily ascribed to a decreasing number of snow-covered days at the southern fringe of the NH seasonal snow layer, where some basins may see the loss of almost all their winter SWE snow storage under the RCP85 scenario. The SCF was also projected to decrease at higher latitudes, albeit significantly less. However, the 1st of April SWE at higher latitudes was projected to increase even though the number of days with snow covered ground was expected to decrease. In all the largest rivers draining into the Arctic Ocean the contribution of snow melt was found to increase significantly and, in some cases, almost double between the periods 1950-1975 and 2075-2100.

The pattern of decreasing SCF in mid latitudes was also observed in Eythorsson et al., (2019) based on the MODIS/Terra snow cover product. Thus, the trends that have already been observed in these areas can be expected to continue, at an accelerated pace throughout the 21st century given the RCP85 trajectory or at a slowly declining pace and stabilizing by the end of the century given the RCP45 trajectory. Increased snowfall at high latitudes is expected due to sea ice decline and increased regional evaporation from the Arctic Ocean (Kopec et al., 2016; Singarayer et al., 2006). This was observed as an increase in SCF in Eythorsson et al., (2019) over the historical MODIS period (2000-2016) and as an increase in the 1st of April SWE in Eythorsson et al., (2023b). The increase in SCF observed in high latitudes in Eythorsson et al., (2019) is expected to reverse as these areas continue to warm and by the end of the century the SCF will have decreased significantly across the entire NH.

Collectively, the results of the work presented in this dissertation show that significant changes have occurred to snow resources in many regions across the NH as estimated based on remotely sensed data from the MODIS/Terra instrument and presented in Eythorsson et al., (2019). Snow Cover Frequency (SCF) was shown to have decreased in many mid-latitude areas whereas around the arctic ocean large areas had seen an increase in the local SCF. These changes to have occurred concomitantly with local climate warming, as estimated from trends in the coverage of KG climate classes, with only the northernmost parts of the Arctic remaining with relatively unchanged climate and snow regimes, as presented in Eythorsson et al., (2019). These trends were replicated and shown to continue at least until the end of the 21st century by modelling NH snow conditions based on the ensemble of downscaled and bias corrected GCM models from the CMIP5 project. The model results revealed a trend of decreasing snow cover frequency across the hemisphere while snow storage volume was projected to increase around the Arctic, as presented in Eythorsson et al., (2023b). The results of both Eythorsson et al., (2019; 2023b) show that the NH snow and climate regimes have undergone significant changes and that these changes can be expected to continue for the foreseeable future, however, these trends were shown to vary significantly depending on region. An analysis of climate and snow changes in Icelandic snow resources showed that the Icelandic climate is expected to change significantly throughout the present century, over the same period snow resources are expected to diminish across the country, as presented in Eythorsson et al., (2023a). Analysis of SCF trends estimated from MODIS/Terra snow cover data revealed observable glacial ablation around the termini of most Icelandic outlet glaciers, whereas over the same time SCF had increased significantly in large areas in the highland. This SCF increase over the MODIS period is likely due to decadal scale oscillations in atmospheric and ocean currents

in the North Atlantic, which have been shown to significantly affect the seasonal mass balance behavior of Icelandic glaciers, as presented in Eythorsson et al., (2018).

4.2 Future Perspectives

The results of this dissertation show that snow resources in the Northern Hemisphere have and are expected to continue undergoing significant changes. These results are in line with the just published 6th Assessment Report (AR6) by the International Panel on Climate Change (IPCC) where it states that there is very high confidence that the NH spring snow cover has been decreasing since 1978 and that further decrease of the NH seasonal snow extent is virtually certain under all plausible emission scenarios (Fox-Kemper et al., 2021). These projections have significant consequences for societies and ecosystems in cold regions, which require further attention and research to optimize local mitigation and adaptation measures in these regions.

The Snow17 model results which was used in Eythorsson et al., 2023a and Eythorsson et al., 2023b were calculated in a 0.2-degree horizontal resolution based on the ensemble average of the 21 bias corrected and downscaled GCMs from the CMIP5 experiment (Taylor et al., 2012). In Iceland, where topography can greatly influence local meteorological characteristics (e.g. Rögnvaldsson et al., 2007), snow cover estimates would benefit from a finer spatial resolution. The results in Figure 3-23 confirm that many topographical effects are smoothed out in the simulated snow cover estimates, as compared to the MODIS snow cover products. To improve the understanding of future changes to snow resources in Iceland these changes should be modelled at a higher resolution e.g. using regional climate models such as the EURO-CORDEX (Jacob et al., 2013).

The long-term trend in snow cover projected in Eythorsson et al., (2023a) and e.g. in (Johannesson et al., 2007) shows a decrease in snow cover across the country, however the short term trend observed both through in situ and satellite observations and shows a trend of increasing SCF in large parts of the country, as shown by Eythorsson et al., (2023a) and Gunnarsson et al., 2019. These results deserve further attention, it is important for water resources managers in Iceland to have the best available estimates of future snow resources and to understand if and then why these trends differ in the short and the long term. It should be investigated whether the short-term increase in SCF is due to short term oscillations in the Iceland climate, stemming from variations in oceanic or atmospheric circulation patterns. Furthermore, the Icelandic snow resources were simulated based on the ensemble average of all the 21 GCMs in the NASA NEX GDDP database. The selection of models into the ensemble impacts the accuracy of the results. It is worth analyzing which of the models show the highest correlation to Icelandic meteorology and only simulate future snow conditions based on those GCMs which show satisfactory simulations of the Icelandic climate.

The results of Eythorsson et al. (2018), showed that the summer mass balance of the Brúarjökull could be predicted satisfactorily based on information on the initial conditions of the surrounding hydro-climatological system at the beginning of the glacial melt season. The model framework developed in Eythorsson et al. (2018), can in essence be applied to any type of predictive modelling where there is a statistical relationship between the predictor and response variables. Given the promising results from Eythorsson et al. (2018), it is worth developing these methods further and apply them to snowmelt, discharge and

reservoir inflow forecasting at various temporal scales, for the key glacially dominated watersheds in Iceland. This could potentially improve streamflow forecasting in Iceland at various lead times, providing valuable information for water resources managers across the country.

The results of Eythorsson et al. (2023b), show that snow coverage is expected to decrease across the NH between the periods 1950-1975 and 2075-2100. However, the mean winter SWE is expected to increase substantially in roughly the same areas which were shown to have experienced an increase in SCF over the period 2000-2016 in Eythorsson et al. (2019). These results deserve further attention. A regional analysis of future scenarios in snow resources should be conducted for the Arctic. Estimates produced by both GCMs as well as regional Arctic climate models such as the Regional Arctic System Model (Cassano et al., 2017; Hamman et al., 2016) should be compared as well as between different snow models. Lastly, the effect of increasing SCF in the historically arid regions of the high Arctic on the earth's radiation budget should be considered.

References

Ackerman, S. A., Holz, R. E., Frey, R., Eloranta, E. W., Maddux, B. C., & McGill, M. (2008). Cloud detection with MODIS. Part II: Validation. *Journal of Atmospheric and Oceanic Technology*, *25*(7), 1073–1086. https://doi.org/10.1175/2007JTECHA1053.1

Adalgeirsdottir, G., Gudmundsson, S., Bjornsson, H., Palsson, F., Johannesson, T., Hannesdottir, H., … Berthier, E. (2011). Modelling the 20th and 21st century evolution of Hoffellsjokull glacier, SE-Vatnajokull, Iceland. *Cryosphere*, Vol. 5, pp. 1961–1975. https://doi.org/10.5194/tc-5-961-2011

Aðalgeirsdóttir, G., Magnússon, E., Pálsson, F., Thorsteinsson, T., Belart, J. M. C., Jóhannesson, T., … Björnsson, H. (2020). Glacier Changes in Iceland From ∼1890 to 2019. *Frontiers in Earth Science*, *0*, 520. https://doi.org/10.3389/FEART.2020.523646

Adam, J. C., Hamlet, A. F., & Lettenmaier, D. P. (2009). Implications of global climate change for snowmelt hydrology in the twenty-first century. *Hydrological Processes*. https://doi.org/10.1002/hyp.7201

AMAP. (2015). AMAP assessment 2015: Temporal Trends in Persistent Organic Pollutants in the Arctic. In *AMAP assessment report*.

Amlien, J. (2008). Remote sensing of snow with passive microwave radiometers—A review of current algorithms. *Norsk Regnesentral Report, 1019*, 52.

Anderson, E. (2006). Snow Accumulation and Ablation Model–SNOW-17. In *Office of Hydrologic Development, National Weather Service*. https://doi.org/10.1038/177563a0

Anderson, E. A. (2002). Calibration of Conceptual Hydrologic Models for Use in River Forecasting. *NOAA Technical Report, NWS 45, Hydrology Labratory*.

Armstrong, R. (2001). Historical Soviet daily snow depth version 2 (HSDSD). *National Snow and Ice Data Center, Boulder, CO. CD-ROM*.

Arsenault, K. R., Houser, P. R., & De Lannoy, G. J. M. (2014). Evaluation of the MODIS snow cover fraction product. *Hydrological Processes*, *28*(3), 980–998. https://doi.org/10.1002/hyp.9636

Augustine, J. A., DeLuisi, J. J., & Long, C. N. (2000). SURFRAD - A National Surface Radiation Budget Network for Atmospheric Research. *Bulletin of the American Meteorological Society*, *81*(10), 2341–2358. https://doi.org/10.1175/1520-0477(2000)081<2341:SANSRB>2.3.CO;2

Ault, T. W., Czajkowski, K. P., Benko, T., Coss, J., Struble, J., Spongberg, A., … Gross, C. (2006). Validation of the MODIS snow product and cloud mask using student and NWS cooperative station observations in the Lower Great Lakes Region. *Remote Sensing of Environment*, *105*(4), 341–353. https://doi.org/10.1016/j.rse.2006.07.004

Bajracharya, S. R., & Mool, P. (2009). Glaciers, glacial lakes and glacial lake outburst floods in the Mount Everest region, Nepal. *Annals of Glaciology*, *50*(53), 81–86. https://doi.org/10.3189/172756410790595895)

Baldocchi, D., Falge, E., Gu, L., Olson, R., Hollinger, D., Running, S., … Wofsy, S. (2001). FLUXNET: A New Tool to Study the Temporal and Spatial Variability of Ecosystem-Scale Carbon Dioxide, Water Vapor, and Energy Flux Densities. *Bulletin of the American Meteorological Society*, *82*(11), 2415–2434. https://doi.org/10.1175/1520-0477(2001)082<2415:FANTTS>2.3.CO;2

Barichivich, J., Briffa, K. R., Myneni, R. B., Osborn, T. J., Melvin, T. M., Ciais, P., … Tucker, C. (2013). Large-scale variations in the vegetation growing season and annual cycle of atmospheric CO2 at high northern latitudes from 1950 to 2011. *Global Change Biology*, *19*(10), 3167–3183. https://doi.org/10.1111/gcb.12283

Barnston, A. G., & Livezey, R. E. (1987). Classification, Seasonality and Persistence of Low-Frequency Atmospheric Circulation Patterns in: Monthly Weather Review Volume 115 Issue 6 (1987). https://doi.org/https://doi.org/10.1175/1520-0493(1987)115%3C1083:CSAPOL%3E2.0.CO;2

Barry, R. G. (2003). Mountain cryospheric studies and the WCRP climate and cryosphere (CliC) project. *Journal of Hydrology*, *282*(1), 177–181. https://doi.org/https://doi.org/10.1016/S0022-1694(03)00253-1

Basang, D., Barthel, K., & Olseth, J. (2017). Satellite and Ground Observations of Snow Cover in Tibet during 2001–2015. *Remote Sensing*, *9*(11), 1201. https://doi.org/10.3390/rs9111201

Beck, H. E., Zimmermann, N. E., McVicar, T. R., Vergopolan, N., Berg, A., & Wood, E. F. (2018). Present and future köppen-geiger climate classification maps at 1-km resolution. *Scientific Data*, *5*(1), 1–12. https://doi.org/10.1038/sdata.2018.214

Belart, J., Magnússon, E., Berthier, E., Gunnlaugsson, Á. Þ., Pálsson, F., Aðalgeirsdóttir, G., … Björnsson, H. (2020). Mass balance of 14 Icelandic glaciers, 1945–2017: spatial variations and links with climate. *Frontiers in Earth Science*, *8*, 163.

Beven, K., & Freer, J. (2001). Equifinality, data assimilation, and uncertainty estimation in mechanistic modelling of complex environmental systems using the GLUE methodology. *Journal of Hydrology*. https://doi.org/10.1016/S0022-1694(01)00421-8

BILLINGS, W. D., & MOONEY, H. A. (1968). The Ecology of Arctic and Alpine Plants. *Biological Reviews*, *43*(4), 481–529. https://doi.org/10.1111/j.1469-185x.1968.tb00968.x

Björnsson, H., Pálsson, F., & Gudmundsson, S. (2001). Jökulsárlón at Breiðamerkurjökull, Vatnajökull, Iceland: 20th century changes and future outlook. *Jökull*, *50*, 1–18.

Bjornsson, Halldor, Olason, E. O., Jónsson, T., & Henriksen, S. (2007). Analysis of a smooth seasonal cycle with daily resolution and degree day maps for Iceland. *Meteorologische Zeitschrift*, 57–69. https://doi.org/10.1127/0941-2948/2007/0188

Bjornsson, Helgi, & Palsson, F. (2008). Icelandic glaciers. *Jökull*, *58*(58), 365–386.

Bjornsson, Helgi, Palsson, F., Gudmundsson, S., Magnusson, E., Adalgeirsdottir, G., Johannesson, T., … Thorsteinsson, T. (2013). Contribution of Icelandic ice caps to sea level rise: Trends and variability since the Little Ice Age. *Geophysical Research Letters*, *40*(8), 1546–1550. https://doi.org/10.1002/grl.50278

Bliss, A., Hock, R., & Radić, V. (2014). Global response of glacier runoff to twenty-first century climate change. *J. Geophys. Res.: Earth Surf.*, *119*(4), 717–730. https://doi.org/10.1002/2013jf002931

Blöschl, G., Hall, J., Parajka, J., Perdigão, R. A. P., Merz, B., Arheimer, B., … Živković, N. (2017). Changing climate shifts timing of European floods. *Science*, *357*(6351), 588–590. https://doi.org/10.1126/SCIENCE.AAN2506

Bojinski, S., Verstraete, M., Peterson, T., Richter, C., Simmons, A., & Zemp, M. (2014). The concept of Essential Climate Variables in support of climate research, applications, and policy. *Bull. Am. Meteorol. Soc.*, *95*(9), 1431–1443. https://doi.org/10.1175/bams-d-13-00047.1

Boone, A. A., Habets, F., Noilhan, J., Clark, D., Dirmeyer, P., Fox, S., … Yang, Z. L. (2004). The Rhône-aggregation land surface scheme intercomparison project: An overview. *Journal of Climate*. https://doi.org/10.1175/1520-0442(2004)017<0187:TRLSSI>2.0.CO;2

Bracegirdle, T. J., Krinner, G., Tonelli, M., Haumann, F. A., Naughten, K. A., Rackow, T., … Wainer, I. (2020). Twenty first century changes in Antarctic and Southern Ocean surface climate in CMIP6. *Atmospheric Science Letters*, *21*(9), e984. https://doi.org/10.1002/ASL.984

Braithwaite, R. J., Konzelmann, T., Marty, C., & Ulesen, O. B. (1998). Errors in daily ablation measurements in northern Greenland, 1993-94, and their implications for glacier climate studies. *Journal of Glaciology*. https://doi.org/10.1017/S0022143000002094

Brown, J., Ferrians, O., Higginbottom, J. A., & Melnikov, E. (2002). *Circum-Arctic Map of Permafrost and Ground-Ice Conditions, Version 2*. Retrieved from https://nsidc.org/data/ggd318#

Brown, R. D. (2000). Northern Hemisphere snow cover variability and change, 1915–97. *Journal of Climate*, *13*(13), 2339–2355.

Brown, R. D., & Brasnett, B. (2010). Canadian Meteorological Centre (CMC) daily snow depth analysis data. *Environment Canada*, 169.

Brynjólfsson, S., Schomacker, A., & Ingólfsson, Ó. (2014). Geomorphology and the Little Ice Age extent of the Drangajökull ice cap, NW Iceland, with focus on its three surge-type outlets. *Geomorphology*, *213*, 292–304. https://doi.org/10.1016/J.GEOMORPH.2014.01.019

Cabedo-Sanz, P., Belt, S. T., Jennings, A. E., Andrews, J. T., & Geirsdóttir, Á. (2016).

Variability in drift ice export from the Arctic Ocean to the North Icelandic Shelf over the last 8000 years: A multi-proxy evaluation. *Quaternary Science Reviews*, *146*, 99–115. https://doi.org/10.1016/J.QUASCIREV.2016.06.012

Callaghan, T. V., Johansson, M., Brown, R. D., Groisman, P. Y., Labba, N., Radionov, V., … Wood, E. F. (2011). Multiple effects of changes in arctic snow cover. *Ambio*, *40*(SUPPL. 1), 32–45. https://doi.org/10.1007/s13280-011-0213-x

Callaghan, T. V., Johansson, M., Brown, R. D., Groisman, P. Y., Labba, N., Radionov, V., … Wood, E. F. (2011). Multiple effects of changes in arctic snow cover. *Ambio*, *40*(SUPPL. 1), 32–45. https://doi.org/10.1007/s13280-011-0213-x

Carenzo, M., Pellicciotti, F., Rimkus, S., & Burlando, P. (2009). Assessing the transferability and robustness of an enhanced temperature-index glacier-melt model. *Journal of Glaciology*, *55*(190), 258–274. https://doi.org/10.3189/002214309788608804

Carr, J. R., Stokes, C., & Vieli, A. (2014). Recent retreat of major outlet glaciers on Novaya Zemlya, Russian Arctic, influenced by fjord geometry and sea-ice conditions. *Journal of Glaciology*, *60*(219), 155–170. https://doi.org/10.3189/2014JoG13J122

Carrera-Hernández, J. J., & Gaskin, S. J. (2007). Spatio temporal analysis of daily precipitation and temperature in the Basin of Mexico. *Journal of Hydrology*, *336*(3), 231–249. https://doi.org/https://doi.org/10.1016/j.jhydrol.2006.12.021

Cassano, J. J., DuVivier, A., Roberts, A., Hughes, M., Seefeldt, M., Brunke, M., … Hamman, J. (2017). Development of the Regional Arctic System Model (RASM): near-surface atmospheric climate sensitivity. *Journal of Climate*, *30*(15), 5729–5753.

Cauvy-Fraunié, S., & Dangles, O. (2019). A global synthesis of biodiversity responses to glacier retreat. *Nature Ecology & Evolution 2019 3:12*, *3*(12), 1675–1685. https://doi.org/10.1038/s41559-019-1042-8

Chang, A T C, Foster, J. L., & Hall, D. K. (1987). Nimbus-7 SMMR derived global snow cover parameters. *Annals of Glaciology*, *9*, 39–44.

Chang, Alfred T C, & Rango, A. (2000). Algorithm theoretical basis document (ATBD) for the AMSR-E snow water equivalent algorithm. *NASA/GSFC, Nov*.

Che, T., Li, X., Jin, R., Armstrong, R., & Zhang, T. (2008). Snow depth derived from passive microwave remote-sensing data in China. *Annals of Glaciology*, *49*, 145–154.

Chen, D., & Chen, H. W. (2013). Using the Koppen classification to quantify climate variation and change: An example for 1901-2010. *Environmental Development*, *6*(1), 69–79. https://doi.org/10.1016/j.envdev.2013.03.007

Chen, Z., Zhou, T., Zhang, L., Chen, X., Zhang, W., & Jiang, J. (2020). Global Land Monsoon Precipitation Changes in CMIP6 Projections. *Geophysical Research Letters*, *47*(14), e2019GL086902. https://doi.org/10.1029/2019GL086902

Choi, G., Robinson, D. A., & Kang, S. (2010). Changing Northern Hemisphere Snow Seasons. *Journal of Climate*, *23*(19), 5305–5310.

https://doi.org/10.1175/2010JCLI3644.1

Choudhury, A., Yadav, A. C., & Bonafoni, S. (2021). A response of snow cover to the climate in the northwest himalaya (Nwh) using satellite products. *Remote Sensing*, *13*(4), 1–22. https://doi.org/10.3390/rs13040655

Christian, J. E., Koutnik, M., & Roe, G. (2018). Committed retreat: Controls on glacier disequilibrium in a warming climate. *Journal of Glaciology*. https://doi.org/10.1017/jog.2018.57

Clark, M. P., Slater, A. G., Barrett, A. P., Hay, L. E., McCabe, G. J., Rajagopalan, B., & Leavesley, G. H. (2006). Assimilation of snow covered area information into hydrologic and land-surface models. *Advances in Water Resources*, *29*(8), 1209–1221. https://doi.org/10.1016/J.ADVWATRES.2005.10.001

Clifford, D. (2010). Global estimates of snow water equivalent from passive microwave instruments: history, challenges and future developments. *International Journal of Remote Sensing*, *31*(14), 3707–3726.

Cohen, J. (1994). Snow cover and climate. *Weather*, *49*(5), 150–156. https://doi.org/10.1002/j.1477-8696.1994.tb05997.x

Cohen, J. L., Furtado, J. C., Barlow, M. A., Alexeev, V. A., & Cherry, J. E. (2012). Arctic warming, increasing snow cover and widespread boreal winter cooling. *Environmental Research Letters*. https://doi.org/10.1088/1748-9326/7/1/014007

Cohen, J., Screen, J. A., Furtado, J. C., Barlow, M., Whittleston, D., Coumou, D., … Jones, J. (2014). Recent Arctic amplification and extreme mid-latitude weather. *Nature Geoscience*. https://doi.org/10.1038/ngeo2234

Connolly, R., Connolly, M., Soon, W., Legates, D. R., Cionco, R. G., & Herrera, V. M. V. (2019). Northern Hemisphere Snow-Cover Trends (1967–2018): A Comparison between Climate Models and Observations. *Geosciences*, *9*(3), 135. https://doi.org/10.3390/geosciences9030135

Cook, B. I., Mankin, J. S., Marvel, K., Williams, A. P., Smerdon, J. E., & Anchukaitis, K. J. (2020). Twenty-First Century Drought Projections in the CMIP6 Forcing Scenarios. *Earth's Future*, *8*(6), e2019EF001461. https://doi.org/https://doi.org/10.1029/2019EF001461

Corripio, J. G. (2004). Snow surface albedo estimation using terrestrial photography. *International Journal of Remote Sensing*, *25*(24), 5705–5729.

Dariane, A. B., Khoramian, A., & Santi, E. (2017). Investigating spatiotemporal snow cover variability via cloud-free MODIS snow cover product in Central Alborz Region. *Remote Sensing of Environment*, *202*, 152–165. https://doi.org/10.1016/j.rse.2017.05.042

De Ruyter de Wildt, M, Oerlemans, J., & Bjornsson, H. (2003). A calibrated mass balance model for Vatnajökull, Iceland. *Jökull*, *52*, 1–20.

De Ruyter de Wildt, MS, Klok, E., & Oerlemans, J. (2003). Reconstruction of the mean specific mass balance of Vatnajokull (Iceland) with a seasonal sensitivity characteristic. *Geografiska Annaler: Series A, Physical Geography*, *85*(1), 57–72. Retrieved from http://onlinelibrary.wiley.com/doi/10.1111/1468-0459.00189/abstract

Debele, B., Srinivasan, R., & Gosain, A. K. (2010). Comparison of process-based and temperature-index snowmelt modeling in SWAT. *Water Resources Management*. https://doi.org/10.1007/s11269-009-9486-2

Dee, D. P., Uppala, S. M., Simmons, A. J., Berrisford, P., Poli, P., Kobayashi, S., … Vitart, F. (2011). The ERA-Interim reanalysis: configuration and performance of the data assimilation system. *Quarterly Journal of the Royal Meteorological Society*, *137*(656), 553–597. https://doi.org/10.1002/QJ.828

Deems, J. S., Fassnacht, S. R., & Elder, K. J. (2006). Fractal distribution of snow depth from LiDAR data. *Journal of Hydrometeorology*, *7*(2), 285–297.

Deems, J. S., Painter, T. H., & Finnegan, D. C. (2013). Lidar measurement of snow depth: a review. *Journal of Glaciology*. https://doi.org/10.3189/2013jog12j154

Derksen, C, Walker, A., LeDrew, E., & Goodison, B. (2003). Combining SMMR and SSM/I data for time series analysis of central North American snow water equivalent. *Journal of Hydrometeorology*, *4*(2), 304–316.

Derksen, Chris. (2008). The contribution of AMSR-E 18.7 and 10.7 GHz measurements to improved boreal forest snow water equivalent retrievals. *Remote Sensing of Environment*, *112*(5), 2701–2710. https://doi.org/https://doi.org/10.1016/j.rse.2008.01.001

Deschamps-Berger, C., Gascoin, S., Berthier, E., Deems, J., Gutmann, E., Dehecq, A., … Dumont, M. (2020). Snow depth mapping from stereo satellite imagery in mountainous terrain: evaluation using airborne lidar data. *Cryosphere Discuss*, 1–28.

Dietz, A.J., Kuenzer, C., Gessner, U., & Dech, S. (2012). Remote sensing of snow – a review of available methods. *International Journal of Remote Sensing*, *33*(13), 4094–4134. https://doi.org/10.1080/01431161.2011.640964

Dietz, Andreas Juergen, Kuenzer, C., Gessner, U., & Dech, S. (2012). Remote sensing of snow – a review of available methods. *International Journal of Remote Sensing*, *33*(13), 4094–4134. https://doi.org/10.1080/01431161.2011.640964

Dong, C. (2018, June 1). Remote sensing, hydrological modeling and in situ observations in snow cover research: A review. *Journal of Hydrology*, Vol. 561, pp. 573–583. https://doi.org/10.1016/j.jhydrol.2018.04.027

Dormann, C. F., Calabrese, J. M., Guillera-Arroita, G., Matechou, E., Bahn, V., Bartoń, K., … Hartig, F. (2018, November 1). Model averaging in ecology: a review of Bayesian, information-theoretic, and tactical approaches for predictive inference. *Ecological Monographs*, Vol. 88, pp. 485–504. https://doi.org/10.1002/ecm.1309

Douville, H., Raghavan, K., Renwick, J., Allan, R. P., Arias, P. A., Barlow, M., … Zolina,

O. (2021). Water Cycle Changes. In V. Masson-Delmotte, P. Zhai, A. Pirani, S. L. Connors, C. Péan, S. Berger, … B. Zhou (Eds.), *Climate Change 2021: The Physical Science Basis. Contribution of Working Group I to the Sixth Assessment Report of the Intergovernmental Panel on Climate Change* (p. 239). Retrieved from https://www.ipcc.ch/report/ar6/wg1/#FullReport

Easterling, D. R. (2002). *United States Historical Climatology Network daily temperature and precipitation data (1871-1997)*. ORNL Oak Ridge National Laboratory (US).

Ellingson, R. G. (1995). Surface longwave fluxes from satellite observations: A critical review. *Remote Sensing of Environment*, *51*(1), 89–97. https://doi.org/10.1016/0034-4257(94)00067-W

Emanuel, K. (2021). Response of Global Tropical Cyclone Activity to Increasing CO2: Results from Downscaling CMIP6 Models. *Journal of Climate*, *34*(1), 57–70. https://doi.org/10.1175/JCLI-D-20-0367.1

Engeset, R. V, Sorteberg, H. K., & Udnaes, H. C. (2017). Snow pillows: Use and verification. In *Snow Engineering Recent Advances and Developments* (pp. 45–52). Routledge.

Essery, R., Morin, S., Lejeune, Y., & B Ménard, C. (2013). A comparison of 1701 snow models using observations from an alpine site. *Advances in Water Resources*. https://doi.org/10.1016/j.advwatres.2012.07.013

Essery, R., Rutter, N., Pomeroy, J., Baxter, R., Stahli, M., Gustafsson, D., … Elder, K. (2009). SnowMIP2: An evalution of forest snow process simulation. *Bulletin of the American Meteorological Society*. https://doi.org/10.1175/2009BAMS2629.1

Etchevers, P., Martin, E., Brown, R., Fierz, C., Lejeune, Y., Bazile, E., … Yang, Z. L. (2004). Validation of the energy budget of an alpine snowpack simulated by several snow models (SnowMIP project). *Annals of Glaciology*.

Eyring, V., Gillett, N. P., Achuta Rao, K. M., Barimalala, R., Barreiro Parrillo, M., Bellouin, N., … Sun, Y. (2021). Human Influence on the Climate System. In V. Masson-Delmotte, P. Zhai, A. Pirani, S. L. Connors, C. Péan, S. Berger, … B. Zhou (Eds.), *ClimateChange 2021: The Physical Science Basis. Contribution of Working Group I to the Sixth Assessment Report of the Intergovernmental Panel on Climate Change* (p. 207). Retrieved from https://www.ipcc.ch/report/ar6/wg1/#FullReport

Eythorsson, D., Gardarsson, S. M., Gunnarsson, A., & Hrafnkelsson, B. (2018). Statistical summer mass-balance forecast model with application to Brúarjökull glacier, South East Iceland. *Journal of Glaciology*, *64*(244). https://doi.org/10.1017/jog.2018.22

Eythorsson, Darri, Gardarsson, S. M., Ahmad, S. K., Hossain, F., & Nijssen, B. (2019). Arctic climate and snow cover trends - Comparing Global Circulation Models with remote sensing observations. *International Journal of Applied Earth Observation and Geoinformation*, *80*, 71–81. https://doi.org/https://doi.org/10.1016/j.jag.2019.04.003

Eythorsson, Darri, Gardarsson, S. M., Gunnarsson, A., & Hrafnkelsson, B. (2018). Statistical summer mass-balance forecast model with application to Brúarjökull glacier, South

East Iceland. *Journal of Glaciology*, *64*(244). https://doi.org/10.1017/jog.2018.22

Eythorsson, Darri, Gardarsson, S. M., Gunnarsson, A., & Sveinsson, O. G. B. (2023). Observed and predicted trends in Icelandic snow conditions for the period 1930–2100. *The Cryosphere*, *17*(1), 51–62. https://doi.org/10.5194/TC-17-51-2023

Eythorsson, Darri, Gardarsson, S. M., & Nijssen, B. (2023). Projected changes to Northern Hemisphere snow conditions over the period 1950–2100, given two emission scenarios. *Remote Sensing Applications: Society and Environment*, *30*, 100954. https://doi.org/10.1016/J.RSASE.2023.100954

Feng, C., Zhang, X., Wei, Y., Zhang, W., Hou, N., Xu, J., … Jiang, B. (2021). Estimation of Long-Term Surface Downward Longwave Radiation over the Global Land from 2000 to 2018. *Remote Sensing 2021*, *Vol. 13*, *Page 1848*, *13*(9), 1848. https://doi.org/10.3390/RS13091848

Fernandes, R., & Zhao, H. (2008). Mapping daily snow cover extent over land surfaces using NOAA AVHRR imagery. *Proceedings of 5th EARSeL Workshop: Remote Sensing of Land Ice and Snow, Bern, Switzerland*, *1113*, 18.

Fierz, C., Armstrong, R. L., Durand, Y., Etchevers, P., Greene, E., McClung, D. M., … Sokratov, S. a. (2009). The international classification for seasonal snow on the ground. In *UNESCO, IHP–VII, Technical Documents in Hydrology, No 83; IACS contribution No 1*.

Finsterwalder, S., & Schunk, H. (1887). Der Suldenferner. *Zeit Schrift Des Deut Schen Und Oesterriechischen Alpenvereins*, *18*, 72–89.

Fontrodona Bach, A., van der Schrier, G., Melsen, L. A., Klein Tank, A. M. G., & Teuling, A. J. (2018). Widespread and Accelerated Decrease of Observed Mean and Extreme Snow Depth Over Europe. *Geophysical Research Letters*. https://doi.org/10.1029/2018GL079799

Foppa, N., Stoffel, A., & Meister, R. (2007). Synergy of in situ and space borne observation for snow depth mapping in the Swiss Alps. *International Journal of Applied Earth Observation and Geoinformation*, *9*(3), 294–310. https://doi.org/https://doi.org/10.1016/j.jag.2006.10.001

Formetta, G., Bancheri, M., David, O., & Rigon, R. (2016). Performance of site-specific parameterizations of longwave radiation. *Hydrology and Earth System Sciences*, *20*(11), 4641–4654. https://doi.org/10.5194/HESS-20-4641-2016

Foster, J. L., Hall, D. K., Chang, A. T. C., Rango, A., Wergin, W., & Erbe, E. (1999). Effects of snow crystal shape on the scattering of passive microwave radiation. *IEEE Transactions on Geoscience and Remote Sensing*, *37*(2), 1165–1168.

Foster, J. L., Hall, D. K., Eylander, J. B., Riggs, G. A., Nghiem, S. V, Tedesco, M., … Casey, K. A. (2011). A blended global snow product using visible, passive microwave and scatterometer satellite data. *International Journal of Remote Sensing*, *32*(5), 1371–1395.

Foster, J., Liston, G., Koster, R., Essery, R., Behr, H., Dumenil, L., … Cohen, J. (1996). Snow cover and snow mass intercomparisons of general circulation models and remotely sensed datasets. *Journal of Climate*, *9*(2), 409–426.

Fox-Kemper, B., Hewitt, H. T., Xiao, C., Aðalgeirsdóttir, G., Drijfhout, S. S., Edwards, T. L., … Yu, Y. (2021). Ocean, Cryosphere and Sea Level Change. In V. Masson-Delmotte, P. Zhai, A. Pirani, S. L. Connors, C. Péan, S. Berger, … B. Zhou (Eds.), *Climate Change 2021: The Physical Science Basis. Contribution of Working Group I to the Sixth Assessment Report of the Intergovernmental Panel on Climate Change* (p. 271). Retrieved from https://www.ipcc.ch/report/ar6/wg1/#FullReport

Fragoso, T. M., Bertoli, W., & Louzada, F. (2018). Bayesian Model Averaging: A Systematic Review and Conceptual Classification. *International Statistical Review*, *86*(1), 1–28. https://doi.org/10.1111/insr.12243

Frey, R. A., Ackerman, S. A., Liu, Y., Strabala, K. I., Zhang, H., Key, J. R., & Wang, X. (2008). Cloud detection with MODIS. Part I: Improvements in the MODIS cloud mask for Collection 5. *Journal of Atmospheric and Oceanic Technology*, *25*(7), 1057–1072. https://doi.org/10.1175/2008JTECHA1052.1

Gabbi, J., Carenzo, M., Pellicciotti, F., Bauder, A., & Funk, M. (2014). A comparison of empirical and physically based glacier surface melt models for long-term simulations of glacier response. *Journal of Glaciology*. https://doi.org/10.3189/2014jog14j011

Gafurov, A., & Bárdossy, A. (2009). Cloud removal methodology from MODIS snow cover product. *Hydrology and Earth System Sciences*, *13*(7), 1361–1373.

Gao, Y., Xie, H., Lu, N., Yao, T., & Liang, T. (2010). Toward advanced daily cloud-free snow cover and snow water equivalent products from Terra–Aqua MODIS and Aqua AMSR-E measurements. *Journal of Hydrology*, *385*(1–4), 23–35.

Gardner, A. (2013). A reconciled estimate of glacier contributions to sea level rise: 2003 to 2009. *Science*, *340*(6134), 852–857. https://doi.org/10.1126/science.1234532

Gardner, A. S., & Sharp, M. J. (2010). A review of snow and ice albedo and the development of a new physically based broadband albedo parameterization. *Journal of Geophysical Research: Earth Surface*, *115*(F1).

Geirsdóttir, Á., Miller, G. H., Axford, Y., & Sædís Ólafsdóttir. (2009). Holocene and latest Pleistocene climate and glacier fluctuations in Iceland. *Quaternary Science Reviews*. https://doi.org/10.1016/j.quascirev.2009.03.013

Geirsdóttir, Á., Miller, G. H., Larsen, D. J., & Ólafsdóttir, S. (2013). Abrupt holocene climate transitions in the northern north atlantic region recorded by synchronized lacustrine records in iceland. *Quaternary Science Reviews*. https://doi.org/10.1016/j.quascirev.2013.03.010

Goodison, B. E., Louie, P. Y. T., & Yang, D. (1998). *WMO solid precipitation measurement intercomparison*.

Gorelick, N., Hancher, M., Dixon, M., Ilyushchenko, S., Thau, D., & Moore, R. (2016).

Google Earth Engine: Planetary-scale geospatial analysis for everyone. *Remote Sensing of Environment*. https://doi.org/10.1016/j.rse.2017.06.031

Guðmundsson, S., Björnsson, H., Jóhannesson, T., Aðalgeirsdóttir, G., Pálsson, F., & Sigurðsson, O. (2009). Similarities and differences in the response to climate warming of two ice caps in Iceland. *Hydrology Research*, *40*(5), 495–502. https://doi.org/10.2166/NH.2009.210

Gunnarsson, A, Garðarsson, S. M., & Sveinsson, Ó. G. B. (2019). Icelandic snow cover characteristics derived from a gap-filled MODIS daily snow cover product. *Hydrol. Earth Syst. Sci.*, *23*(7), 3021–3036. https://doi.org/10.5194/hess-23-3021-2019

Gunnarsson, Andri, Gardarsson, S. M., Pálsson, F., Jóhannesson, T., & Sveinsson, Ó. G. B. (2021). Annual and inter-annual variability and trends of albedo of Icelandic glaciers. *The Cryosphere*, *15*(2), 547–570.

H Souri, A., & Azizi, A. (2013). Removing Bowtie Phenomenon by Correction of Panoramic Effect in MODIS Imagery. *International Journal of Computer Applications,Published by Foundation of Computer Science, New York, USA.*, *68*, 12–16.

Hall, D. K., Foster, J. L., & Chang, A. T. C. (1982). Measurement and Modeling of Microwave Emission from Forested Snowfields in Michigan. *Hydrology Research*, *13*(3), 129–138. https://doi.org/10.2166/NH.1982.0011

Hall, D. K., Salomonson, V. V., & Riggs, G. A. (2016). MODIS/Terra Snow Cover Daily L3 Global 500m Grid. Version 6. *Boulder, Colorado USA: NASA National Snow and Ice Data Center Distributed Active Archive Center*.

Hall, Dorothy K., Hall, D. K., Riggs, G. A., Digirolamo, N. E., & Román, M. O. (2019). Evaluation of MODIS and VIIRS cloud-gap-filled snow-cover products for production of an Earth science data record. *Hydrology and Earth System Sciences*, *23*(12), 5227–5241. https://doi.org/10.5194/hess-23-5227-2019

Hall, Dorothy K, Riggs, G. A., Foster, J. L., & Kumar, S. V. (2010). Development and evaluation of a cloud-gap-filled MODIS daily snow-cover product. *Remote Sensing of Environment*, *114*(3), 496–503.

Hall, Dorothy K, Riggs, G. A., & Salomonson, V. V. (1995). Development of methods for mapping global snow cover using moderate resolution imaging spectroradiometer data. *Remote Sensing of Environment*, *54*(2), 127–140.

Hall, Dorothy K, Riggs, G. A., & Salomonson, V. V. (2006). MODIS/Terra Snow Cover Daily L3 Global 500m Grid V005 2000-01-01 to 2016-12-31. Retrieved January 5, 2017, from Boulder, Colorado USA: National Snow and Ice Data Center. Digital Media website: https://nsidc.org/data/mod10a1

Halldór Björnsson, Árný E. Sveinbjörnsdóttir, Anna K. Daníelsdóttir, Árni Snorrason, Bjarni D. Sigurðsson, Einar Sveinbjörnsson, Gísli Viggósson, Jóhann Sigurjónsson, Snorri Baldursson, S. Þ. & T. J. (2018). Hnattrænar loftslagsbreytingar og áhrif þeirra á íslandi - Skýrsla vísindanefndar um loftslagsbreytingar. In *Veðurstofa Íslands*. Retrieved from http://www.umhverfisraduneyti.is/media/PDF_skrar/visindanefndloftslagsbreytingar.p

df

Hamman, J., Nijssen, B., Brunke, M., Cassano, J., Craig, A., DuVivier, A., … Osinski, R. (2016). Land surface climate in the regional Arctic system model. *Journal of Climate*, *29*(18), 6543–6562.

Hanna, E., Jónsson, T., & Box, J. E. (2001). Recent changes in Icelandic climate. *Spring*, 3–9. https://doi.org/10.1256/wea.80.04

Hanna, E., Jónsson, T., & Box, J. E. (2004). An analysis of Icelandic climate since the nineteenth century. *International Journal of Climatology*, *24*(10), 1193–1210. https://doi.org/10.1002/joc.1051

Hannesdóttir, H., Björnsson, H., Pálsson, F., Adalgeirsdóttir, G., & Gudmundsson, S. (2015). Changes in the southeast Vatnajokull ice cap, Iceland, between ∼1890 and 2010. *Cryosphere*, *9*(2), 565–585. https://doi.org/10.5194/TC-9-565-2015

Hannesdóttir, Hrafnhildur, Aðalgeirsdóttir, G., Jóhannesson, T., Guðmundsson, S., Crochet, P., Ágústsson, H., … Björnsson, H. (2015). Downscaled precipitation applied in modelling of mass balance and the evolution of southeast Vatnajökull, Iceland. *Journal of Glaciology*, *61*(228), 799–813. https://doi.org/10.3189/2015JOG15J024

Hannesdóttir, Hrafnhildur, Björnsson, H., Pálsson, F., Aðalgeirsdóttir, G., & Guðmundsson, S. (2016). Variations of southeast vatnajökull ice cap (iceland) 1650–1900 and reconstruction of the glacier surface geometry at the little ice age maximum. *Http://Dx.Doi.Org/10.1111/Geoa.12064*, *97*(2), 237–264. https://doi.org/10.1111/GEOA.12064

Hauser, S., & Schmitt, A. (2021). Glacier Retreat in Iceland Mapped from Space: Time Series Analysis of Geodata from 1941 to 2018. *PFG – Journal of Photogrammetry, Remote Sensing and Geoinformation Science 2021*, *1*, 1–19. https://doi.org/10.1007/S41064-021-00139-Y

Helmert, J., Şorman, A. Ş., Montero, R. A., De Michele, C., de Rosnay, P., Dumont, M., … Arslan, A. N. (2018, December 1). Review of snow data assimilation methods for hydrological, land surface, meteorological and climate models: Results from a COST harmosnow survey. *Geosciences (Switzerland)*, Vol. 8, p. 489. https://doi.org/10.3390/geosciences8120489

Hirabayashi, Y., Tanoue, M., Sasaki, O., Zhou, X., & Yamazaki, D. (2021). Global exposure to flooding from the new CMIP6 climate model projections. *Scientific Reports 2021 11:1*, *11*(1), 1–7. https://doi.org/10.1038/s41598-021-83279-w

Hjort, N. L., & Claeskens, G. (2003). Frequentist Model Average Estimators. *Journal of the American Statistical Association*, *98*(464), 879–899. https://doi.org/10.1198/016214503000000828

Hock, R. (2003). Temperature index melt modelling in mountain areas. *Journal of Hydrology*. https://doi.org/10.1016/S0022-1694(03)00257-9

Hock, R. (2005). Glacier melt: A review of processes and their modelling. *Progress in*

Physical Geography. https://doi.org/10.1191/0309133305pp453ra

Hofer, S., Lang, C., Amory, C., Kittel, C., Delhasse, A., Tedstone, A., … Fettweis, X. (2020). Doubling of future Greenland Ice Sheet surface melt revealed by the new CMIP6 high-emission scenario. *EGUGA*, 19502. Retrieved from https://ui.adsabs.harvard.edu/abs/2020EGUGA..2219502H/abstract

Hofer, S., Lang, C., Amory, C., Kittel, C., Delhasse, A., Tedstone, A., & Fettweis, X. (2020). Greater Greenland Ice Sheet contribution to global sea level rise in CMIP6. *Nature Communications 2020 11:1, 11*(1), 1–11. https://doi.org/10.1038/s41467-020-20011-8

Hoffman, R. N., Kumar, V. K., Boukabara, S. A., Ide, K., Yang, F., & Atlas, R. (2018). Progress in forecast skill at three leading global operational NWP centers during 2015-17 as seen in summary assessment metrics (SAMs). *Weather and Forecasting*. https://doi.org/10.1175/WAF-D-18-0117.1

Höge, M., Guthke, A., & Nowak, W. (2019, May 1). The hydrologist's guide to Bayesian model selection, averaging and combination. *Journal of Hydrology*, Vol. 572, pp. 96–107. https://doi.org/10.1016/j.jhydrol.2019.01.072

Hopkinson, C., & Demuth, M. N. (2006). Using airborne lidar to assess the influence of glacier downwasting on water resources in the Canadian Rocky Mountains. *Canadian Journal of Remote Sensing*, *32*(2), 212–222.

Hori, M., Sugiura, K., Kobayashi, K., Aoki, T., Tanikawa, T., Kuchiki, K., … Enomoto, H. (2017). A 38-year (1978–2015) Northern Hemisphere daily snow cover extent product derived using consistent objective criteria from satellite-borne optical sensors. *Remote Sensing of Environment*, *191*, 402–418. https://doi.org/10.1016/j.rse.2017.01.023

Huss, M. (2011). Present and future contribution of glacier storage change to runoff from macroscale drainage basins in Europe. *Water Resour. Res.*, *47*(7), W07511. https://doi.org/10.1029/2010wr010299

Huss, Matthias, & Hock, R. (2018). Global-scale hydrological response to future glacier mass loss. *Nature Climate Change 2018 8:2*, *8*(2), 135–140. https://doi.org/10.1038/s41558-017-0049-x

Hyvärinen, O., Eerola, K., Siljamo, N., & Koskinen, J. (2009). Comparison of snow cover from satellite and numerical weather prediction models in the Northern Hemisphere and Northern Europe. *Journal of Applied Meteorology and Climatology*, *48*(6), 1199–1216.

Icelandic Meterological Office. (2023). Tímaraðir fyrir valdar veðurstöðvar. Retrieved August 15, 2023, from https://vedur.is/vedur/vedurfar/medaltalstoflur/

Icelandic Meterologocial Office. (2008). *Reglur um veðurathuganir, skýrslurfærslu og skeytasendingar á skeytastöðvum*. Retrieved from https://www.vedur.is/media/vedurstofan/utgafa/greinargerdir/1995/leidbeiningar_2003_v2.pdf

Icelandic Meterologocial Office. (2021). *Gagnabanki Veðurstofu Íslands, afgreiðsla nr.*

2021-12-15/01. Reykjavik.

IPCC. (2021). *Climate Change 2021: The Physical Science Basis. Contribution of Working Group I to the Sixth Assessment Report of the Intergovernmental Panel on Climate Change* (V. Masson-Delmotte, P. Zhai, A. Pirani, S. L. Connors, C. Péan, S. Berger, … B. Zhou, Eds.). Retrieved from https://www.ipcc.ch/report/ar6/wg1/#FullReport

Jacob, D., Petersen, J., Eggert, B., Alias, A., Christensen, O. B., Bouwer, L. M., … Yiou, P. (2013). EURO-CORDEX: new high-resolution climate change projections for European impact research. *Regional Environmental Change 2013 14:2*, *14*(2), 563–578. https://doi.org/10.1007/S10113-013-0499-2

Jarvis, C. H., & Stuart, N. (2001). A Comparison among Strategies for Interpolating Maximum and Minimum Daily Air Temperatures. Part II: The Interaction between Number of Guiding Variables and the Type of Interpolation Method. *Journal of Applied Meteorology*, *40*(6), 1075–1084. https://doi.org/10.1175/1520-0450(2001)040<1075:ACASFI>2.0.CO;2

Jevrejeva, S., Palanisamy, H., & Jackson, L. P. (2020). Global mean thermosteric sea level projections by 2100 in CMIP6 climate models. *Environmental Research Letters*, *16*(1), 014028. https://doi.org/10.1088/1748-9326/ABCEEA

Johannesson, T., Adalgeirsdottir, G., Bjornsson, H., Crochet, P., Eliasson, B. E., Gudmundsson, S., … Thorsteinsson, T. (2007). *Effect of climate change on hydrology and hydro-resoures in Iceland*. Reykjavik.

Jóhannesson, T., Björnsson, H., Magnússon, E., Guðmundsson, S., Pálsson, F., Sigurðsson, O., … Berthier, E. (2013). Ice-volume changes, bias estimation of mass-balance measurements and changes in subglacial lakes derived by lidar mapping of the surface of Icelandic glaciers. *Annals of Glaciology*, *54*(63), 63–74. https://doi.org/10.3189/2013AOG63A422

Jóhannesson, T., Pálmason, B., Hjartarson, Á., Jarosch, A. H., Magnússon, E., Belart, J. M. C., & Gudmundsson, M. T. (2020). Non-surface mass balance of glaciers in Iceland. *Journal of Glaciology*, *66*(258), 685–697.

Jónsdóttir, J. F., Uvo, C. B., & Clarke, R. T. (2008). Trend analysis in Icelandic discharge, temperature and precipitation series by parametric methods. *Hydrology Research*, *39*(5–6), 425–436. https://doi.org/10.2166/NH.2008.002

Jónsson, T. (2001). *Langtímasveiflur I. Snjóhula og snjókoma.* Reykjavik.

Juszak, I., & Pellicciotti, F. (2013). A comparison of parameterizations of incoming longwave radiation over melting glaciers: Model robustness and seasonal variability. *Journal of Geophysical Research Atmospheres*, *118*(8), 3066–3084. https://doi.org/10.1002/JGRD.50277

Jylhä, K., Tuomenvirta, H., Ruosteenoja, K., Niemi-Hugaerts, H., Keisu, K., & Karhu, J. A. (2010). Observed and Projected Future Shifts of Climatic Zones in Europe and Their Use to Visualize Climate Change Information. *Weather, Climate, and Society*, *2*(2), 148–167. https://doi.org/10.1175/2010wcas1010a.1

Kääb, A., Wessels, R., Haeberli, W., Huggel, C., Kargel, J., & Khalsa, S. (2003). Rapid ASTER imaging facilitates timely assessment of glacier hazards and disasters. *Eos*, *84*(13), 117. https://doi.org/10.1029/2003eo130001

Kalra, A., Ahmad, S., & Nayak, A. (2013). Increasing streamflow forecast lead time for snowmelt-driven catchment based on large-scale climate patterns. *Advances in Water Resources*, *53*, 150–162. https://doi.org/10.1016/j.advwatres.2012.11.003

Kang, D. H., Gao, H., Shi, X., Islam, S. U., & Déry, S. J. (2016). Impacts of a Rapidly Declining Mountain Snowpack on Streamflow Timing in Canada's Fraser River Basin. *Scientific Reports*. https://doi.org/10.1038/srep19299

Kapnick, S. B., & Delworth, T. L. (2013). Controls of global snow under a changed climate. *Journal of Climate*. https://doi.org/10.1175/JCLI-D-12-00528.1

Kaser, G., Großhauser, M., & Marzeion, B. (2010). Contribution potential of glaciers to water availability in different climate regimes. *Proc. Natl Acad. Sci. USA (PNAS)*, *107*(47), 20 223-20 227. https://doi.org/10.1073/pnas.1008162107

Kavetski, D., Kuczera, G., & Franks, S. W. (2006). Calibration of conceptual hydrological models revisited: 1. Overcoming numerical artefacts. *Journal of Hydrology*. https://doi.org/10.1016/j.jhydrol.2005.07.012

Kelly, R. (2009). The AMSR-E snow depth algorithm: Description and initial results. *Journal of the Remote Sensing Society of Japan*, *29*(1), 307–317.

Kerr, R. A. (2000, June 16). A North Atlantic climate pacemaker for the centuries. *Science*, Vol. 288, pp. 1984–1986. https://doi.org/10.1126/science.288.5473.1984

Klein Tank, A. M. G., & Konnen, G. P. (2003). Trends in Indices of Daily Temperature and Precipitation Extremes in Europe, 1946 - 99. *Journal of Climate*, *16*(22), 3665–3680. https://doi.org/10.1175/1520-0442(2003)016<3665:TIIODT>2.0.CO;2

Knudsen, K. L., Søndergaard, M. K. B., Eiríksson, J., & Jiang, H. (2008). Holocene thermal maximum off North Iceland: Evidence from benthic and planktonic foraminifera in the 8600–5200 cal year BP time slice. *Marine Micropaleontology*, *67*(1–2), 120–142. https://doi.org/10.1016/J.MARMICRO.2007.11.003

Kok, R. J. de, Steiner, J. F., Litt, M., Wagnon, P., Koch, I., Azam, M. F., & Immerzeel, W. W. (2020). Measurements, models and drivers of incoming longwave radiation in the Himalaya. *International Journal of Climatology*, *40*(2), 942. https://doi.org/10.1002/JOC.6249

König, M., Winther, J., & Isaksson, E. (2001). Measuring snow and glacier ice properties from satellite. *Reviews of Geophysics*, *39*(1), 1–27.

Kopec, B. G., Feng, X., Michel, F. A., & Posmentier, E. S. (2016). Influence of sea ice on Arctic precipitation. *Proceedings of the National Academy of Sciences*, *113*(1), 46–51. https://doi.org/10.1073/pnas.1504633113

Köppen, W. (1884). Die Wärmezonen der Erde, nach der Dauer der heissen, gemässigten

und kalten Zeit und nach der Wirkung der Wärme auf die organische Welt betrachtet. *Meteorologische Zeitschrift*, *1*(21), 5–226.

Köppen, W. P., & Geiger, R. (1968). *Klima der Erde: Climate of the Earth*. Perthes.

Kottek, M., Grieser, J., Beck, C., Rudolf, B., & Rubel, F. (2006). World map of the Köppen-Geiger climate classification updated. *Meteorologische Zeitschrift*, *15*(3), 259–263. https://doi.org/10.1127/0941-2948/2006/0130

Kraus, K., & Pfeifer, N. (1998). Determination of terrain models in wooded areas with airborne laser scanner data. *ISPRS Journal of Photogrammetry and Remote Sensing*, *53*(4), 193–203.

Krinner, G., Derksen, C., Essery, R., Flanner, M., Hagemann, S., Clark, M., … Zhu, D. (2018). ESM-SnowMIP: Assessing snow models and quantifying snow-related climate feedbacks. *Geoscientific Model Development*. https://doi.org/10.5194/gmd-11-5027-2018

Kulkarni, A. V, & Karyakarte, Y. (2014). Observed changes in Himalayan glaciers. *Current Science*, *106*(2), 237–244. Retrieved from http://www.jstor.org/stable/24099804

Kumar, S., Mocko, D., Vuyovich, C., & Peters-Lidard, C. (2020). Impact of surface albedo assimilation on snow estimation. *Remote Sensing*, *12*(4), 645.

Kustas, W. P., Rango, A., & Uijlenhoet, R. (1994). A simple energy budget algorithm for the snowmelt runoff model. *Water Resources Research*. https://doi.org/10.1029/94WR00152

Kuusisto, E. (1980). On the Values and Variability of Degree-Day Melting Factor in Finland. *Hydrology Research*. https://doi.org/10.2166/nh.1980.0011

Lang, H., & Braun, L. (1990). On the information content of air temperature in the context of snow melt estimation. *Hydrology of Mountainous Areas*.

Langdon, P. G., Caseldine, C. J., Croudace, I. W., Jarvis, S., Wastegård, S., & Crowford, T. C. (2011). A chironomid-based reconstruction of summer temperatures in NW Iceland since AD 1650. *Quaternary Research*, *75*(3), 451–460. https://doi.org/10.1016/J.YQRES.2010.11.007

Larsen, D. J., Miller, G. H., Geirsdóttir, Á., & Thordarson, T. (2011). A 3000-year varved record of glacier activity and climate change from the proglacial lake Hvítárvatn, Iceland. *Quaternary Science Reviews*, *30*(19–20), 2715–2731. https://doi.org/10.1016/J.QUASCIREV.2011.05.026

Lee, J. Y., Marotzke, J., Bala, G., Cao, L., Corti, S., Dunne, J. P., … Zhou, T. (2021). Future Global Climate: Scenario-Based Projections and Near-Term Information. In V. Masson-Delmotte, P. Zhai, A. Pirani, S. L. Connors, C. Péan, S. Berger, … B. Zhou (Eds.), *Climate Change 2021: The Physical Science Basis. Contribution of Working Group I to the Sixth Assessment Report of the Intergovernmental Panel on Climate Change* (p. 200). Retrieved from https://www.ipcc.ch/report/ar6/wg1/#FullReport

Lemke, P., Ren, J., Alley, R. B., Allison, I., Carrasco, J., Flato, G., … Thomas, R. H. (2007). Observations: changes in snow, ice and frozen ground Climate Change 2007: The Physical Science Basis. Contribution of Working Group I to the Fourth Assessment Report of the Intergovernmental Panel on Climate Change. *Cambridge University Press. UK, Cambridge*, 337–383.

Levitus, S., Antonov, J. I., Boyer, T. P., Baranova, O. K., Garcia, H. E., Locarnini, R. A., … Zweng, M. M. (2012). World ocean heat content and thermosteric sea level change (0-2000m), 1955-2010. *Geophysical Research Letters*, *39*(10). https://doi.org/10.1029/2012GL051106

Li, C., Su, F., Yang, D., Tong, K., Meng, F., & Kan, B. (2018). Spatiotemporal variation of snow cover over the Tibetan Plateau based on MODIS snow product, 2001–2014. *International Journal of Climatology*, *38*(2), 708–728. https://doi.org/10.1002/joc.5204

Liang, T., Zhang, X., Xie, H., Wu, C., Feng, Q., Huang, X., & Chen, Q. (2008). Toward improved daily snow cover mapping with advanced combination of MODIS and AMSR-E measurements. *Remote Sensing of Environment*, *112*(10), 3750–3761.

Lievens, H., Demuzere, M., Marshall, H.-P., Reichle, R. H., Brucker, L., Brangers, I., … De Lannoy, G. J. M. (2019). Snow depth variability in the Northern Hemisphere mountains observed from space. *Nature Communications 2019 10:1*, *10*(1), 1–12. https://doi.org/10.1038/s41467-019-12566-y

Liston, G. E., & Hiemstra, C. A. (2011). The changing cryosphere: Pan-Arctic snow trends (1979-2009). *Journal of Climate*, *24*(21), 5691–5712. https://doi.org/10.1175/JCLI-D-11-00081.1

López-Moreno, J. I., & Nogués-Bravo, D. (2006). Interpolating local snow depth data: an evaluation of methods. *Hydrological Processes*, *20*(10), 2217–2232. https://doi.org/https://doi.org/10.1002/hyp.6199

Louis, J.-F. (1979). A parametric model of vertical eddy fluxes in the atmosphere. *Boundary-Layer Meteorology 1979 17:2*, *17*(2), 187–202. https://doi.org/10.1007/BF00117978

LP-DAAC. (2004). Global 30 Arc-Second Elevation Data Set GTOPO30.

Lucas, R. M., & Harrison, A. R. (1990). Snow observation by satellite: A review. *Remote Sensing Reviews*, *4*(2), 285–348.

Lyu, K., Zhang, X., & Church, J. A. (2020). Regional Dynamic Sea Level Simulated in the CMIP5 and CMIP6 Models: Mean Biases, Future Projections, and Their Linkages. *Journal of Climate*, *33*(15), 6377–6398. https://doi.org/10.1175/JCLI-D-19-1029.1

Magnússon, E., Pálsson, F., Björnsson, H., & Guðmundsson, S. (2013). *Removing the ice cap of Öræfajökull central volcano, SE-Iceland: Mapping and interpretation of bedrock topography, ice volumes, subglacial troughs and implications for hazards assessments*.

Magnússon, Eyjólfur, Pálsson, F., & Björnsson, H. (2009). *Breytingar á austanverðum Skeiðarárjökli og farvegi Skeiðarár 1997-2009 og framtíðarhorfur*. Reykjavik.

Magnusson, J., Wever, N., Essery, R., Helbig, N., Winstral, A., & Jonas, T. (2015). Evaluating snow models with varying process representations for hydrological applications. *Water Resources Research*. https://doi.org/10.1002/2014WR016498

Malmros, J. K., Mernild, S. H., Wilson, R., Tagesson, T., & Fensholt, R. (2018). Snow cover and snow albedo changes in the central Andes of Chile and Argentina from daily MODIS observations (2000–2016). *Remote Sensing of Environment*, *209*, 240–252. https://doi.org/10.1016/J.RSE.2018.02.072

Marks, D., Kimball, J., Tingey, D., & Link, T. (1998). The sensitivity of snowmelt processes to climate conditions and forest cover during rain-on-snow: a case study of the 1996 Pacific Northwest flood. *Hydrological Processes*. https://doi.org/10.1002/(SICI)1099-1085(199808/09)12:10/11<1569::AID-HYP682>3.0.CO;2-L

Marshall, S. J., Björnsson, H., Flowers, G. E., & Clarke, G. K. C. (2005). Simulation of Vatnajökull ice cap dynamics. *Journal of Geophysical Research: Earth Surface*. https://doi.org/10.1029/2004JF000262

Marthews, T. R., Malhi, Y., & Iwata, H. (2012). Calculating downward longwave radiation under clear and cloudy conditions over a tropical lowland forest site: An evaluation of model schemes for hourly data. *Theoretical and Applied Climatology*, *107*(3–4), 461–477. https://doi.org/10.1007/S00704-011-0486-9

Marti, R., Gascoin, S., Berthier, E., Pinel, M. de, Houet, T., & Laffly, D. (2016). Mapping snow depth in open alpine terrain from stereo satellite imagery. *The Cryosphere*, *10*(4), 1361–1380.

Martin, E., & Lejeune, Y. (1998). Turbulent fluxes above the snow surface. *Annals of Glaciology*. https://doi.org/10.3189/1998aog26-1-179-183

Marzeion, B., Cogley, J., Richter, K., & Parkes, D. (2014). Attribution of global glacier mass loss to anthropogenic and natural causes. *Science*, *345*(6199), 919–921. https://doi.org/10.1126/science.1254702

Marzeion, B., Jarosch, A., & Hofer, M. (2012). Past and future sea-level change from the surface mass balance of glaciers. *Cryosphere*, *6*(6), 1295–1322. https://doi.org/10.5194/tc-6-1295-2012

Maslanik, J., Stroeve, J., Fowler, C., & Emery, W. (2011). Distribution and trends in Arctic sea ice age through spring 2011. *Geophysical Research Letters*. https://doi.org/10.1029/2011GL047735

Maurer, J. M., Schaefer, J. M., Rupper, S., & Corley, A. (2019). Acceleration of ice loss across the Himalayas over the past 40 years. *Science Advances*. https://doi.org/10.1126/sciadv.aav7266

Maurice G Kendall. (1975). Rank Correlation Methods. In *London Griffin*.

McCune, B., & Keon, D. (2002). Equations for potential annual direct incident radiation and heat load. *Journal of Vegetation Science*. https://doi.org/10.1111/j.1654-1103.2002.tb02087.x

Melkonian, A. K., Willis, M. J., Pritchard, M. E., & Stewart, A. J. (2016). Recent changes in glacier velocities and thinning at Novaya Zemlya. *Remote Sensing of Environment*, *174*, 244–257. https://doi.org/10.1016/j.rse.2015.11.001

Menne, M. J., Durre, I., Vose, R. S., Gleason, B. E., & Houston, T. G. (2012). An Overview of the Global Historical Climatology Network-Daily Database. *Journal of Atmospheric and Oceanic Technology*, *29*(7), 897–910. https://doi.org/10.1175/JTECH-D-11-00103.1

Meromy, L., Molotch, N. P., Link, T. E., Fassnacht, S. R., & Rice, R. (2013). Subgrid variability of snow water equivalent at operational snow stations in the western USA. *Hydrological Processes*, *27*(17), 2383–2400. https://doi.org/https://doi.org/10.1002/hyp.9355

Metsämäki, S. J., Anttila, S. T., Markus, H. J., & Vepsäläinen, J. M. (2005). A feasible method for fractional snow cover mapping in boreal zone based on a reflectance model. *Remote Sensing of Environment*, *95*(1), 77–95.

Miller, S. D., Lee, T. F., & Fennimore, R. L. (2005). Satellite-based imagery techniques for daytime cloud/snow delineation from MODIS. *Journal of Applied Meteorology*, *44*(7), 987–997.

Miller, S. L., Elder, K., Cline, D., Davis, R. E., & Ochs, E. (2003). Use of LIDAR for measuring snowpack depth. *AGU Fall Meeting Abstracts*, *2003*, C42C-05.

Miller, W. P., Piechota, T. C., Gangopadhyay, S., & Pruitt, T. (2011). Development of streamflow projections under changing climate conditions over Colorado River basin headwaters. *Hydrology and Earth System Sciences*. https://doi.org/10.5194/hess-15-2145-2011

Ministerrådet, N. (2012). *Climate Change and Energy Systems.* 228.

Mizukami, N., & Koren, V. (2008). Methodology and Evaluation of Melt Factor Parameterization for Distributed SNOW- 17. *Abstract Id. H31J-08*. American Geophysical Union, Fall Meeting 2008.

Molotch, N. P., Colee, M. T., Bales, R. C., & Dozier, J. (2005). Estimating the spatial distribution of snow water equivalent in an alpine basin using binary regression tree models: The impact of digital elevation data and independent variable selection. *Hydrological Processes*. https://doi.org/10.1002/hyp.5586

Moriasi, D. N., Arnold, J. G., Van Liew, M. W., Binger, R. L., Harmel, R. D., & Veith, T. L. (2007). Model evaluation guidelines for systematic quantification of accuracy in watershed simulations. *Transactions of the ASABE*, *50*(3), 885–900. https://doi.org/10.13031/2013.23153

Mosavi, A., Ozturk, P., & Chau, K. W. (2018). Flood prediction using machine learning models: Literature review. *Water (Switzerland)*. https://doi.org/10.3390/w10111536

Mote, P. W., Hamlet, A. F., Clark, M. P., & Lettenmaier, D. P. (2005). Declining mountain snowpack in western north America. *Bulletin of the American Meteorological Society*.

https://doi.org/10.1175/BAMS-86-1-39

Mudryk, L. R., Derksen, C., Kushner, P. J., & Brown, R. (2015). Characterization of Northern Hemisphere snow water equivalent datasets, 1981-2010. *Journal of Climate*. https://doi.org/10.1175/JCLI-D-15-0229.1

Mudryk, L., Santolaria-Otín, M., Krinner, G., Ménégoz, M., Derksen, C., Brutel-Vuilmet, C., … Essery, R. (2020). Historical Northern Hemisphere snow cover trends and projected changes in the CMIP6 multi-model ensemble. *Cryosphere*, *14*(7), 2495–2514. https://doi.org/10.5194/TC-14-2495-2020

Nawri, N., Pálmason, B., Petersen, G. N., Björnsson, H., & Þorsteinsson, S. (2017). The ICRA atmospheric reanalysis project for Iceland. *Icel Meteorol Off*, *5*.

Nijssen, B., Bowling, L. C., Lettenmaier, D. P., Clark, D. B., El Maayar, M., Essery, R., … Yang, Z. L. (2003). Simulation of high latitude hydrological processes in the Torne-Kalix basin: PILPS Phase 2(e) 2: Comparison of model results with observations. *Global and Planetary Change*. https://doi.org/10.1016/S0921-8181(03)00004-3

Notaro, M., Lorenz, D., Hoving, C., & Schummer, M. (2014). Twenty-first-century projections of snowfall and winter severity across central-eastern North America. *Journal of Climate*. https://doi.org/10.1175/JCLI-D-13-00520.1

Notz, D., & Community, S. (2020). Arctic Sea Ice in CMIP6. *Geophysical Research Letters*, *47*(10), e2019GL086749. https://doi.org/10.1029/2019GL086749

Notz, D., Jahn, A., Holland, M., Hunke, E., Massonnet, F., Stroeve, J., … Vancoppenolle, M. (2016). The CMIP6 Sea-Ice Model Intercomparison Project (SIMIP): Understanding sea ice through climate-model simulations. *Geoscientific Model Development*, *9*(9), 3427–3446. https://doi.org/10.5194/GMD-9-3427-2016

Nowicki, S. M. J., Payne, A., Larour, E., Seroussi, H., Goelzer, H., Lipscomb, W., … Shepherd, A. (2016). Ice Sheet Model Intercomparison Project (ISMIP6) contribution to CMIP6. *Geoscientific Model Development*, *9*(12), 4521–4545. https://doi.org/10.5194/GMD-9-4521-2016

O'Neel, S., McNeil, C., Sass, L. C., Florentine, C., Baker, E. H., Peitzsch, E., … Fagre, D. (2019). Reanalysis of the US Geological Survey Benchmark Glaciers: Long-term insight into climate forcing of glacier mass balance. *Journal of Glaciology*. https://doi.org/10.1017/jog.2019.66

Ohmura, A. (2002). Physical Basis for the Temperature-Based Melt-Index Method. *Journal of Applied Meteorology*. https://doi.org/10.1175/1520-0450(2001)040<0753:pbfttb>2.0.co;2

Ólafsson, H., Furger, M., & Brümmer, B. (2007). The weather and climate of Iceland. *Meteorologische Zeitschrift*, *16*(1), 5–8. https://doi.org/10.1127/0941-2948/2007/0185

Paik, S., & Min, S.-K. (2020). Quantifying the Anthropogenic Greenhouse Gas Contribution to the Observed Spring Snow-Cover Decline Using the CMIP6 Multimodel Ensemble. *Journal of Climate*, *33*(21), 9261–9269. https://doi.org/10.1175/JCLI-D-20-0002.1

Painter, T. H., Rittger, K., McKenzie, C., Slaughter, P., Davis, R. E., & Dozier, J. (2009). Retrieval of subpixel snow covered area, grain size, and albedo from MODIS. *Remote Sensing of Environment*. https://doi.org/10.1016/j.rse.2009.01.001

Pálsson, F., Gudmundsson, S., Björnsson, H., Berthier, E., Magnússon, E., Gudmundsson, S., & Haraldsson, H. (2012). Mass and volume changes of Langjökull ice cap, Iceland, ~1890 to 2009, deduced from old maps, satellite images and in situ mass balance measurements. *Undefined*.

Palsson, F., Gunnarsson, A., Adalgeirsdottir, G., Jonsson, T., Steinthorsson, S., & Palsson, H. (2014). *Vatnajokull: Mass balance, melt water drainage and surface velocity of the glacial year 2013-14*.

Pálsson, Finnur, Magnússon, E., & Björnsson, H. (2016). *Greinargerð um könnun á legu vatnaskila Skaftár og Hverfisfljóts og stöðugleika þeirra þegar jökullinn hörfar*. Reykjavik.

Palter, J. B. (2015). The Role of the Gulf Stream in European Climate. *Annual Review of Marine Science*, *7*(1), 113–137. https://doi.org/10.1146/annurev-marine-010814-015656

Parajka, J, Pepe, M., Rampini, A., Rossi, S., & Blöschl, G. (2010). A regional snow-line method for estimating snow cover from MODIS during cloud cover. *Journal of Hydrology*, *381*(3–4), 203–212.

Parajka, Juraj, Haas, P., Kirnbauer, R., Jansa, J., & Blöschl, G. (2012). Potential of time-lapse photography of snow for hydrological purposes at the small catchment scale. *Hydrological Processes*, *26*(22), 3327–3337. https://doi.org/10.1002/HYP.8389

Paulescu, M., Paulescu, E., Gravila, P., & Badescu, V. (2013). Solar Radiation Measurements. In *Weather Modeling and Forecasting of PV Systems Operation* (pp. 17–42). https://doi.org/10.1007/978-1-4471-4649-0_2

Payne, A. J., Nowicki, S., Abe-Ouchi, A., Agosta, C., Alexander, P., Albrecht, T., … Zwinger, T. (2021). Future sea level change under CMIP5 and CMIP6 scenarios from the Greenland and Antarctic ice sheets. *Geophysical Research Letters*, *14*, e2020GL091741. https://doi.org/10.1029/2020GL091741

Peel, M. C., Finlayson, B. L., & Mcmahon, T. A. (2007). Updated world map of the Koppen-Geiger climate classification. *HESSD Earth Syst. Sci. Discuss*, *4*(4), 439–473. https://doi.org/10.1127/0941-2948/2006/0130

Pepe, M., Brivio, P. A., Rampini, A., Nodari, F. R., & Boschetti, M. (2005). Snow cover monitoring in Alpine regions using ENVISAT optical data. *International Journal of Remote Sensing*, *26*(21), 4661–4667.

Poli, P., Hersbach, H., Dee, D. P., Berrisford, P., Simmons, A. J., Vitart, F., … Fisher, M. (2016). ERA-20C: An Atmospheric Reanalysis of the Twentieth Century. *Journal of Climate*, *29*(11), 4083–4097. https://doi.org/10.1175/JCLI-D-15-0556.1

Pulliainen, J., & Hallikainen, M. (2001). Retrieval of regional snow water equivalent from

space-borne passive microwave observations. *Remote Sensing of Environment*, *75*(1), 76–85.

Pulliainen, J. T., Grandell, J., & Hallikainen, M. T. (1999). HUT snow emission model and its applicability to snow water equivalent retrieval. *IEEE Transactions on Geoscience and Remote Sensing*, *37*(3), 1378–1390.

Putnam, A. E., Schaefer, J. M., Denton, G. H., Barrell, D. J. A., Finkel, R. C., Andersen, B. G., … Doughty, A. M. (2012). Regional climate control of glaciers in NewÂ Zealand and Europe during the pre-industrial Holocene. *Nature Geoscience*. https://doi.org/10.1038/ngeo1548

Radić, V., Bliss, A., Beedlow, A., Hock, R., Miles, E., & Cogley, J. (2013). Regional and global projections of twenty-first century glacier mass changes in response to climate scenarios from global climate models. *Climate Dyn.*, *42*(1–2), 37–58. https://doi.org/10.1007/s00382-013-1719-7

Raleigh, M. S., & Clark, M. P. (2014). Are temperature-index moels appropriate for assessing climate change impacts on snowmelt? *Proceeding of the Western Snow Conference 2014*.

Reutebuch, S. E., McGaughey, R. J., Andersen, H.-E., & Carson, W. W. (2003). Accuracy of a high-resolution lidar terrain model under a conifer forest canopy. *Canadian Journal of Remote Sensing*, *29*(5), 527–535.

RGI Consortium. (2019). *Randolph Glacier Inventory - A Dataset of Global Glacier Outlines, Version 6. [Iceland]*. https://doi.org/doi: https://doi.org/10.7265/4m1f-gd79

Roach, L. A., Dörr, J., Holmes, C. R., Massonnet, F., Blockley, E. W., Notz, D., … Bitz, C. M. (2020). Antarctic Sea Ice Area in CMIP6. *Geophysical Research Letters*, *47*(9), e2019GL086729. https://doi.org/10.1029/2019GL086729

Roberts, M. J., Camp, J., Seddon, J., Vidale, P. L., Hodges, K., Vannière, B., … Wu, L. (2020). Projected Future Changes in Tropical Cyclones Using the CMIP6 HighResMIP Multimodel Ensemble. *Geophysical Research Letters*, *47*(14), e2020GL088662. https://doi.org/10.1029/2020GL088662

Robinson, D. A. (1993). Hemispheric snow cover from satellites. *Annals of Glaciology*, *17*, 367–371. https://doi.org/DOI: 10.3189/S0260305500013112

Rodell, B. M., Houser, P. R., Jambor, U., Gottschalck, J., Mitchell, K., Meng, C., … Toll, D. (2004). THE GLOBAL LAND DATA ASSIMILATION SYSTEM This powerful new land surface modeling system integrates data from advanced observing systems to support improved forecast model initialization and hydrometeorological investigations. *Bull. Amer. Meteor. Soc.* https://doi.org/10.1

Rodell, M, & Houser, P. R. (2004). Updating a land surface model with MODIS-derived snow cover. *Journal of Hydrometeorology*, *5*(6), 1064–1075.

Rodell, Matthew, Houser, P. R., Jambor, U., Gottschalck, J., Mitchell, K., Meng, C. J., … Toll, D. (2004). The Global Land Data Assimilation System. *Bulletin of the American*

Meteorological Society. https://doi.org/10.1175/BAMS-85-3-381

Roegnvaldsson, O., Jonsdottir, J. F., & Olafsson, H. (2007). Numerical simulations of precipitation in the complex terrain of Iceland - Comparison with glaciological and hydrological data. *Meteorologische Zeitschrift*, *16*(1), 71–85. https://doi.org/10.1127/0941-2948/2007/0174

Romanov, P., Gutman, G., & Csiszar, I. (2000). Automated monitoring of snow cover over North America with multispectral satellite data. *Journal of Applied Meteorology*, *39*(11), 1866–1880.

Rosenthal, W., & Dozier, J. (1996). Automated mapping of montane snow cover at subpixel resolution from the Landsat Thematic Mapper. *Water Resources Research*, *32*(1), 115–130.

Ryan, W. A., Doesken, N. J., & Fassnacht, S. R. (2008). Evaluation of ultrasonic snow depth sensors for US snow measurements. *Journal of Atmospheric and Oceanic Technology*, *25*(5), 667–684.

Saavedra, F. A., Kampf, S. K., Fassnacht, S. R., & Sibold, J. S. (2018). Changes in Andes snow cover from MODIS data, 2000-2016. *Cryosphere*, *12*(3), 1027–1046. https://doi.org/10.5194/TC-12-1027-2018

Salomonson, V. V., & Appel, I. (2006). Development of the aqua MODIS NDSI fractional snow cover algorithm and validation results. *IEEE Transactions on Geoscience and Remote Sensing*. https://doi.org/10.1109/TGRS.2006.876029

Sante, F. Di, Coppola, E., & Giorgi, F. (2021). Projections of river floods in Europe using EURO-CORDEX, CMIP5 and CMIP6 simulations. *International Journal of Climatology*, *41*(5), 3203–3221. https://doi.org/10.1002/JOC.7014

Schaefli, B., Hingray, B., Niggli, M., & Musy, A. (2010). A conceptual glacio-hydrological model for high mountainous catchments. *Hydrology and Earth System Sciences Discussions*. https://doi.org/10.5194/hessd-2-73-2005

Schomacker, A. (2010). Expansion of ice-marginal lakes at the Vatnajökull ice cap, Iceland, from 1999 to 2009. *Geomorphology*, *119*(3–4), 232–236. https://doi.org/10.1016/J.GEOMORPH.2010.03.022

Sen, P. K. (1968). Estimates of the Regression Coefficient Based on Kendall's Tau. *Journal of the American Statistical Association*, *63*(324), 1379–1389. https://doi.org/10.1080/01621459.1968.10480934

Serreze, M. C., & Barry, R. G. (2011). Processes and impacts of Arctic amplification: A research synthesis. *Global and Planetary Change*, *77*(1–2), 85–96. https://doi.org/10.1016/j.gloplacha.2011.03.004

Serreze, M. C., & Francis, J. A. (2006). The arctic amplification debate. *Climatic Change*, *76*(3–4), 241–264. https://doi.org/10.1007/s10584-005-9017-y

Serreze, M. C., & Stroeve, J. (2015). Arctic sea ice trends, variability and implications for

seasonal ice forecasting. *Philosophical Transactions of the Royal Society A: Mathematical, Physical and Engineering Sciences*, *373*(2045). https://doi.org/10.1098/rsta.2014.0159

Sexton, J. O., Song, X. P., Feng, M., Noojipady, P., Anand, A., Huang, C., … Townshend, J. R. (2013). Global, 30-m resolution continuous fields of tree cover: Landsat-based rescaling of MODIS vegetation continuous fields with lidar-based estimates of error. *International Journal of Digital Earth*. https://doi.org/10.1080/17538947.2013.786146

Sheffield, J., Goteti, G., & Wood, E. F. (2006). Development of a 50-year high-resolution global dataset of meteorological forcings for land surface modeling. *Journal of Climate*. https://doi.org/10.1175/JCLI3790.1

Shu, Q., Wang, Q., Song, Z., Qiao, F., Zhao, J., Chu, M., & Li, X. (2020). Assessment of Sea Ice Extent in CMIP6 With Comparison to Observations and CMIP5. *Geophysical Research Letters*, *47*(9), e2020GL087965. https://doi.org/10.1029/2020GL087965

Sicre, M.-A., Hall, I. R., Mignot, J., Khodri, M., Ezat, U., Truong, M.-X., … Knudsen, K.-L. (2011). Sea surface temperature variability in the subpolar Atlantic over the last two millennia. *Paleoceanography*, *26*(4). https://doi.org/10.1029/2011PA002169

Sigurðsson, O., & Jóhannesson, T. (2014). *Samantekt um snjómælingar á hálendi Íslands*. Reykjavik.

Sing, P., & Kumar, N. (1996). Determination of snowmelt factor in the Himalayan region. *Hydrological Sciences Journal*. https://doi.org/10.1080/02626669609491504

Singarayer, J. S., Bamber, J. L., Valdes, P. J., Singarayer, J. S., Bamber, J. L., & Valdes, P. J. (2006). Twenty-First-Century Climate Impacts from a Declining Arctic Sea Ice Cover. *Journal of Climate*, *19*(7), 1109–1125. https://doi.org/10.1175/JCLI3649.1

Singh, P., Kumar, N., & Arora, M. (2000). Degree-day factors for snow and ice for Dokriani Glacier, Garhwal Himalayas. *Journal of Hydrology*. https://doi.org/10.1016/S0022-1694(00)00249-3

Sivapalan, M. (2003). Prediction in ungauged basins: a grand challenge for theoretical hydrology. *Hydrological Processes*. https://doi.org/10.1002/hyp.5155

Slater, A. G., Schlosser, C. A., Desborough, C. E., Pitman, A. J., Henderson-Sellers, A., Robock, A., … Xue, Y. (2002). The Representation of Snow in Land Surface Schemes: Results from PILPS 2(d). *Journal of Hydrometeorology*. https://doi.org/10.1175/1525-7541(2001)002<0007:trosil>2.0.co;2

Slater, Andrew G., & Clark, M. P. (2006). Snow Data Assimilation via an Ensemble Kalman Filter. *Journal of Hydrometeorology*, *7*(3), 478–493. https://doi.org/10.1175/JHM505.1

Solberg, R., Wangensteen, B., Metsämäki, S., Nagler, T., Sandner, R., Rott, H., … Pulliainen, J. (2010). GlobSnow snow extent product guide product version 1.0. *European Space Angency, Finland*.

Sommer, C., Malz, P., Seehaus, T. C., Lippl, S., Zemp, M., & Braun, M. H. (2020). Rapid

glacier retreat and downwasting throughout the European Alps in the early 21st century. *Nature Communications 2020 11:1*, *11*(1), 1–10. https://doi.org/10.1038/s41467-020-16818-0

Stigter, E. M., Wanders, N., Saloranta, T. M., Shea, J. M., Bierkens, M. F. P., & Immerzeel, W. W. (2017). Assimilation of snow cover and snow depth into a snow model to estimate snow water equivalent and snowmelt runoff in a Himalayan catchment. *Cryosphere*. https://doi.org/10.5194/tc-11-1647-2017

Straneo, F., & Heimbach, P. (2013, December 4). North Atlantic warming and the retreat of Greenland's outlet glaciers. *Nature*, Vol. 504, pp. 36–43. https://doi.org/10.1038/nature12854

Sturm, M., Holmgren, J., & Liston, G. E. (1995). A seasonal snow cover classification system for local to global applications. *Journal of Climate*, *8*(5), 1261–1283.

Tait, A. B. (1998). Estimation of snow water equivalent using passive microwave radiation data. *Remote Sensing of Environment*, *64*(3), 286–291.

Tank, A. M. G. K., Wijngaard, J. B., Können, G. P., Böhm, R., Demarée, G., Gocheva, A., … Petrovic, P. (2002). Daily dataset of 20th-century surface air temperature and precipitation series for the European Climate Assessment. *International Journal of Climatology*, *22*(12), 1441–1453. https://doi.org/10.1002/JOC.773

Taylor, K. E., Stouffer, R. J., & Meehl, G. A. (2012). An overview of CMIP5 and the experiment design. *Bulletin of the American Meteorological Society*, Vol. 93, pp. 485–498. https://doi.org/10.1175/BAMS-D-11-00094.1

Thorsteinsson, T., & Björnstrom Halldór. (2013). Climate Change and Energy Systems. Impacts, risk and Adaptation in the Nordic Baltic countries. *International Journal of Applied Engineering Research*, *8*(March), 228.

Thorsteinsson, T., Einarsson, B., & Kjartansson, V. (2004). *Afkoma Hofsjokuls 1997-2004*.

Thrasher, B., Melton, F., & Weile, W. (2006). NASA Earth Exchange Global Daily Downscaled Projections (NEX-GDDP) | CDS. Retrieved May 1, 2017, from NASA NEX website: https://cds.nccs.nasa.gov/nex-gddp/

Tsai, Y.-L. S., Dietz, A., Oppelt, N., & Kuenzer, C. (2019). Remote Sensing of Snow Cover Using Spaceborne SAR: A Review. *Remote Sensing 2019, Vol. 11, Page 1456*, *11*(12), 1456. https://doi.org/10.3390/RS11121456

U.S. Army Corps of Engineers. (1998). Runoff From Snowmelt. *Engineering and Design*.

Ukkola, A. M., Kauwe, M. G. De, Roderick, M. L., Abramowitz, G., & Pitman, A. J. (2020). Robust Future Changes in Meteorological Drought in CMIP6 Projections Despite Uncertainty in Precipitation. *Geophysical Research Letters*, *47*(11), e2020GL087820. https://doi.org/10.1029/2020GL087820

Vaganov, E. A., Hughes, M. K., Kirdyanov, A. V., Schweingruber, F. H., & Silkin, P. P. (1999). Influence of snowfall and melt timing on tree growth in subarctic Eurasia.

Nature. https://doi.org/10.1038/22087

van Vuuren, D. P., Edmonds, J., Kainuma, M., Riahi, K., Thomson, A., Hibbard, K., … Rose, S. K. (2011). The representative concentration pathways: An overview. *Climatic Change*, *109*(1), 5–31. https://doi.org/10.1007/s10584-011-0148-z

Vavrus, S. (2007). The role of terrestrial snow cover in the climate system. *Climate Dynamics*, *29*(1), 73–88. https://doi.org/10.1007/s00382-007-0226-0

Wang, A., Xu, L., & Kong, X. (2018). Assessments of the Northern Hemisphere snow cover response to 1.5 and 2.0°C warming. *Earth System Dynamics*. https://doi.org/10.5194/esd-9-865-2018

Wang, B., Jin, C., & Liu, J. (2020). Understanding Future Change of Global Monsoons Projected by CMIP6 Models. *Journal of Climate*, *33*(15), 6471–6489. https://doi.org/10.1175/JCLI-D-19-0993.1

Wang, H., Zhang, X., & Zou, G. (2009). Frequentist model averaging estimation: a review. *Journal of Systems Science and Complexity*, *22*(September), 732–748. https://doi.org/10.1007/s11424-009-9198-y

Wang, L., Derksen, C., & Brown, R. (2008). Detection of pan-Arctic terrestrial snowmelt from QuikSCAT, 2000–2005. *Remote Sensing of Environment*, *112*(10), 3794–3805. https://doi.org/https://doi.org/10.1016/j.rse.2008.05.017

Wang, L., Sharp, M., Brown, R., Derksen, C., & Rivard, B. (2005). Evaluation of spring snow covered area depletion in the Canadian Arctic from NOAA snow charts. *Remote Sensing of Environment*, *95*(4), 453–463.

Wang, T., Fetzer, E. J., Wong, S., Kahn, B. H., & Yue, Q. (2016). Validation of MODIS cloud mask and multilayer flag using CloudSat-CALIPSO cloud profiles and a cross-reference of their cloud classifications. *Journal of Geophysical Research*, *121*(19), 11620–11635. https://doi.org/10.1002/2016JD025239

Wang, X., & Xie, H. (2009). New methods for studying the spatiotemporal variation of snow cover based on combination products of MODIS Terra and Aqua. *Journal of Hydrology*, *371*(1–4), 192–200.

Warren, S. G. (2019). Optical properties of ice and snow. *Philosophical Transactions of the Royal Society A: Mathematical, Physical and Engineering Sciences*. https://doi.org/10.1098/rsta.2018.0161

Winther, J., Gerland, S., Ørbæk, J. B., Ivanov, B., Blanco, A., & Boike, J. (1999). Spectral reflectance of melting snow in a high Arctic watershed on Svalbard: some implications for optical satellite remote sensing studies. *Hydrological Processes*, *13*(12-13), 2033–2049.

WMO. (2014). *Global Cryosphere Watch*. Vienna.

Xuejin, T., Zhenni, W., Xingmin, M., Peng, G., Guangju, Z., Wenyi, S., & Chaojun, G. (2019). Spatiotemporal changes in snow cover over China during 1960–2013.

Atmospheric Research, *218*, 183–194. https://doi.org/10.1016/J.ATMOSRES.2018.11.018

Yunlong, W., Huang, X., Hui, L., Sun, Y., Qisheng, F., & Tiangang, L. (2018). Tracking Snow Variations in the Northern Hemisphere Using Multi-Source Remote Sensing Data (2000–2015). *Remote Sensing*, *10(1)*(136). https://doi.org/doi:10.3390/rs10010136

Zampieri, M., Toreti, A., Schindler, A., Scoccimarro, E., & Gualdi, S. (2017). Atlantic multi-decadal oscillation influence on weather regimes over Europe and the Mediterranean in spring and summer. *Global and Planetary Change*, *151*, 92–100. https://doi.org/10.1016/j.gloplacha.2016.08.014

Zemp, M., Huss, M., Thibert, E., Eckert, N., McNabb, R., Huber, J., … Cogley, J. G. (2019). Global glacier mass changes and their contributions to sea-level rise from 1961 to 2016. *Nature 2019 568:7752*, *568*(7752), 382–386. https://doi.org/10.1038/s41586-019-1071-0

Zemp, Michael, Frey, H., Gortner-Roer, I., Nussbaumer, S. U., Hoelzle, M., Paul, F., … Vincent, C. (2015). Historically unprecedented global glacier decline in the early 21st century. *Journal of Glaciology*, *61*(228), 745–762. https://doi.org/10.3189/2015JoG15J017

Zeng, X., Broxton, P., & Dawson, N. (2018). Snowpack Change From 1982 to 2016 Over Conterminous United States. *Geophysical Research Letters*. https://doi.org/10.1029/2018GL079621

Zeng, X., Zhao, M., & Dickinson, R. E. (1998). Intercomparison of Bulk Aerodynamic Algorithms for the Computation of Sea Surface Fluxes Using TOGA COARE and TAO Data. *Journal of Climate*, *11*(10), 2628–2644. https://doi.org/10.1175/1520-0442(1998)011<2628:IOBAAF>2.0.CO;2

Zhai, J., Mondal, S. K., Fischer, T., Wang, Y., Su, B., Huang, J., … Uddin, M. J. (2020). Future drought characteristics through a multi-model ensemble from CMIP6 over South Asia. *Atmospheric Research*, *246*, 105111. https://doi.org/10.1016/J.ATMOSRES.2020.105111

Zhang, J., Zhao, L., Deng, S., Xu, W., & Zhang, Y. (2017). A critical review of the models used to estimate solar radiation. *Renewable and Sustainable Energy Reviews*, *70*, 314–329. https://doi.org/10.1016/J.RSER.2016.11.124

Zhang, Y., & Ma, N. (2018). Spatiotemporal variability of snow cover and snow water equivalent in the last three decades over Eurasia. *Journal of Hydrology*, *559*, 238–251. https://doi.org/10.1016/J.JHYDROL.2018.02.031

Zhong, X., Zhang, T., Kang, S., & Wang, J. (2021). Spatiotemporal variability of snow cover timing and duration over the Eurasian continent during 1966–2012. *Science of The Total Environment*, *750*, 141670. https://doi.org/10.1016/J.SCITOTENV.2020.141670

Zhu, X., Lee, S.-Y., Wen, X., Wei, Z., Ji, Z., Zheng, Z., & Dong, W. (2021). Historical evolution and future trend of Northern Hemisphere snow cover in CMIP5 and CMIP6

models. *Environmental Research Letters*, *16*(6), 065013. https://doi.org/10.1088/1748-9326/AC0662

Zuzel, J. F., & Cox, L. M. (1975). Relative importance of meteorological variables in snowmelt. *Water Resources Research*. https://doi.org/10.1029/WR011i001p00174

Appendix A - Statistical Summer Mass-Balance Forecast Model with Application to Brúarjökull Glacier, South East Iceland

Journal of Glaciology (2018), Page 1 of 10 doi: 10.1017/jog.2018.22

Statistical summer mass-balance forecast model with application to Brúarjökull glacier, South East Iceland

DARRI EYTHORSSON,[1] SIGURDUR M. GARDARSSON,[1] ANDRI GUNNARSSON,[2] BIRGIR HRAFNKELSSON[3]

[1]*Faculty of Civil and Environmental Engineering, University of Iceland, Hjardarhaga 2-6, Reykjavik 107, Iceland*
[2]*Research and Development Division, Landsvirkjun, Haaleitisbraut 68, Reykjavik 103, Iceland*
[3]*Department of Mathematics, Faculty of Physical Sciences, University of Iceland, Reykjavik 107, Iceland*
Correspondence: Darri Eythorsson <dae5@hi.is>

ABSTRACT. Forecasting of glacier mass balance is important for optimal management of hydrological resources, especially where glacial meltwater constitutes a significant portion of stream flow, as is the case for many rivers in Iceland. In this study, a method was developed and applied to forecast the summer mass balance of Brúarjökull glacier in southeast Iceland. In the present study, many variables measured in the basin were evaluated, including glaciological snow accumulation data, various climate indices and meteorological measurements including temperature, humidity and radiation. The most relevant single predictor variables were selected using correlation analysis. The selected variables were used to define a set of potential multivariate linear regression models that were optimized by selecting an ensemble of plausible models showing good fit to calibration data. A mass-balance estimate was calculated as a uniform average across ensemble predictions. The method was evaluated using fivefold cross-validation and the statistical metrics Nash–Sutcliffe efficiency, the ratio of the root mean square error to the std dev. and percent bias. The results showed that the model produces satisfactory predictions when forced with initial condition data available at the beginning of the summer melt season, between 15 June and 1 July, whereas less reliable predictions are produced for longer lead times.

KEYWORDS: glacier mass balance, glacier modelling, ice and climate, melt-surface

1. INTRODUCTION

Water storage in snow and ice is an important factor in the hydrological cycle in many regions of high altitudes and latitudes like Iceland, where 11% of the country is covered by glaciers (Bjornsson and Palsson, 2008). Simulation and prediction of melt behavior provide valuable information for water resources management, e.g. regarding reservoir fill rates, potential power production and load on hydraulic structures. Short-term predictions of a few days improve daily operations and risk analysis, whereas longer term prediction of seasonal melt behavior assists in the systematic optimization of networks of reservoirs and diversions.

Prior work in melt modeling of Icelandic glaciers has focused on either empirical (degree day) and physical (energy balance) modeling approaches. Both have shown good performance for simulating glacial mass balance (e.g. De Ruyter de Wildt and others, 2003b; Marshall and others, 2005; Carenzo and others, 2009; Engelhardt and others, 2014). Empirical approaches to mass-balance modeling have been considered sufficient when the underlying physical processes need not be resolved (e.g. Réveillet and others, 2017). More recently, the vast potential of remote-sensing data has been increasingly applied to snowmelt estimation in basins where little information is available (Kalra and others, 2013; Qiu and others, 2014; Drolon and others, 2016).

Observations have shown that across the globe glaciers are losing mass and retreating. These studies have further concluded that the rapid retreat in the early 21st century is without precedent on a global scale (Barnett and others, 2005; Liu and others, 2015; Zemp and others, 2015; Roe and others, 2017). In line with the trend of glaciers globally, Icelandic glaciers have experienced retreat in recent years and their mass loss since the end of the 19th century has been shown to be responsible for 0.03 mm sea level rise globally (Bjornsson and others, 2013). Studies of the response of Icelandic glaciers to the expected climate change have shown that the country's main ice caps will mostly disappear over the next two centuries, leaving glaciers only at the highest elevations (Aðalgeirsdóttir and others, 2006, 2011).

Studies have predicted that increased glacial ablation will result in increased river runoff in Icelandic rivers throughout the 21st century (Jonsdóttir, 2010; Gudmundsson and others, 2011; Matthews and others, 2015). While little prior work exists on summer mass-balance modeling of Icelandic glaciers, several studies have considered the subject in other regions. These attempts have either employed statistical modeling techniques or used physical models forced with climate simulations (Fujita and Ageta, 2000; Schöner and Böhm, 2007).

The present study considers the prediction of the summer mass balance of Brúarjökull in SE Iceland. The Brúarjökull catchment, which is more than 90% glacierized, was harnessed for hydropower generation by the construction of the Halslon reservoir in 2006 (Gardarsson and Eliasson, 2006). Due to its hydroelectric potential, data have been recorded on hydro-meteorological variables in the catchment, including measurements of glacier mass balance since 1993 (De Ruyter de Wildt and others, 2003a, b; Rasmussen, 2005).

Brúarjökull covers an area of 1550 km^2, making it the largest outlet glacier of the Vatnajökull ice cap, representing

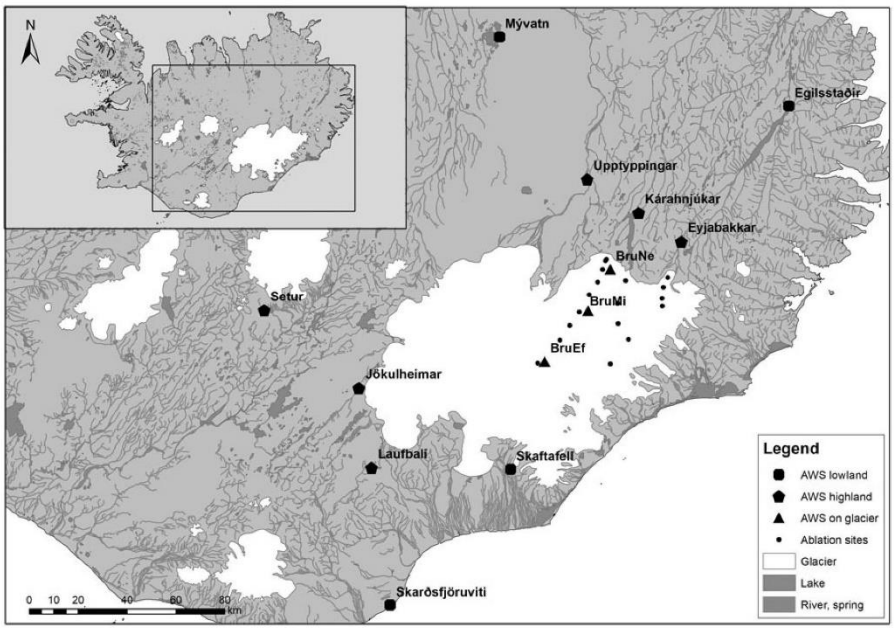

Fig. 1. Location of mass-balance points and automatic weather stations (AWS) which collect the meteorological data that were used in the study (Data on land cover from National Land Survey of Iceland).

~19% of the total area covered by the ice cap. The glacier ranges in elevation from 600 to ~1550 m a.s.l. and the mean equilibrium line lies at an altitude ~ 1200 m a.s.l. (Bjornsson and Palsson, 2008). The glacier slopes gently toward the central Icelandic highland plateau and is classified as a surging outlet glacier with a surge frequency of 80–100 years, the last one occurring in 1964 (Kjær and others, 2008). Unlike other outlets of the ice cap, Brúarjökull is not underlain by geothermal areas. Due to the proximity to surrounding volcanoes, its surface is periodically covered in volcanic tephra, thus decreasing its albedo (Larsen, 1998; Moller and others, 2014). In the three main volcanoes near the basin, Bárðarbunga, Grímsvötn and Kverkfjöll, tephra events occur on average ~15 eruptions per century (Oladottir and others, 2011).

The forcing of physically based melt models with meteorological forecast model output on seasonal time scales inevitably incurs the large uncertainty in the forcing data. In this paper, statistical modeling was investigated to attempt the prediction of summer mass balance directly from the initial conditions of the system on the forecast date, thereby minimizing the uncertainties. The motivation for the study was to investigate whether the mass balance of the Brúarjökull could be predicted at the beginning of the melt season and to develop a simple operational model for reservoir operators. The goal of the study was to assess the predictive power of the information available by employing statistical approaches and the impact of lead times on predictions.

2. DATA

The data used in the present study consisted of glaciological mass-balance measurements, meteorological variables measured around the Brúarjökull basin, and climate indices which have been shown to correlate with Icelandic weather patterns (e.g. Baldwin and others, 2003; Hanna and others, 2004).

2.1. Glaciological measurements

Winter accumulation and summer ablation of Vatnajökull are measured in biannual measurement surveys at the boundaries of the melt season in spring and autumn. Winter accumulation is estimated by drilling ice cores and the summer ablation is measured from ablation wires or rods that are placed on the glacier in spring, when winter accumulation is measured (Thorsteinsson and others, 2004). The annual net mass balance is calculated as the sum of the winter accumulation and the summer ablation. Figure 1 shows the approximate location of mass-balance sites on the surface of Brúarjökull as small circles.

The annual mass balance within each catchment on the glacier has been estimated based on the ablation stake measurements by extrapolating across the area (Palsson and others, 2014). The summer mass balance within the Halslon reservoir catchment was used as the response variable in the present study, while the winter accumulation at the various accumulation sites was used as an input variable. It should be noted that the estimated mass balance did not include liquid precipitation that fell on the glacier during the summer nor snow that melted outside the survey period. Furthermore, the uncertainty in the mass-balance measurements is not reported. The glaciological summer mass-balance data were selected as response variable based on the overlap of the shorter time series of discharge for the reservoir inflow which started in 2007.

2.2. Meteorological variables

Data were obtained from eight automatic weather stations (AWS) in and around the Brúarjökull basin. Three AWS on the glacier surface were used at elevations of 850, 1200 and 1400 m a.s.l. denoted as BruNe, BruMi and BruEf, respectively. The stations are designed to collect measurements of the components of the snow surface energy balance, shown as triangles in Figure 1. Time series of the measurements were acquired as daily averages of the following parameters: air temperature, relative humidity, net radiation, wind speed and surface albedo.

Data from ten land-based AWS surrounding the Brúarjökull basin were obtained, six based in the central highlands and four in the lowlands. The locations of the land-based AWS are shown as squares and pentagons in Figure 1. Time series were obtained as mean daily values of the following parameters: air temperature, dew point temperature, vapor pressure, relative humidity, atmospheric pressure and wind speed, and additionally precipitation measurements from the AWS at Egilsstadir.

2.3. Climatological variables

Icelandic climate has been shown to be significantly influenced by prevailing ocean conditions surrounding the island as well as changes in the large-scale circulations in the North Atlantic Ocean (Hanna and others, 2001). Large-scale changes in atmospheric circulation have also been shown to correlate significantly with long-term Icelandic climate trends (e.g. Hanna and others, 2004).

To incorporate information on the variability in the ocean conditions surrounding Iceland, the following two datasets were acquired: monthly averages of the Atlantic Multidecadal Oscillation (AMO) index (Enfield and others, 2001) and quarterly averages of the heat content of the Northern Atlantic (60–0°W, 30–65°N) measured in the top 700 m of the ocean by the US National Oceanic Data Center (NODC). The AMO index is defined from the trends in Sea Surface Temperature (SST) in the North Atlantic and has been shown to be correlated with temperature and precipitation patterns in Europe (Ghosh and others, 2017; Zampieri and others, 2017). Furthermore, the heat transport through the North Atlantic by the warm Gulf Stream has been shown to be a key factor in determining the climate of Northern Europe (e.g. Palter, 2015).

To incorporate information about the atmospheric circulations into the model, monthly averages of the North Atlantic Oscillation Index (NAOI) were acquired from the US National Oceanic and Atmospheric Administration (NOAA). The NAOI is a measure of the changes in the difference in atmospheric pressure at sea level between the Icelandic and the Azores. Studies have shown the NAOI to be significantly correlated with temperature and precipitation patterns in Iceland (Hanna and others, 2004).

3. METHODS

3.1. Time series

The data were obtained as hourly or daily averages from the AWS and as point measurements of the winter accumulation data and climatological indices. The AWS data were aggregated to average values to represent the initial conditions of the system at four different dates in spring, specifically for the periods beginning on 1 April and ending on 15 May, 1 June, 15 June and 1 July.

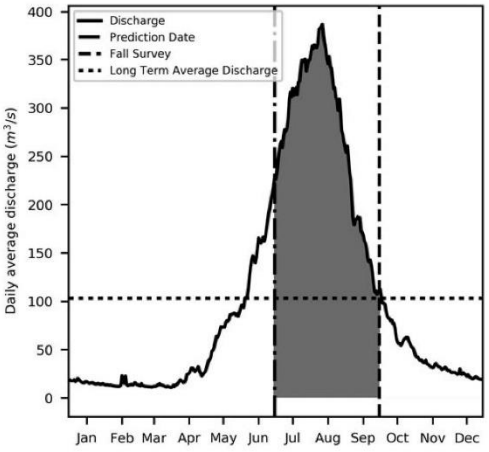

Fig. 2. Average daily discharge into Halslon reservoir for the period 2007–2015. The shaded area represents a proxy for the predicted mass balance.

The main aim of the study was to predict the summer inflow into the Hálslón Reservoir. Due to the short time series of inflow (2007–2015) the summer mass balance of Brúarjökull was selected as a proxy. Figure 2 shows the average daily discharge into the Halslon reservoir, where the shaded area shows the period between the forecast date on 1 July to the time of the fall ablation survey when the total summer mass balance of the glacier is calculated. The mass-balance data do not represent hydrological fluxes such as the drainage from the 10% of the basin, which is de-glacierized, baseflow and basal melt due to geothermal fluxes and liquid precipitation that falls on the glacier in summer. Despite this, we consider that the summer mass balance of the 90% glacierized portion of the basin offers a good representation of the inter-annual variability of net summer inflow into the reservoir. Thus, the total inflow, represented by the shaded area under the curve, will be significantly correlated to the summer mass balance, the quantity to be predicted in the present study.

The method was initially applied to 1 July data; then predictions of the summer mass balance were produced for each of the dates to assess the evolution of the predictive performance of the modeling approach in the period leading up to the summer melt season. The availability of the acquired data overlapped for the period 2001–2015, which was selected as the study period for the research. A breakdown of the input variables screened in the study along with their correlation to Brúarjökull summer mass balance is given in Appendix A.

The number of years used in the present study were $N = 15$. The input data were aggregated to a single average value for each year that represented the initial conditions of the system prior to the date of prediction. The data were split into training and test sets using the K-fold cross-validation method. In the present study, K was selected as 5 and the dataset was split into five subsets, each using three observations to test the model and 12 observations for calibration. A

fivefold cross-validation was selected over a leave-one-out approach (where $K = N$) to reduce the variance in the error estimates (James and others, 2013).

3.2. Variable selection

In the present study, many predictor variables were considered, whereas the number of observations of the response variable were few. To reduce the number of predictors and prevent model overfitting, variables were selected that showed a significant correlation with the response variable, the observed mass balance of the glacier. The variables were ranked by their r^2 value, and variables with r^2 values above a certain threshold were selected for further model development. The threshold value for variable selection was determined by sensitivity analysis of model results, as described in the subsequent sections.

3.3. Multivariate model ensemble

The selected variables can be used to create many multivariate regression models, none of which may be obviously superior to any of the others. Rather than selecting any single model, an ensemble of all potential competing models was developed. The selected variables were used to calculate a set of all possible multivariate linear regression models comprising five or fewer input variables. The input variables were limited to five due to computational limitations and the potential risk of overfitting the short time series. The optimal number of input parameters to include in the models of the ensemble was investigated by sensitivity analysis of model results with a range of numbers of input parameters, as described in subsequent sections.

3.4. Multi-model inference

Selection of any single one of the regression models in the set of possible models would recognize the existence of several potential and competing models and introduce additional uncertainty in the estimator due to the model selection. Unless the uncertainty associated with model selection is accounted for, overconfident estimates of model predictions may be inferred (Wang and others, 2009).

An alternative to selecting a single model is to average the prediction over a range of plausible models. This technique, called model averaging, incorporates the uncertainty associated with model selection into predictions of unknown variables (Hjort and Claeskens, 2003). The model averaging approach has in recent years been applied to several hydrological model applications (Diks and Vrugt, 2010; Tsai, 2010).

Methods for model averaging include Bayesian model averaging (BMA) and frequentist model averaging (FMA). In BMA, model uncertainty is evaluated by assigning prior probabilities to all models being considered, whereas in the FMA, no prior probabilities are required and all estimators are determined by the data (Buckland and others, 1997; Raftery and others, 1997; Hoeting and others, 1999). In the present study, the FMA approach to model averaging was chosen as it relies only on the available data.

The response variable was estimated from a model ensemble by calculating the ensemble average. Several weighting functions have been reported in the literature to incorporate the measures of model plausibility into model averaging, based, for example, on goodness-of-fit metrics Akaike information criterion (Buckland and others, 1997), Bayesian information criterion and focused information criterion (FIC) (Burnham and Anderson, 2002; Zhang and others, 2012). Other strategies for weight function selection include the minimization of Mallow's C_p criterion and weight choice based on the unbiased estimator of risk (Liang and others, 2011). In cases where little prior information is available on the likelihood of each model, or models having similar priors, assigning a uniform weight to each model is a reasonable choice (Raftery and others, 1997). In the present study, a uniform weight was selected.

3.5. Optimal subset of models

Another important consideration of the model averaging methodology is the selection of a set of models over which to average. A complete Bayesian solution to the problem is to average over the entire set of possible models (Madigan and Raftery, 1994). However, as the set of potential models can become large, averaging over the entire set may not be practical. To reduce the number of models to be considered, Madigan and Raftery (1994) suggested excluding models that poorly fit the calibration data.

The quality of each model in the set of possible models was assessed by several evaluation metrics. Moriasi and others (2007) surveyed several model evaluation metrics for watershed simulations and recommended using three metrics: the Nash–Sutcliffe efficiency (*NSE*), the ratio of the root mean square error to the std dev. of measured data (*RSR*) and the percent bias (*PBIAS*) for evaluation of hydrological models (Moriasi and others, 2007). These three metrics were selected for model evaluation in the present study; their mathematical formulations are described as:

$$\mathrm{NSE} = 1 - \frac{\sum_{i=1}^{n}\left(Y_i^{\mathrm{obs}} - Y_i^{\mathrm{sim}}\right)^2}{\sum_{i=1}^{n}\left(Y_i^{\mathrm{obs}} - Y^{\mathrm{mean}}\right)^2}, \quad (1)$$

$$\mathrm{RSR} = \frac{\mathrm{RMSE}}{\mathrm{STDEV}_{\mathrm{obs}}} = \frac{\sqrt{\sum_{i=1}^{n}\left(Y_i^{\mathrm{obs}} - Y_i^{\mathrm{sim}}\right)^2}}{\sqrt{\sum_{i=1}^{n}\left(Y_i^{\mathrm{obs}} - Y^{\mathrm{mean}}\right)^2}}, \quad (2)$$

$$\mathrm{PBIAS} = \frac{\sum_{i=1}^{n}\left(Y_i^{\mathrm{obs}} - Y_i^{\mathrm{sim}}\right)\times(100)}{\sum_{i=1}^{n}\left(Y_i^{\mathrm{obs}}\right)}, \quad (3)$$

where n is the number of data points in the dataset, Y_i^{obs} is the observed mass balance in the ith year, Y_i^{sim} is the simulated mass balance in the ith year and Y^{mean} is the mean observed mass balance. Moriasi and others (2007) suggested that a model simulation could be judged as satisfactory if $NSE > 0.5$, $RSR < 0.7$ and $PBIAS < \pm 25\%$.

An ensemble of plausible models was created by evaluating all models in the set of possible multivariate regression models in accordance with the recommended values of *NSE*, *RSR* and *PBIAS*. Models with $NSE < 0.5$, $RSR > 0.7$ and $PBIAS > \pm 25\%$ were eliminated from further analysis and the remaining models were stored for multi-model inference.

Madigan and Raftery (1994) suggested that, in the case of models that fit the calibration data equally well, the less complicated model should be selected as it receives more support from the data. In the present study, a sensitivity analysis was

Table 1. *NSE* of different model configurations with varying $r^2_{threshold}$ and number input variables, optimal value of *NSE* = 1

	Number of variables				
	1	2	3	4	5
$r^2_{threshold}$					
0.2	−0.09	0.48	0.53	0.51	0.44
0.25	−0.03	0.55	0.56	0.54	0.48
0.3	0.23	0.69	0.71	0.71	0.66
0.35	0.24	0.61	0.64	0.64	0.44

Table 3. *PBIAS* of different model configurations, optimal value of *PBIAS* = 0

	Number of variables				
	1	2	3	4	5
$r^2_{threshold}$					
0.2	0.76	2.55	2.45	3.15	4.29
0.25	0.85	2.46	2.39	3.02	3.66
0.3	−2.65	−0.08	0.41	0.75	1.23
0.35	−3.05	−0.75	0.38	0.47	1.45

performed on model predictions by varying the number of allowed input variables in the models and thus identifying the optimal number of variables to include.

The model averaging estimate of glacier ablation, $\hat{A}$, is then given by

$$\hat{A} = \frac{1}{M}\sum_{k=1}^{M}\hat{A}_k, \quad (4)$$

where the index k denotes the kth model considered, M is the total number of models and $\hat{A}_k$ is the estimated ablation based on the kth model. The uncertainty in the estimate is taken as the spread in predicted values of the ensemble of models.

4. RESULTS AND DISCUSSION

4.1. Multimodel inference

The selection of a threshold value of r^2 for variable selection and the number of input variables used in the model were optimized by performing a sensitivity analysis of the model results. The results were evaluated using the metrics *NSE*, *RSR* and *PBIAS* and were calculated using four threshold values of r^2 [0.2, 0.25, 0.3, 0.35] and five options for the number of model input variables [1, 2, 3, 4, 5]. Model ensembles were calculated for each combination of model options and the ensemble mean was used to calculate the evaluation metrics. The use of the median ensemble response was also investigated and yielded almost identical results. Tables 1–3 show the results for the evaluation metrics: *NSE*, *RSR* and *PBIAS*, respectively, while Table 4 shows the total number of models in each ensemble.

The results of the sensitivity analysis showed that the optimal values of *NSE* and *RSR* were obtained using a threshold value of $r^2 = 0.3$ and constraining the number of input parameters in the models to four (optimal results are highlighted in Tables 2–4). In terms of *PBIAS*, the optimal configuration was found with a threshold $r^2 = 0.3$ and two input variables in the models. However, the *PBIAS* of several configurations showed very low bias including the optimal configuration in terms of *NSE* and *RSR*. Hence it was concluded that the optimal model ensemble was achieved by selecting potential input variables with $r^2 > 0.3$ and restricting the number of inputs into each model in the ensemble to three. As shown in Table 4, this model ensemble contains 35 plausible models.

Table 2. *RSR* of different model configurations, optimal value of *RSR* = 0

	Number of variables				
	1	2	3	4	5
$r^2_{threshold}$					
0.2	1.04	0.72	0.69	0.69	0.75
0.25	1.01	0.67	0.66	0.68	0.72
0.3	0.88	0.56	0.53	0.53	0.58
0.35	0.87	0.62	0.60	0.59	0.75

4.2. Variable selection

The time series of all the acquired potential input variables were assessed based on their correlation with the observed summer mass balance of Brúarjökull. Variables with a correlation coefficient below a set threshold value of 0.3 as determined in Section 4.1 were eliminated from further analysis. The variables selected for model development and their corresponding r^2 values are presented in Table 5.

4.3. Model evaluation

The model was evaluated according to its ability to predict observed values of mass balance of the glacier in terms of the evaluation metrics *NSE*, *RSR* and *PBIAS* described in Section 3.5. The models were evaluated using fivefold cross-validation; thus, the data were split five ways providing 12 observations for calibration, leaving three observations for model evaluation for each fold. Table 5 shows the evaluation metrics obtained in the present study for each of the five folds used for cross-validation.

The results in Table 6 show that for four out of the five folds, all evaluation metrics indicated a satisfactory prediction in accordance with the specifications of Moriasi and others (2007). However, for the third fold, evaluated with

Table 4. Number of models in the ensemble of plausible models with different configurations of number of input variables and threshold r^2 value

	Number of variables				
	1	2	3	4	5
$r^2_{threshold}$					
0.2	15	105	455	1365	3003
0.25	11	55	165	330	462
0.3	7	21	35	35	21
0.35	5	10	10	5	1

Table 5. Final variables selected for model development and their correlation to the observed summer mass balance of Brúarjökull, given as r^2 values

Variable	Location	r^2
Net radiation	BruNe (850 m a.s.l)	0.65
AMO index	Atlantic Ocean	0.48
Albedo	BruNe (850 m a.s.l)	0.47
Albedo	BruMi (1200 m a.s.l)	0.36
Atmospheric pressure	Karahnjukar	0.35
Precipitation	Egilsstadir	0.33
Ocean heat content	North Atlantic	0.32

Table 6. Evaluation metrics for model averaged predictions using fivefold cross-validation

Evaluation period	NSE	RSR	PBIAS (%)
2001–2003	0.71	0.53	4.9
2004–2006	0.66	0.57	10.7
2007–2009	−0.72	1.3	−3.2
2010–2012	0.75	0.49	−6.1
2013–2015	0.87	0.35	−8.7

Models show satisfactory performance with NSE > 0.5, RSR < 0.7 and PBIAS ⩽ ±25%.

observations from the period 2007–2009, low *NSE* and high *RSR* values were observed, whereas PBIAS was within acceptable range.

Figure 3 shows the observed mass balance of the Brúarjökull for the study period with predicted values from each fold in a box and whiskers plot. The observed summer mass balance is shown as black stars; the notch in the box represents the median of the ensemble predictions, while the ends of the box represent the upper and lower quartiles; the whiskers encompass the range of all ensemble predictions. Considering the time series of simulated and observed values shown in Figure 3 during the period 2007–2009, both were very close to the long-term average mass balance of the glacier. When the observed values were close to the mean value, the denominator in Eqns (1) and (2) took on a small value, inflating the evaluation metrics, *NSE* and *RSR*. Thus, during periods where the mass balance is consistently close to the mean, these metrics may provide a poor indication of the quality of the model outputs.

The results in Figure 3 show that the range of ensemble predictions encompasses the observed values for all observations in the study period except 2004 and 2012. Furthermore, the ensemble mean provides a reasonable estimate of the observed mass balance for the range of observations considered. The evaluation metrics described in Eqns (1)–(3) were calculated for all predictions yielding values of $NSE = 0.71$, $RSR = 0.54$ and PBIAS = 0.27%. The results suggest that the model has satisfactory performance with low bias for under- or overpredicting the mass balance.

4.4. Model performance in time

The results described in the previous sections were obtained using data available on 1 July. To assess how the predictive performance of the method evolved over time in spring, as the melt season approached predictions were calculated for data available for 15 May, 1 June and 15 June. Table 6 shows the evaluation metrics observed for predictions at each of these dates compared with 1 July.

The evaluation metrics presented in Table 7 show that the predictive information in the data diminished quickly as the lead time increased to dates prior to 1 July. For predictions made on 15 May, negative values of *NSE* were observed, indicating that the model predictions performed worse than simply reporting the mean mass balance of the glacier.

Figure 4 shows the predictions from the model suite using data from the four dates in spring. The results show that for longer lead times, the spread in ensemble predictions increased. Especially, ensembles for the years 2008 and 2009 showed a large variability in model outputs. The model also had poorer performance in predicting the extremes of the observations with longer lead times. The results show that predictions made prior to 1 July were less reliable and the earliest time when satisfactory predictions could be made was between 15 June and 1 July.

Figure 5 shows the correlation of the selected input variables shown in Table 5 to the Brúarjökull summer mass balance at the four forecast dates in spring. The table shows that the key predictor on 1 July forecast, net radiation at BruNe, has much less predictive power earlier in the spring. The same applies to the albedo at both BruNe and BruMi, which show

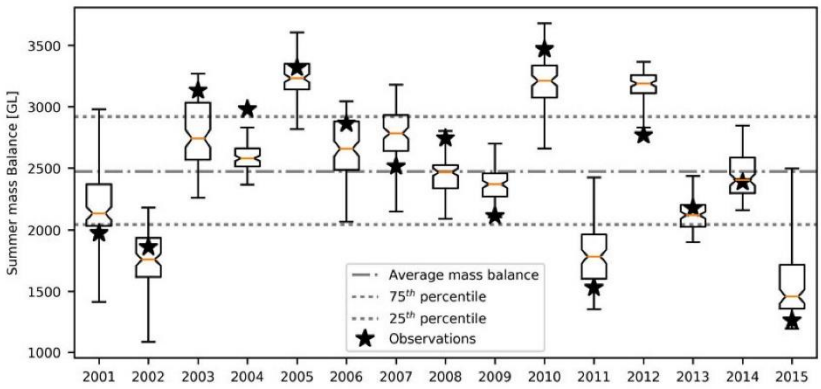

Fig. 3. Model averaged predictions of Brúarjökull summer mass balance for all fivefold cross-validations. Observed glacier mass balance is shown as black stars.

Table 7. Evaluation metrics for predictions with longer lead times with models showing satisfactory performance on 1 July

Forecast date	NSE	RSR	PBIAS (%)
15 May	−0.95	1.39	9.2
1 June	0.13	0.93	3.2
15 June	0.45	0.75	2.7
1 July	0.71	0.54	0.27

Satisfactory performance is defined as models having $NSE > 0.5$, $RSR < 0.7$ and $PBIAS \leqslant \pm 25\%$.

some predictive power on 15 June but none earlier. This suggests that spring snow conditions on the glacier are not indicative of the summer melt. By the end of June, as the melt season is beginning on the glacier, these variables start showing the power to predict the summer melt patterns.

The precipitation at Egilsstadir and atmospheric pressure at Karahnjukar similarly show little to no correlation to the summer mass balance on the earliest forecast dates. This suggests that the precipitation patterns in late spring and early summer play an important role in determining the summer melt, whereas precipitation patterns during the winter are less important in determining the ultimate summer melt. This can also be deduced from the fact that none of the winter accumulation measurements showed correlation to the observed summer mass balance.

The AMO index and the North Atlantic Ocean Heat content, however, show a persistent correlation to the summer mass balance throughout all the forecast dates. This suggests that a large portion of the inter-annual variability in Icelandic glacier mass balance is affected by the large-scale oceanic circulations and heat transport in the North Atlantic Ocean. The trends in these variables persist in much longer time frames than local climate conditions and contain significant predictive power for glacial mass-balance forecasts at least as early as the end of the first annual quarter. These results suggest that a significant portion of the variability in summer mass balance of Icelandic glaciers can be forecast well in advance of the melt season with lead times up to the length of the autocorrelative time scales of the AMO index.

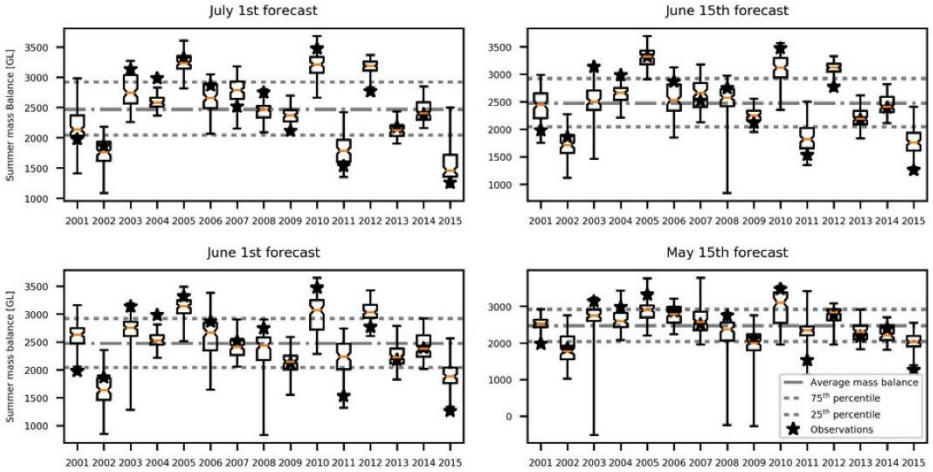

Fig. 4. Model averaged predictions of Brúarjökull summer mass balance for all fivefold cross-validations. The optimal model found with 1 July data was forced with earlier data at three different dates between 15 May and 15 June.

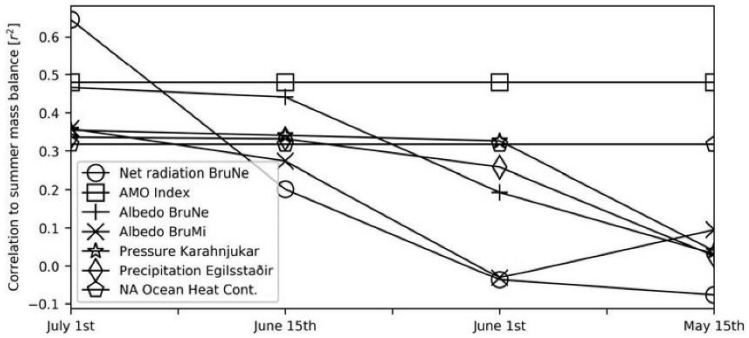

Fig. 5. Correlation of the selected predictor variables to Brúarjökull summer mass balance on four forecast dates in Spring.

Lastly, we note that the NAOI did not show any correlation to the summer mass balance. This suggests that large-scale atmospheric circulation in the North Atlantic, while indicative of Icelandic climate, is not an important factor in summer melt patterns of Icelandic glaciers. Hence, in terms of glacial mass balance, the ocean circulation in the North Atlantic is a much more important variable than atmospheric circulation.

5. CONCLUSION

The study showed that, of all the potential input variables available in the basin, seven showed a significant correlation with the summer mass balance. The variables deemed to contain predictive information at the beginning of the melt season were associated with average net radiation, glacier albedo, precipitation, atmospheric pressure and heat flux in the North Atlantic. It was observed that out of all potential multivariate regression models incorporating these variables, only a few adequately predicted summer mass balance. As selection of any single model would cause additional uncertainty in the estimation of the response variable due to model selection, an ensemble of plausible multivariate regression models was calculated and the average of the model results was used to predict the glacier mass balance.

The selection of a subset of plausible models over which to average was investigated. The results suggest that the optimal subset was found by eliminating models with poor fit to calibration data. Sensitivity analysis of model predictions suggested that the optimal number of input variables to include in the models was three and with variables exhibiting significant correlation included as inputs. The results showed that, in terms of the model evaluation measures *NSE*, *RSR* and PBIAS, satisfactory predictions of summer mass balance could be made by calculating a uniform average of model forecasts over the set of plausible models.

Investigation of the lead time with which predictions are calculated showed that model performance becomes less reliable as simulations are performed earlier in spring. Satisfactory predictions can be produced between 15 June and 1 July, at which time the melt season is beginning and predictions of summer melt volumes are valuable to water resources managers.

ACKNOWLEDGEMENTS

We thank the University of Iceland Research Fund which is supporting the first author. The project was also supported by the Energy Research Fund of the National Energy Company, Landsvirkjun by grants no. MEI-03-2015 and DOK-02-2017. We thank Landsvirkjun, the Icelandic Meteorological office and the Marine Research Institute for help with data gathering. We also thank Sverrir Gudmundsson and Finnur Palsson at the Institute of Natural Sciences at the University of Iceland, Oli Pall Geirsson at the Science Institute of the University of Iceland, Oli Gretar Blondal Sveinsson, executive VP for R&D at Landsvirkjun, and Ulfar Linnet, Manager of resources at Landsvirkjun, for numerous valuable suggestions to improve the paper.

REFERENCES

Aðalgeirsdóttir G, Johannesson T, Bjornsson H, Palsson F and Sigurdsson O (2006) Response of Hofsjokull and southern Vatnajokull, Iceland, to climate change. *J. Geophys. Res. Earth Surf.*, **111**, F03001 (doi: 10.1029/2005jf000388)

Aðalgeirsdóttir G and 6 others (2011) Modelling the 20th and 21st century evolution of Hoffellsjokull glacier, SE-Vatnajokull, Iceland. *Cryosphere* **5**, 961–975 (doi: 10.5194/tc-5–961–2011)

Baldwin MP and 5 others (2003) Stratospheric memory and skill of extended-range weather forecasts. Science (New York, N.Y.), **301**(5633), 636–640 (doi: 10.1126/science.1087143)

Barnett TP, Adam JC and Lettenmaier DP (2005) Potential impacts of a warming climate on water availability in snow-dominated regions. *Nature*, **438**(7066), 303–309 (doi: 10.1038/nature04141)

Bjornsson H and Palsson F (2008) Icelandic glaciers. *Jökull*, **58**(58), 365–386.

Bjornsson H and 6 others (2013) Contribution of Icelandic ice caps to sea level rise: trends and variability since the Little Ice Age. *Geophys. Res. Lett.*, **40**(8), 1546–1550 (doi: 10.1002/grl.50278)

Buckland ST, Burnham KP and Augustin NH (1997) Model selection: an integral part of inference. *Biometrics*, **53**(2), 603 (doi: 10.2307/2533961)

Burnham KP and Anderson DR (2002) *Model selection and multimodel inference*, Springer, New York (doi: 10.1007/978-3-319-02868-2_3)

Carenzo M, Pellicciotti F, Rimkus S and Burlando P (2009) Assessing the transferability and robustness of an enhanced temperature-index glacier-melt model. *J. Glaciol.*, **55**(190), 258–274 (doi: 10.3189/002214309788608804)

De Ruyter de Wildt M, Klok E and Oerlemans J (2003a) Reconstruction of the mean specific mass-balance of Vatnajokull (Iceland) with a seasonal sensitivity characteristic. *Geogr. Ann. Ser. A Phys. Geogr.*, **85**(1), 57–72. (doi: 10.1111/1468-0459.00189)

De Ruyter de Wildt M, Oerlemans J and Bjornsson H (2003b) A calibrated mass-balance model for Vatnajökull, Iceland. *Jökull*, **52**, 1–20.

Diks CGH and Vrugt JA (2010) Comparison of point forecast accuracy of model averaging methods in hydrologic applications. *Stoch. Environ. Res. Risk Assess.*, **24**(6), 809–820 (doi: 10.1007/s00477-010-0378-z)

Drolon V, Maisongrande P, Berthier E, Swinnen E and Huss M (2016) Monitoring of seasonal glacier mass-balance over the European Alps using low-resolution optical satellite images. *J. Glaciol.*, **62**(235), 912–927 (doi: 10.1017/jog.2016.78)

Enfield DB, Mestas-Nuñez AM and Trimble PJ (2001) The Atlantic multidecadal oscillation and its relation to rainfall and river flows in the continental U.S. *Geophys. Res. Lett.*, **28**(10), 2077–2080 (doi: 10.1029/2000GL012745)

Engelhardt M, Schuler TV and Andreassen LM (2014) Contribution of snow and glacier melt to discharge for highly glacierised catchments in Norway. *Hydrol. Earth Syst. Sci.*, **18**(2), 511–523 (doi: 10.5194/hess-18-511-2014)

Fujita K and Ageta Y (2000) Effect of summer accumulation on glacier mass-balance on the Tibetan Plateau revealed by mass-balance model. *J. Glaciol.*, **46**(153), 244–252 (https://doi.org/10.3189/172756500781832945)

Gardarsson SM and Eliasson J (2006) Influence of climate warming on Halslon reservoir sediment filling. *Nord. Hydrol.*, **26**, 553–569 (doi: 10.2166/nh.2006.014)

Ghosh R, Müller WA, Baehr J and Bader J (2017) Impact of observed North Atlantic multidecadal variations to European summer climate: a linear baroclinic response to surface heating. *Clim. Dyn.*, **48**(11–12), 3547–3563 (doi: 10.1007/s00382-016-3283-4)

Gudmundsson S and 6 others (2011) Response of Eyjafjallajokull, Torfajokull and Tindfjallajokull ice caps in Iceland to regional warming, deduced by remote sensing. *Polar Res.*, **30** (doi: 10.3402/Polar.V30i0.7282)

Hanna E, Jónsson T and Box JE (2001) Recent changes in Icelandic climate. *Spring*, **61**, 3–9 (doi: 10.1256/wea.80.04)

Hanna E, Jónsson T and Box JE (2004) An analysis of Icelandic climate since the nineteenth century. *Int. J. Climatol.*, **24**(10), 1193–1210 (doi: 10.1002/joc.1051)

Hjort NL and Claeskens G (2003) Frequentist model average estimators. *J. Am. Stat. Assoc.*, **98**(464), 879–899 (doi: 10.1198/016214503000000828)

Hoeting JA, Madigan D, Raftery AE and Volinsky CT (1999) Bayesian model averaging: a tutorial. *Stat. Sci.*, **14**(4), 382–417 (doi: 10.2307/2676803)

James G, Witten D, Tibshirani R and Hastie T (2013) *An introduction to statistical learning with applications in R*, Springer, New York (doi: 10.1007/978-1-4614-7138-7)

Jonsdóttir JF (2010) A runoff map based on numerically simulated precipitation and a projection of future runoff in Iceland. *Hydrol. Sci. J.*, **53**, 100–111 (doi: 10.1623/hysj.53.1.100)

Kalra A, Ahmad S and Nayak A (2013) Increasing streamflow forecast lead time for snowmelt-driven catchment based on large-scale climate patterns. *Adv. Water Resour.*, **53**, 150–162 (doi: 10.1016/j.advwatres.2012.11.003)

Kjær KH, Korsgaard NJ and Schomacker A (2008) Impact of multiple glacier surges – a geomorphological map from Bruarjokull, East Iceland. *J. Maps*, **4**(1), 5–20 (doi: 10.4113/jom.2008.91)

Larsen G (1998) Eight centuries of periodic volcanism at the center of the Iceland hotspot revealed by glacier tephrostratigraphy. *Geology*, **26**(10), 943–946 (doi: 10.1130/0091-7613(1998)026<0943:ECOPVA>2.3.CO;2)

Liang H, Zou G, Wan ATK and Zhang X (2011) Optimal weight choice for frequentist model average estimators. *J. Am. Stat. Assoc.*, **106**(495), 1053–1066 (doi: 10.1198/jasa.2011.tm09478)

Liu W and 5 others (2015) Impacts of climate change on hydrological processes in the Tibetan Plateau: a case study in the Lhasa River basin. *Stoch. Environ. Res. Risk Assess.*, **29**(7), 1809–1822 (doi: 10.1007/s00477-015-1066-9)

Madigan D and Raftery AE (1994) Model selection and accounting for model uncertainty in graphical models using Occam's Window. *J. Am. Stat. Assoc.*, **89**(428), 1535–1546 (doi: 10.1080/01621459.1994.10476894)

Marshall SJ, Bjornsson H, Flowers GE and Clarke GKC (2005) Simulation of Vatnajokull ice cap dynamics. *J. Geophys. Res. Earth Surf.*, **110**, F03009 (doi: 10.1029/2004JF000262)

Matthews T, Hodgkins R, Gudmundsson S, Palsson F and Bjornsson H (2015) Inter-decadal variability in potential glacier surface melt energy at Vestari Hagafellsjokull (Langjokull, Iceland) and the role of synoptic circulation. *Int. J. Climatol.*, **35**(10), 3041–3057 (doi: https://doi.org/10.1002/joc.4191)

Moller R and 7 others (2014) MODIS-derived albedo changes of Vatnajokull (Iceland) due to tephradeposition from the 2004 Grimsvotn eruption. *Int. J. Appl. Earth Obs. Geoinf.*, **26**(1), 256–269 (doi: 10.1016/j.jag.2013.08.005)

Moriasi DN and 5 others (2007) Model evaluation guidelines for systematic quantification of accuracy in watershed simulations. *Trans. ASABE*, **50**(3), 885–900 (doi: 10.13031/2013.23153)

Oladottir BA, Larsen G and Sigmarsson O (2011) Holocene volcanic activity at Grimsvotn, Bardarbunga and Kverkfjoll subglacial centres beneath Vatnajokull, Iceland. *Bull. Volcanol.*, **73**(9), 1187–1208 (doi: 10.1007/S00445-011-0461-4)

Palsson F and 5 others (2014) *Vatnajokull: mass-balance, melt water drainage and surface velocity of the glacial year 2013–14*. Landsvirkjun. Report No LV-2014-138 (Retrieved 01/05/2017, http://gogn.lv.is/files/2014/2014-138.pdf)

Palter JB (2015) The role of the Gulf Stream in European climate. *Ann. Rev. Mar. Sci.*, **7**(1), 113–137 (doi: 10.1146/annurev-marine-010814-015656)

Qiu L, You J, Qiao F and Peng D (2014) Simulation of snowmelt runoff in ungauged basins based on MODIS: a case study in the Lhasa River basin. *Stoch. Environ. Res. Risk Assess.*, **28**(6), 1577–1585 (doi: 10.1007/s00477-013-0837-4)

Raftery AE, Madigan D and Hoeting JA (1997) Bayesian model averaging for linear regression models. *J. Am. Stat. Assoc.*, **92**(437), 179–191 (doi: 10.1080/01621459.1997.10473615)

Rasmussen LA (2005) Mass-balance of Vatnajokull reconstructed back to 1958. *Jokull*, **55**, 139–146

Réveillet M, Vincent C, Six D and Rabatel A (2017) Which empirical model is best suited to simulate glacier mass-balances? *J. Glaciol.*, **63**(237), 39–54 (doi: 10.1017/jog.2016.110)

Roe GH, Baker MB and Herla F (2017) Centennial glacier retreat as categorical evidence of regional climate change. *Nat. Geosci.*, **10**(2), 95–99 (doi: 10.1038/ngeo2863)

Schöner W and Böhm R (2007) A statistical mass-balance model for reconstruction of LIA ice mass for glaciers in the European Alps. *Ann. Glaciol.*, **44**, 161–169 (doi: 10.3189/172756407782871639)

Thorsteinsson T, Einarsson B and Kjartansson V (2004) *Afkoma Hofsjokuls 1997–2004*. Icelandic National Energy Authority, Reykjavik, Report NO OS-2004/029

Tsai FTC (2010) Bayesian model averaging assessment on groundwater management under model structure uncertainty. *Stoch. Environ. Res. Risk Assess.*, **24**(6), 845–861 (doi: 10.1007/s00477-010-0382-3)

Wang H, Zhang X and Zou G (2009) Frequentist model averaging estimation: a review. *J. Syst. Sci. Complex.*, **22**, 732–748 (doi: 10.1007/s11424-009-9198-y)

Zampieri M, Toreti A, Schindler A, Scoccimarro E and Gualdi S (2017) Atlantic multi-decadal oscillation influence on weather regimes over Europe and the Mediterranean in spring and summer. *Glob. Planet. Change*, **151**, 92–100 (doi: 10.1016/j.gloplacha.2016.08.014)

Zemp M and 38 others (2015) Historically unprecedented global glacier decline in the early 21st century. *J. Glaciol.*, **61**(228), 745–762 (doi: 10.3189/2015JoG15J017)

Zhang X, Wan ATK and Zhou SZ (2012) Focused information criteria, model selection, and model averaging in a tobit model with a nonzero threshold. *J. Bus. Econ. Stat.*, **30**(1), 132–142 (doi: 10.1198/jbes.2011.10075)

APPENDIX A

See Table A1.

Table A1. Breakdown of the potential input variables surveyed along with their correlation to Brúarjökull summer mass balance

Variable	Location	Period	$R^2_{adjusted}$	Variable	Location	Period	$R^2_{adjusted}$
Net radiation	BruNe	Q2	0.645	Relative humidity	Hvalsnes	Q2	0.050
AMO	North Atlantic	Past month	0.479	Dew point temperature	Eyjabakkar	Q1	0.045
Albedo	BruNe	Q2	0.466	Relative humidity	Myvatn	Q1	0.026
Albedo	BruMi	Q2	0.359	Outgoing longwave radiation	BruNe	Q2	0.014
Atmospheric pressure	Karahnjukar	Q2	0.355	Winter accumulation	BB0	Winter	0.013
Precipitation	Egilsstaðir	Q2	0.336	Winter accumulation	B10	Winter	0.008

Table A1. (*Cont.*)

Variable	Location	Period	$R^2_{adjusted}$	Variable	Location	Period	$R^2_{adjusted}$
Heat content	North Atlantic Ocean	Past month	0.318	Relative humidity	BruMi	Q1	0.007
Reflected solar radiation	BruNe	Q2	0.298	Wind speed	Myvatn	Q1	0.004
Wind speed	Myvatn	Q2	0.291	Wind speed	Upptyppingar	Q1	0.000
Winter accumulation	B12	Winter	0.261	Temperature	Skaftafell	Q2	−0.003
Atmospheric pressure	Eyjabakkar	Q2	0.259	Outgoing longwave radiation	BruMi	Q2	−0.004
Atmospheric pressure	Egilsstaðir	Q2	0.256	Wind speed	Karahnjukar	Q1	−0.004
Wind speed	Egilsstaðir	Q2	0.232	Vapor pressure	Karahnjukar	Q2	−0.008
Temperature	Eyjabakkar	Q2	0.227	Temperature	Egilsstaðir	Q2	−0.017
Winter accumulation	B19	Winter	0.218	Positive degree days	BruNe	Q1	−0.021
Wind direction	BruNe	Q2	0.200	Atmospheric pressure	Laufbali	Q2	−0.023
Atmospheric pressure	Egilsstaðir	Q1	0.195	Negative degree days	BruNe	Q1	−0.024
Wind speed	Hvalsnes	Q2	0.192	Temperature	BruNe	Q1	−0.027
Winter accumulation	B16	Winter	0.191	Temperature	Egilsstaðir	Q1	−0.030
Relative humidity	Jökulheimar	Q2	0.191	Atmospheric pressure	Teighorn	Q2	−0.030
Incoming longwave radiation	BruNe	Q2	0.187	Wind speed	BruNe	Q1	−0.030
Atmospheric pressure	Eyjabakkar	Q1	0.182	Dew point temperature	Karahnjukar	Q2	−0.033
Temperature	Karahnjukar	Q2	0.182	Relative humidity	Eyjabakkar	Q1	−0.033
Sea temperature anomaly	North Atlantic	Past month	0.180	Wind direction	Upptyppingar	Q1	−0.034
Albedo	Brune	Q1	0.177	Wind speed	Eyjabakkar	Q1	−0.035
Relative humidity	Jökulheimar	Q2	0.167	Wind speed	Setur	Q2	−0.037
Wind speed	Laufbali	Q2	0.158	Temperature	Teighorn	Q2	−0.044
Wind speed	Skarðsfjöruviti	Q2	0.157	Relative humidity	Eyjabakkar	Q2	−0.046
Winter accumulation	B13	Winter	0.157	Temperature	Laufbali	Q2	−0.046
Relative humidity	BruNe	Q1	0.155	Winter accumulation	B09	Winter	−0.047
Reflected solar radiation	BruMi	Q2	0.152	Temperature	BruMi	Q2	−0.049
Winter accumulation	Bru	Winter	0.151	Wind direction	BruNe	Q1	−0.051
Relative humidity	Karahnjukar	Q2	0.146	Incoming solar radiation	BruMi	Q2	−0.051
Wind speed	Skaftafell	Q2	0.143	Wind direction	Karahnjukar	Q2	−0.055
Temperature	Eyjabakar	Q1	0.139	Precipitation	Egilsstaðir	Q1	−0.055
Wind speed	BruMi	Q2	0.139	Atmospheric pressure	Jökulheimar	Q2	−0.056
Temperature	Setur	Q2	0.135	Temperature	Skarðsfjöruviti	Q2	−0.056
Incoming longwave radiation	BruNe	Q1	0.133	Wind direction	Upptyppingar	Q2	−0.058
Wind speed	Egilsstaðir	Q1	0.126	Incoming longwave radiation	BruMi	Q2	−0.060
Winter accumulation	BUD	Winter	0.124	Wind speed	BruNe	Q2	−0.060
Positive degree days	BruMi	Q2	0.117	Wind direction	Karahnjukar	Q1	−0.064
Reflected solar radiation	BruNe	Q1	0.116	Atmospheric pressure	Setur	Q2	−0.065
Wind speed	Upptyppingar	Q2	0.116	Incoming solar radiation	BruNe	Q2	−0.066
Wind speed	Eyjabakkar	Q2	0.110	Wind direction	Eyjabakkar	Q2	−0.068
Incoming solar radiation	BruNe	Q1	0.107	Relative humidity	Myvatn	Q2	−0.068
Temperature	Jökulheimar	Q2	0.107	Wind direction	Eyjabakkar	Q1	−0.068
Winter accumulation	B18	Winter	0.106	Negative degree days	BruNe	Q2	−0.069
Net radiation	BruMi	Q2	0.103	NAOI	North Atlantic	Past month	−0.069
Wind speed	Jökulheimar	Q2	0.102	Negative degree days	BruMi	Q2	−0.071
Relative humidity	BruNe	Q2	0.098	Wind Speed	Teighorn	Q2	−0.072
Atmospheric pressure	Karahnjukar	Q1	0.097	Wind direction	BruMi	Q2	−0.072
Wind speed	Karahnjukar	Q2	0.097	Relative humidity	Skaftafell	Q2	−0.074
Dew point temperature	Karahnjukar	Q1	0.088	Temperature	Hvalsnes	Q2	−0.075
Temperature	Myvatn	Q2	0.080	Temperature	BruNe	Q2	−0.075
Temperature	Myvatn	Q1	0.078	Vapor pressure	Eyjabakkar	Q2	−0.075
Temperature	Karahnjukar	Q1	0.070	Relative humidity	Karahnjukar	Q1	−0.077
Outgoing longwave radiation	BruNe	Q1	0.069	Relative humidity	Egilsstaðir	Q1	−0.077
Winter accumulation	B14	Winter	0.067	Dew point temperature	Eyjabakkar	Q2	−0.077
Vapor pressure	Eyjabakkar	Q1	0.067	Positive degree days	BruNe	Q2	−0.082
Relative humidity	Egilsstaðir	Q2	0.054	Net radiation	BruNe	Q1	−0.090

MS received 25 August 2017 and accepted in revised form 15 February 2018

Appendix B – Arctic Climate and Snow Cover Trends – Comparing Global Circulation Models with Remote Sensing Observations

Int J Appl Earth Obs Geoinformation 80 (2019) 71–81

Contents lists available at ScienceDirect

Int J Appl Earth Obs Geoinformation

journal homepage: www.elsevier.com/locate/jag

Arctic climate and snow cover trends – Comparing Global Circulation Models with remote sensing observations

Darri Eythorsson[a,*], Sigurdur M. Gardarsson[a], Shahryar K. Ahmad[b], Faisal Hossain[b], Bart Nijssen[b]

[a] Faculty of Civil and Environmental Engineering, University of Iceland, Iceland
[b] Faculty of Civil and Environmental Engineering, University of Washington, United States

ARTICLE INFO

Keywords:
Snow Cover Frequency
Köppen-Geiger climate classifications
MODIS
Google Earth Engine
Trend analysis

ABSTRACT

This study assessed the impact of climate change on snow resources in the Arctic. Climate was classified for the period 1950–2100 according to the Köppen-Geiger (KG) classification system using the ensemble average of NASA-NEX CMIP5 projections for the rcp 4.5 scenario. Snow Cover Frequency (SCF) in days/year was calculated from the MODIS10A1 snow product and the SCF trends were calculated across the Arctic for the MODIS period (2001–2016). Ten pollution monitoring areas in the Arctic lowlands, especially vulnerable to climate change impacts, were selected for analyzing the climate and snow regimes. In seven of the ten areas we observed significant changes in the climate during the MODIS period and these same areas also showed the largest SCF trends. At lower latitudes we observed decreasing SCF, while further north, by the shores of the Arctic seas, SCF has increased. Averaged across the Arctic we observed a 0.91 days/year decrease in SCF. Our results show that across the Arctic warmer climate classes have and will continue to replace polar tundra and cold summer regions. Based on the CMIP5 simulations, we expect the coverage of the currently dominant Arctic climate class, Cold climate with cold summers and no dry season (*Dfc*), to decline by about 40% by 2100 and be replaced by climate classes associated with warm (*Dfb, Dsb, Dwb*) and hot (*Dfa, Dsa, Dwa*) summers.

1. Introduction

We studied the impact of climate change on snow resources in the Arctic. The historical and future expected climate warming was assessed, as estimated by Global Circulations Model (GCM) projections for the rcp 4.5 scenario. We combined information on the climate trends with satellite observations of snow cover to investigate the climate impact on snow resources in the area. The results were analyzed to identify physical drivers for the observed changes on a regional basis and assess the future evolution of the Arctic snow regime. The specific research questions we considered were whether there has been and/or can we expect significant changes in the Arctic climate and, if climate change has occurred, can it be detected by remote sensing observations of the local snow cover?

The climate in the Arctic has been warming at twice the global rate and polar regions are expected to experience the most rapid climate change globally (Larsen et al., 2015). Among the impacts that have been observed already are melting permafrost (Lawrence et al., 2008), declining sea ice concentrations (Notz and Stroeve, 2016), species migrations (Thuiller et al., 2008) and extreme weather events (Cohen et al., 2014). These impacts, which are expected to further advance in the future, will drastically impact Arctic societies and ecosystems (Overland et al., 2013). An essential factor for societal adaptation in the Arctic will be to understand the impact of changing climate regimes on local water resources, which are stored in the landscape as ice and snow for large portions of the year (Diffenbaugh et al., 2013; Eliasson et al., 2017).

A key estimate of the availability of snow resources from remote sensing is Snow Cover Frequency (SCF), the number of snow-covered days per year. SCF can indicate growing season length and habitat suitability (Barichivich et al., 2013) and is an important geophysical feature as snow cover will reflect most of the inbound solar radiation (Cohen, 1994). As it is an important element in several land surface processes, SCF is an important variable in geophysical simulations, e.g. hydrological modelling in cold regions (Bokhorst et al., 2016). Due to its importance, snow cover has been a key observation target for remote sensing using satellites since the 1960's (Cohen, 1994; Guan et al., 2013). Many instruments have been deployed to map global snow cover using various sensor technologies including optical sensors (e.g. Landsat, AVHRR, MODIS, GOES) and microwave technology (e.g. SMMR and AMSR-E) (Dietz et al., 2012). Data from these sensors have, for example, been assimilated in hydrological models to improve

* Corresponding author.
E-mail address: dae5@hi.is (D. Eythorsson).

https://doi.org/10.1016/j.jag.2019.04.003
Received 26 November 2018; Received in revised form 3 April 2019; Accepted 8 April 2019

streamflow simulations (Huang et al., 2017).

Among the best estimates of future climate conditions are GCM projections, whose skill has improved in recent years and which are the basis for developing and implementing societal adaptation strategies (Stocker et al., 2013). We used the ensemble average of the CMIP5 projections for the Representative Concentration Pathway (rcp) 4.5 emission scenario to represent historical and future climate conditions, respectively (Taylor et al., 2012). The GCM output can be used to classify regional climate into different climate regimes. Climate change can then be quantified by analyzing changes of these regimes over time (Chen and Chen, 2013). A widely accepted classification scheme is the Köppen-Geiger (KG) climate classification system, which classifies climate regimes based on temperature and precipitation estimates (Köppen, 1918). The KG system has been used in a variety of disciplines to estimate both global and local impacts of climate change (Chen and Chen, 2013) and as a method to validate GCM results (Lohmann et al., 1993). With the availability of gridded high resolution climate simulations and improved computational capabilities, these maps can now be produced with higher spatial and temporal resolution allowing for a more detailed analysis of climate changes (Kottek et al., 2006; Spinoni et al., 2015).

In this study we analyzed SCF trends using MODIS data that is available for the period (2001–2016) to investigate how they compare with climate changes predicted by recent GCM projections. We argue that if significant changes in the climate and snow regimes coincide in space and time, longer term GCM projections can be considered more reliable and can be used to predict long term SCF trends.

Our hypothesis is that the warming trend that has been observed in the Arctic would result in a decreasing trend in snow cover across the area. We expect this trend to be more pronounced at lower latitudes but also present further north. Our results indicate that the interaction between the climate and snow regimes is not this straightforward, as in some locations we observed a significant increase in SCF simultaneously with a shift toward warmer climate.

2. Materials and methods

2.1. Tools and datasets

In this study the Google Earth Engine (GEE) (Gorelick et al., 2016) was used for all spatial analysis, while some of the statistical analysis and plotting of the results was performed in Python using the SciPy toolbox (Oliphant, 2007). All the datasets used in the study were available in the GEE data catalog. Graphs were created using Pyplot and maps were produced in ArcGIS.

Representative Concentration Pathway (rcp) 4.5 is a stabilization scenario in which total radiative forcing will be stabilized before 2100 by employment of a range of technologies and strategies for reducing greenhouse gas emissions (van Vuuren et al., 2011). The NASA NEX dataset (Thrasher et al., 2006) was used to estimate daily climate conditions by calculating the ensemble average of the CMIP5 projections for the rcp 4.5 scenario (van Vuuren et al., 2011; Taylor et al., 2012). The NASA NEX dataset contains downscaled projections of the 21 GCMs from the CMIP5 model inter-comparison project (Taylor et al., 2012). The CMIP5 calculations were performed in support of the fifth assessment report of the International Panel on Climate Change (IPCC AR5) (Taylor et al., 2012). The NASA NEX dataset is bias-corrected as it contains the CMIP5 GCM reproduction of historic climate.

The MOD10A1.005 MODIS/Terra dataset was used for daily snow cover classifications. The GE data catalog provides the MODIS global daily snow cover products MOD10A1 (Terra) and MYD10A1 (Aqua) (Hall et al., 2006). These datasets contain gridded daily snow cover identified using the Normalized Difference Snow Index (NDSI). The MODIS/Terra product was selected over MODIS/Aqua due to the failure of the band 6 detectors on MODIS/Aqua which impact the calculation of the NDSI (Barnes et al., 2003). Several studies conducted to validate the MODIS snow products have shown good performance compared to other satellite-derived snow results (Maurer et al., 2003) and to ground observations (Xu et al., 2017). The MOD09GA dataset from NASA EOSDIS LP DAAC was used for information about the nadir angle of the MODIS observations.

For calculations involving elevation, we used the GTOPO30 30 arc-second global digital elevation model (LP-DAAC, 2004).

2.2. Study areas

We selected ten pollution monitoring areas within the Arctic boundary defined by the Arctic Monitoring and Assessment Program (AMAP) of the Arctic Council as our study areas. For comparison, analysis was also performed for the entire AMAP area. These ten areas were selected as they are considered especially vulnerable to human development and climate change (AMAP, 2015). The study areas were restricted to the Arctic coastline and lowlands and code was written in GEE to select only data from elevations below 500 m a.s.l. The study areas are shown in Fig. 1. The study areas refer to 70% of the total AMAP area and 92% of the AMAP area below 500 m.a.s.l. We analyzed the Arctic lowlands in our study, because we expect the greatest changes to the climate and snow regimes in these areas. Furthermore, these lower elevation areas are where most human development is located and are the most important areas for wildlife and vegetation habitat. At higher elevation in the Arctic, where glaciation is much more common, large changes in snow or climate were not expected and any changes would be of less consequence for Arctic societies and ecology.

The study areas were manually approximated using the geography tools in the JavaScript version of GEE, while the AMAP boundary was obtained and uploaded as an asset to GEE. The AMAP boundary and the selected pixels of the study areas are shown in Fig. 1.

2.3. Climate classification trends

KG climate classifications were calculated globally at 0.2-degree horizontal resolution. We implemented an algorithm in GEE to classify each pixel based on the KG classification criteria which are summarized in Appendix A (Kottek et al., 2006; Peel et al., 2007). The classification consists of five main classes, each with two levels of subclasses, yielding a total of 30 climate classes. Thus, for example, an area classified with the main class *D – Cold*, second subclass *f – no dry season* and the third subclass *b – warm summer*, would have the code *Dfb*. The algorithm was applied to the Arctic region to calculate annual KG classifications for the duration of the NASA NEX dataset (1951–2100) for the rcp 4.5 scenario.

The ensemble average of the climate models was calculated and taken as an estimate of future conditions. We chose to use the ensemble average of the 21 GCMs in the NEX dataset for rcp 4.5 to run the KG categorical classification scheme. We used the ensemble average as this is a good representative of the of future climate states defined by the rcp 4.5 scenario of the CMIP5 GCM ensemble.

For this study, climate change was estimated as a change in the KG classification for each grid cell due to a change in temperature and precipitation patterns in that same grid cell over varying time periods (Beck et al., 2005). The proportional coverage of each climate class within each study area was found for each year, yielding a time series of proportional KG class coverage in each area. We calculated KG classes for the full period of the NEX dataset (1951–2099) while SCF was estimated using MODIS data available for the period (2001–2016). We

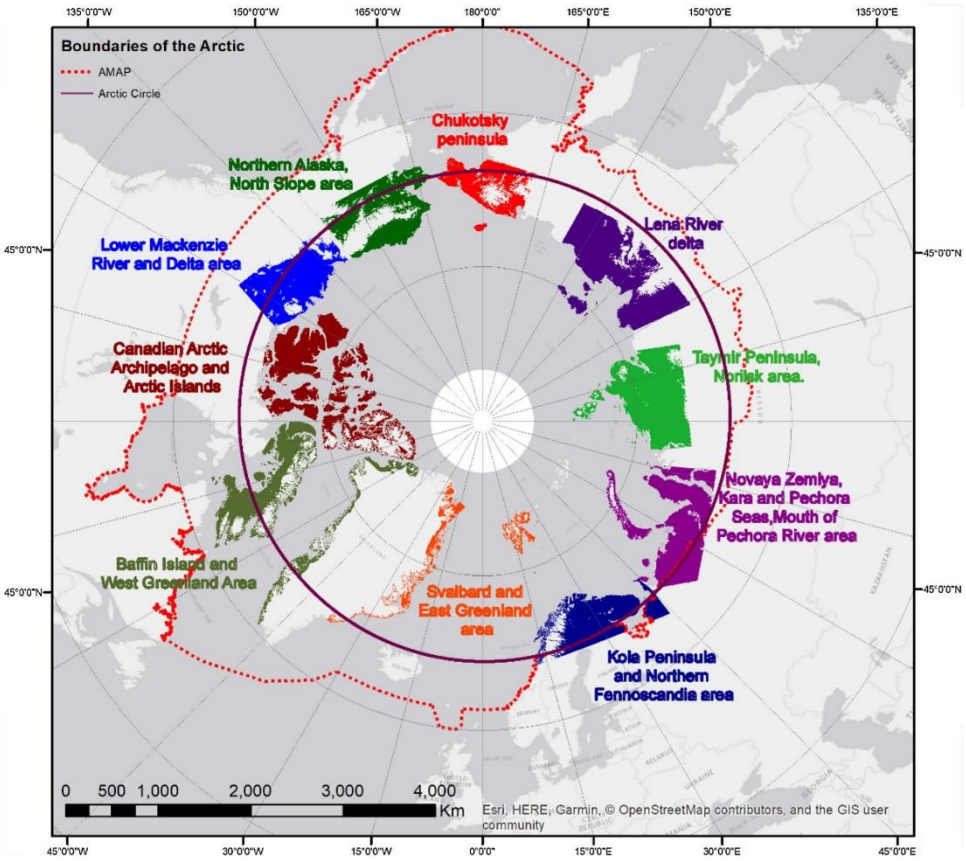

Fig. 1. The Arctic AMAP area and the selected pixels of the ten study areas below 500 m. a.s.l.
Data: AMAP (2015).

used the SCF time series to attempt to validate the GCM projections as we argue that significant changes in the climate and snow regime should coincide in time and space; the projections can then be used to predict future SCF trends and to assess them for periodicity.

2.4. Snow cover frequency trends

We calculated annual SCF at a 500 m × 500 m resolution across the Arctic based on the MODIS10A1.005 snow cover product. We re-mapped the MODIS10A1 dataset to provide a binary classification of snow cover for all valid observations by assigning pixels with value 1 (snow/ice) or 0 (no snow/ice). Observations with zenith angles greater than 25° were filtered out to reduce the so-called *panoramic "bow-tie" effect*. This is a panoramic distortion that is exacerbated by the curvature of the earth, causing overlap in satellite scan lines, leading to data repetition, which is known to cause systematic error in snow mapping in general (Souri and Azizi, 2013) and decreasing accuracy of the MODIS cloud cover mask specifically (Ackerman et al., 2008). Information about the sensor nadir angle was extracted from the MOD09GA dataset and merged with the remapped MOD10A1. The snow cover detection algorithm used to develop MOD10A1 uses all the MODIS swaths acquired in a given day to select the best observation using the NDSI (Baker, 2011).

The MODIS cloud detection algorithm has been evaluated over polar areas and has exhibited misclassification rates for daytime observations of as high as 20% (Liu et al., 2004). With the release of the fifth collection of MODIS imagery significant improvements have been made to the cloud mask (Frey et al., 2008). Wang et al. (2016) compared the MODIS cloud mask to the CloudSat-Cloud-Aerosol and Infrared Pathfinder Satellite Observations (CALIPSO) (C-C) and found 77.8% agreement between the methods (Wang et al., 2016). Ackerman et al., 2008 compared the MODIS cloud mask with ground-based Lidar and satellite-borne Laser Altimeter data and found 85% agreement among the methods. Ault et al. (2006) compared the MODIS cloud cover detection to field observations and found agreement between 86–92%. Based on these studies, we used the MOD10A1 data as is, without additional cloud masking. In this study, missing observations because of, for example, cloud cover or polar night were masked by assigning them a null

value. Pixels with null values that also occurred between consecutive swaths with high nadir angles were rejected. These procedures reduced the number of valid observations annually so that across the Arctic we observed on average 60 valid observations/year per pixel

We calculated the annual SCF for each pixel by filtering the image collection by year and counting the number of times each pixel was covered in snow, dividing by the number of valid observations in each year. Annual SCF maps were calculated for the period of MODIS observations (2001–2016) based on all valid MODIS observations. We did not perform any gap-filling on the MODIS snow cover product to avoid introducing bias in case the number of valid observations is correlated to snow cover. The trend in SCF over the MODIS time series was estimated by linear regression and Sen's estimator of slope method (Sen, 1968) at each pixel. The statistical significance of the trend line was then assessed, using both the non-parametric Mann-Kendall trend test (Maurice and Kendall, 1975) and Sen's estimator of slope methods, as described in the following sections.

2.5. Comparing trends in KG class coverage and SCF

In each study area the timeseries of proportional KG coverage were investigated for evidence of statistically meaningful change during the period of overlap (2001–2016) using the non-parametric Mann-Kendall and Sen's estimator of slope methods. Confidence levels of $\alpha = 0.05$ and $\alpha = 0.01$ were selected as thresholds for reporting statistically significant results. The threshold values of α were selected as this has been a tradition in quantitative research. However, as a value of slightly less than 0.05 only provides a weak argument against the null hypothesis (Wasserstein and Lazar, 2016), p-values are reported for all analyses performed in this study to report the strength of the evidence against the null hypothesis.

The evidence for statistical significance of the trends in SCF and KG class coverage was assessed. Since the distribution of the data is unknown and not assumed to be normally distributed, we estimated the significance of trend using the non-parametric Sen's slope method (Sen, 1968) and the Mann-Kendall hypothesis test (Kendall 1975). Both of these methods have frequently been used to quantify significance of trend in hydro-meteorological time series (Drapela and Drapelova, 2011; Gocic and Trajkovic, 2013). The null hypothesis was that there was no monotonic trend in the data: H_0: $s = 0$, while the alternative hypothesis was that a monotonic trend was present: H_1: $|s| > 0$. Maps were developed showing areas with significant evidence for the rejection of the null hypothesis.

The significance of the trend identified by linear regression was assessed using the Mann-Kendall test. The test was applied using the *ee.Reducer.kendallsCorrelation()* function in GEE and the *stats.kendalltau*() function in SciPy was used. Significant values of τ were estimated from the large sample approximation which is valid for $n > 10$. *Z*-values corresponding to these significance levels were found for the standard normal distribution (Helsel and Hirsch, 2002).

The trend was also estimated using Sen's slope method, which is less sensitive to outliers. The method was applied using the *ee.Reducer.sensSlope()* function in GEE and the *stats.mstats.theilslopes*() function in SciPy. The slope was estimated between all data points in the time series and ordered from smallest to largest. Sen's slope estimate was calculated to give the mean of the slope estimates. The confidence intervals about the slope estimate were calculated for $\alpha = 0.01$ and $\alpha = 0.05$. The slope was determined to be statistically different from zero if the upper and lower confidence intervals shared the same sign (Gocic and Trajkovic, 2013).

3. Results

3.1. Trends in climate classifications

We classified Arctic climate annually for the period 1951–2100 as per the methods described in Section 2.3. We calculated the proportional coverage of each climate class in each study area for each year in the record. Our results showed that, across the Arctic and especially at lower latitudes, climate classes associated with warmer and longer summers have been replacing colder climates. Our results further show that these trends are expected to continue throughout the 21st century.

Fig. 2 shows the climate classifications for the years 1951 and 2099. The figure shows that cold climate with warm summers and no dry season (*Dfb*), which historically has been the main climate class in the continental subarctic, will spread northward until at least the end of the current century, replacing climates associated with cold summers and very cold winters. Fig. 2 shows that all the main climate classes within the Arctic belong to the groups of Cold (*D*) or Polar (*E*) climate.

Table 1 shows the average coverage of the polar and cold climate classes within the Arctic AMAP boundary for the decades 1951–1960 and 2090–2099 grouped by sub category. Table 1 also shows the change in coverage of the same classes during this period. The results show that all classes associated with polar and cold climate with very cold winters are expected to decline during the period. On average, cold climate with cold summers is expected to decline, although the dry/cold summer class (*Dsc*) is expected to expand by half. All climate classes associate with warm and hot summers are expected to more than double during the present century. We note that KG class *Dfd*, cold climate with very cold winters and no dry season was not observed.

Fig. 3 shows the time series of proportional coverage for the main groups of climate classes in the Arctic AMAP area during the period 1951–2099 with a rolling 15-year average. Our results show that throughout the period cold climate classes with cold summers (*Dfc, Dsc* and *Dwc*) are the most common Arctic climates below 500 m.a.s.l. Fig. 3 shows that classes with very cold winters (*Dwd* and *Dsd*) and polar climates (*ET* and *EF*) decline steadily throughout the study period. Climate classes with warm (*Dfb, Dsb* and *Dwb*) and hot summers (*Dfa, Dsa* and *Dwa*) consistently increase in coverage throughout the period, with the rate of increase accelerating after year 2000. Our results show that in the beginning of the period the cold summer classes are rapidly replacing polar (*ET* and *EF*) and very cold winter (*Dwd* and *Dsd*) climate classes, with cold summer classes reaching a peak coverage around year 2020. In the latter part of the period classes with warm (*Dfb, Dwb* and *Dsb*) and hot summers (*Dfa, Dwa* and *Dsa*) advance further north into the Arctic, causing a net decline in the coverage of the cold summer climate classes.

Our results show that by the end of the 21st century the coverage of the most common Arctic climate class in the beginning of the period, cold climate with cold summers and no dry season (*Dfc*) will have decreased by about 40%. The second most common class, Polar tundra (*ET*) is expected to decrease by 34% during the same period. We expect that as these colder climate classes recede further north, climate classes associated with warm and hot summers will expand in coverage by 185% and 733% respectively.

3.2. SCF trends

We estimated the SCF trends in the Arctic using linear regression and the Sen's slope estimator method, as described in Section 2.4. The methods showed good agreement and yielded similar slope estimates. The evidence for the significance of the trends was estimated using the Sen's slope estimator test and the Mann-Kendall trend test for the Sen's slope and linear regression trends, respectively.

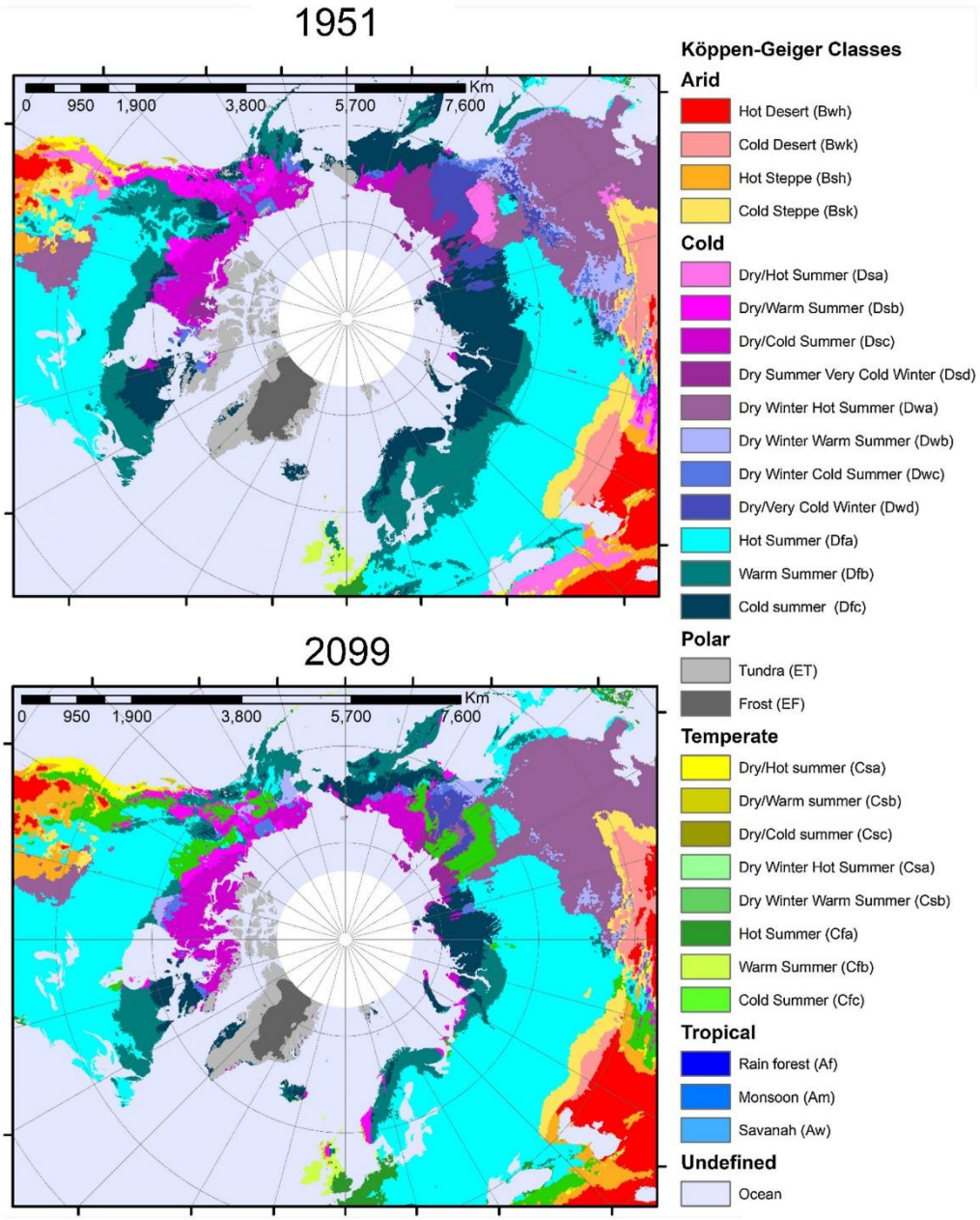

Fig. 2. Examples of annual Köppen-Geiger (KG) classification maps, for year 1951 (upper) and 2099 (lower).

Fig. 4 shows areas with significant SCF slope as highlighted (blue for decreasing SCF and red for increasing SCF) for both statistical methods and significance levels of $\alpha = 0.05$ and $\alpha = 0.01$. The results show that, in general, both methods identify the same areas as exhibiting significant SCF slope. However, the Mann-Kendall method identified areas with permanent snow cover as having a significant increase in SCF, most notably on the Greenland ice sheet. The Sen's method was less sensitive to outliers due to pixel misclassification and did not

Table 1
Coverage of Polar and Cold climate classes within the Arctic AMAP boundary and changes between 1951–1960 and 2090–2099.

		1951–1960	2090–2099	Net Change
	Polar	**26.4%**	**17.3%**	**−35%**
	Polar Frost (EF)	0.4%	0.1%	−86%
	Polar Tundra (*ET*)	26.0%	17.2%	−34%
Cold Climate	**Very Cold Winters**	**15.9%**	**3.1%**	**−80%**
	Dry Winters (*Dwd*)	4.3%	0.1%	−97%
	Dry Summers (*Dsd*)	11.5%	3.0%	−74%
	Cold Summers	**49.1%**	**43.8%**	**−11%**
	No Dry Season (*Dfc*)	30.4%	18.0%	−41%
	Dry Winters (*Dwc*)	2.9%	1.8%	−36%
	Dry Summers (*Dsc*)	15.8%	23.9%	51%
	Warm Summers	**6.6%**	**18.7%**	**185%**
	No Dry Season (*Dfb*)	4.3%	12.9%	197%
	Dry Winters (*Dwb*)	0.2%	1.2%	518%
	Dry Summers (*Dsb*)	2.1%	4.6%	126%
	Hot Summers	**2.0%**	**16.9%**	**733%**
	No Dry Season (*Dfa*)	0.9%	7.6%	770%
	Dry Winters (*Dwa*)	0.5%	1.1%	125%
	Dry Summers (*Dsa*)	0.7%	8.3%	1099%

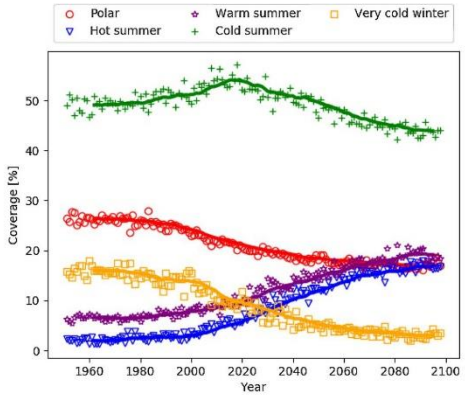

Fig. 3. Proportional coverage of the most common groups of KG classes in the Arctic, below 500 m.a.s.l. for the period 1951–2099. A 15-year rolling mean is shown as solid line.

exhibit this behavior in glaciated terrain. Hence, for further analysis of the results, Sen's method was used. The results in Fig. 4 show large areas of decreasing SCF at lower latitudes surrounding the Arctic circle, whereas at higher latitudes, around the shoreline of the Arctic seas patterns of increasing SCF were observed. Averaged across the arctic AMAP area below 500 m.a.s.l, the findings suggest a decrease in the SCF of 0.25%/year, or 9.1 days/decade, in the period 2001–2016.

3.3. Comparison of SCF and climate trends

We calculated the trends in annual coverage of the two most common KG classes and the average SCF trend in each of the ten study areas, as defined in Section 2.5. The trends were calculated for the overlapping period (2001–2016).

Fig. 5 shows the time series of proportional KG class coverage and SCF for this period. The results differed between areas with changes being evident in some places, whereas in other areas no clear changes were observed, neither for the snow nor the climate regimes. In general, warmer climate classes were observed to replace colder ones during the study period.

Furthermore, we assessed the evidence for the statistical significance of the KG trend line in each study area, using the methods described in Section 2.5. We also calculated the percentage of each area where a significant SCF trend was observed. Table 2 shows the changes in the two most common KG climate classes in all study areas and the result of the statistical analysis of whether the changes can be considered statistically significant. Table 2 also shows the portion of each area where a statistically significant SCF trend was observed, as described in Fig. 4. The table shows the total portion of significant SCF trends as well as the portions of positive and negative SCF trends. The results show that in seven study areas we identified a statistically significant trend in the coverage of one or both of the two main climate classes. These areas also had the biggest portion of statistically significant SCF trends (4.8–13.6% at $\alpha = 0.05$). In the three areas where the climate had not changed statistically significantly - Taymir Peninsula & the Norilsk area, Svalbard & Eastern Greenland area and the Canadian Arctic Archipelago – we also observed the smallest portion of significant SCF trends (< 2% at $\alpha = 0.05$). Hence, the results shown in Table 2 are consistent in that the most pronounced changes in snow cover were observed in areas where the most significant climate change had occurred.

Our results show that, across the AMAP area polar tundra (*ET*) has retreated significantly while at the same time SCF has decreased significantly in 2.8% of the area and increased in 0.8%, at the $\alpha = 0.05$ confidence level. Table 2 shows that in different study areas these trends vary considerably, although in all cases polar or cold summer climate classes are replaced by warmer climate classes.

In both the Lower Mackenzie river delta and the Northern Alaska & North slope area we observed climate with dry/hot summers (*Dsb*) advancing significantly while SCF has been increasing. In the Lena River Delta area cold summer regions with very cold winters (*Dfd*) have receded and cold/dry summer (*Dsc*) regions have advanced while SCF has increased. In the Chukotsky Peninsula, Polar Tundra (*ET*) has receded while SCF has increased. In these four areas we observed a pattern of warmer climate classes advancing at the same time as SCF is increasing. We suggest that the increased SCF observed are driven by changes in the precipitation regime, however, the KG classes that are changing in these areas do not lend themselves to detailed analysis of precipitation patterns.

In both the Kola Peninsula area and the Novaya Zemiya & Pechora Seas area, cold summer regions (*Dfc*) have receded and warm summer regions (*Dfb*) have advanced while SCF has decreased. On Baffin Island and in Western Greenland, polar tundra (*ET*) has receded and cold summer climate (*Dfc*) has advanced while SCF has increased and decreased by about the same amount.

4. Discussion

In this study we compared trends in climate change and snow cover frequency in the Arctic. Our results showed that KG climate classes associated with warm summers have been spreading northward in the Arctic, replacing cold summer climates and polar tundra. These changes are most evident at lower latitudes while colder climate classes are more persistent further north. This is consistent with the snow cover changes we observed at lower latitudes where we saw a decreasing SCF trend around the Arctic perimeter. These results also support our original hypothesis that warming climate would lead to decreasing

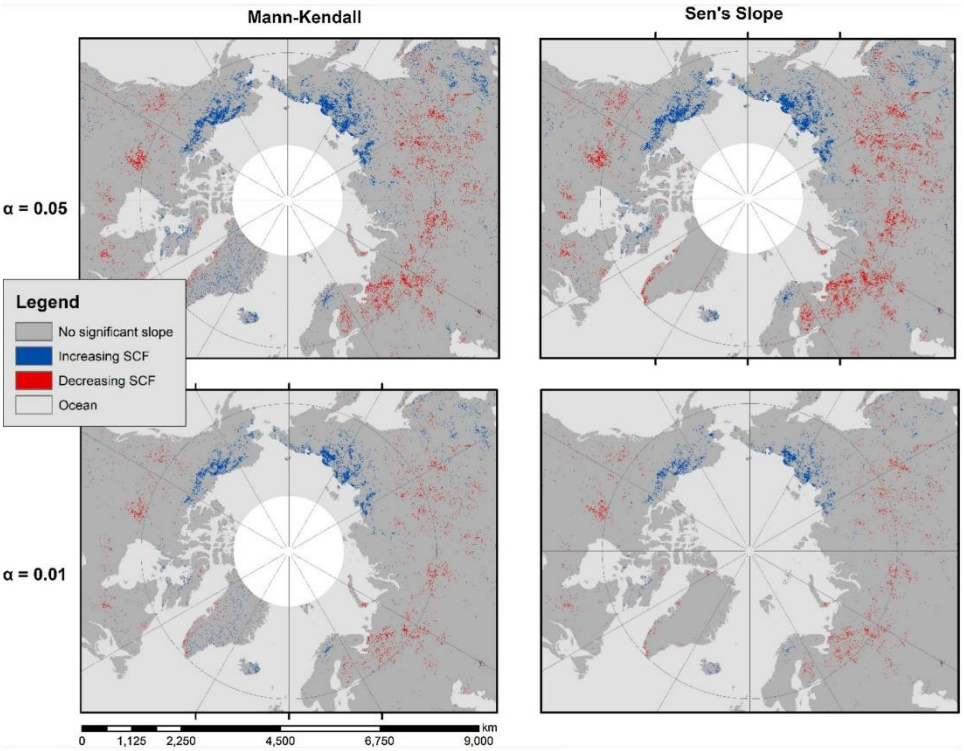

Fig. 4. Areas of significant slope in SCF, at significance levels α = 0.05 and α = 0.01 using the Mann Kendall hypothesis test (left) and Sen's slope estimator (right) (blue: increasing SCF, red: decreasing SCF) (For interpretation of the references to colour in this figure legend, the reader is referred to the web version of this article).

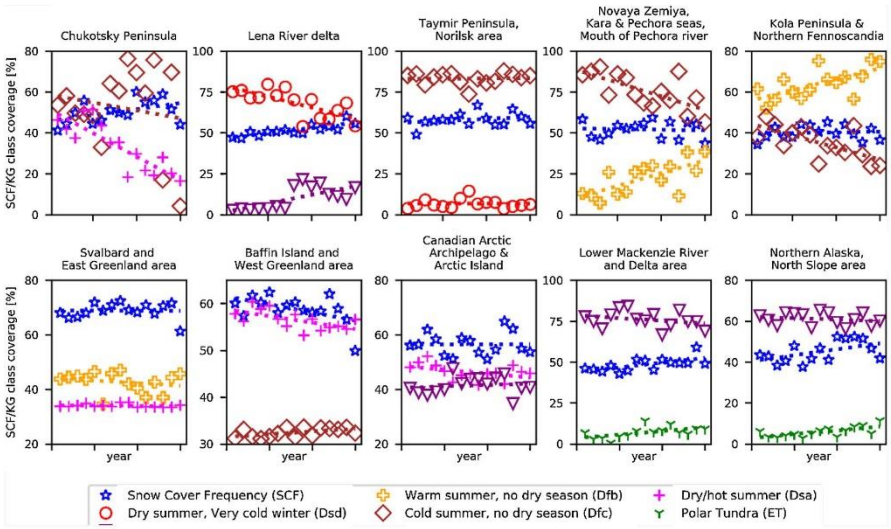

Fig. 5. SCF and proportional coverage of the two most common KG classes in each study area below 500 m.a.s.l. for the period 2001–2016. Trends were estimated with an ordinary least square linear regression (note, for clarity the subplots have differing scales on the vertical axis).

Table 2
Changes in coverage of the two main KG classes in the period 2001–2016 and the percentage of study areas below 500 m.a.s.l. showing a significant SCF trend. Significant results at the $\alpha = 0.05$ confidence level are in bold.

	1st KG Class				2nd KG class				SCF significant area [%] (%pos. / %neg.)	
Area	Name	Change 2001–2016 [%]	MK p-value	Sen's slope	Name	Change 2001–2016 [%]	MK p-value	Sen's slope	$\alpha = 0.05$	$\alpha = 0.01$
Arctic AMAP area	Cold summer no dry season (Dfc)	−7.7%	0.255	inSign	**Tundra (ET)**	**−5.99%**	**0.025**	**Sign**	3.6 (+0.8/−2.8)	0.9 (+0.2/−0.7)
Chukotsky Peninsula	Cold summer no dry season (Dfc)	−21.60%	0.72	inSign	**Tundra (ET)**	**−77.00%**	**0.0006**	**Sign**	11.5 (+11.4/−0.07)	3.7 (+3.7/−0.0)
Lena River Delta	**Cold summer very cold winter (Dfd)**	**−25.30%**	**0.006**	**Sign**	**Cold/dry summers (Dsc)**	**490.50%**	**0.005**	**Sign**	13.6 (+12.9/−0.7)	6.4 (+6.2/−0.2)
Taymir Peninsula, Norilsk Area	Cold summer no dry season (Dfc)	0.70%	0.881	inSign	Dry summer very cold Winter (Dsd)	13.30%	0.805	inSign	1.8 (+1.4/−0.4)	0.4 (+0.3/−0.1)
Novaya Zemiya, Kara & Pechora Seas, Mouth of Pechora River	**Cold summer no dry season (Dfc)**	**−30.20%**	**0.009**	**Sign**	**Warm summer no dry season (Dfb)**	**198.60%**	**0.006**	**Sign**	4.8 (+0.5/−4.3)	1.6 (+0.1/−1.5)
Kola Peninsula & Northern Fennoscandia	**Warm summer no dry season (Dfb)**	**29.60%**	**0.009**	**Sign**	**Cold summer no dry season (Dfc)**	**−62.20%**	**0.003**	**Sign**	9.1 (+2.3/−6.8)	3.6 (+0.7/−0.29)
Svalbard and Eastern Greenland	Warm summer no dry season (Dfb)	−3.40%	0.52	inSign	Tundra (ET)	−1.30%	0.21	inSign	1.2 (+0.6/−1.6)	0.9 (+0.2/−0.7)
Baffin Island and West Greenland Area	**Tundra (ET)**	**−7.00%**	**0.025**	**Sign**	**Cold summer no dry season (Dfc)**	**5.00%**	**0.042**	**Sign**	7.8 (+3.1/−4.7)	3.0 (+1.1/−1.9)
Canadian Arctic Archipelago & Arctic Islands	Tundra (ET)	−8.10%	0.255	inSign	Cold/dry summers (Dsc)	6.50%	0.22	inSign	1.3 (+0.08/−1.2)	0.5 (+0.2/−0.3)
Lower Mackenzie River and Delta area	Cold/dry summers (Dsc)	−11.29%	0.21	inSign	**Dry/hot summers (Dsa)**	**32.78%**	**0.02**	**Sign**	11.3 (+10.7/−0.6)	4.5 (+4.3/−0.2)
Northern Alaska and North slope area	Cold/dry summers (Dsc)	4.03%	0.45	inSign	**Dry/hot summers (Dsa)**	**84%**	**0.006**	**Sign**	11.1 (+11.05/−0.05)	4.3 (+4.3/−0.0)

frequency of snow coverage. At high latitudes, however, around the Arctic shores, we observed increasing SCF trends in many areas, the opposite of our original hypothesis. This pattern was most obvious in areas close to the Bering Strait, and to a lesser extent in areas close to the Barents and Norwegian Seas.

We observed that 8.3% of the Arctic AMAP area has undergone a significant change in SCF in the MODIS period (2001–2016). Averaged across the Arctic SCF has decreased by 0.25%/year or by 9.1 days per decade. These findings agree with prior studies on changes to the snow regime in the area. Yunlong et al. (2018) used MODIS, AMSR-e and the IMS snow cover extent product to develop cloud-free daily snow cover extent maps and estimated a decrease in Northern Hemisphere (NH) Snow Covered Days (SCD) by 5.3 days/decade over the MODIS period; Hori et al. (2017) combined MODIS and AVHRR data to derive a daily Snow Cover Extent (SCE) product for the Northern Hemisphere and found a decreasing trend of 10 days/ decade over large areas of the NH during the period 1978–2015; Liston and Hiemstra (2011) modeled NH snow cover using MERRA reanalysis data and found a decrease in SCD by 2.5 days per decade across the Arctic in the period 1979 – 2009. On average these studies suggest that the frequency of snow cover in the Arctic has decreased by 6.7 days/decade.

In seven study areas of ten we observed evidence for statistically significant climate change during the period 2001–2016 These areas also showed the largest portions of statistically significant SCF trends. These areas have in common proximity to marine areas where sea ice concentration has decreased significantly in recent years (Maslanik et al., 2011). The three areas where no significant climate change and limited SCF trends were detected are all located in the far north and two are in or near the central continental Arctic where sea ice concentrations have not changed as dramatically. These results are consistent with previous findings that suggest that the decreasing sea ice concentrations in the surrounding seas have resulted in increased precipitation over these historically arid areas (Kopec et al., 2016). Although consistent with models (Singarayer et al., 2006) the increasing SCF trends we observed in this study are not found in the studies of Yunlong et al. (2018) or Hori et al. (2017).

In our study we used the MODIS TERRA snow cover product to quantify changes in snow cover. We did not use the MODIS AQUA products due to known issues with band 6 (Barnes et al., 2003). We calculated the SCF rather than performing gap filling and calculating the SCD to prevent adding uncertainty associated with the gap filling method. We suggest that further work should be done to validate and compare gap-filled and multi-sensor snow products to ground-based observations and modeling results to limit and quantify the uncertainty associated with these data. We note that the MODIS period, 2001–2016 is rather short, and trends during this short period can be induced by low frequency cyclical climate patterns, or by a small amount of extreme weather events. However, combined with the climate data we argue that trends observed in both the snow and climate regime during this period can be considered reliable. Both the KG climate classification and presence of snow cover are primarily dependent on precipitation and temperature. Although the mapping from the precipitation and temperature fields to the climate classification and SCF is quite different, our results show that statistically significant changes in these regimes are correlated and that snow cover trends are a useful indicator of assessing changes to regional climate.

Our analysis of climate classifications in the Arctic for the period 1951–2099 suggests that, according to the CMIP5 projections for rcp 4.5, the changes observed during the MODIS era are part of a larger trend that will continue throughout the present century. Given the consistency of the climate trends and their correlation to local snow cover changes, the SCF trends observed in the period 2001–2016 are unlikely to be an artifact of natural periodicity in the climate regime. We expect the northward progress of warmer climate classes will continue at least throughout the present century, as will the decreasing SCF trends as observed in this study. At the same time at higher latitudes, we expect SCF to continue increasing as sea ice concentration continues to decrease.

5. Conclusions

Across the Arctic we observed a consistent trend of warmer climate classes, associated with longer and warmer summers, spreading ever northward. In seven of ten study areas we observed evidence for significant climate change occurring in the period 2001–2016. In these same areas, we also observed the largest SCF trends. In general, we observed decreasing SCF trends at lower latitudes while further north, in the areas bordering the Arctic seas, we observed increasing SCF trends. This increase in SCF at high latitudes has most likely been from increased precipitation due to increasing humidity that results from a declining sea ice concentration. These results are consistent with prior studies in the area.

Our results show that, according to the CMIP5 projections for rcp 4.5, the climate changes observed in the Arctic since 2001 are part of a larger climatic trend that is expected to continue at least throughout the present century. Based on these projections we expect decreasing SCF trends to spread northward, while at higher latitudes, we expect SCF to continue increasing as sea ice concentrations decrease. These changes will impact the Arctic ecosystem, local communities and current exploitation of natural resources and potential utilization of new areas and resources, such as for mining, oil/gas extraction, and transportation.

Conflicts of interest

The authors declare no conflict of interest. The funding sponsors had no role in the design of the study; in the collection, analyses, or interpretation of data; in the writing of the manuscript; nor in the decision to publish the results.

Acknowledgments

We thank the University of Iceland Research Fund which is supporting the first author through the doctoral grants of the University of Iceland Research Fund and the Icelandic National Energy Company, Landsvirkjun, which supported the first author through the Energy Research Fund with grant no. DOK-02-2017. We also acknowledge the assistance of the facilitators at a workshop on scientific writing, arranged by Aalto University, Helsinki, Finland, and IWA/YWP Finland in August 2018.

Appendix A. Köppen-Geiger Classification Criteria

See Table A1.

Table A1
Criteria for Köppen-Geiger classifications and their symbols.

1st	2nd	3rd	Description	Criteria*
A			Tropical	$T_{cold} \geq 18$
	f		-Rain forest	$P_{dry} \geq 60$
	m		-Monsoon	Not Af and $P_{dry} \geq 100\text{-}MAP/25$
	w		-Savannah	Not Af and $P_{dry} < 100\text{-}MAP/25$
B			Arid	$MAP < 10*P_{threshold}$
	w		-Desert	$MAP < 5*P_{threshold}$
	s		-Steppe	$MAP \geq 5*P_{threshold}$
		H	-Hot	$MAT \geq 18$
		K	-Cold	$MAT < 18$
C			Temperate	$T_{hot} > 10$ & $0 < T_{cold} < 18$
	s		-Dry Summer	$P_{sdry} < 40$ & $P_{sdry} < P_{wwet}/3$
	w		-Dry Winter	$P_{wdry} < P_{swet}/10$
	f		-Without dry season	Not Cs or Cw
		A	-Hot Summer	$T_{hot} \geq 22$
		B	-Warm Summer	Not a & $T_{mon}10 \geq 4$
		C	-Cold Summer	Not a or b & $1 \leq T_{mon}10 \leq 4$
D			Cold	$T_{hot} > 10$ and $T_{cold} \leq 0$
	s		-Dry Summer	$P_{sdry} < 40$ & $P_{sdry} < P_{wwet}/3$
	w		-Dry Winter	$P_{wdry} < P_{swet}/10$
	f		-Without dry season	Not Ds and Not Dw
		A	-Hot Summer	$T_{hot} \geq 22$
		B	-Warm Summer	Not a & $T_{mon}10 \geq 4$
		C	-Cold Summer	Not a, b or d
		D	-Very Cold Winter	Not a or b & $T_{cold} < -38$
E			Polar	$T_{hot} < 10$
	T		-Tundra	$T_{hot} > 0$
	F		-Frost	$T_{hot} \leq 0$

References

Ackerman, S.A., Holz, R.E., Frey, R., Eloranta, E.W., Maddux, B.C., McGill, M., 2008. Cloud detection with MODIS. Part II: validation. J. Atmos. Oceanic Technol. 25 (7), 1073–1086. https://doi.org/10.1175/2007JTECHA1053.1.

AMAP, 2015. AMAP Assessment 2015: Temporal Trends in Persistent Organic Pollutants in the Arctic. AMAP Assessment Report.

Ault, T.W., Czajkowski, K.P., Benko, T., Coss, J., Struble, J., Spongberg, A., et al., 2006. Validation of the MODIS snow product and cloud mask using student and NWS cooperative station observations in the Lower Great Lakes Region. Remote Sens. Environ. 105 (4), 341–353. https://doi.org/10.1016/j.rse.2006.07.004.

Baker, N., 2011. Joint Polar Satellite System (JPSS) VIIRS Snow Cover Algorithm Theoretical Basis Document (ATBD). Northrop Grumman Aerospace Syst., Redondo Beach, Calif, pp. 1–52.

Barichivich, J., Briffa, K.R., Myneni, R.B., Osborn, T.J., Melvin, T.M., Ciais, P., et al., 2013. Large-scale variations in the vegetation growing season and annual cycle of atmospheric CO2 at high northern latitudes from 1950 to 2011. Glob. Change Biol. 19 (10), 3167–3183. https://doi.org/10.1111/gcb.12283.

Barnes, W.L., Xiong, X., Salomonson, V.V., 2003. Status of Terra MODIS and Aqua MODIS. Adv. Space Res. 32 (11), 2099–2106. https://doi.org/10.1016/S0273-1177(03)90529-1.

Beck, C., Grieser, J., Rudolf, B., 2005. A New Monthly Precipitation Climatology for the Global Land Areas for the Period 1951 to 2000 Vol. 2004 Klimastatusbericht KSB.

Bokhorst, S., Pedersen, S.H., Brucker, L., Anisimov, O., Bjerke, J.W., Brown, R.D., et al., 2016. Changing Arctic snow cover: a review of recent developments and assessment of future needs for observations, modelling, and impacts. Ambio 45, 516. https://doi.org/10.1007/s13280-016-0770-0.

Chen, D., Chen, H.W., 2013. Using the Köppen classification to quantify climate variation and change: an example for 1901-2010. Environ. Dev. 6 (1), 69–79. https://doi.org/10.1016/j.envdev.2013.03.007.

Cohen, J., 1994. Snow cover and climate. Weather 49 (5), 150–156. https://doi.org/10.1002/j.1477-8696.1994.tb05997.x.

Cohen, J., Screen, J.A., Furtado, J.C., Barlow, M., Whittleston, D., Coumou, D., et al., 2014. Recent Arctic amplification and extreme mid-latitude weather. Nat. Geosci. 7, 627–637. https://doi.org/10.1038/ngeo2234.

Dietz, A.J., Kuenzer, C., Gessner, U., Dech, S., 2012. Remote sensing of snow – a review of available methods. Int. J. Remote Sens. 33 (13), 4094–4134. https://doi.org/10.1080/01431161.2011.640964.

Diffenbaugh, N.S., Scherer, M., Ashfaq, M., 2013. Response of snow-dependent hydrologic extremes to continued global warming. Nat. Clim. Change. https://doi.org/10.1038/nclimate1732.

Drapela, K., Drapelova, I., 2011. Application of Mann-Kendall test and the Sen's slope estimates for trend detection in deposition data from Bily Kriz (Beskydy Mts., the Czech Republic) 1997—2010. Beskydy 4 (2), 133–146. Retrieved from. http://www.mendelu.cz/dok_server/slozka.pl?id=57763%5Cndownload=88743.

Eliasson, K., Ulfarsson, G.F., Valsson, T., Gardarsson, S.M., 2017. Identification of development areas in a warming Arctic with respect to natural resources, transportation, protected areas, and geography. Futures 85, 14–29. https://doi.org/10.1016/j.futures.2016.11.005.

Frey, R.A., Ackerman, S.A., Liu, Y., Strabala, K.I., Zhang, H., Key, J.R., Wang, X., 2008. Cloud detection with MODIS. Part I: improvements in the MODIS cloud mask for Collection 5. J. Atmos. Oceanic Technol. 25 (7), 1057–1072. https://doi.org/10.1175/2008JTECHA1052.1.

Gocic, M., Trajkovic, S., 2013. Analysis of changes in meteorological variables using Mann-Kendall and Sen's slope estimator statistical tests in Serbia. Glob. Planet. Change 100, 172–182. https://doi.org/10.1016/j.gloplacha.2012.10.014.

Gorelick, N., Hancher, M., Dixon, M., Ilyushchenko, S., Thau, D., Moore, R., 2016. Google Earth Engine: planetary-scale geospatial analysis for everyone. Remote Sens. Environ. 202, 18–27. https://doi.org/10.1016/j.rse.2017.06.031.

Guan, B., Molotch, N.P., Waliser, D.E., Jepsen, S.M., Painter, T.H., Dozier, J., 2013. Snow water equivalent in the Sierra Nevada: blending snow sensor observations with snowmelt model simulations. Water Resour. Res. 49 (8), 5029–5046. https://doi.org/10.1002/wrcr.20387.

Hall, D.K., Riggs, G.A., Salomonson, V.V., 2006. MODIS/Terra Snow Cover Daily L3 Global 500m Grid V005 2000-01-01 to 2016-12-31. Retrieved January 5, 2017, from. https://nsidc.org/data/mod10a1.

Helsel, D.R., Hirsch, R.M., 2002. Statistical methods in water resources. Techniques of Water-Resources Investigations of the United States Geological Survey Vol. 36. pp. 524. https://doi.org/10.2307/1269385.

Hori, M., Sugiura, K., Kobayashi, K., Aoki, T., Tanikawa, T., Kuchiki, K., et al., 2017. A 38-year (1978–2015) Northern Hemisphere daily snow cover extent product derived using consistent objective criteria from satellite-borne optical sensors. Remote Sens. Environ. 191, 402–418. https://doi.org/10.1016/j.rse.2017.01.023.

Huang, C., Newman, A.J., Clark, M.P., Wood, A.W., Zheng, X., 2017. Evaluation of snow data assimilation using the ensemble Kalman filter for seasonal streamflow prediction in the western United States. Hydrol. Earth Syst. Sci. https://doi.org/10.5194/hess-21-635-2017.

Kopec, B.G., Feng, X., Michel, F.A., Posmentier, E.S., 2016. Influence of sea ice on Arctic precipitation. Proc. Natl. Acad. Sci. 113 (1), 46–51. https://doi.org/10.1073/pnas.1504633113.
Köppen, W., 1918. Klassifikation der Klimate nach Temperatur, Niederschlag und Jahresablauf (Classification of climates according to temperature, precipitation and seasonal cycle). Petermanns Geographische Mitteilungen.
Kottek, M., Grieser, J., Beck, C., Rudolf, B., Rubel, F., 2006. World map of the Köppen-Geiger climate classification updated. Meteorol. Z. 15 (3), 259–263. https://doi.org/10.1127/0941-2948/2006/0130.
Larsen, J.N., Anisimov, O.A., Constable, A., Hollowed, A.B., Maynard, N., Prestrud, P., et al., 2015. Polar regions. Climate Change 2014: Impacts, Adaptation and Vulnerability: Part B: Regional Aspects: Working Group II Contribution to the Fifth Assessment Report of the Intergovernmental Panel on Climate Change. https://doi.org/10.1017/CBO9781107415386.008.
Lawrence, D.M., Slater, A.G., Tomas, R.A., Holland, M.M., Deser, C., 2008. Accelerated Arctic land warming and permafrost degradation during rapid sea ice loss. Geophys. Res. Lett. 35, L11506. https://doi.org/10.1029/2008GL033985.
Liston, G.E., Hiemstra, C.A., 2011. The changing cryosphere: Pan-Arctic snow trends (1979–2009). J. Clim. 24 (21), 5691–5712. https://doi.org/10.1175/JCLI-D-11-00081.1.
Liu, Y., Key, J.R., Frey, R.A., Ackerman, S.A., Menzel, W.P., 2004. Nighttime polar cloud detection with MODIS. Remote Sens. Environ. 92 (2), 181–194. https://doi.org/10.1016/j.rse.2004.06.004.
Lohmann, U., Sausen, R., Bengtsson, L., Cubasch, U., Perlwitz, J., Roeckner, E., 1993. The Koppen climate classification as a diagnostic tool for general circulation models. Clim. Res. 3 (3), 177–193. https://doi.org/10.3354/cr003177.
LP-DAAC, 2004. Global 30 Arc-Second Elevation Data Set GTOPO30.
Maslanik, J., Stroeve, J., Fowler, C., Emery, W., 2011. Distribution and trends in Arctic sea ice age through spring 2011. Geophys. Res. Lett. 38, L13502. https://doi.org/10.1029/2011GL047735.
Maurer, E.P., Rhoads, J.D., Dubayah, R.O., Lettenmaier, D.P., 2003. Evaluation of the snow-covered area data product from MODIS. Hydrol. Process. 17 (1), 59–71. https://doi.org/10.1002/hyp.1193.
Maurice, G., Kendall, 1975. Rank Correlation Methods. Griffin, London.
Notz, D., Stroeve, J., 2016. Observed Arctic sea-ice loss directly follows anthropogenic CO2 emission. Science 354, 747–750. https://doi.org/10.1126/science.aag2345.
Oliphant, T.E., 2007. Python for scientific computing. Comput. Sci. Eng. 9 (3), 10–20. https://doi.org/10.1109/MCSE.2007.58.
Overland, J.E., Wang, M., Walsh, J.E., Stroeve, J.C., 2013. Future Arctic climate changes: adaptation and mitigation time scales. Earth's Future 2, 68–74. https://doi.org/10.1002/2013EF000162.Received.
Peel, M.C., Finlayson, B.L., Mcmahon, T.A., 2007. Updated world map of the Koppen-Geiger climate classification. HESSD Earth Syst. Sci. Discuss 4 (4), 439–473. https://doi.org/10.1127/0941-2948/2006/0130.
Sen, P.K., 1968. Estimates of the regression coefficient based on Kendall's Tau. J. Am. Stat. Assoc. 63 (324), 1379–1389. https://doi.org/10.1080/01621459.1968.10480934.
Singarayer, J.S., Bamber, J.L., Valdes, P.J., Singarayer, J.S., Bamber, J.L., Valdes, P.J., 2006. Twenty-first-century climate impacts from a declining Arctic sea ice cover. J. Clim. 19 (7), 1109–1125. https://doi.org/10.1175/JCLI3649.1.
Souri, A.H., Azizi, A., 2013. Removing bowtie phenomenon by correction of panoramic effect in MODIS imagery. Int. J. Comput. Appl. 68, 12–16 Published by Foundation of Computer Science, New York, USA.
Spinoni, J., Vogt, J., Naumann, G., Carrao, H., Barbosa, P., 2015. Towards identifying areas at climatological risk of desertification using the Köppen-Geiger classification and FAO aridity index. Int. J. Climatol. 35 (9), 2210–2222. https://doi.org/10.1002/joc.4124.
Stocker, T.F., Qin, D., Plattner, G.K., Tignor, M.M.B., Allen, S.K., Boschung, J., et al., 2013. Climate change 2013 the physical science basis: Working Group I contribution to the fifth assessment report of the intergovernmental panel on climate change. Climate Change 2013 the Physical Science Basis: Working Group I Contribution to the Fifth Assessment Report of the Intergovernmental Panel on Climate Change. https://doi.org/10.1017/CBO9781107415324.
Taylor, K.E., Stouffer, R.J., Meehl, G.A., 2012. An overview of CMIP5 and the experiment design. Bull. Am. Meteorol. Soc. 93, 485–498. https://doi.org/10.1175/BAMS-D-11-00094.1.
Thrasher, B., Melton, F., Weile, W., 2006. NASA Earth Exchange Global Daily Downscaled Projections (NEX-GDDP) | CDS. Retrieved May 1, 2017, from. https://cds.nccs.nasa.gov/nex-gddp/.
Thuiller, W., Albert, C., Araújo, M.B., Berry, P.M., Cabeza, M., Guisan, A., et al., 2008. Predicting global change impacts on plant species' distributions: future challenges. Perspect. Plant Ecol. Evol. Syst. https://doi.org/10.1016/j.ppees.2007.09.004.
van Vuuren, D.P., Edmonds, J., Kainuma, M., Riahi, K., Thomson, A., Hibbard, K., et al., 2011. The representative concentration pathways: an overview. Clim. Change 109 (1), 5–31. https://doi.org/10.1007/s10584-011-0148-z.
Wang, T., Fetzer, E.J., Wong, S., Kahn, B.H., Yue, Q., 2016. Validation of MODIS cloud mask and multilayer flag using CloudSat-CALIPSO cloud profiles and a cross-reference of their cloud classifications. J. Geophys. Res. 121 (19), 11620–11635. https://doi.org/10.1002/2016JD025239.
Wasserstein, R.L., Lazar, N.A., 2016. The ASA's statement on p-values: context, process, and purpose. Am. Stat. 70 (2), 129–133. https://doi.org/10.1080/00031305.2016.1154108.
Xu, W., Ma, H., Wu, D., Yuan, W., 2017. Assessment of the daily cloud-free MODIS Snow-cover product for monitoring the snow-cover phenology over the Qinghai-Tibetan Plateau. Remote Sens. 9 (6). https://doi.org/10.3390/rs9060585.
Yunlong, W., Huang, X., Hui, L., Sun, Y., Qisheng, F., Tiangang, L., 2018. Tracking snow variations in the Northern Hemisphere using multi-source remote sensing data (2000–2015). Remote Sens. 10 (1), 136. https://doi.org/10.3390/rs10010136.

Appendix C - Observed and Predicted Trends in Icelandic Snow Conditions for the period 1930-2100

The Cryosphere, 17, 51–62, 2023
https://doi.org/10.5194/tc-17-51-2023

The Cryosphere Open Access EGU

Observed and predicted trends in Icelandic snow conditions for the period 1930–2100

Darri Eythorsson[1], **Sigurdur M. Gardarsson**[1], **Andri Gunnarsson**[2], **and Oli Gretar Blondal Sveinsson**[2]

[1]Faculty of Civil and Environmental Engineering, University of Iceland, Reykjavik, Iceland
[2]Research and Development Division, Landsvirkjun, Reykjavik, Iceland

Correspondence: Darri Eythorsson (dae5@hi.is)

Received: 4 July 2022 – Discussion started: 18 August 2022
Revised: 2 December 2022 – Accepted: 9 December 2022 – Published: 10 January 2023

Abstract. This study presents an estimate of historical snow conditions in Iceland and a projection of these conditions, given different emission scenarios. Historical snow conditions were estimated using in situ observations from manned meteorological stations over the period 1930–2021 and by remotely sensed observations from the MODIS instruments over the period 2001–2021. Historical and future climate conditions, as described by each of the 21 general circulation models (GCM) from the 5th iteration of the Coupled Model Intercomparison Project (CMIP5) as contained in the NASA Earth Exchange (NEX) Global Daily Downscaled Projections (GDDP) dataset, were used to simulate snow conditions in Iceland over the period 1950–2100 under the Representative Concentration Pathways (RCP) RCP4.5 and RCP8.5 with the SNOW-17 model. The results show an increase in the average annual snow cover frequency (SCF) over the historical record detected both in the in situ (1930–2021) and remotely sensed data (2001–2021). Average annual snow depth measurements also revealed an increasing trend over the historical record. Simulated snow conditions show a substantial decrease in both snow water equivalent (SWE) and SCF over the period 1950–2100, a trend more pronounced under RCP8.5 as compared to RCP4.5.

1 Introduction

The Icelandic climate is categorized as maritime, with mild winters, cold summers, strong winds, frequent precipitation and large spatiotemporal variations in weather and microclimate (Bjornsson et al., 2007; Ólafsson et al., 2007). It is strongly influenced by ocean conditions in the North Atlantic (e.g., Massé et al., 2008) and mass balance trends of Icelandic glaciers are highly correlated with changes in large-scale ocean circulations (Eythorsson et al., 2018). Since the Last Glacial Maximum (LGM) the average annual air temperature in Iceland has increased by about 4 °C (Geirsdóttir et al., 2013; Knudsen et al., 2008; Langdon et al., 2011; Larsen et al., 2011; Sicre et al., 2011). The average air temperature in Iceland has risen by 0.08 °C/decade since the 1850's, comparable to the global average, and by 0.5 °C/decade over the period 1980–2016 (Bjornsson et al., 2018). Since 1890 the Icelandic glaciers have lost about 16 % of their mass and 18 % of their surface area, contributing about 1.5 mm of global sea level rise (Aðalgeirsdóttir et al., 2020; Bjornsson et al., 2013) and are expected to lose most of their remaining mass over the next two centuries at the current pace (Adalgeirsdottir et al., 2006; Bjornsson and Palsson, 2008; Jóhannesson et al., 2004; Schmidt et al., 2020). Runoff in Iceland is generally expected to increase in winter as less water is stored in the snowpack and runoff from glaciers is expected to increase until at least the middle of the 21st century (Blöschl et al., 2017; Jónsdóttir, 2008), the rate of which is expected to vary depending on ocean conditions in the North Atlantic, where recent cooling has led to a slowdown in mass loss of Icelandic glaciers (Noël et al., 2022). Spring melt is generally predicted to begin earlier and autumn snow cover to occur later (Johannesson et al., 2007). Analysis of a recently developed gap-filled MODIS snow cover product suggests that the snow cover duration has increased during the period 2000–2018 for all months expect October and November (Gunnarsson et al., 2019). Understanding of future expected changes to snow in Iceland is important for water resources management as it constitutes

Published by Copernicus Publications on behalf of the European Geosciences Union.

a considerable portion of the regional hydrological cycle, especially in the interior highlands where the majority of the country's energy production occurs, in hydropower plants fed by glacial rivers.

Snow cover monitoring by satellite remote sensing has been studied since the 1960s and several global snow cover products have been produced based on these observations. (Dong, 2018; Frei et al., 2012; Robinson et al., 1993). The MODIS instruments on the Terra and Aqua satellites (Dietz et al., 2012) provide a good balance of spatial and temporal resolution, with two daily observations and 500 m × 500 m pixels (Aalstad et al., 2020). An important variable for snow remote sensing is the snow cover frequency (SCF), the number of days with snow cover divided by the number of valid observations per year (Nolin et al., 2021), which is related to e.g., growing season length and habitability (Callaghan et al., 2011). The SCF is a key variable in the Earth's energy balance (Cohen, 1994) and can be used to analyze the impacts of climate change on the cryosphere (Brown and Mote, 2009).

Snow condition estimates by both general circulation models (GCM) and regional climate models (RCM) capture the main traits of annual snow cycles but are know to contain biases due to their relatively simple snow schemes (Frei et al., 2018; Matiu and Hanzer, 2022). In general the GCM-RCM pair predicts continuation of the ongoing reduction in average snow conditions until the middle of the 21st century (Verfaillie et al., 2018). Improved estimates of snow conditions have been achieved, e.g., using various re-analysis (e.g., Fiddes et al., 2019), downscaling (Fiddes et al., 2022; Smiatek et al., 2016) and data assimilation methods applied either to GCM-RCM snow projections or projections of snow conditions by different snow models forced with downscaled and/or bias corrected GCM-RCM data (e.g., Hanzer et al., 2018).

Many snow models have been developed and described in the literature (e.g., Krinner et al., 2018; Magnusson et al., 2015). The SNOW-17 model was developed for the US National Water Service where it has been used for operational snow forecasting for the past several decades (Anderson, 2006). The SNOW-17 model has been applied to several regional climate change studies (Miller et al., 2011; Notaro et al., 2014) and has shown good correlation to MODIS snow-covered area (SCA) observations (Franz and Karsten, 2013) . A key advantage of the SNOW-17 model is that it is a conceptual model which simulates snowpack conditions based on a temperature index which is both more computationally efficient compared to full energy balance models and requires fewer and simpler forcing data variables.

The objective of this study was to analyze observed trends and predict the development of snow conditions in Iceland under different plausible climate scenarios. This article presents an analysis of historical and future trends in Icelandic climate and snow conditions. Improved understanding of how local snow resources are likely to respond to changing climate conditions is important as these changes are expected to impact local communities and ecosystems as well as changing the challenges and opportunities for exploiting natural resources in cold areas (Eliasson et al., 2017). In this study changes to historical snow cover properties were estimated based on both in situ and remotely sensed observations. Future snow conditions were projected by modeling based on a globally downscaled and bias corrected ensemble of GCMs from the 5th iteration of the Coupled Model Intercomparison Project (CMIP5). The novelty of this study is the analysis of an extended dataset of in situ records of snow conditions in Iceland combined with a reliable remotely sensed dataset of snow conditions in the area and the comparison of these observations with snow conditions simulated using a trusted snow model.

2 Methods

2.1 Tools and datasets

2.1.1 In situ snow observations

Data on in situ snow measurements at manned monitoring stations were acquired from the Icelandic Meteorological Office (IMO) (Icelandic Meteorological Office, 2021). The data contain all observations and manual measurements of local snow depth (SND), snow cover status (SNC), precipitation (R), precipitation class (RTEG), and a visual estimate of surrounding mountain snow cover status (SNCM) for a total of 266 manned observation stations that have recorded snow data in the period 1930–2021. The SNCM is measured with the intent to represent the SNCM in the highlands at 550–650 m a.s.l. in the mountains visible from each observation station, as best applicable to the site of each station. The SNC is measured with the intent to represent the average snow cover status in the near vicinity of the observation station, within 1 km radius (Icelandic Meteorological Office, 2008).

Figure 1 (left panel) shows the locations of the monitoring stations that have recorded SNC continuously for at least 20 years at some time during 1930–2021. The figure shows that the observations are spread around the lowlands near the coastline with more sparse observations in the interior highlands. Figure 1 (right panel) shows the number of IMO stations reporting snow variable observations over the period 1930–2021 and the average annual snow depth across all stations for the same period. The number of stations reporting snow data was below 10 until 1950 and rapidly increased thereafter, the number of stations recording snow cover status increased prior to those recording snow depth, from the 1960s onwards snow depth has been recorded at more than 60 stations. Figure 1 (right panel) shows that the average annual snow depth from all stations has remained similar throughout the study period.

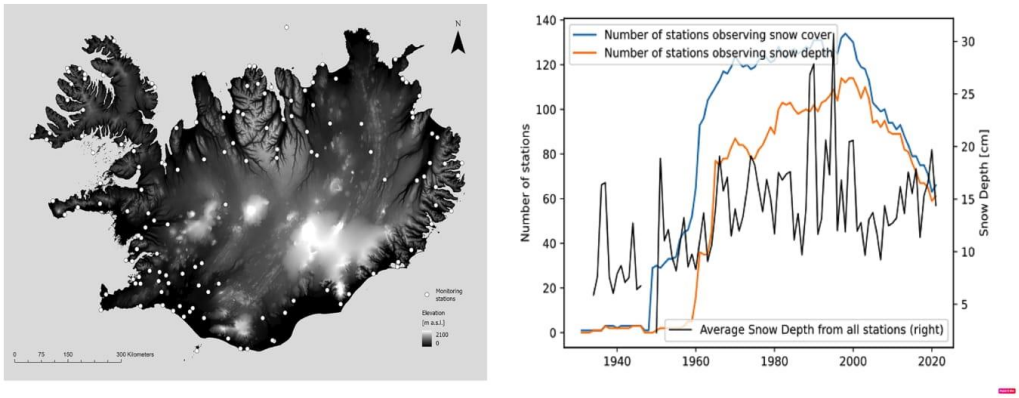

Figure 1. Left panel: topography of Iceland (National Land Survey of Iceland, 2016) and the location of IMO monitoring stations where snow has been measured continuously for at least 20 years in the period 1930–2021. Right panel: number of IMO stations observing snow variables and the average annual snow depth from all stations over time (Icelandic Meteorological Office, 2021).

2.1.2 Remote sensing and geospatial data

The MOD10A1.006 and MYD10A1.006 daily snow cover products from the MODIS instruments on NASA's Aqua and Terra satellites (Hall and Riggs, 2016a, b) were used to estimate spatial changes in snow cover over the period of the 2001–2021 water years. The NDSI_Snow_Cover band was used to estimate the presence of snow in each pixel. The band contains the value of the normalized difference snow index (NDSI) which leverages the fact that snow is highly reflective within the visible spectrum but not the shortwave infrared (Painter et al., 2009; Dozier, 1989). The NDSI values in each pixel are given in a range of 0–100 where a value of NDSI > 0 often indicates the presence of some snow in the pixel and a value of 100 that the pixel is likely fully snow covered. The NDSI is not to be confused with fractional snow covered area (FSCA) which is a measure of the fractional snow coverage of a pixel although there exist commonly used transformations between MODIS, FSCA and NDSI, including linear (Salomonson and Appel, 2006), inverse linear (Fiddes et al., 2019) and other regression methods (Alonso-González et al., 2021). Results from the Sentinel-2 mission have also shown good performance of other NDSI-FSCA transformations (Gascoin et al., 2020). Regression methods have shown good performance on medium resolution observations such as from MODIS, whereas higher resolution observations have been shown to benefit from spectral unmixing (Aalstad et al., 2020; Cortés et al., 2014). The NDSI_Snow_ Cover_Basic_QA band was used to select observations by quality estimation. A 10×10 m DEM (IslandDEM) was used for topographical information (National Land Survey of Iceland, 2016).

2.1.3 Climate data

The NASA Earth Exchange (NEX) Global Daily Downscaled Projections (GDDP) dataset (Thrasher et al., 2012) was used as an estimate of historical and future climate. The dataset contains global minimum and maximum near surface air temperatures and surface precipitation rates, as estimated by 21 globally downscaled and bias-corrected CMIP5 GCMs, in 0.2° horizontal resolution for the period 1950–2100. It is noted that the CMIP6 version of the NEX-GDDP dataset was published after the conclusion of the present study and could be considered in future studies (Thrasher et al., 2022). Daily average temperature was calculated as the mean of daily minimum and maximum temperatures and the ensemble mean was used to represent future climate. Climate and land cover data from the Global Land Data Assimilation System V 2.0 (GLDAS-2) (Rodell et al., 2004) dataset was used for parameter estimation and permafrost extent data from the Arctic Permafrost Map (WGS43261) were also used for parameter estimation (Brown et al., 2002).

2.2 Data processing

2.2.1 In situ observations

The SND is recorded for all days with snow covered ground, in cm, SNC and SNCM are classified by visual observation as: 0 = no snow, 2 = patchy snow cover, 4 = fully covered ground (Icelandic Meteorological Office, 2008). The SND for 1 April was calculated for all stations with more than 20 years of continuous snow depth measurements within the period 1930–2021 ($n = 89$). The annual snow cover frequency (SCF) was calculated for all stations with more than 20 years of continuous snow cover status observations within

the period 1930–2021 ($n = 93$). The SCF was calculated as the number of days with snow covered ground divided by the number of days in the year, for both fully snow covered ground (SNC or SNCM = 4) and for patchy to full snow cover status (SNC or SNCM $\geq$ 2). The SCF was calculated both for observations on the immediate surroundings of the observation site (SFC) and on the surrounding mountains (SFCM).

2.2.2 Remotely sensed observations

A binary snow cover classification was derived from the MOD10A1.006 and MYD10A1.006 snow cover products (Hall and Riggs, 2016a, b). Data from the NDSI_Snow_Cover band was selected for observations with the highest quality estimate (NDSI_Snow_Cover_Basic_QA = 0). The daily mean of NDSI_Snow_Cover band was calculated from both snow cover products. Pixels with NDSI_Snow_Cover > 0 were classified as snow cover (1), and others as no snow (0). The average annual SCF was calculated by counting the number of snow-covered days and dividing by the number of days with valid observations in each pixel, per hydrological year. The SCF was calculated based on the highest quality observations, thus excluding lower quality observations as well as missing data due to cloud cover. The availability of MODIS data during polar darkness is a temporal limitation for the dataset.

2.2.3 Snow modeling

Daily snowpack in Iceland was simulated for each hydrological year in the period 1950–2100 using the SNOW-17 model (Anderson, 2006). The model was run in a 0.2° resolution with daily average precipitation and temperature data from each of the 21 downscaled and bias corrected CMIP5 GCMs in the NASA NEX GDDP dataset (Thrasher et al., 2012). The model was initialized at the start of each hydrological year in the study period to prevent snow accumulation between years. The model was applied to each of the 21 CMIP5 GCMs in the NASA NEX GDDP dataset and to both the RCP4.5 and RCP8.5 scenarios. These scenarios were chosen to represent both a business as usual scenario (RCP8.5) and a stabilization scenario (RCP4.5) where anthropogenic climate forcing is assumed to be stabilized by the end of the century. The SNOW-17 algorithm was coded in Google Earth Engine (GEE), the simulations were performed in GEE and the input data were accessed through the GEE data catalog.

The SNOW-17 uses 10 model parameters that must be specified by the user for each location. In this study the SNOW-17 parameters were determined at the model resolution across Iceland based on local topography, ecology and hydrology. The recommendations provided by the author of the model (Anderson, 2006) were followed for all model parameters except the melt factors MFMAX and MFMIN, which are key model parameters that describe the relation between surface air temperature and snowmelt. For the melt factors the methods of Mizukami and Koren (2008) were followed as they incorporate information about the local slope, aspect, shading, vegetation cover and local shortwave energy balance. The method for parameter determination was selected as calibration of parameters influenced by prevailing climate conditions would cause bias across the time scales considered in this study, although it incurs the uncertainty associated with parameter estimation. The supporting data used for parameter determination were SWE, surface air temperature, precipitation and snowfall rates, near surface wind speed, land cover classification and net solar radiation from the Global Land Data Assimilation System V 2.0 Dataset (GLDAS-2), a 10 × 10 m Digital Elevation Model (DEM) of Iceland (IslandDEM) and permafrost extent data from the Arctic Permafrost Map (WGS43261). Table 1 summarizes the description of each of the SNOW-17 model parameters and presents the value ranges, units, source methodology and supporting datasets used for the determination.

The yearly 1 April SWE was extracted for each ensemble member. The annual SCF was also calculated for each ensemble member as the number of times a model grid cell contained snow per year divided by the number of days in that year. The 1 April SWE was used as it has a long history of use as a snow metric for streamflow forecasting and the SCF was used as it has been suggested as a more appropriate snow metric for a changing climate (Nolin et al., 2021).

2.2.4 Data analysis

This study analyzed a large amount of data on Icelandic snow conditions with the purpose of studying long-term trends in snow conditions based on publicly available authoritative datasets. The presence of a statistically significant trend in the time series of in situ observed mean annual SCF and SND was estimated using the Mann-Kendall trend test and by using Sens's estimator of slope method for the MODIS observations. Both of these tests have often been applied to trend analysis in snow cover studies (Notarnicola, 2020; Yilmaz et al., 2019). The Sen's slope method was applied to the remotely sensed observations as it is tolerant to outliers (e.g., Nguyen et al., 2022). The trend test p-values were calculated for the annual SCF and SND time series. If $p<0.05$ the change in the observed data was assumed to be unlikely due to random variability, indicating a presence of a monotonic trend. The average annual snow rain ratio in Iceland was estimated from the ensemble mean of air temperature and surface precipitation data from the NEX-GDDP dataset by applying a simple rain / snow partitioning scheme, where precipitation is classified as snow under a set temperature threshold (0 °C). The GEE (Gorelick et al., 2016) was used to access data, perform simulations and analyze results. Statistical analysis was performed using GEE and the SciPy toolbox (Oliphant, 2007). ArcMap 10.7.1 was used to produce maps showing the results.

Table 1. SNOW-17 model parameters and the value ranges, units, source methods and supporting data used for each.

Parameter	Range	Units	Supporting data	Methodology
Gauge under-catch factor (GCF)	1.0	–	–	Andersson (2006)
Maximum melt factor (MFMAX)	0.7–2.4	$\mathrm{mm\,°C^{-1}\cdot 6\,h^{-1}}$	IslandDEM GLDAS-2	Mizukami and Koren (2008)
Minimum melt factor (MFMIN)	0.001–1.5	$\mathrm{mm\,°C^{-1}\cdot 6\,h^{-1}}$	IslandDEM GLDAS-2	Mizukami and Koren (2008)
Average wind during rain on snow (UADJ)	0.02–0.4	$\mathrm{mm\,mb^{-1}}$	GLDAS-2	Andersson (2006)
Temperature determining rain or snow (PXTEMP)	−1–3	°C	GLDAS-2	Andersson (2006)
Base temperature where melt occurs (MBASE)	0	°C	–	Andersson (2006)
Maximum negative melt factor (NMF)	0.05–0.3	$\mathrm{mm\,°C^{-1}\cdot 6\,h^{-1}}$	GLDAS-2	Andersson (2002)
Antecedent temperature index (TIPM)	0.05–0.2	–	GLDAS-2	Andersson (2002)
Physical liquid water holding capacity (PLWHC)	0.02–0.3	%	GLDAS-2	Andersson (2002)
Constant basal melt rate (DAYGM)	0–0.3	$\mathrm{mm\,d^{-1}}$	WGS43261	Andersson (2006)

3 Results

3.1 Historical snow cover trends

Figure 2a shows the average temperatures and precipitation in Iceland over the period 1950–2021 as estimated from the ensemble mean of the 21 GCMs in the GDDP dataset. The figure shows that both temperature and precipitation have a positive trend during the period while the variability in precipitation has been more than for temperature observations. Figure 2b shows the annual average SCF for all IMO monitoring stations for the period 1950–2021, calculated for local (circles) and mountain (triangles) snow cover status both based on only observations of fully snow-covered ground (SNC or SNCM = 4) and including patchy snow cover status (SNC or SNCM ≥ 2), the in situ data are shown with a 10-year rolling average and a linear trendline. The figure shows the average annual SCF estimated from the MODIS Terra and Aqua snow cover products (black markers) for observations above (stars) and below (crosses) 500 m a.s.l. The figure shows an increasing trend for all observations and that the MODIS observations below and above 500 m a.s.l. correspond well with snow cover status observations around the observation sites and in the surrounding mountains, respectively. Figure 2c shows the average annual snow depth (SND) of all IMO monitoring stations for the period 1950–2021 with a linear trend line and a 10-year rolling average. Due to the considerable increase in the number of stations reporting snow measurements in the 1950s, as illustrated in Fig. 1, data prior to that were not used for trend analyses. The figure shows an increasing trend of SND over the period with the highest values recorded by the end of the 20th century.

The results in Fig. 2 show that on average both SND and SCF in Iceland have a positive trend over the period 1950–2021. The trend is more apparent when considering both full and patchy snow cover status, (SNC or SNCM ≥ 2) and the data reveal considerable natural climate variability. The MODIS estimates of SCF below and above 500 m a.s.l. are comparable to the in situ estimates of local and mountain SCF, respectively.

Figure 3 shows the estimated average annual snow / rain ratio and the projected average annual changes to precipitation and temperature in Iceland over the period 1950–2100 compared to 1950–1960 averages (temperature = −3.35 °C, precipitation 1028 $\mathrm{mm\,yr^{-1}}$) given two emission scenarios. The figure shows that as both temperature and precipitation are expected to experience a continuation of the ongoing increase from the 1950–1960 average the average annual snow / rain ratio across Iceland is expected to decrease continually, from around 0.6 to around 0.2 and 0.1 for RCP4.5 and RCP8.5, respectively. This trend will be apparent sooner at lower elevations where air temperatures are closer to the

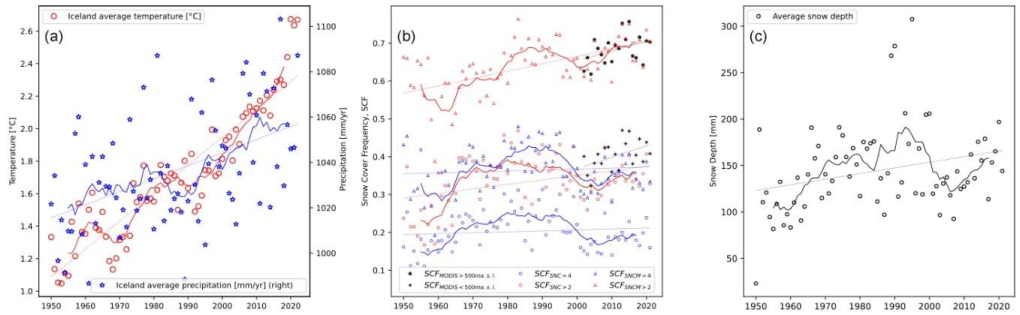

Figure 2. **(a)** Average annual temperature and precipitation in Iceland over the period 1950–2021 as estimated by the ensemble mean of NASA NEX-GDDP. **(b)** Annual average SCF for all IMO monitoring stations for the period 1950–2021 and **(c)** average annual snow depth of all IMO monitoring stations. The solid lines represent a 10-year rolling average.

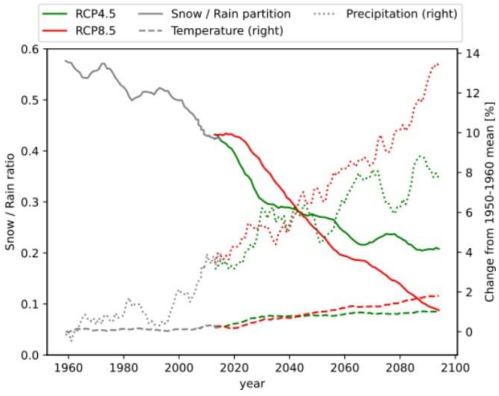

Figure 3. Estimated average annual snow / rain ratio and projected changes for average annual temperature and precipitation in Iceland for the period 1950–2100 given the RCP4.5 and RCP8.5 emission scenarios.

snow / rain partitioning threshold. At higher elevations the observed increase in precipitation will result in a temporarily thicker snowpack overall, as air temperatures are further from reaching the threshold, which would offset the increased winter snowmelt and shorten the snow cover duration associated with temperature rise until the threshold is reached.

Table 2 summarizes the statistical significance of the estimated snow trends, estimated using the Mann-Kendall trend test, for both the period of extensive historical records (1950–2021) and the MODIS period (2001–2021), in terms of p values. The values for the historical trends are calculated from 1950 as the number of stations reporting snow data are few prior to the 1950s, as shown in Fig. 1. The results show that the increasing SCF and SND trends observed in Fig. 2 are statistically significant over the period 1950–2021 for all SCF estimates except for observations of SNCM = 4 (fully snow-covered mountains). Over the MODIS period 2001–2021 the trend is significant for all metrics except for observations of SNC = 4 and for MODIS observations above 500 m a.s.l.

Figure 4a shows the relative change in annual SCF over Iceland as estimated from MODIS observations over the period 2001–2021. Figure 4b shows areas where the trend line is statistically significant ($\alpha = 0.05$) for both MODIS and in situ observations (SNC = 4) shown as symbols. Blue regions and markers show areas where the SCF had significantly increased and the red areas with decreasing SCF. The results show that many areas in Iceland have experienced a significant change in the local SCF, both as estimated from MODIS data and from in-situ snow cover status observations over the period 2001–2021. Most of these areas have experienced an increase in SCF, especially the eastern highlands and the mountainous regions of northern and northwestern Iceland. A few areas showed significant decreases in the SCF and most of those were located at the termini of the country's major outlet glaciers, where a retreat has been well documented (Hannesdóttir et al., 2019; Aðalgeirsdóttir et al., 2020; Hauser and Schmitt, 2021) or in coastal areas. The areas where the largest change in SCF is observed from MODIS data over the period 2001–2021 are those where geophysical surface changes have occurred, e.g., due to glacial retreat. All manned observation sites where a decrease in SCF or SND had occurred over the period were located at low elevation in coastal areas except for one.

3.2 Projected seasonal snow conditions

Figure 5 shows the results of the simulation of daily snow conditions in Iceland for the period 1950–2100 for both representative concentration pathways (RCP) RCP4.5 and RCP8.5. Figure 5a shows the average winter SWE across Ice-

Table 2. Statistical significance of the linear SCD and SCF trend lines, estimated using the Mann-Kendall (MK) trend test, for the full historical period (1950–2021) and the MODIS period (2001–2021). Statistically significant trend lines at the $\alpha = 0.05$ level are shown in bold.

	Trend [% per decade]		p-value	
	1950–2021	2001–2021	1950–2021	2001–2021
SCFM (SNCM $\geq$ 2)	0.1	4.3	$\mathbf{1.4 \times 10^{-6}}$	**0.02**
SCFM (SNCM = 4)	0.0025	2.1	0.9	0.07
SCF (SNC $\geq$ 2)	0.1	3.7	**0.025**	**0.01**
SCF (SNC = 4)	0.002	1.9	0.6	0.06
SND	0.05	3.0	**0.006**	**0.002**
MODIS below 500 m a.s.l.	–	2.9	–	**0.04**
MODIS above 500 m a.s.l.	–	2.4	–	0.11
MODIS all elevations	–	2.6	–	**0.04**

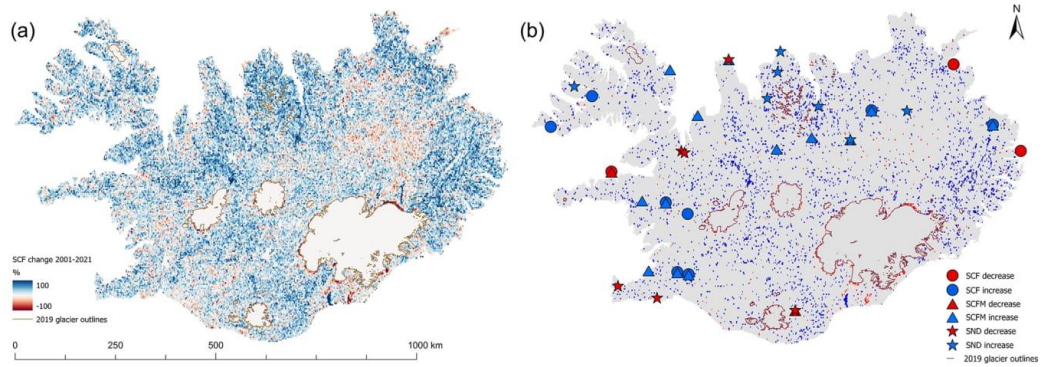

Figure 4. (a) Percentage relative change in annual SCF over Iceland as estimated from MODIS over the period 2001–2021. **(b)** Areas where the SCF trend line is statistically significant ($\alpha = 0.05$) for both MODIS and in situ observations (SNC = 4), where in situ observations are shown with symbols. The 2019 outlines of glaciers and the ice divides of their major outlet glaciers are shown with black lines (Hannesdóttir et al., 2020).

land and 5b shows the simulated average annual SCF along with in situ and MODIS-derived SCF estimates.

Figure 5 shows that both SWE and SCF are expected to decrease in Iceland over the course of the 21st century and that this decrease has been ongoing throughout the study period. Figure 5b shows that MODIS-derived SCF estimates over the period 2001–2021 fit well with the simulated values. In situ observations of local and mountain snow cover status (SNC or SNCM > 2) fall below and above the simulated averages, respectively, as expected. However, although observed and simulated SCF estimates fit well with the magnitude and variability of each other, their trend is opposite. The observational data show an increasing SCF trend while the simulations show a decreasing trend over the historical period 1950–2020. This pattern of opposing trends is also observed in terms of snow magnitude as the simulated SWE estimates show a decrease in SWE, whereas the observed snow depth measurements (shown in Fig. 2) show a significant increase ($p = 1.54 \times 10^{-5}$) over the period 1930–2021. The results also illustrate the substantial natural climate variability in Icelandic snow conditions.

The results in Fig. 2 show a positive trend for temperature and precipitation in Iceland over the period 1950–2021. Increasing temperatures result in enhanced snowmelt, which is apparent in a flat or decreasing SCF in coastal regions (shown in Fig. 4), whereas at higher elevations the increased precipitation enhance winter snow accumulation leading to higher SCF despite the enhanced snowmelt during summer, leading to a countrywide increase in average SCF. This effect of increased snow cover at high elevations can be expected to persist until temperatures have risen above freezing for a considerable portion of the winter at the highest elevations as well, after which snow cover is expected to decrease at all elevations. Due to variability in the Icelandic landscape and topography this effect should be more apparent when simulated at a finer spatial resolution.

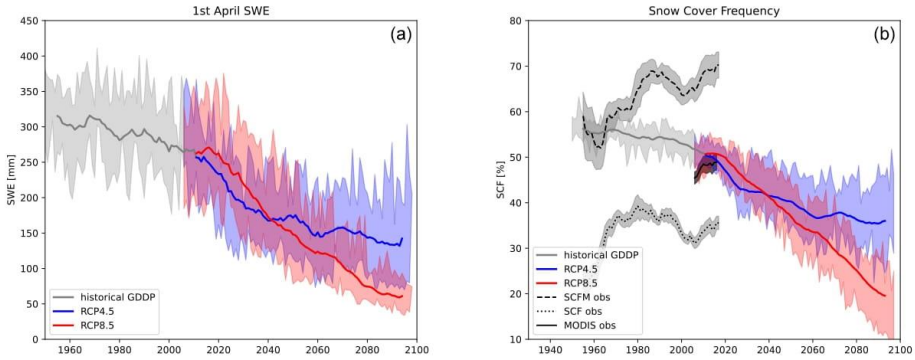

Figure 5. (a) Simulated average winter SWE across Iceland for both RCP4.5 (green) and RCP8.5 (red). **(b)** simulated average annual SCF across Iceland as projected by RCP4.5 and RCP8.5 compared to observations from monitoring stations of mountain and local snow cover status as well as the MODIS snow cover products. The shaded area represents the upper and lower quantiles of the ensemble simulations and one standard deviation from the mean of the observations. The solid line shows a 10-year moving average.

Recent studies have suggested a regional cooling in the ocean temperatures surrounding Iceland due to changes in the thermohaline circulation in the North Atlantic Ocean (Caesar et al., 2018). This regional cooling, which has been connected to a temporary slowing of glacial ablation in Iceland (Noël et al., 2022), would explain the opposing trends observed in Fig. 5 as this regional cooling is poorly represented in the CMIP5 models used for the snow simulations in this study. The North Atlantic cooling trend is projected to halt around 2050 given the results of the Community Earth System Model version 2 (Danabasoglu et al., 2020).

4 Discussion and conclusion

The analysis of snow observations showed a significant increase in both snow cover frequency (SCF) and 1 April SWE, both as estimated from in situ observations over the period 1930–2021 and from observations from the MODIS instruments on NASA's Terra and Aqua satellites over the period 2001–2021. The MODIS observations were comparable with in situ observations of both local and mountain snow cover status. The results also revealed a large natural variability in snow conditions, which was expected due to the sensitivity of the Icelandic climate to fluctuations in large-scale atmospheric and ocean circulations in the North Atlantic region (e.g., Hanna et al., 2004; Massé et al., 2008). The results showed a significant increase in average annual snow depth over all stations for the period 1930–2021.

Simulated SCF was consistent with SCF estimates from both MODIS and in situ observations for the historical period, although the simulated trend was opposite to the trends in both observational datasets. The simulations show that SCF is expected to significantly decrease over the projected period 2006–2100 especially below 500 m a.s.l., where snow cover is expected to become a rare occurrence by the end of the period, given the RCP8.5 emission scenario. The simulated SWE shows a significant decrease in SWE over the period 1950–2021 whereas average annual SND from all IMO stations has a positive trend over the same period. The results show that the water storage in Icelandic winter snowpack could decrease by about half or 3/4 under the RCP4.5 and RCP8.5 emission scenarios, respectively, over the period 1950–2100.

The results of this study suggest that the increased SCF in Iceland, observed both from remotely sensed and in situ data, is associated with increased precipitation causing a more frequent and thicker snowpack which persists longer, despite enhanced melt rates. This is consistent with Bjornsson et al. (2018) who found annual precipitation to have increased by about 10 % during the period 1980–2015. This increasing trend was also observed by Gunnarsson et al. (2019) who used multisource satellite remote sensing data to show that there had been an increase in snow cover in Iceland for all months except October and November over the period (2000–2017). The simulated snow conditions are also in agreement with previous projections of a decrease in SCF and snow mass across Iceland, as the rising average temperature causes spring melts to begin earlier and autumn snow cover to occur later (e.g., Johannesson et al., 2007).

The results presented in this study deserve further investigation. Observations of snow conditions reveal a large natural variability which may be affected by large scale circulations in atmospheric and ocean circulations in the North Atlantic as well as global temperature changes. The observations of both snow cover and snow depth indicate an increasing trend in these variables over the historical period whereas simulated snow conditions predict a decrease in both over the course of the present century, the extent of which is depen-

Table 3. Underlying research datasets used in this study.

Dataset	Purpose	Reference	DOI:
NASA NEX-GDDP	Model forcing	Thrasher et al. (2012)	https://doi.org/10.5194/hess-16-3309-2012 https://ds.nccs.nasa.gov/thredds/catalog/bypass/NEX-GDDP/catalog.html
GLDAS-2	Parameter estimation	Beaudoing and Rodell (2020)	https://doi.org/10.5067/E7TYRXPJKWOQ
Arctic Permafrost Extent (WGS43261)	Parameter estimation	Brown et al. (2002)	https://doi.org/10.7265/skbg-kf16
IslandDEM	Parameter estimation and analysis	–	https://www.lmi.is/is/landupplysingar/gagnagrunnar/nidurhal
MYD10A1.006 MOD10A1.006	Remotely sensed snow observations	Hall and Riggs (2016a, b)	https://doi.org/10.5067/MODIS/MOD10A1.006 https://doi.org/10.5067/MODIS/MYD10A1.006
IMO snow observations	In situ snow observations	–	fyrirspurnir@vedur.is

dent on future emission scenarios. The observed increases in SCF and SWE could be part of natural climate variability induced by low-frequency cyclical climate patterns, or by a small amount of extreme weather events. The causes and the impacts of these changes to Icelandic ecology and society should be better understood as future changes to snow conditions will impact the hydrological cycle, which will further affect the local ecology, hazard assessments, water resources management, and hydropower production in the country.

Code and data availability. All data used for the analysis in this study are freely available and were accessed either through the Google Earth Engine database or by direct correspondence with the data provider. The datasets used in this study and their source literature and links are provided in Table 3. The code for the snow model and/or the remote sensing analysis can be made available upon request.

Author contributions. DE and SMG designed the experiments. DE developed the code, performed the analysis and prepared the manuscript. DE and AG gathered, assessed, and prepared the data. SMG, AG and OGBS reviewed the manuscript and provided significant consultation and contributions throughout the work.

Competing interests. The contact author has declared that none of the authors has any competing interests.

Disclaimer. Publisher's note: Copernicus Publications remains neutral with regard to jurisdictional claims in published maps and institutional affiliations.

Acknowledgements. We thank the University of Iceland Research Fund which is supporting the first author through a doctoral grant.

Financial support. This research has been supported by the Háskóli Íslands, Raunvísindastofnun, Háskóli Íslands (grant no. HI16050205).

Review statement. This paper was edited by Masashi Niwano and reviewed by Kristoffer Aalstad and one anonymous referee.

References

Aalstad, K., Westermann, S., and Bertino, L.: Evaluating satellite retrieved fractional snow-covered area at a high-Arctic site using terrestrial photography, Remote Sens. Environ., 239, 111618, https://doi.org/10.1016/J.RSE.2019.111618, 2020.

Aðalgeirsdóttir, G., Johannesson, T., Bjornsson, H., Palsson, F., and Sigurosson, O.: Response of Hofsjokull and southern Vatnajokull, Iceland, to climate change, J. Geophys. Res. Surf., 111, F03001, https://doi.org/10.1029/2005jf000388, 2006.

Aðalgeirsdóttir, G., Magnússon, E., Pálsson, F., Thorsteinsson, T., Belart, J. M. C., Jóhannesson, T., Hannesdóttir, H., Sigurðsson, O., Gunnarsson, A., Einarsson, B., Berthier, E., Schmidt, L. S., Haraldsson, H. H., and Björnsson, H.: Glacier Changes in Iceland From ∼1890 to 2019, Front. Earth Sci., 8, 523646, https://doi.org/10.3389/FEART.2020.523646, 2020.

Alonso-González, E., Gutmann, E., Aalstad, K., Fayad, A., Bouchet, M., and Gascoin, S.: Snowpack dynamics in the Lebanese mountains from quasi-dynamically downscaled ERA5 reanalysis updated by assimilating remotely sensed fractional snow-covered area, Hydrol. Earth Syst. Sci., 25, 4455–4471, https://doi.org/10.5194/hess-25-4455-2021, 2021.

Anderson, E. A.: Calibration of conceptual models for use in river forecasting, Hydrology Lab., Silver Spring, MD, National Weather Service, 2002.

Anderson, E.: Snow Accumulation and Ablation Model–SNOW-17, Office of Hydrologic Development, National Weather Service, https://doi.org/10.1038/177563a0, 2006.

Beaudoing, H. and Rodell, M.: GLDAS Noah Land Surface Model L4 3 hourly 0.25 × 0.25 degree V2.1, Greenbelt, Maryland, USA, Goddard Earth Sciences Data and Information Services Center (GES DISC), NASA/GSFC/HSL [data set], https://doi.org/10.5067/E7TYRXPJKWOQ, 2022.

Bjornsson, H. and Palsson, F.: Icelandic glaciers, Jökull, 58, 365–386, 2008.

Bjornsson, H., Olason, E. O., Jónsson, T., and Henriksen, S.: Analysis of a smooth seasonal cycle with daily resolution and degree day maps for Iceland, Meteorol. Z., 16, 57–69, https://doi.org/10.1127/0941-2948/2007/0188, 2007.

Bjornsson, H., Palsson, F., Gudmundsson, S., Magnusson, E., Adalgeirsdottir, G., Johannesson, T., Berthier, E., Sigurdsson, O., and Thorsteinsson, T.: Contribution of Icelandic ice caps to sea level rise: Trends and variability since the Little Ice Age, Geophys. Res. Lett., 40, 1546–1550, https://doi.org/10.1002/grl.50278, 2013.

Bjornsson, H., Sigurdsson, B., Davidsdottir, B., Olafsson, J., Asthorsson, O., Olafsdottir, S., Baldursson, T., and Jonsson, T.: Climate Change and it's impact on Iceland – Report of the scientific committee on Climate Change, Icelandic Meteorological Office, ISSN 978-9935-9414-0-4, 2018.

Blöschl, G., Hall, J., Parajka, J., Perdigão, R. A. P., Merz, B., Arheimer, B., Aronica, G. T., Bilibashi, A., Bonacci, O., Borga, M., Čanjevac, I., Castellarin, A., Chirico, G. B., Claps, P., Fiala, K., Frolova, N., Gorbachova, L., Gül, A., Hannaford, J., Harrigan, S., Kireeva, M., Kiss, A., Kjeldsen, T. R., Kohnová, S., Koskela, J. J., Ledvinka, O., Macdonald, N., Mavrova-Guirguinova, M., Mediero, L., Merz, R., Molnar, P., Montanari, A., Murphy, C., Osuch, M., Ovcharuk, V., Radevski, I., Rogger, M., Salinas, J. L., Sauquet, E., Šraj, M., Szolgay, J., Viglione, A., Volpi, E., Wilson, D., Zaimi, K., and Živković, N.: Changing climate shifts timing of European floods, Science, 357, 588–590, https://doi.org/10.1126/SCIENCE.AAN2506, 2017.

Brown, J., Ferrians, O., Higginbottom, J. A., and Melnikov, E.: Circum-Arctic Map of Permafrost and Ground-Ice Conditions, Version 2, Boulder, Colorado USA, National Snow and Ice Data Center [data set], https://doi.org/10.7265/skbg-kf16, 2002.

Brown, R. D. and Mote, P. W.: The response of Northern Hemisphere snow cover to a changing climate, J. Clim., 22, 2124–2145, https://doi.org/10.1175/2008JCLI2665.1, 2009.

Caesar, L., Rahmstorf, S., Robinson, A., Feulner, G., and Saba, V.: Observed fingerprint of a weakening Atlantic Ocean overturning circulation, Nature, 556, 191–196, https://doi.org/10.1038/s41586-018-0006-5, 2018.

Callaghan, T. V., Johansson, M., Brown, R. D., Groisman, P. Y., Labba, N., Radionov, V., Bradley, R. S., Blangy, S., Bulygina, O. N., Christensen, T. R., Colman, J. E., Essery, R. L. H., Forbes, B. C., Forchhammer, M. C., Golubev, V. N., Honrath, R. E., Juday, G. P., Meshcherskaya, A. V., Phoenix, G. K., Pomeroy, J., Rautio, A., Robinson, D. A., Schmidt, N. M., Serreze, M. C., Shevchenko, V. P., Shiklomanov, A. I., Shmakin, A. B., Sköld, P., Sturm, M., Woo, M. K., and Wood, E. F.: Multiple effects of changes in arctic snow cover, Ambio, 40, 32–45, https://doi.org/10.1007/s13280-011-0213-x, 2011.

Cohen, J.: Snow cover and climate, Weather, 49, 150–156, https://doi.org/10.1002/j.1477-8696.1994.tb05997.x, 1994.

Cortés, G., Girotto, M., and Margulis, S. A.: Analysis of sub-pixel snow and ice extent over the extratropical Andes using spectral unmixing of historical Landsat imagery, Remote Sens. Environ., 141, 64–78, https://doi.org/10.1016/J.RSE.2013.10.023, 2014.

Danabasoglu, G., Lamarque, J. F., Bacmeister, J., Bailey, D. A., DuVivier, A. K., Edwards, J., Emmons, L. K., Fasullo, J., Garcia, R., Gettelman, A., Hannay, C., Holland, M. M., Large, W. G., Lauritzen, P. H., Lawrence, D. M., Lenaerts, J. T. M., Lindsay, K., Lipscomb, W. H., Mills, M. J., Neale, R., Oleson, K. W., Otto-Bliesner, B., Phillips, A. S., Sacks, W., Tilmes, S., van Kampenhout, L., Vertenstein, M., Bertini, A., Dennis, J., Deser, C., Fischer, C., Fox-Kemper, B., Kay, J. E., Kinnison, D., Kushner, P. J., Larson, V. E., Long, M. C., Mickelson, S., Moore, J. K., Nienhouse, E., Polvani, L., Rasch, P. J., and Strand, W. G.: The Community Earth System Model Version 2 (CESM2), J. Adv. Model. Earth Syst., 12, e2019MS001916, https://doi.org/10.1029/2019MS001916, 2020.

Dietz, A. J., Kuenzer, C., Gessner, U., and Dech, S.: Remote sensing of snow – a review of available methods, Int. J. Remote Sens., 33, 4094–4134, https://doi.org/10.1080/01431161.2011.640964, 2012.

Dong, C.: Remote sensing, hydrological modeling and in situ observations in snow cover research: A review, J. Hydrol., 561, 573–583, https://doi.org/10.1016/j.jhydrol.2018.04.027, 2018.

Dozier, J.: Spectral signature of alpine snow cover from the landsat thematic mapper, Remote Sens. Environ., 28, 9–22, https://doi.org/10.1016/0034-4257(89)90101-6, 1989.

Eliasson, K., Ulfarsson, G. F., Valsson, T., and Gardarsson, S. M.: Identification of development areas in a warming Arctic with respect to natural resources, transportation, protected areas, and geography, Futures, 85, 14–29, https://doi.org/10.1016/j.futures.2016.11.005, 2017.

Eythorsson, D., Gardarsson, S. M., Gunnarsson, A., and Hrafnkelsson, B.: Statistical summer mass-balance forecast model with application to Brúarjökull glacier, South East Iceland, J. Glaciol., 64, 311–320, https://doi.org/10.1017/jog.2018.22, 2018.

Fiddes, J., Aalstad, K., and Westermann, S.: Hyper-resolution ensemble-based snow reanalysis in mountain regions using clustering, Hydrol. Earth Syst. Sci., 23, 4717–4736, https://doi.org/10.5194/hess-23-4717-2019, 2019.

Fiddes, J., Aalstad, K., and Lehning, M.: TopoCLIM: rapid topography-based downscaling of regional climate model output in complex terrain v1.1, Geosci. Model Dev., 15, 1753–1768, https://doi.org/10.5194/gmd-15-1753-2022, 2022.

Franz, K. J. and Karsten, L. R.: Calibration of a distributed snow model using MODIS snow covered area data, J. Hydrol., 494, 160–175, https://doi.org/10.1016/j.jhydrol.2013.04.026, 2013.

Frei, A., Tedesco, M., Lee, S., Foster, J., Hall, D. K., Kelly, R., and Robinson, D. A.: A review of global satellite-derived snow products, Adv. Space Res., 50, 1007–1029, https://doi.org/10.1016/j.asr.2011.12.021, 2012.

Frei, P., Kotlarski, S., Liniger, M. A., and Schär, C.: Future snowfall in the Alps: projections based on the EURO-CORDEX regional climate models, The Cryosphere, 12, 1–24, https://doi.org/10.5194/tc-12-1-2018, 2018.

Gascoin, S., Dumont, Z. B., Deschamps-Berger, C., Marti, F., Salgues, G., López-Moreno, J. I., Revuelto, J., Michon, T., Schattan, P., and Hagolle, O.: Estimating fractional snow cover in open terrain from Sentinel-2 using the normalized difference snow index, Remote Sens., 12, 2904, https://doi.org/10.3390/RS12182904, 2020.

Geirsdóttir, Á., Miller, G. H., Larsen, D. J., and Ólafsdóttir, S.: Abrupt holocene climate transitions in the northern north atlantic region recorded by synchronized lacustrine records in iceland, Quat. Sci. Rev., 70, 48–62, https://doi.org/10.1016/J.QUASCIREV.2013.03.010, 2013.

Gorelick, N., Hancher, M., Dixon, M., Ilyushchenko, S., Thau, D., and Moore, R.: Google Earth Engine: Planetary-scale geospatial analysis for everyone, Remote Sens. Environ., 202, 18–27, https://doi.org/10.1016/j.rse.2017.06.031, 2016.

Gunnarsson, A., Garðarsson, S. M., and Sveinsson, Ó. G. B.: Icelandic snow cover characteristics derived from a gap-filled MODIS daily snow cover product, Hydrol. Earth Syst. Sci., 23, 3021–3036, https://doi.org/10.5194/hess-23-3021-2019, 2019.

Hall, D. K. and Riggs, G. A.: MODIS/Aqua Snow Cover Daily L3 Global 500m SIN Grid, Version 6, Boulder, Colorado USA, NASA National Snow and Ice Data Center Distributed Active Archive Center [data set], https://doi.org/10.5067/MODIS/MYD10A1.006 (last access: 22 December 2022), 2016a.

Hall, D. K. and Riggs, G. A.: MODIS/Terra Snow Cover Daily L3 Global 500m SIN Grid, Version 6, Boulder, Colorado USA, NASA National Snow and Ice Data Center Distributed Active Archive Center [sata set], https://doi.org/10.5067/MODIS/MOD10A1.006 (last access: 22 December 2022), 2016b.

Hanna, E., Jónsson, T., and Box, J. E.: An analysis of Icelandic climate since the nineteenth century, Int. J. Climatol., 24, 1193–1210, https://doi.org/10.1002/joc.1051, 2004.

Hannesdóttir, H., Sigurðsson, O., Þrastarson, R. H., Guðmundsson, S., Belart, J. M. C., Pálsson, F., Magnússon, E., Víkingsson, S., Kaldal, I., and Jóhannesson, T.: A national glacier inventory and variations in glacier extent in Iceland from the Little Ice Age maximum to 2019, Jökull, 70, 111–118, https://doi.org/10.33799/jokull2020.70.001, 2019.

Hannesdóttir, H., Sigurðsson, O., Þrastarson, R. H., Guðmundsson, S., Belart, J. M. C., Pálsson, F., Magnússon, E., Víkingsson, S., Kaldal, I., and Jóhannesson, T.: A national glacier inventory and variations in glacier extent in Iceland from the Little Ice Age maximum to 2019, Jokull, 2020, 1–34, https://doi.org/10.33799/JOKULL2020.70.001, 2020.

Hanzer, F., Förster, K., Nemec, J., and Strasser, U.: Projected cryospheric and hydrological impacts of 21st century climate change in the Ötztal Alps (Austria) simulated using a physically based approach, Hydrol. Earth Syst. Sci., 22, 1593–1614, https://doi.org/10.5194/hess-22-1593-2018, 2018.

Hauser, S. and Schmitt, A.: Glacier Retreat in Iceland Mapped from Space: Time Series Analysis of Geodata from 1941 to 2018, PFG – J. Photogramm. Remote Sens. Geoinf. Sci. 2021, 1, 1–19, https://doi.org/10.1007/S41064-021-00139-Y, 2021.

Icelandic Meterologocial Office: Reglur um veðurathuganir, skýrslurfærslu og skeytasendingar á skeytastöðvum, Reykjavik, https://www.vedur.is/media/vedurstofan/utgafa/greinargerdir/1995/leidbeiningar_2003_v2.pdf (last access: 22 December 2022), 2008.

Icelandic Meterologocial Office: Gagnabanki Veðurstofu Íslands, afgreiðsla nr. 2021-12-15/01 [data set], Reykjavik, 2021 (can be accessed by direct communication with the IMO).

Johannesson, T., Aðalgeirsdottir, G., Bjornsson, H., Palsson, F., and Sigurdsson, O.: Response of glaciers and glacier runoff in Iceland to climate change, edited by: Jarvet, A., in: Proceedings of the 23rd Nordic Hydrological Conference, 8–12 August 2004, Tallinn, Estonia, 2004.

Johannesson, T., Adalgeirsdottir, G., Bjornsson, H., Crochet, P., Eliasson, B. E., Gudmundsson, S., Jonsdóttir, J. F., Olafsson, H., Palsson, F., Rognvaldss, On, O., Sigurdsson, O., Snorrasson, A., Sveinsson, O. G. B., and Thorsteinsson, T.: Effect of climate change on hydrology and hydro-resoures in Iceland, Reykjavik, Report for the VO project, National Energy Authority, ISBN 978-9979-68-224-0, 2007.

Jónsdóttir, J. F., Uvo, C. B., and Clarke, R. T.: Trend analysis in Icelandic discharge, temperature and precipitation series by parametric methods, Hydrol. Res., 39, 425–436, https://doi.org/10.2166/NH.2008.002, 2008.

Knudsen, K. L., Søndergaard, M. K. B., Eiríksson, J., and Jiang, H.: Holocene thermal maximum off North Iceland: Evidence from benthic and planktonic foraminifera in the 8600–5200 cal year BP time slice, Mar. Micropaleontol., 67, 120–142, https://doi.org/10.1016/J.MARMICRO.2007.11.003, 2008.

Krinner, G., Derksen, C., Essery, R., Flanner, M., Hagemann, S., Clark, M., Hall, A., Rott, H., Brutel-Vuilmet, C., Kim, H., Ménard, C. B., Mudryk, L., Thackeray, C., Wang, L., Arduini, G., Balsamo, G., Bartlett, P., Boike, J., Boone, A., Chéruy, F., Colin, J., Cuntz, M., Dai, Y., Decharme, B., Derry, J., Ducharne, A., Dutra, E., Fang, X., Fierz, C., Ghattas, J., Gusev, Y., Haverd, V., Kontu, A., Lafaysse, M., Law, R., Lawrence, D., Li, W., Marke, T., Marks, D., Ménégoz, M., Nasonova, O., Nitta, T., Niwano, M., Pomeroy, J., Raleigh, M. S., Schaedler, G., Semenov, V., Smirnova, T. G., Stacke, T., Strasser, U., Svenson, S., Turkov, D., Wang, T., Wever, N., Yuan, H., Zhou, W., and Zhu, D.: ESM-SnowMIP: assessing snow models and quantifying snow-related climate feedbacks, Geosci. Model Dev., 11, 5027–5049, https://doi.org/10.5194/gmd-11-5027-2018, 2018.

Langdon, P. G., Caseldine, C. J., Croudace, I. W., Jarvis, S., Wastegård, S., and Crowford, T. C.: A chironomid-based reconstruction of summer temperatures in NW Iceland since AD 1650, Quat. Res., 75, 451–460, https://doi.org/10.1016/J.YQRES.2010.11.007, 2011.

Larsen, D. J., Miller, G. H., Geirsdóttir, Á., and Thordarson, T.: A 3000-year varved record of glacier activity and climate change from the proglacial lake Hvítárvatn, Iceland, Quat. Sci. Rev., 30, 2715–2731, https://doi.org/10.1016/J.QUASCIREV.2011.05.026, 2011.

Magnusson, J., Wever, N., Essery, R., Helbig, N., Winstral, A., and Jonas, T.: Evaluating snow models with varying process representations for hydrological applications, Water Resour. Res., 51, 2707–2723, https://doi.org/10.1002/2014WR016498, 2015.

Massé, G., Rowland, S. J., Sicre, M. A., Jacob, J., Jansen, E., and Belt, S. T.: Abrupt climate changes for Iceland during the last millennium: Evidence from high resolution sea ice reconstructions, Earth Planet. Sci. Lett., 269, 565–569, https://doi.org/10.1016/j.epsl.2008.03.017, 2008.

Matiu, M. and Hanzer, F.: Bias adjustment and downscaling of snow cover fraction projections from regional climate models using remote sensing for the European Alps, Hydrol. Earth Syst. Sci., 26, 3037–3054, https://doi.org/10.5194/hess-26-3037-2022, 2022.

Miller, W. P., Piechota, T. C., Gangopadhyay, S., and Pruitt, T.: Development of streamflow projections under changing climate conditions over Colorado River basin headwaters, Hydrol. Earth Syst. Sci., 15, 2145–2164, https://doi.org/10.5194/hess-15-2145-2011, 2011.

Mizukami, N., and Koren, V.: Methodology and evaluation of melt factor parameterization for distributed SNOW-17, AGU Fall Meeting Abstracts, Vol. 2008, 2008.

National Land Survey of Iceland: IcelandDEM_2016, Akranes, National Land Survey of Iceland [data set], https://www.lmi.is/is/landupplysingar/gagnagrunnar/nidurhal (last access: 22 December 2022), 2016.

Nguyen, H. M., Ouillon, S., and Vu, V. D.: Sea Level Variation and Trend Analysis by Comparing Mann–Kendall Test and Innovative Trend Analysis in Front of the Red River Delta, Vietnam (1961–2020), Water (Switzerland), 14, 1709, https://doi.org/10.3390/W14111709, 2022.

Noël, B., Aðalgeirsdóttir, G., Pálsson, F., Wouters, B., Lhermitte, S., Haacker, J. M., and van den Broeke, M. R.: North Atlantic Cooling is Slowing Down Mass Loss of Icelandic Glaciers, Geophys. Res. Lett., 49, e2021GL095697, https://doi.org/10.1029/2021GL095697, 2022.

Nolin, A. W., Sproles, E. A., Rupp, D. E., Crumley, R. L., Webb, M. J., Palomaki, R. T., and Mar, E.: New snow metrics for a warming world, Hydrol. Process., 35, e14262, https://doi.org/10.1002/HYP.14262, 2021.

Notarnicola, C.: Hotspots of snow cover changes in global mountain regions over 2000–2018, Remote Sens. Environ., 243, 111781, https://doi.org/10.1016/J.RSE.2020.111781, 2020.

Notaro, M., Lorenz, D., Hoving, C., and Schummer, M.: Twenty-first-century projections of snowfall and winter severity across central-eastern North America, J. Clim., 27, 6526–6550, https://doi.org/10.1175/JCLI-D-13-00520.1, 2014.

Ólafsson, H., Furger, M., and Brümmer, B.: The weather and climate of Iceland, Meteorol. Z., 16, 5–8, https://doi.org/10.1127/0941-2948/2007/0185, 2007.

Oliphant, T. E.: Python for scientific computing, Comput. Sci. Eng., 9, 10–20, https://doi.org/10.1109/MCSE.2007.58, 2007.

Painter, T. H., Rittger, K., McKenzie, C., Slaughter, P., Davis, R. E., and Dozier, J.: Retrieval of subpixel snow covered area, grain size, and albedo from MODIS, Remote Sens. Environ., 113, 868–879, https://doi.org/10.1016/j.rse.2009.01.001, 2009.

Robinson, D. A., Dewey, K. F., and Heim, R. R.: Global Snow Cover Monitoring: An Update, Bull. Am. Meteorol. Soc., 74, 1689–1696, https://doi.org/10.1175/1520-0477(1993)074<1689:GSCMAU>2.0.CO;2, 1993.

Rodell, M., Houser, P. R., Jambor, U., Gottschalck, J., Mitchell, K., Meng, C. J., Arsenault, K., Cosgrove, B., Radakovich, J., Bosilovich, M., Entin, J. K., Walker, J. P., Lohmann, D., and Toll, D.: The Global Land Data Assimilation System, Bull. Am. Meteorol. Soc., 85, 381–394, https://doi.org/10.1175/BAMS-85-3-381, 2004.

Salomonson, V. V. and Appel, I.: Development of the aqua MODIS NDSI fractional snow cover algorithm and validation results, IEEE Trans. Geosci. Remote Sens., 44, 1747–1756, https://doi.org/10.1109/TGRS.2006.876029, 2006.

Schmidt, L. S., Aðalgeirsdóttir, G., Pálsson, F., Langen, P. L., Guðmundsson, S., and Björnsson, H.: Dynamic simulations of Vatnajökull ice cap from 1980 to 2300, J. Glaciol., 66, 97–112, https://doi.org/10.1017/jog.2019.90, 2020.

Sicre, M.-A., Hall, I. R., Mignot, J., Khodri, M., Ezat, U., Truong, M.-X., Eiríksson, J., and Knudsen, K.-L.: Sea surface temperature variability in the subpolar Atlantic over the last two millennia, Paleoceanography, 26, PA4218, https://doi.org/10.1029/2011PA002169, 2011.

Smiatek, G., Kunstmann, H., and Senatore, A.: EURO-CORDEX regional climate model analysis for the Greater Alpine Region: Performance and expected future change, J. Geophys. Res.-Atmos., 121, 7710–7728, https://doi.org/10.1002/2015JD024727, 2016.

NASA Earth Exchange Global Daily Downscaled Projections (NEX-GDDP)|CDS: https://cds.nccs.nasa.gov/nex-gddp/, last access: 1 May 2017.

Thrasher, B., Maurer, E. P., McKellar, C., and Duffy, P. B.: Technical Note: Bias correcting climate model simulated daily temperature extremes with quantile mapping, Hydrol. Earth Syst. Sci., 16, 3309–3314, https://doi.org/10.5194/hess-16-3309-2012 (data available at: https://ds.nccs.nasa.gov/thredds/catalog/bypass/NEX-GDDP/catalog.html, last access: 6 December 2022), 2012.

Thrasher, B., Wang, W., Michaelis, A., Melton, F., Lee, T., and Nemani, R.: NASA Global Daily Downscaled Projections, CMIP6, Sci. Data, 9, 1–6, 2022.

Verfaillie, D., Lafaysse, M., Déqué, M., Eckert, N., Lejeune, Y., and Morin, S.: Multi-component ensembles of future meteorological and natural snow conditions for 1500 m altitude in the Chartreuse mountain range, Northern French Alps, The Cryosphere, 12, 1249–1271, https://doi.org/10.5194/tc-12-1249-2018, 2018.

Yilmaz, Y. A., Aalstad, K., and Sen, O. L.: Multiple Remotely Sensed Lines of Evidence for a Depleting Seasonal Snowpack in the Near East, Remote Sens. 2019, 11, 483, https://doi.org/10.3390/RS11050483, 2019.

Appendix D - Projected Changes to Northern Hemisphere Snow Conditions over the period 1950-2100, given two emission scenarios

Remote Sensing Applications: Society and Environment 30 (2023) 100954

Contents lists available at ScienceDirect

Remote Sensing Applications: Society and Environment

journal homepage: www.elsevier.com/locate/rsase

Projected changes to Northern Hemisphere snow conditions over the period 1950–2100, given two emission scenarios

Darri Eythorsson [a, *], Sigurdur M. Gardarsson [a], Bart Nijssen [b]

[a] Faculty of Civil and Environmental Engineering, University of Iceland, Reykjavík, Iceland
[b] Faculty of Civil and Environmental Engineering, University of Washington, Seattle, USA

ABSTRACT

In this study Northern Hemisphere (NH) snow conditions were simulated and analyzed for the period 1950–2100 under two emission scenarios RCP45 and RCP85. Daily snow conditions were simulated using the Snow17 model run on the Google Earth Engine (GEE) parallel cloud computing platform with each of the 21 GCMs in the NASA NEX GDDP dataset. The model was evaluated based on Snow Water Equivalent (SWE) and Snow Cover Area (SCA) data from the GLDAS-2 dataset and SCA remote sensing data from the MODIS/Terra instrument. The results showed that both NH SWE and the number of Snow-Covered Days (SCD) have and will continue to decrease at lower latitudes, whereas in many high latitude regions SWE is expected to increase, even as SCD is decreasing. The average annual NH SCD is expected to decrease by 12.5% and 23.1% between the periods 1950–1975 and 2075–2100, under RCP45 and RCP85, respectively. Between the same periods however, the NH mean winter SWE is expected to increase slightly in the beginning of the period under both RCPs. By 2100, SWE will have reduced to the 1950–1975 level under RCP45. Under RCP85, SWE will be 10% lower than the 1950–1975 level. These changes will pose a great challenge for water resource management across a wide spectrum, including impacting current way of living.

1. Introduction

This study presents an analysis of the evolution of Northern Hemisphere (NH) snow conditions over the period 1950–2100 under two different emission scenarios, RCP45 and RCP85 (Meinshausen et al., 2011). Daily snowpack conditions were simulated across the NH in 0.2-degree horizontal resolution using a conceptual snow model, Snow17 (Anderson, 2006). The model was run using daily average precipitation and temperature data from the NASA-NEX GDDP dataset (Thrasher et al., 2012), which contains the ensemble of downscaled and bias corrected Global Circulation Models (GCMs) from the CMIP5 project (Taylor et al., 2012). The model simulations were evaluated for the historic period using remote sensing data from the MODIS/Terra snow cover product (Hall et al., 2016) and meteorological data from the Global Land Data Assimilation System (GLDAS) (Rodell et al., 2004).

The AR6 report by the Intergovernmental Panel on Climate Change (IPCC) states with very high confidence that the NH spring snow cover has decreased since 1978 and that further decrease of NH seasonal snow extent is virtually certain under all plausible emission scenarios (Fox-Kemper et al., 2021). These changes will have major hydrological, ecological and societal implications in cold regions (e.g. Eliasson et al., 2017; Instanes et al., 2016). Changes to NH snow conditions have been observed in several studies. Yunlong et al. (2018) using MODIS, IMS and AMSR-E data, estimated a decrease in NH snow cover by 5.3 days/decade since 2001. Hori et al. (2017) found an average decrease in Snow Cover Extent of 10 days/decade in large areas of the NH since 1978, using MODIS and AVHRR data. Eythorsson et al. (2019) estimated a decrease in Arctic Snow Cover Frequency (SCF) of 9.1 days/decade since 2001 using MODIS data. Fontrodona Bach et al. (2018) studied in situ snow depth data across Europe and found an average decrease in mean snow depth of 12.2% per decade. Mudryk et al. (2020) estimated a snow mass loss trend in NH of −5 Gt/yr for all months from December to May for the period 1981–2018 based on 6 observational snow products. The range in estimated changes to

* Corresponding author.
E-mail address: dae5@hi.is (D. Eythorsson).

https://doi.org/10.1016/j.rsase.2023.100954
Received 23 December 2022; Received in revised form 6 March 2023; Accepted 8 March 2023
Available online 15 March 2023

NH snow cover illustrate the uncertainty in observing this complex phenomenon using different observational data sources (e.g. Brown and Robinson, 2011). Connolly et al. (2019) showed an observed trend of decreasing snow cover in the NH, which exceeded that predicted by all CMIP5 models over the period 1967–2018.

Under future climate scenarios observed snow trends are expected to continue and even amplify (van Oldenborgh et al., 2013; Vihma et al., 2016). Successful adaptation to a changing hydrological regime in these regions is therefore reliant on skillful predictions of future snow conditions (Scheepers et al., 2018). Wang et al. (2018) compared the snow cover simulations in the NH from the CMIP5 project and the Community Earth System Model (Kay et al., 2015) under different emission scenarios and found that all models predicted a decreasing frequency of snow cover. Brown and Mote (2009) analyzed the sensitivity of snow variables to future climate warming and found that the number of Snow-Covered Days (SCD) was the most sensitive to different levels of warming. Mudryk et al. (2020) analyzed snow projections in the CMIP6 ensemble and showed that NH spring snow extent is on average expected to decrease by 8%/1 °C of global surface air temperature (GSAT) increase relative to the 1995–2014 average.

The goal of this paper was to study spatio-temporal changes to NH snow conditions under different emission scenarios across the hemisphere and in selected study basins. The novelty is that a dedicated and well documented snow model (Snow17) was used to model NH snow conditions based on downscaled and bias corrected temperature and precipitation estimates from the CMIP5 GCM ensemble. GCM snow parameter estimates are known to contain biases due to their relatively simple snow schemes (Matiu and Hanzer, 2022) as well as in their temperature and precipitation estimates which are the key parameters for snow modelling (Jacob et al., 2013). Thus, using Snow17 with downscaled and bias corrected input data will give improved simulations of snow conditions. To illustrate the effect of predicted climatic changes in different regions the results were mapped to selected individual watersheds in the NH as these are the spatial units of concern for water resources management.

2. Methods

2.1. Data

Daily average downscaled and bias corrected precipitation and temperature were calculated from the GLDAS-2 and NASA NEX-GDDP dataset and used to run the Snow17 model. The Bias-Correction Spatial Disaggregation (BCSD) method is used to downscale the input data. It is a statistical downscaling algorithm specifically developed to address the current limitations of global GCM outputs (Maurer and Hidalgo, 2008; Thrasher et al., 2012; Wood et al., 2004). Snow data from the MODIS10A01.V006 and GLDAS-2 datasets were used to evaluate the model results. Permafrost data from the WGS43261 dataset, land cover data from the GLCF dataset, elevation data from the GTOPO30 dataset and various parameters from the GLDAS-2 dataset were used for parameter estimation. The spatial data used in this study were mapped to the model resolution, 0.2°, in GEE using the native ee.Image.reproject() function. Table 1 summarizes the datasets used in the project.

2.2. Data processing

Google Earth Engine (GEE) (Gorelick et al., 2016) was used to access data, perform the model simulations as well as spatio-temporal and statistical analysis of the results. GEE is an emerging platform for large scale analysis of remote sensing and geoinformation and has commonly been applied in hydrological research (e.g. Chen and Zhao, 2022; Liu et al., 2022), including snow cover mapping (Banerjee et al., 2021; Eythorsson et al., 2019; Snapir et al., 2019) and regional snow modelling based on downscaled climate projections (Eythorsson et al., 2022).

Table 1
Datasets used in this study.

Dataset	Description	Variables	Purpose	Reference
MOD10A1 v006	MODIS/Terra snow cover product.	- NDSI_Snow_Cover	Model evaluation	Hall et al. (2016)
GLDAS-2	Global daily hydrometeorological data	- SWE_inst - Tair_f_inst - Rainf_f_tavg - Wind_f_inst - SWdown_f_tavg - tree_canopy_cover - SnowDepth_inst	- Model evaluation - Parameter estimation	Rodell et al. (2004)
NASA NEX-GDDP	Ensemble of 21 daily downscaled and bias corrected GCMs from the CMIP5 project.	- tasmin - tasmax - pr	Model forcing	Thrasher et al. (2006)
GTOPO30	Global Digital Elevation Map (DEM)	- elevation	Parameter estimation	LP-DAAC (2004)
GLCF	Global Land Cover Data	- tree_canopy_cover	Parameter estimation	Sexton et al. (2013)
WGS43261	Arctic permafrost map.	- Permafrost extent	Parameter estimation	Brown et al. (2002)

2.2.1. Snow model

In this study the Snow17 model was used to simulate daily snow conditions in the Northern Hemisphere (NH) for the period 1950–2100 at a 0.2-degree resolution. The model was developed as part of the Unites States National Water Service River Forecast System (US NWSRS) and is used for operational snow forecasting (Anderson, 2006). It is a conceptual snow accumulation and melt model that uses a temperature index approach to simulate the key processes occurring in a body of snow including heat storage, water retention, transmission of liquid water, and snowmelt. The model takes in temperature and precipitation data, simulates a single layer snowpack, and returns its Snow Water Equivalent (SWE) as well as outflow (snowmelt and precipitation runoff). It has been applied to regional studies to evaluate the climate change impact on snow conditions (e.g. Miller et al., 2011; Notaro et al., 2014). Snow17 simulations have been evaluated based on the MODIS snow cover products with good results (Franz and Karsten, 2013).

Snow17 requires several model parameters, which must be specified by the user. In this study, model parameters were determined in a distributed grid at the model resolution based on previously published guidelines for the Snow17 model, thereby accounting for local conditions. The recommendations of the model author (Anderson, 2006; 2006) were followed for most of the parameters. For the melt factors MFMIN and MFMAX, which are the key parameters governing snow melt rates, the methods proposed by Mizukami and Koren (2008) were used as they incorporate information on the local surface energy balance, such as shading, aspect, slope, vegetation cover and average solar irradiance, into the determination of the local melt factor which were determined based on local shading, aspect and slope, estimated from based on the GTOPO-30 digital elevation model as well as local vegetation cover and average solar irradiance estimated based on the GLDAS-2 dataset.

Apart from the melt factors, the parameters with the greatest influence on model performance are the gage under-catch factor *SUCF* and the average wind during rain on snow *UADJ*. The *SUCF* corrects the amount of new snow recorded for each time step to account for gage catch deficiency, blowing snow across areal divides and sublimation. The forcing datasets that were used in this project have been corrected for gage catch deficiencies (Rodell et al., 2004; Sheffield et al., 2006). When simulation across long time periods and large areas with multiple snow fall events, gage catch deficiencies can be assumed to cancel out (Anderson, 2006). *UADJ* describes the average wind function during rain on snow events and is used in the model to estimate the sensible and latent heat transfer components of the snowpack *SEB*. *UADJ* was estimated as the average wind speed from the GLDAS-2 wind field for the period 1950–1999. Of the minor parameters *PXTEMP* determines the ratio of rain versus snow in precipitation. *MBASE* describes the temperature at which melt occurs, set as 0 °C globally in this study. *NMF* is the negative melt factor which determines the energy exchange at the snow-air boundary when melt is not occurring. It has the same seasonal variation as the melt factors and is estimated based on average snow density. *TIPM* is the antecedent temperature index which describes snowpack temperatures near the surface and is estimated based on average snow depths. *PLWHC* describes the physical liquid water holding capacity of the snow and was estimated based on average snow depths. *DAYGM* is the constant basal melt rate occurring at the snow/ground boundary and was estimated based on permafrost extent data.

The Snow17 parameters were estimated based on environmental data, including data on SWE, precipitation rates, surface air temperatures and near surface wind velocity, land cover classification and solar radiation from the GLDAS-2 dataset, topographical data from the GTOPO-30 digital elevation model and permafrost extent from the Arctic Permafrost Map (WGS43261). Table 2 presents a summary of the Snow17 parameters, their description, ranges, values, and source methodologies.

2.2.2. Model evaluation

The model was evaluated based on historical Snow Water Equivalent (SWE) and Snow Cover Area (SCA) data for the 2004 water year. The evaluation simulation was performed using temperature and precipitation inputs from the GLDAS-2 dataset. The model simulations were compared to a) SWE and SCA data from the GLDAS-2 dataset and b) SCA data from MODIS/TERRA snow cover dataset (MOD10A1.v006). The simulations were evaluated based on the 2004 water year as it had average SWE and SCA conditions across the NH within that period of overlap between the input and evaluation data.

The model performance was evaluated by calculating the ratio between root mean square error and the standard deviation (RSR) of daily SCA estimates across the NH. RSR is a recommended evaluation metrics for hydrologically relevant processes (e.g. Sthapit et al., 2022) and simulations are generally considered satisfactory if RSR <0.7 (Moriasi et al., 2007). The average spatial correlation between the modelled and observed SWE and SCA was also calculated across the NH over the study period as the Pearson's Correlation coefficient, R.

Table 2
Snow17 parameters, description, value ranges and estimation methodology.

Parameter	Description	Range	Units	Methodology
SUCF	Gage under-catch factor	1.0	–	Anderson (2006)
MFMAX	Maximum Melt Factor	0.7–2.4	mm/°C*6h	Mizukami & Koren (2008)
MFMIN	Minimum Melt Factor	0.001–1.5	mm/°C*6h	Mizukami & Koren (2008)
UADJ	Average wind during rain on snow	0.02–0.4	mm/mb	Anderson (2006)
PXTEMP	Temperature determining rain/snow	−1–3	°C	Anderson (2006)
MBASE	Base temp. where melt occurs	0	°C	Anderson (2006)
NMF	Maximum negative melt factor	0.05–0.3	mm/°C*6h	Anderson (2006)
TIPM	Antecedent temperature index	0.05–0.2	–	Anderson (2006)
PLWHC	Liquid water holding capacity	0.02–0.3	%	Anderson (2006)
DAYGM	Constant basal melt rate	0–0.3	mm/day	Anderson (2006)

2.2.3. Snow projections

The Snow17 model was run with each of the 21 downscaled and bias corrected GCM's in the NASA-NEX GDDP dataset using daily precipitation and temperature data for the period 1950–2100. The model was initialized at the beginning of each water year so that it would not store water between years. The annual number of snow-covered days was calculated for each water year in the study period by calculating the number of days where SWE >0 between October 1st and September 31st annually. The yearly mean winter SWE was estimated by calculating the mean simulated SWE between the dates December 22nd and March 20th for each water year in the study period. The relative changes in the annual mean winter SWE and SCD between 1950-1975 and 2075–2100 were calculated for both RCP45 and RCP85. The average annual 1st April SWE was calculated across the NH. Lastly, the relative changes in SWE and SCD were analyzed in a selection of large snow impacted watersheds across the NH with different hydrological characteristics, shown in Fig. 1.

3. Results and discussion

3.1. Model evaluation

The model simulations were evaluated based on Snow Cover Area (SCA) and Snow Water Equivalent (SWE) data for the 2004 water year. The model was run with input data from the GLDAS-2 dataset. Simulated SWE values were compared to GLDAS-2 SWE data and simulated SCA was compared to SCA estimated from both MODIS/TERRA data and GLDAS-2.

Table 3 shows the average spatial correlation coefficient between the daily modelled and observed SWE and SCA across the NH for the 2004 water year. The upper number in shows the average Pearson's correlation, R, and the lower number within parenthesis the associated two-sided p-value.

The results shown in Table 3 suggest that there is a high correlation between the simulated and observational SCA and SWE estimates. It is notable that both correlation estimates for SCA were higher than the correlation between MODIS and the GLDAS2 snow field ($R = 0.7$, $p = 0.028$). The RSR between the daily SCA simulations MODIS observations was 0.13 and 0.39 between the simulations and the GLDAS-2 snow observations. For comparison the RSR between the two observational datasets was 0.34. The model evaluation showed that the model produced satisfactory simulations of SCA in the NH comparable to both observational datasets. The model results showed a high correlation to both SWE and SCA observations comparable to the correlation of the observational datasets to each other. This suggests that the model satisfactorily simulates large scale SCA and SWE conditions in the NH and is thus expected to provide a reasonable estimate of future snow conditions within that domain when forced with downscaled and bias corrected climate projections.

3.2. Snow projections

The average annual SCD and mean winter SWE were calculated for the first and last quarter centuries of the dataset, that is, the 3rd quarter of the 20th century 1950–1975; and the 4th quarter of the 21st century 2075–2100, respectively.

Fig. 2 shows i) the mean SCD for 1950–1975; ii) the percentage change in SCD between 2075-2100 and 1950–1975 under RCP45; and iii) same as ii) but for RCP85. The results show that SCF in the NH is expected to decrease during the present century in almost all regions, under both emission scenarios. The only areas that show an increasing SCD are on the border of the Tibetan Plateau and

Fig. 1. River basins in the Northern Hemisphere for which changes in SCD and SWE were analyzed.

Table 3
Average spatial correlation coefficient, R, between the modelled and observed SWE and SCA across the NH for the 2004 water year. The lower number within parenthesis the associated two-sided p-value.

Observation data	Parameter	R (p)
GLDAS-2	SWE	0.77 (0.008)
GLDAS-2	SCA	0.77 (0.002)
MODIS	SCA	0.81 (0.027)

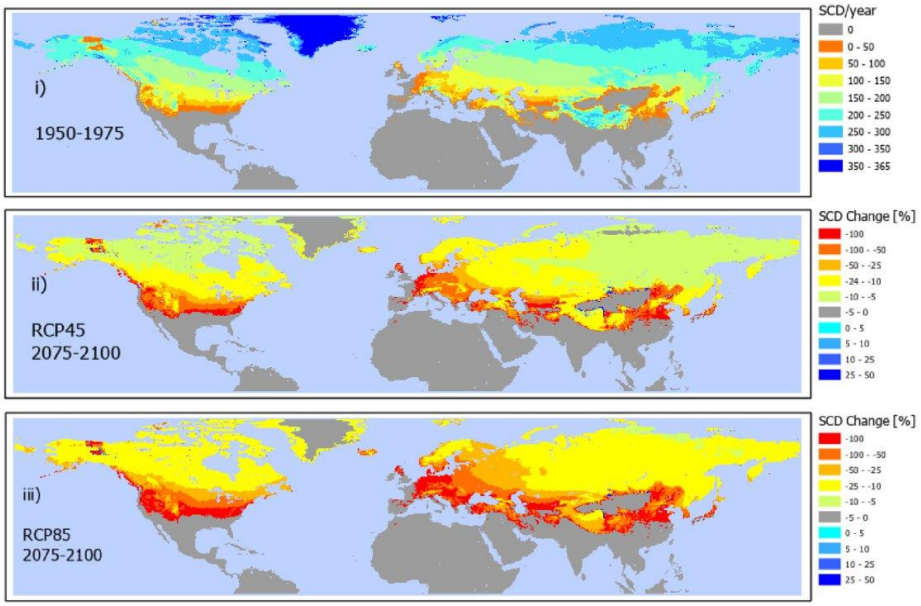

Fig. 2. i) Mean number of Snow-Covered Days (SCD) for the period 1950–1975, ii) percentage change in SCD between 2075-2100 and 1950–1975 under RCP45 and iii) same as ii) but for RCP85.

the Gobi Desert. Snow cover is expected to disappear almost completely in many mid-latitude areas at the periphery of the current seasonal snow extent. Large regions in Central Europe, Northern Middle East, Northern China as well as in the Northern part of the conterminous USA are expected to be mostly snow free throughout the year by the end of the present century. This pattern of decreasing SCD globally which is readily observable under both emission scenarios is more pronounced under RCP85 than RCP45.

Fig. 3 shows i) the mean winter (SWE) for 1950–1975; ii) the percentage change in SWE between 2075-2100 and 1950–1975 under RCP45; and iii) same as ii) but for RCP85. The results show that the mean winter SWE is expected to decrease in mid latitude areas of the NH during the 21st century. At higher latitudes however, mean winter SWE is expected to increase, in some cases by more than 100%. The biggest relative increase in mean winter SWE is expected to occur in the high Arctic areas around the Bering strait, eastern Siberia and the north-western coast of North America as well as in the southwestern Tibetan Plateau. These patterns of increasing SWE at high latitudes are due to increasing winter precipitation that stems from an intensification of the hydrological cycle as air temperatures rise and surrounding sea ice decreases (Maslanik et al., 2011). These patterns are readily observable under both emission scenarios but more pronounced under RCP85 than RCP45.

Fig. 4 shows the NH annual SCD (left) and mean winter SWE (right) as compared to a 1950 baseline. The results show SCD is expected to decrease linearly throughout the 21st century under RCP85 but would stabilize at about 85% of 1950 levels by 2100 under RCP45. The NH mean winter SWE is expected to increase under both emission scenarios. Given the RCP85 scenario NH mean winter SWE is expected to peak around mid-21st century and then start to decline, whereas under RCP45 NH mean winter SWE is expected to increase throughout the century to more than 4% above 1950 levels.

Fig. 4 shows that the frequency of snow cover is expected to decrease significantly throughout the 21st century given both emission scenarios. The results shown in Fig. 2 shows that most of this decrease will occur at lower latitudes where the winter snow season will shorten. The results in Fig. 4 show that this decrease in SCD is already underway, which is in an agreement with several earlier studies which have found decreasing snow cover in the NH in recent decades (Connolly et al., 2019; Eythorsson et al., 2019; Mudryk et al., 2020; Yunlong et al., 2018)

Fig. 4 also shows that the NH mean winter SWE is expected to increase slightly in the beginning of the period and decline after about 2020 down to 1950–1975 levels by 2100 under rcp45 but about 10% under the 1950–1975 average under rcp85. Fig. 3 shows increasing SWE in the Arctic, whereas at lower latitudes, SWE is decreasing, suggesting that total snow storage in the NH may remain at present levels despite decreasing SCF. This increase in Arctic SWE is consistent with prior findings (e.g. Kopec et al., 2016; Singarayer et al., 2006) and can be attributed to increasing precipitation, which in turn stems from decreasing sea-ice concentrations in the Arctic Ocean, which brings more atmospheric moisture to these areas. The results show that SWE is expected to increase throughout the 21st century under RCP45, whereas under RCP85 the NH mean winter SWE is expected to peak in the second half of the century, as the declining snowpack at lower latitudes overtakes the increasing arctic SWE. This pattern of decreasing SWE at lower latitudes and increasing SWE in the Arctic are consistent with prior studies (e.g. Wang et al., 2018).

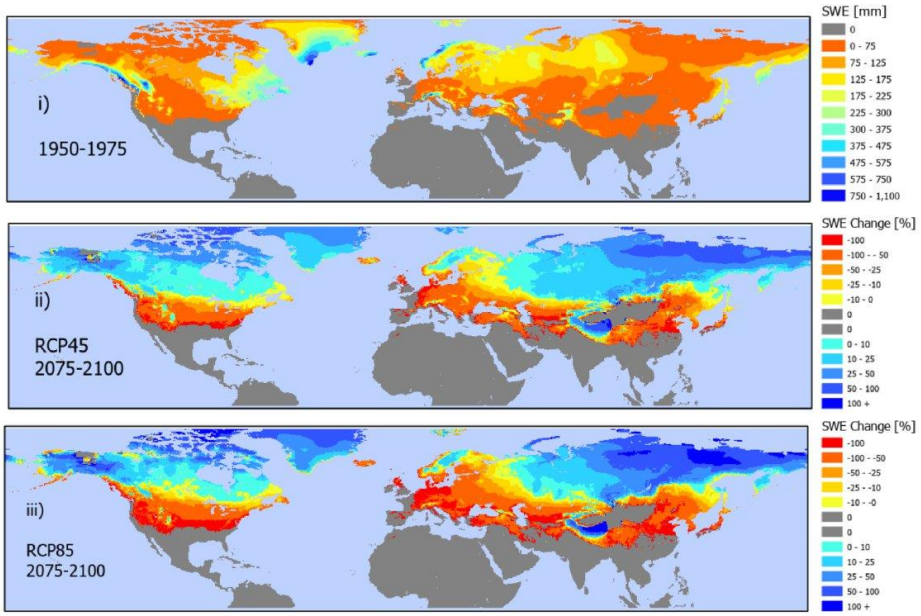

Fig. 3. Mean winter Snow Water Equivalent (SWE) for the period 1950–1975, ii) percentage change in SWE between 2075-2100 and 1950–1975 under RCP45 and iii) same as ii) but for RCP85.

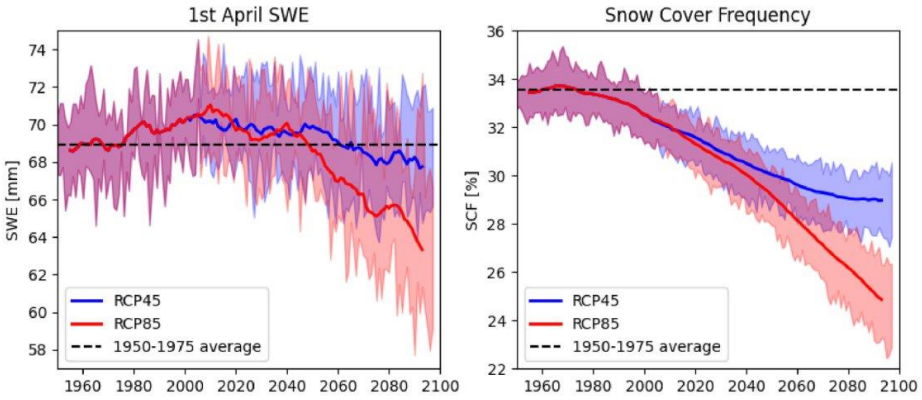

Fig. 4. Annual Snow Cover Frequency (SCF) (right) and 1st of April Snow Water Equivalent (SWE) across the NH (right). The shaded areas represent the upper and lower quantiles of the ensemble simulations, and the solid line a 10-year moving average.

Table 4 shows the relative change in SWE and SCD between 1950-1975 and 2075–2100 in the study basins. Basins where mean winter SWE is expected to increase by more than 10% under RCP45 are colored blue, likewise the basins where mean winter SWE is expected to decrease by more than 10% are colored red, basins where mean winter SWE is expected to change by less than 10% are colored grey. Based on the UN-adjusted population count, 30.1% of the NH population lives within the boundaries of these watersheds (CIESIN, 2018).

Fig. 5 shows the study basins, blue basins showed more than 10% increase in SWE, red basins showed more than 10% decrease in SWE while grey basins showed less than 10% change in SWE, under RCP45. The results show that all study basins discharging into the Arctic Ocean are expected to experience a more than 10% increase in mean winter SWE whereas at lower latitude basins SWE are mostly expected to decrease. Table 4 shows that this decrease is most pronounced in mid-latitude rivers of central Europe (Elbe, Oder, Rhone, Vistula, Danube and Dnieper) and North America (Mississippi, Columbia, and Colorado). Basins in the Himalaya region are expected to experience both decreasing SCD and SWE, although, not as pronounced.

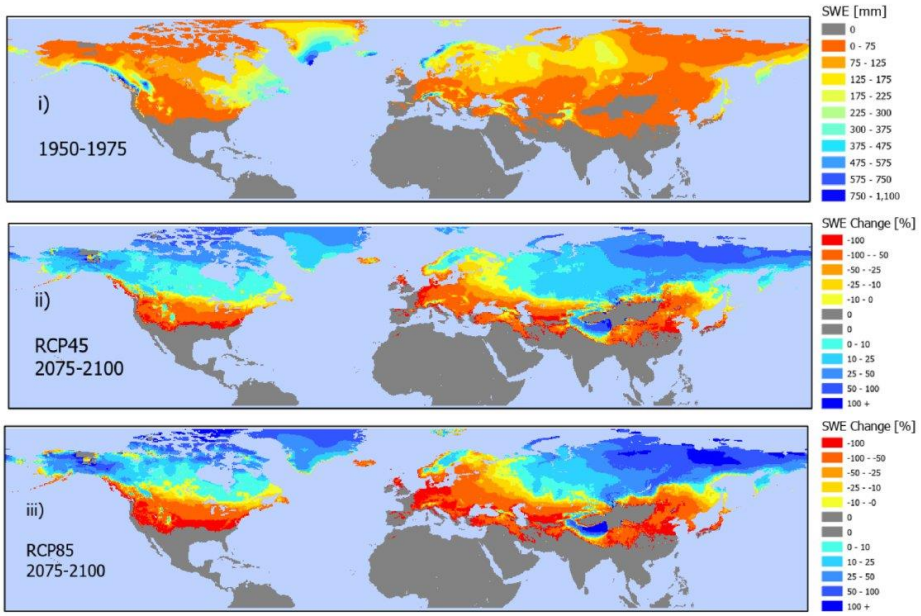

Fig. 3. Mean winter Snow Water Equivalent (SWE) for the period 1950–1975, ii) percentage change in SWE between 2075-2100 and 1950–1975 under RCP45 and iii) same as ii) but for RCP85.

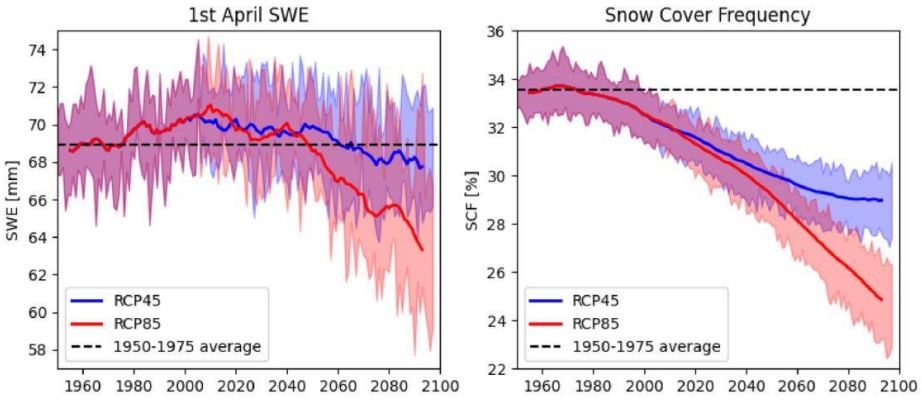

Fig. 4. Annual Snow Cover Frequency (SCF) (right) and 1st of April Snow Water Equivalent (SWE) across the NH (right). The shaded areas represent the upper and lower quantiles of the ensemble simulations, and the solid line a 10-year moving average.

Table 4 shows the relative change in SWE and SCD between 1950-1975 and 2075–2100 in the study basins. Basins where mean winter SWE is expected to increase by more than 10% under RCP45 are colored blue, likewise the basins where mean winter SWE is expected to decrease by more than 10% are colored red, basins where mean winter SWE is expected to change by less than 10% are colored grey. Based on the UN-adjusted population count, 30.1% of the NH population lives within the boundaries of these watersheds (CIESIN, 2018).

Fig. 5 shows the study basins, blue basins showed more than 10% increase in SWE, red basins showed more than 10% decrease in SWE while grey basins showed less than 10% change in SWE, under RCP45. The results show that all study basins discharging into the Arctic Ocean are expected to experience a more than 10% increase in mean winter SWE whereas at lower latitude basins SWE are mostly expected to decrease. Table 4 shows that this decrease is most pronounced in mid-latitude rivers of central Europe (Elbe, Oder, Rhone, Vistula, Danube and Dnieper) and North America (Mississippi, Columbia, and Colorado). Basins in the Himalaya region are expected to experience both decreasing SCD and SWE, although, not as pronounced.

Table 4
Relative change in SWE and SCD (in %) between 1950-1975 and 2075–2100 in the study basins. Basins colored blue have more than 10% increase in mean winter SWE over the period, red colored basins showed more than 10% decrease in SWE and grey colored basins had less than 10% change in SWE, under the RCP45 emission scenario.

Basin	*Latitude*	*RCP45*		*RCP85*	
		Δ SWE [%]	*Δ SCD [%]*	*Δ SWE [%]*	*Δ SCD [%]*
Indigirka	High	56.7	−6.4	97.3	−10.9
Kolyma	High	46.5	−6.5	74.1	−11.4
Lena	High	31.8	−7.2	52.5	−12.5
Yukon	High	33.4	−14.0	48.4	−20.9
Ob	High	28.4	−9.2	18.7	−19.2
Yenisey	High	26.4	−7.8	42.0	−14.7
Mackenzie	High	12.3	−9.0	14.3	−16.2
Volga	Mid	2.5	−15.9	−9.8	−30.2
Dalälven	Mid	−3.9	−15.6	−22.6	−33.4
Fraser	Mid	−4.9	−20.2	−29.1	−36.6
Saskatchewan-Nelson	Mid	0.5	−12.9	−12.6	−23.6
Indus	Low	−4.0	−14.6	−7.1	−23.1
Mekong	Low	−8.0	−5.0	−11.8	−9.5
Ganges-Brahmaputra	Low	−15.7	−12.9	−20.8	−18.7
St. Lawrence	Mid	−19.8	−20.9	−44.0	−43.7
Amur	Mid	−25.8	−20.0	−42.9	−26.4
Don	Mid	−24.1	−21.7	−61.6	−48.1
Dnieper	Mid	−34.7	−25.9	−84.0	−68.5
Yangtze	Low	−27.0	−21.3	−31.4	−26.3
Seine	Low	−46.8	−45.8	−46.9	−45.9
Colorado	Low	−43.0	−40.7	−53.2	−51.3
Columbia	Low	−55.9	−53.5	−73.2	−72.4
Mississippi	Low	−58.4	−48.7	−73.4	−66.4
Rhone	Low	−76.8	−70.6	−81.4	−76.9
Danube	Low	−78.8	−67.5	−92.8	−89.0
Rhine	Mid	−94.3	−91.2	−97.5	−97.0
Vistula	Mid	−81.3	−58.7	−99.0	−96.2
Oder	Mid	−95.9	−90.9	−99.5	−99.0
Elbe	Low	−92.0	−81.6	−99.8	−99.0

Fig. 5. Changes to mean winter SWE in the study basins. Blue basins showed more than 10% increase in SWE, red basins showed more than 10% decrease in SWE while grey basins showed less than 10% change in SWE, under the RCP45 emission scenario. (For interpretation of the references to color in this figure legend, the reader is referred to the Web version of this article.)

The results in Table 4 show that the SCD is expected to decrease in all the study basins, under both emission scenarios. The decrease is greater under the RCP85 scenario than under RCP45, with some basins expected to experience an almost complete loss of snow cover. Fig. 5 shows that despite decreasing SCD the mean winter SWE is expected to increase in all the northernmost basins. The results presented in Table 4 and Fig. 5 show that in general lower latitude basins are expected to experience a more pronounced decrease in snow cover and snow water equivalent magnitude whereas higher latitude basins are expected to see less decrease in snow cover and all high latitude basins are expected to experience an increase in snow water equivalent. Fig. 5 shows that although projected changes in snow conditions in general correlate with latitude, other factors such as elevation, local climatology and topography

influence how snow conditions are expected to change over the course of the study period, as e.g., illustrated by the Himalayan basins, Indus and Mekong, which are forecast to see less change to snow conditions despite their low latitude.

The declining snow pack conditions in the basins of the continental subarctic have been well documented, both in North America (e.g. Kang et al., 2016; Mote et al., 2005) and Europe (e.g. Fontrodona Bach et al., 2018). Both SWE and SCD have decreased across the conterminous United States over the period 1982–2016 (Zeng et al., 2018), which is consistent with the results of this study. Decreasing snow cover, snow storage and snow melt runoff in the Himalaya region has been documented e.g. by Maurer et al. (2019) and Stigter et al. (2017), which are consistent with the findings of the present study. In the Arctic region, the results of this study are consistent with prior studies which have found increasing snow cover (e.g. Cohen et al., 2012; Eythorsson et al., 2019) and snow storage (Callaghan et al., 2011) in recent decades. Vaganov et al. (1999) showed that increasing snowfall in Northern Eurasia has been shown to have decreased the length of the regional growing season. The results presented in this study show that the trend of declining snowpack at lower latitudes and increasing SWE in large high latitude areas in the Arctic is expected continue at a steady or increasing pace, at least for the next few decades.

4. Conclusion

This study presents an analysis of simulated snow conditions across the Northern Hemisphere (NH) for the period 1950–2100 given the RCP45 and RCP85 emission scenarios. The model parameters were determined at the model resolution based on best practices given long term local environmental conditions. The model performance showed high correlations between simulations and two observational datasets. In this study simulations are based on downscaled environmental input data, thereby projecting future snow conditions at a finer spatial resolution than in the CMIP5 models. Modelling at a finer spatial resolution better accounts for local environmental conditions thus making the projections more relevant for local and regional water resources management. Here, future snow conditions are simulated using a well-documented snow model based on bias-corrected GCM temperature and precipitation projections, whose bias in GCM projections have been documented (e.g. Jacob et al., 2013), thereby providing less distorted projections of future snow conditions than GCMs, which have been shown to contain bias in snow projections specifically due to relatively simple snow schemes (Matiu and Hanzer, 2022).

The results presented in this study are agree with the conclusion of the recently published AR6 report by the IPCC that show a decreasing frequency of snow cover in the NH. The results are also in line with previous studies which have shown increasing snow cover and snow volume at high latitudes in the Arctic. The snow simulations presented in this study project that these trends will continue at least for the next few decades. Under RCP45 NH snow cover is expected to stabilize at around 85% of 1950–1975 levels in the second half of the 21st century while under RCP NH snow cover will decrease at an accelerating pace until at least 2100.

The amount of water stored as snow in the winter season will generally decrease at lower latitudes and at lower elevations whereas it is expected to increase in the Arctic. As an example, under RCP85 the mean winter SWE is expected to decrease by up to 99% in the Vistula, Oder, and Elbe River basins and increase up to 97% in the Indigirka River basin. Basins with sources in highly elevated basins such as the Indus, Ganges-Brahmaputra and Mekong are expected to experience considerably less changes to snow conditions than other, low latitude basins.

Between the periods 1950–1975 and 2075–2100 the NH SCD is expected to decrease by 12.5% and 23.1% under the RCP45 and RCP85, respectively, whereas the 1st of April SWE in the NH expected to increase slightly in the beginning of the period and then decline back to 1950 levels under rcp45 and to about 10% under 1950–1975 levels by 2100. These changes will pose a great challenge for water resource management across a wide spectrum, including impacting current way of living, as is for example already evident in the Colorado river basin (Lukas and Payton, 2020).

Ethical statement

1) This material is the authors' own original work, which has not been previously published elsewhere. 2) The paper is not currently being considered for publication elsewhere. 3) The paper reflects the authors' own research and analysis in a truthful and complete manner.

Author contribution

DE/SMG/BN designed the experiments. DE developed the data code, performed the analysis, and prepared the manuscript. BN and SMG reviewed the results and the manuscript and provided significant consultations and contributions throughout the work.

Code/data availability

All data used in this study are freely available. The code for the snow model and/or the analysis can be made available upon request.

Declaration of competing interest

The authors declare that they have no known competing financial interests or personal relationships that could have appeared to influence the work reported in this paper.

Data availability

Data will be made available on request.

References

Anderson, E., 2006. Snow accumulation and ablation model–SNOW-17. In: Office of Hydrologic Development. National Weather Service. https://doi.org/10.1038/177563a0.

Banerjee, A., Chen, R., Meadows, M.E., Sengupta, D., Pathak, S., Xia, Z., Mal, S., 2021. Tracking 21st century climate dynamics of the Third Pole: an analysis of topo-climate impacts on snow cover in the central Himalaya using Google Earth Engine. Int. J. Appl. Earth Obs. Geoinf. 103, 102490. https://doi.org/10.1016/J.JAG.2021.102490.

Brown, J., Ferrians, O., Higginbottom, J.A., Melnikov, E., 2002. Circum-arctic map of permafrost and ground-ice conditions. *Version 2.* Retrieved from. https://nsidc.org/data/ggd318#.

Brown, R.D., Robinson, D.A., 2011. Northern Hemisphere spring snow cover variability and change over 1922-2010 including an assessment of uncertainty. Cryosphere. https://doi.org/10.5194/tc-5-219-2011.

Brown, Ross D., Mote, P.W., 2009. The response of Northern Hemisphere snow cover to a changing climate. J. Clim. 22 (8), 2124–2145. https://doi.org/10.1175/2008JCLI2665.1.

Callaghan, T.V., Johansson, M., Brown, R.D., Groisman, P.Y., Labba, N., Radionov, V., et al., 2011. Multiple effects of changes in arctic snow cover. Ambio 40 (Suppl. 1), 32–45. https://doi.org/10.1007/s13280-011-0213-x.

Center for International Earth Science Information Network - CIESIN - Columbia University, 2018. Gridded Population of the World, Version 4 (GPWv4): Population Count Adjusted to Match 2015 Revision of UN WPP Country Totals.

Chen, Z., Zhao, S., 2022. Automatic monitoring of surface water dynamics using Sentinel-1 and Sentinel-2 data with Google Earth Engine. Int. J. Appl. Earth Obs. Geoinf. 113, 103010. https://doi.org/10.1016/J.JAG.2022.103010.

Cohen, J.L., Furtado, J.C., Barlow, M.A., Alexeev, V.A., Cherry, J.E., 2012. Arctic warming, increasing snow cover and widespread boreal winter cooling. Environ. Res. Lett. https://doi.org/10.1088/1748-9326/7/1/014007.

Connolly, R., Connolly, M., Soon, W., Legates, D.R., Cionco, R.G., Herrera, V.M.V., 2019. Northern hemisphere snow-cover trends (1967–2018): a comparison between climate models and observations. Geosciences 9 (3), 135. https://doi.org/10.3390/geosciences9030135.

Eliasson, K., Ulfarsson, G.F., Valsson, T., Gardarsson, S.M., 2017. Identification of development areas in a warming Arctic with respect to natural resources, transportation, protected areas, and geography. Futures 85, 14–29. https://doi.org/10.1016/j.futures.2016.11.005.

Eythorsson, D., Gardarsson, S.M., Ahmad, S.K., Hossain, F., Nijssen, B., 2019. Arctic climate and snow cover trends - comparing Global Circulation Models with remote sensing observations. Int. J. Appl. Earth Obs. Geoinf. 80, 71–81. https://doi.org/10.1016/j.jag.2019.04.003.

Eythorsson, D., Gardarsson, S.M., Gunnarsson, A., Sveinsson, O.G.B., 2022. Observed and predicted trends in Icelandic snow conditions for the period 1930–2100. EGUsphere 1–14.

Fontrodona Bach, A., van der Schrier, G., Melsen, L.A., Klein Tank, A.M.G., Teuling, A.J., 2018. Widespread and accelerated decrease of observed mean and extreme snow depth over Europe. Geophys. Res. Lett. https://doi.org/10.1029/2018GL079799.

Fox-Kemper, B., Hewitt, H.T., Xiao, C., Aðalgeirsdóttir, G., Drijfhout, S.S., Edwards, T.L., Yu, Y., 2021. Ocean, cryosphere and sea level change. In: Masson-Delmotte, V., Zhai, P., Pirani, A., Connors, S.L., Péan, C., Berger, S., Zhou, B. (Eds.), Climate Change 2021: the Physical Science Basis. Contribution of Working Group I to the Sixth Assessment Report of the Intergovernmental Panel on Climate Change. p. 271. Retrieved from. https://www.ipcc.ch/report/ar6/wg1/#FullReport.

Franz, K.J., Karsten, L.R., 2013. Calibration of a distributed snow model using MODIS snow covered area data. J. Hydrol. https://doi.org/10.1016/j.jhydrol.2013.04.026.

Gorelick, N., Hancher, M., Dixon, M., Ilyushchenko, S., Thau, D., Moore, R., 2016. Google earth engine: planetary-scale geospatial analysis for everyone. Remote Sense Environ. https://doi.org/10.1016/j.rse.2017.06.031.

Hall, D.K., Salomonson, V.V., Riggs, G.A., 2016. MODIS/Terra Snow Cover Daily L3 Global 500m Grid. NASA National Snow and Ice Data Center Distributed Active Archive Center, Boulder, Colorado USA. Version 6.

Hori, M., Sugiura, K., Kobayashi, K., Aoki, T., Tanikawa, T., Kuchiki, K., et al., 2017. A 38-year (1978–2015) Northern Hemisphere daily snow cover extent product derived using consistent objective criteria from satellite-borne optical sensors. Remote Sense Environ. 191, 402–418. https://doi.org/10.1016/j.rse.2017.01.023.

Instanes, A., Kokorev, V., Janowicz, R., Bruland, O., Sand, K., Prowse, T., 2016. Changes to freshwater systems affecting Arctic infrastructure and natural resources. J. Geophys. Res.: Biogeosciences. https://doi.org/10.1002/2015JG003125.

Jacob, D., Petersen, J., Eggert, B., Alias, A., Christensen, O.B., Bouwer, L.M., Yiou, P., 2013. EURO-CORDEX: new high-resolution climate change projections for European impact research. Reg. Environ. Change 14 (2), 563–578. https://doi.org/10.1007/S10113-013-0499-2. 2013 14:2.

Kang, D.H., Gao, H., Shi, X., Islam, S.U., Déry, S.J., 2016. Impacts of a rapidly declining mountain snowpack on streamflow timing in Canada's fraser river basin. Sci. Rep. https://doi.org/10.1038/srep19299.

Kay, J.E., Deser, C., Phillips, A., Mai, A., Hannay, C., Strand, G., et al., 2015. The community earth system model (CESM) large ensemble project : a community resource for studying climate change in the presence of internal climate variability. Bull. Am. Meteorol. Soc. https://doi.org/10.1175/BAMS-D-13-00255.1.

Kopec, B.G., Feng, X., Michel, F.A., Posmentier, E.S., 2016. Influence of sea ice on Arctic precipitation. Proc. Natl. Acad. Sci. USA 113 (1), 46–51. https://doi.org/10.1073/pnas.1504633113.

Liu, Y., Zhang, H., Zhang, M., Cui, Z., Lei, K., Zhang, J., et al., 2022. Vietnam wetland cover map: using hydro-periods Sentinel-2 images and Google Earth Engine to explore the mapping method of tropical wetland. Int. J. Appl. Earth Obs. Geoinf. 115, 103122. https://doi.org/10.1016/J.JAG.2022.103122.

Lp-DAAC, 2004. Global 30 Arc-Second Elevation Data Set GTOPO30.

Lukas, J.J., Payton, E.A., 2020. Colorado River Basin Climate and Hydrology: State of the Science. Western Water Assessment, University of Colorado Boulder, Cooperative.

Maslanik, J., Stroeve, J., Fowler, C., Emery, W., 2011. Distribution and trends in Arctic sea ice age through spring 2011. Geophys. Res. Lett. https://doi.org/10.1029/2011GL047735.

Matiu, M., Hanzer, F., 2022. Bias adjustment and downscaling of snow cover fraction projections from regional climate models using remote sensing for the European Alps. Hydrol. Earth Syst. Sci. 26 (12), 3037–3054. https://doi.org/10.5194/HESS-26-3037-2022.

Maurer, E.P., Hidalgo, H.G., 2008. Utility of daily vs. monthly large-scale climate data: an intercomparison of two statistical downscaling methods. Hydrol. Earth Syst. Sci. 12 (2), 551–563. https://doi.org/10.5194/HESS-12-551-2008.

Maurer, J.M., Schaefer, J.M., Rupper, S., Corley, A., 2019. Acceleration of ice loss across the Himalayas over the past 40 years. Sci. Adv. https://doi.org/10.1126/sciadv.aav7266.

Meinshausen, M., Smith, S.J., Calvin, K., Daniel, J.S., Kainuma, M.L.T., Lamarque, J., et al., 2011. The RCP greenhouse gas concentrations and their extensions from 1765 to 2300. Climatic Change. https://doi.org/10.1007/s10584-011-0156-z.

Miller, W.P., Piechota, T.C., Gangopadhyay, S., Pruitt, T., 2011. Development of streamflow projections under changing climate conditions over Colorado River basin headwaters. Hydrol. Earth Syst. Sci. https://doi.org/10.5194/hess-15-2145-2011.

Mizukami, N., Koren, V., 2008. Methodology and Evaluation of Melt Factor Parameterization for Distributed SNOW- 17. *Abstract Id. H31J-08.* American Geophysical Union. Fall Meeting 2008.

Moriasi, D.N., Arnold, J.G., Van Liew, M.W., Binger, R.L., Harmel, R.D., Veith, T.L., 2007. Model evaluation guidelines for systematic quantification of accuracy in watershed simulations. Trans. ASABE 50 (3), 885–900. https://doi.org/10.13031/2013.23153.

Mote, P.W., Hamlet, A.F., Clark, M.P., Lettenmaier, D.P., 2005. Declining mountain snowpack in western north America. Bull. Am. Meteorol. Soc. https://doi.org/10.1175/BAMS-86-1-39.

Mudryk, L., Santolaria-Otín, M., Krinner, G., Ménégoz, M., Derksen, C., Brutel-Vuilmet, C., et al., 2020. Historical Northern Hemisphere snow cover trends and

projected changes in the CMIP6 multi-model ensemble. Cryosphere 14 (7), 2495–2514. https://doi.org/10.5194/TC-14-2495-2020.
Notaro, M., Lorenz, D., Hoving, C., Schummer, M., 2014. Twenty-first-century projections of snowfall and winter severity across central-eastern North America. J. Clim. https://doi.org/10.1175/JCLI-D-13-00520.1.
Rodell, M., Houser, P.R., Jambor, U., Gottschalck, J., Mitchell, K., Meng, C.J., Toll, D., 2004. The global land data assimilation system. Bull. Am. Meteorol. Soc. https://doi.org/10.1175/BAMS-85-3-381.
Scheepers, H., Wang, J., Gan, T.Y., Kuo, C.C., 2018. The impact of climate change on inland waterway transport: effects of low water levels on the Mackenzie River. J. Hydrol. https://doi.org/10.1016/j.jhydrol.2018.08.059.
Sexton, J.O., Song, X.P., Feng, M., Noojipady, P., Anand, A., Huang, C., et al., 2013. Global, 30-m resolution continuous fields of tree cover: landsat-based rescaling of MODIS vegetation continuous fields with lidar-based estimates of error. Int. J. Digital Earth. https://doi.org/10.1080/17538947.2013.786146.
Sheffield, J., Goteti, G., Wood, E.F., 2006. Development of a 50-year high-resolution global dataset of meteorological forcings for land surface modeling. J. Clim. https://doi.org/10.1175/JCLI3790.1.
Singarayer, J.S., Bamber, J.L., Valdes, P.J., Singarayer, J.S., Bamber, J.L., Valdes, P.J., 2006. Twenty-first-century climate impacts from a declining arctic Sea Ice cover. J. Clim. 19 (7), 1109–1125. https://doi.org/10.1175/JCLI3649.1.
Snapir, B., Momblanch, A., Jain, S.K., Waine, T.W., Holman, I.P., 2019. A method for monthly mapping of wet and dry snow using Sentinel-1 and MODIS: application to a Himalayan river basin. Int. J. Appl. Earth Obs. Geoinf. 74, 222–230. https://doi.org/10.1016/J.JAG.2018.09.011.
Sthapit, E., Lakhankar, T., Hughes, M., Khanbilvardi, R., Cifelli, R., Mahoney, K., Rafieeinasab, A., 2022. Evaluation of snow and streamflows using noah-MP and WRF-hydro models in aroostook river basin, Maine. Water 2022 (14), 2145. https://doi.org/10.3390/W14142145. 14(14), 2145.
Stigter, E.M., Wanders, N., Saloranta, T.M., Shea, J.M., Bierkens, M.F.P., Immerzeel, W.W., 2017. Assimilation of snow cover and snow depth into a snow model to estimate snow water equivalent and snowmelt runoff in a Himalayan catchment. Cryosphere. https://doi.org/10.5194/tc-11-1647-2017.
Taylor, K.E., Stouffer, R.J., Meehl, G.A., 2012. An overview of CMIP5 and the experiment design. Bull. Am. Meteorol. Soc. 93, 485–498. https://doi.org/10.1175/BAMS-D-11-00094.1.
Thrasher, B., Maurer, E.P., McKellar, C., Duffy, P.B., 2012. Technical Note: bias correcting climate model simulated daily temperature extremes with quantile mapping. Hydrol. Earth Syst. Sci. 16 (9), 3309–3314. https://doi.org/10.5194/HESS-16-3309-2012.
Thrasher, Bridget, Melton, F., Weile, W., 2006. NASA Earth Exchange Global Daily Downscaled Projections (NEX-GDDP) | CDS. Retrieved May 1, 2017, from NASA NEX website: https://cds.nccs.nasa.gov/nex-gddp/.
Vaganov, E.A., Hughes, M.K., Kirdyanov, A.V., Schweingruber, F.H., Silkin, P.P., 1999. Influence of snowfall and melt timing on tree growth in subarctic Eurasia. Nature. https://doi.org/10.1038/22087.
van Oldenborgh, G.J., Collins, M., Arblaster, J., Christensen, J.H., Marotzke, J., Power, S., et al., 2013. Annex I: Atlas of Global and Regional Climate Projections. Retrieved from. https://www.ipcc.ch/site/assets/uploads/2018/02/WG1AR5_AnnexI_FINAL-1.pdf.
Vihma, T., Screen, J., Tjernström, M., Newton, B., Zhang, X., Popova, V., et al., 2016. The atmospheric role in the Arctic water cycle: a review on processes, past and future changes, and their impacts. J. Geophys. Res.: Biogeosciences. https://doi.org/10.1002/2015JG003132.
Wang, A., Xu, L., Kong, X., 2018. Assessments of the Northern Hemisphere snow cover response to 1.5 and 2.0°C warming. Earth Syst. Dynamic. https://doi.org/10.5194/esd-9-865-2018.
Wood, A.W., Leung, L.R., Sridhar, V., Lettenmaier, D.P., 2004. Hydrologic implications of dynamical and statistical approaches to downscaling climate model outputs. Climatic Change 62 (1), 189–216. https://doi.org/10.1023/B:CLIM.0000013685.99609.9E. 2004 62:1.
Yunlong, W., Huang, X., Hui, L., Sun, Y., Qisheng, F., Tiangang, L., 2018. Tracking snow variations in the northern hemisphere using multi-source remote sensing data (2000–2015). Rem. Sens. 10 (1), 136. https://doi.org/10.3390/rs10010136.
Zeng, X., Broxton, P., Dawson, N., 2018. Snowpack change from 1982 to 2016 over conterminous United States. Geophys. Res. Lett. https://doi.org/10.1029/2018GL079621.